Modelling Human Glomerulosclerosis *in vitro*

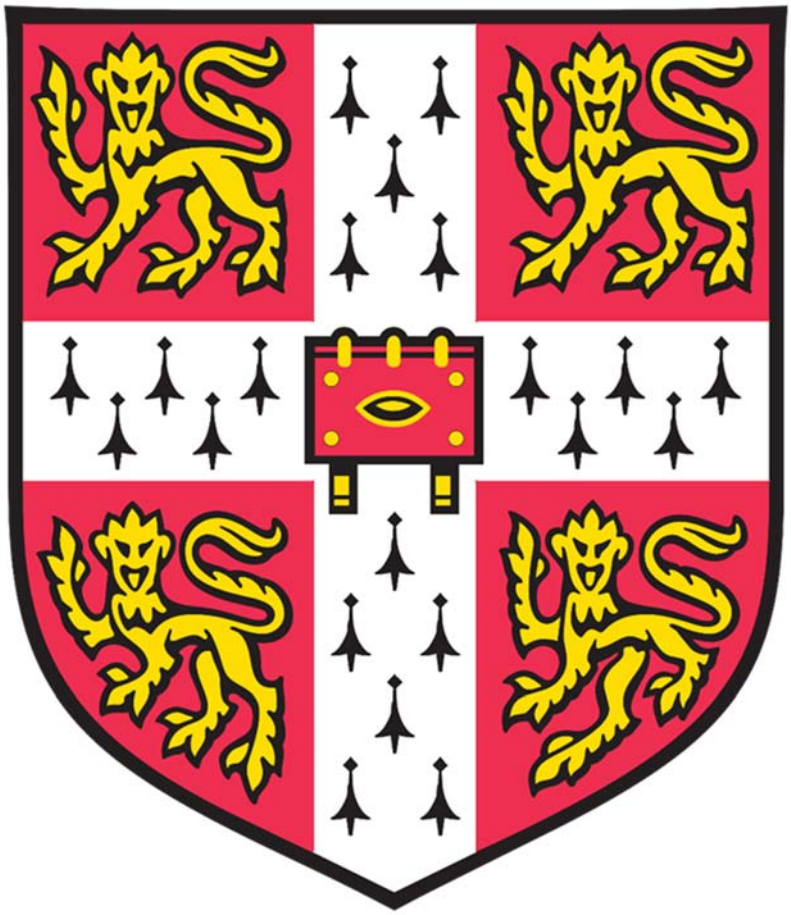

Yvonne Clare Sewell

Trinity Hall College

Thesis submitted for the degree of Doctor of Philosophy

January 2021

Department of Medicine

University of Cambridge

Preface

This dissertation is the result of my own original research conducted from September 2015 until February 2020 at the Department of Medicine, University of Cambridge, UK. This work includes nothing which is the outcome of work done in collaboration except as declared in the Preface and specified in the text.

This work is not substantially the same as any that I have submitted, or, is being concurrently submitted for a degree or diploma or other qualification at the University of Cambridge or any other University or similar institution except as declared in the Preface and specified in the text. I further state that no substantial part of my dissertation has already been submitted, or, is being concurrently submitted for any such degree, diploma or other qualification at the University of Cambridge or any other University or similar institution except as declared in the Preface and specified in the text

This thesis does not exceed the prescribed word limit of 60,000 for the Clinical Medicine and Clinical Veterinary Medicine Degree Committee

Acknowledgements

This work has been conducted as part of a collaboration between the University of Cambridge and MedImmune, Cambridge under the MedImmune/Cambridge PhD Programme in Biomedical Research. Funding for this work has come from the NIHR Cambridge Biomedical Research Centre and MedImmune, Cambridge.

Supervision has been provided, with great thanks, from both the University of Cambridge and MedImmune, Cambridge. Professor John Bradley within the Department of Medicine at the University of Cambridge and Dr Carol Moreno Quinn within the Early Cardiovascular, Renal and Metabolism (CVRM) at MedImmune, Cambridge. I am indebted for the support, encouragement and kindness.
I would like to acknowledge the members of the Bradley group within the Department of Medicine at the University of Cambridge as well as the employees of MedImmune, Cambridge for the welcoming laboratory environment for me to conduct my experiments. I would particularly like to acknowledge Dr Rafia Al-Lamki, who has provided me with many practical skills, including her HOC technique, as well as support and mentorship.

I have had the privilege of access to many different resources throughout my PhD which I would like to acknowledge. Firstly, my research was supported by the Cambridge NIHR BRC Cell Phenotyping Hub, with advice and support provided with imaging. I would also like to gratefully acknowledge the Cambridge Advanced Imaging Centre for their support and assistance in this work. Through MedImmune, I was involved in collaboration with Dr Jaakko Patrakka and his research group at the

Karolinska Institute and would like to acknowledge them for sharing knowledge of podocyte isolation. The Human Research Tissue Bank and Cambridge Biorepository for Translational Medicine, both within the Cambridge University Hospitals NHS Foundation Trust, provided me with patient tissue for my work, I would like to acknowledge their help and guidance with this element of my work. I would also like to acknowledge and sincerely thank the patients who had consented for their tissue to be used in such scientific research.

Finally, to my husband David and my daughter Isla. You are my inspiration and motivation, my supporters and endless sources of love. I truly could not have achieved this without you.

Yvonne Clare Sewell 2021

Abstract

Modelling Human Glomerulosclerosis *in vitro*

Yvonne Clare Sewell, Trinity Hall College

Glomerulosclerosis is a feature of many chronic kidney diseases. Glomeruli are composed of glomerular endothelial cells (GECs), podocytes (PODs) and mesangial cells (MCs), and dysregulation in the interaction between these cell types results in glomerulosclerosis. This is characterised by excessive extracellular matrix deposition and cell dysfunction leading to disproportionate MC proliferation and POD loss. Animal models of glomerulosclerosis often do not reflect disease pathophysiology and 2D glomerular cell monocultures provide limited insight into a disease in which cellular crosstalk and interaction are fundamental. This thesis describes a 3D tri-culture model in which GECs, PODs and MCs are co-cultured in a collagen matrix and used to model human glomerulosclerosis with the treatment of TGF-β. Fibrosis is replicated in the 3D tri-culture model with nodule formation and upregulated fibrotic/inflammatory-associated gene expression. Whilst many cytokines were identified as playing a role in the development of fibrosis in the 3D tri-culture, TGF-β and CTGF were demonstrated as key inducers of fibrosis. With a synergistic relationship, both cytokines required targeting for successful attenuation of fibrosis. Direct targeting of TGF-β is impractical due to its varied and systemic modes of action. Integrin αvβ8 activates LTGF-β to TGF-β, and inhibition of αvβ8 proved to reduce TGF-β evoked fibrosis in the 3D tri-culture model. This thesis concludes that the intimate interaction of glomerular cells both physically and via signalling mechanisms in the 3D tri-culture model mimic the *in vivo* state both morphologically and pathophysiologically. This is required for successful study, identification and assessment of potential therapeutic targets of glomerulosclerosis.

Author Publications

A 3D tri-culture system reveals that activin receptor-like kinase5 and connective tissue growth factor drive human glomerulosclerosis

John P Waters[1]*, Yvonne C Richards[1], Jeremy N Skepper[2], Mark Southwood[3], Paul D Upton[1], Nicholas W Morrell[1], Jordan S Pober[4] and John R Bradley[1]

[1]Department of Medicine, University of Cambridge, Addenbrooke's Hospital and NIHR Cambridge Biomedical Research Centre, Cambridge, UK.[2]Department of Physiology, Development and Neuroscience, University of Cambridge, Cambridge, UK.[3]Department of Pathology, Papworth Hospital, Papworth Everard, Cambridge, UK.[4]Department of Immunobiology, Yale School of Medicine, New Haven, CT, USA

J Pathol. 2017 Nov;243(3):390-400. doi: 10.1002/path.4960. Epub 2017 Oct 3.

Modelling human glomerulosclerosis *in vitro* using a 3-dimensional tri-culture system

Yvonne Richards[1], John Waters[1], Carol Moreno Quinn[2], John R. Bradley[1]

[1]Department of Medicine, University of Cambridge, Addenbrooke's Hospital and NIHR Cambridge Biomedical Research Centre, Cambridge, UK. [2]MedImmune, Cambridge, UK.

Poster presented at: ERA-EDTA 54th Annual Congress; 2016 Jun 3-6; Madrid, Spain.

Novel renal disease model

Yvonne Richards[1], John Waters[1], John R. Bradley[1]

[1]Department of Medicine, University of Cambridge, Addenbrooke's Hospital and NIHR Cambridge Biomedical Research Centre, Cambridge, UK

WIPO (PCT): WO2017199034A1 (Application filed by Cambridge Enterprise Limited)

Abstract:
The invention relates to a renal disease model comprising: a matrix which comprises glomerular endothelial cells, mesangial cells and podocytes; and an agent which induces renal disease morphology. This invention also relates to methods of making and using the same, and kits thereof.

Table of Contents

Abbreviations

Abbreviation	Definition
1D11	Anti-TGF-β Antibody
2D	Two-Dimensional
3D	Three-Dimensional
ActR-IIA	Type II-A Activin Receptor
ActR-IIB	Type II-B Activin Receptor
ALK5i	ALK5 Inhibitor
BA	Beta-actin
BCA assay	Bicinchoninic Acid Assay
bFGF/FGF2	Basic Fibroblast Growth Factor
BMP7	Bone Morphogenic Protein 7
BMPR-II	Type II Bone Morphogenetic Protein Receptor
BRC	Cambridge Biomedical Research Centre
BSA	Bovine Serum Albumin
C60s	60mmx150mm Dishes
CAIC	Cambridge Advanced Imaging Centre
CBTM	Cambridge Biorepository for Translational Medicine
CCL2/MCP-1	C-C motif chemokine 2/ Monocyte Chemoattractant Protein 1
CHO	Chinese hamster ovary
CKD	Chronic Kidney Disease
cryo-EM	Cryogenic Electron Microscopy
CTGF	Connective Tissue Growth Factor
CTGF nAb	CTGF Neutralising Antibody
CUH	Cambridge University Hospital
CVRM	Cardiovascular, Renal and Metabolism
DN	Diabetic Nephropathy
DPBS	Dulbecco's Phosphate Buffered Saline
ECGS	Endothelial Cell Growth Supplement
ECM	Extracellular Matrix
ECM	Endothelial Cell Medium
EF-1	Elongation Factor-1
EGF	Epidermal Growth Factor

EHS	Engelbreth-Holm-Swarm
EMT	Epithelial to Mesenchymal Transition
EndMT	Endothelial to Mesenchymal Transition
EP2 Receptor	Prostaglandin E2 Receptor 2
FBS	Foetal Bovine Serum
FCS	Foetal Calf Serum
fGECs	Foetal Glomerular Endothelial Cells
FGF	Fibroblast Growth Factor
FGFR	FGF Receptor
fMCs	Foetal Mesangial Cells
fPODs	Foetal Podocytes
FSGS	Focal Segmental Glomerulosclerosis
GA	Gentamicin/Amphotericin
GBM	Glomerular Basement Membrane
gDNA	genomic DNA
GEC	Glomerular Endothelial Cell
GFP	Green Fluorescent Protein
GFR	Glomerular Filtration Rate
HB-EGF	Heparin-binding EGF-like Growth Factor
HGF	Hepatocyte Growth Factor
HK genes	Housekeeping genes
HMVECs	Human Dermal Microvascular Endothelial Cells
HOC	Human Organ Culture
HRP	Horseradish Peroxidase
HTRB	Human Research Tissue Bank
HUVECs	Human Umbilical Vein Endothelial Cells
IF	Immunofluorescence
IHC	Immunohistochemistry
IL-1R	IL-1 Receptor
IL-1α	Interleukin 1α
IL-1β	Interleukin 1β
iPS Cells	Induced Pluripotent Stem Cells
ITS	Insulin, Apo-transferrin and sodium selenite

kDa	Kilodalton
LAP	Latency Associated Peptide
LTGF-β	Latent TGF-β
MC	Mesangial Cell
MCM	Mesangial Cell Medium
MMP	Matrix Metalloproteinase
MsCGS	Mesangial Cell Growth Supplement
MT1-MMP	Membrane Type 1-MMP
NF-κB	Nuclear Factor κB
NIHR	National Institute for Health Research
NIP228	Isotype Control Antibody
NLRP3 inflammasome	Nucleotide-binding domain and Leucine-rich Repeat Pyrin domain-containing protein 3 inflammasome
NPHS2	Podocin gene
P/S	Penicillin/Streptomycin Solution
PAI-1	Plasminogen activator inhibitor-1
PBS	Phosphate-Buffered Saline
PBST	PBS containing Tween 20
PDGF-BB	Platelet-derived Growth Factor BB
PDGFR	PDGF Receptors
PDGFR-β	PDGF Receptor β
PFA	Paraformaldehyde
PGA	Polyglycolic Acid
pI	Isoelectric Point
PI3K	Phosphatidylinositol-3 Kinase
POD	Podocyte
pX	Passage Number
RGD	Arginine – Glycine – Aspartic acid
RTK	Receptor Tyrosine Kinases
RT-qPCR	Quantitative Reverse Transcription PCR
SDS-PAGE	Sodium Dodecyl Sulfate Polyacrylamide Gel Electrophoresis
SEM	Scanning Electron Microscopy
Ski	Sloan-Kettering Institute proto-oncogene

SnoN	Ski-related novel gene, non Alu-containing
SNPs	Single Nucleotide Polymorphisms
STR	Short Tandem Repeat
STZ	Streptozotocin
T0	Time Zero
T1D	Type I Diabetes
T2D	Type II Diabetes
TBS	Tris-buffered Saline
TC	Tissue Culture
TEM	Transmission Electron Microscopy
TGFB1	Transforming Growth Factor-β 1 gene
TGF-α	Transforming Growth Factor-α
TGF-β	Transforming Growth Factor-β
TGF-βR-I/ALK5	Type I TGF-β Receptor
TGF-βR-II	Type II TGF-β Receptor
TGIF	TG-interacting factor
TNFR-I/p55	Type I Tumour Necrosis Factor Receptor
TNFR-II/p75	Type II Tumour Necrosis Factor Receptor
TNF-α	Tumour Necrosis Factor-α
ULEX	Ulex europaeus agglutinin I
UUO	Unilateral Ureteral Obstruction
V1	Version 1
V2	Version 2
VEGF	Vascular Endothelial Growth Factor
WT-1	Wilms' tumour protein
α-SMA	α-Smooth Muscle Actin

List of Tables & Figures

Tables

Figures

Chapter 1 – Introduction

Glomerulosclerosis

Chronic kidney disease (CKD) is a prominent cause of morbidity and mortality worldwide. Approximately 60,000 premature deaths a year within the UK are a result of CKD. Treatment is focussed upon slowing progression and preventing complications.[1] The principal cause of progressive CKD is diabetes, which is increasing in prevalence across the world. Renal replacement therapy is the only option for those with progressive renal disease who reach end-stage kidney failure.[2, 3]

Renal fibrosis is one of the key hallmarks of CKD, regardless of disease aetiology. It is characterised by excessive extracellular matrix (ECM) deposition, abolishing the fine structures of the kidney and impairing the organ's function.[4-6] The resultant scarring occurs within the tubular interstitium and glomeruli; glomerulosclerosis is a feature of diabetic nephropathy (DN) and idiopathic focal segmental glomerulosclerosis (FSGS), and many other primary renal and systemic kidney diseases.[7-9]

The glomerulus consists of a basement membrane partitioning the capillaries and mesangium from podocytes, which line Bowman's space. Three distinctive cell types, glomerular endothelial cells (GEC), mesangial cells (MC) and the podocyte (POD) interact intimately, directly or via paracrine cytokine/growth factor signalling for the glomerulus to function effectively.[10, 11] MCs are a specialised pericyte contractile cell type whose interaction with the abluminal surface of GECs is important for both stabilisation and re-modelling, as well as in development. PODs are a highly differentiated polarised epithelial cell type with long cytoplasmic processes, which divide into individual foot processes that integrate with those of neighbouring PODs and so forming filtration slits, otherwise known as the slit diaphragm.[12] The slit diaphragm is a specialised intracellular junction with several highly important functions such as further filtration and cell survival.[12, 13]

A key feature of glomerular disease is proteinuria. Proteins leak across an impaired glomerular filtration barrier and contribute to the progression of renal disease.[14, 15] Glomerular filtration rate (GFR) is a measure of the rate of filtration of fluid from the glomerular capillaries into the Bowman's capsule per unit time, and another measure used to define the extent of glomerular damage.[16]

Glomerulosclerosis is contributed to and affected by the three glomerular cell types; the MC is often termed the "cornerstone" of the disease because the enlarged mesangial compartment is a major hallmark of glomerulosclerosis.[17] This enlargement is due to a combination of MC matrix deposition, cellular hypertrophy and proliferation. The GEC apoptosis seen is related to the loss of glomerular capillaries, and thus loss of glomerular function.[18] Loss of the POD cell type is typical in glomerulosclerosis, a major problem because this highly differentiated cell type may have limited ability to proliferate *in situ*. POD loss may provide an early indication of glomerular disease and have

a key role in glomerulosclerosis.[19, 20] Loss of PODs predicts disease progression of diabetic nephropathy, FSGS and IgA nephropathy.[20]

Multiple cellular events are involved in the pathogenesis of glomerulosclerosis and renal fibrosis, with complex pathways and mechanisms. Renal fibrosis cannot be established by a distinct cell type alone, despite numerous studies pointing to a specific cellular event as key. Simply put, renal fibrosis is a failed wound-healing response. It has long been considered that patients with CKD would pass a juncture where the extent of fibrotic damage becomes irreversible and dialysis and transplantation become inevitable. In the last 20 years, evidence has been gathered to suggest that kidney fibrosis and scarring can be halted and even reversed by targeting specific molecules and growth factors.[21-25]

Cytokines, Growth Factors & Integrins of Fibrosis

Many cytokines and growth factors are involved in the initiation and progression of fibrosis. Some of those involved in key signalling pathways studied in this work are described, and their role in the development of renal fibrosis are described in the next chapter.

Transforming growth factor-β (TGF-β) and its intracellular mediators, SMADS, are widely accepted to be of major importance in disease pathogenesis.[17, 18, 26, 27] In CKD TGF-β is upregulated in both animal models and humans.[28-30]

A member of the TGF-β superfamily, TGF-β regulates diverse functions, including proliferative and inflammatory responses. Many responses are cell-type specific. There are three isoforms of TGF-β (TGF-β1, TGF-β2 and TGF-β3), which are secreted by various cell types. Secreted TGF-β is bound to a latency associated peptide (LAP), rendering it inactive. In the kidney, latent TGF-β (LTGF-β) is deposited within the extracellular matrix. Proteolytic cleavage removes the LAP and activates TGF-β, allowing binding to its type II receptor (TGF-βR-II), which activates the type I receptor (TGF-βR-I/ALK5).[18, 31] Receptor activation induces phosphorylation of receptor mediated SMADs (SMAD2 and SMAD3), which form a complex with a common mediator SMAD (SMAD4) that translocates into the nucleus and regulates target gene transcription; inhibitory SMADs (SMAD6 and SMAD7) compete with SMAD2/SMAD3 for ALK5.[32] Other signalling pathways stimulated by TGF-β include Rho-like GTPases, the phosphatidylinositol-3 kinase (PI3K)/Akt and Ras-MEK-ERK MAP kinase pathways.[27, 33]

Many other cytokines and growth factors are involved in the regulation of fibrosis, often exhibiting crosstalk with TGF-β; a number of these were studied as part of this thesis and will be briefly introduced here. Bone morphogenic protein 7 (BMP7) is a member of the TGF-β superfamily, which like TGF-β has effects on numerous cellular functions in many cell types. BMP7 antagonises TGF-β-dependent fibrosis, stimulating various repair processes in kidney disease.[34-36] BMP7 is highly

expressed in the kidney; in animal models of kidney disease expression is suppressed.[37-39] BMP7 signals by binding to a type II receptor (there are three type-II BMP receptors; type II-A Activin receptor (ActR-IIA), type II-B Activin receptor (ActR-IIB) or type II bone morphogenetic protein receptor (BMPR-II)), which phosphorylates specific type I receptors (ALK2, ALK3 and ALK6) and activates receptor mediated SMADs (SMAD1, SMAD5 and SMAD8) with the mediator SMAD4, in common with the TGF-β pathway.[31, 32] BMP7 also shares with TGF-β the ability to activate other signalling pathways, such as ERK MAP kinase. [38]

Connective tissue growth factor (CTGF) is a cytokine that has emerged as an important player in kidney fibrosis, with TGF-β a potent inducer of CTGF.[40-42] CTGF has a somewhat cooperative role with TGF-β. CTGF has been reported both *in vitro* and *in vivo* to be required for several TGF-β functions, as well as inhibiting BMP7.[41, 43, 44] Stimulation of inflammation may be a way in which CTGF contributes to fibrosis. The cytokine can initiate C-C motif chemokine 2(CCL2/MCP-1) induction, and activate the nuclear factor κB (NF-κB) pathway.[45, 46] CTGF has no single receptor but modulates fibrosis through various molecular pathways.

Platelet-derived growth factor BB (PDGF-BB) forms a dimer involved in many biological processes; best described concerning its role in vascular biology, this includes renal fibrosis and MC proliferation.[47-49] PDGFs bind to three PDGF receptors (PDGFR), signalling through Ras-MAPK and PI3K pathways. PDGFR-beta (PDGFR-β) is used as a marker for MCs, with renal expression of PDGF and PDGFRs being mesenchymal.[48, 49]

The growth factor epidermal growth factor (EGF) and its receptors, similar to CTGF, is involved in the induction of fibrosis whilst also acting synergistically with TGF-β.[42, 50] EGF signals through the ERBB family of four receptor tyrosine kinases (RTK), named ERBB1-4.[51] EGF can be excreted in urine and may act as a biomarker for disease progression, as EGF excretion decreases with disease severity.[52]

Basic fibroblast growth factor (bFGF/FGF2) has also been implicated in CKD by behaving as a potent mitogen for cortical kidney fibroblasts, adding to POD injury and enhancing GEC apoptosis induced by tumour necrosis factor-α (TNF-α).[53-55] bFGF is named for its basic isoelectric point (pI), part of the 22 member fibroblast growth factor (FGF) family, bFGF elicits its effects through four FGF receptors (FGFR).[56-58] bFGF, like other FGFs, is pleiotropic in nature with roles in angiogenesis, cell proliferation and migration.

Hepatocyte growth factor (HGF), unlike the other growth factors highlighted, antagonise the pro-fibrotic action of TGF-β, highlighting HGF as a candidate for use in combatting fibrotic diseases.[59-63] HGF regulates diverse cellular processes via the RTK c-MET.[64]

Various inflammatory molecules have been implicated in renal disease, including TNF-α.[65-71] TNF-α seems to have a central role in the pathogenesis of fibrotic kidney diseases such as diabetic

nephropathy.[66, 67, 69, 70] Immune cells produce TNF-α, including macrophages and T lymphocytes, but MCs can also synthesise this cytokine.[67, 72-74] Two TNF receptors, type I TNF receptor(TNFR-I/p55) and type II TNF receptor (TNFR-II/p75) signal shared and opposing functions, including differentiation, proliferation and cell death.[75]

Interleukin 1α (IL-1α) and interleukin 1β (IL-1β) induce inflammatory processes implicated in CKD. IL-α exists constitutively in epithelial cells; while in other cell types, such as endothelial cells and MCs, the IL-α precursor is expressed upon activation.[76, 77] IL-1β secretion is mainly restricted to activated circulating monocytes.[76, 77] IL-1α and IL-1β elicit a variety of biological effects, including fibrosis.[78, 79]

One receptor studied in this work is the integrin αvβ8. Integrins are cell adhesion receptors, which enable bi-directional signalling across the cell membrane, facilitating cell adhesion and activating intracellular signalling.[80, 81] Integrins are heterodimers of non-covalent α and β subunits. There are 18 distinct α subunits and 8 distinct β subunits, resulting in 24 identified integrins in humans.[80, 81] Ubiquitously expressed within the kidney is the αv subunit, which exists in five isoforms, one being αvβ8. αvβ8 binds the LTGF-β complex and is implicated in the balance of inactive and active TGF-β.[82, 83]

The Study of Fibrosis

Kidney fibrosis has been studied both *in vitro* and *in vivo*. *In vitro* models are generally limited by the lack of representation of the crosstalk between cell types seen in complex cellular *in vivo* networks. Several animal models used to study glomerulosclerosis are discussed in the literature review; the Adriamycin® (doxorubicin) rodent models use Adriamycin® (Pfizer, NY, USA) to induce renal injury, which is structurally and functionally similar to human FSGS.[84] The renal injury seen in streptozotocin (STZ) rodent models of type I diabetes (T1D) resembles human DN; the chemical is toxic to insulin-producing beta-cells of the pancreas.[85, 86] The *db/db* mouse model has a point mutation in the gene coding the leptin receptor, resulting in hyperphagia and obesity. These mice develop diabetes that mimics human type II diabetes (T2D).[87, 88] Injection of an anti-Thy1 monoclonal antibody into a rat induces Thy-1 nephritis, simulating human IgA nephropathy.[89] Alport mice are genetically engineered and have a *Col4a3* knockout. This gene codes for the α3 chain of type IV collagen. Human Alport syndrome is caused by mutations in COL4A3, COL4A4 and/or COL4A5 (α3, α4, α5 chains of type IV collagen) with glomerulosclerosis a key characteristic.[90, 91] The 5/6 nephrectomy is a rodent surgical model of kidney disease, with glomerulosclerosis, that is evoked by unilateral nephrectomy and either partial infarction or amputation of the poles of the remaining kidney; the morphological and functional damage shows similarity to human CKD.[92, 93]The unilateral ureteral obstruction (UUO) rodent model involves surgical intervention to cause kidney damage by complete ureteral obstruction, which

induces inflammation and fibrosis; clinical obstructive nephropathy involves partial obstruction, UUO models have been developed to imitate this in neonatal rodents but are challenging to perform.[89, 94] UUO models are used primarily to study interstitial fibrosis, yet are useful to study progressive renal fibrosis. Many more animal models can be used in the study of glomerulosclerosis, including non-rodent models; rodent models are used most commonly due to their size, cost and ease of maintenance as well as life cycle length. However, all animal models used in the study of glomerulosclerosis have the same problems and disadvantages in that they involve insults that often do not reflect the aetiology of human disease, they can take substantial periods of time to evolve and may be poor predictors of therapeutic responses in humans. Thus, there is a need for more clinically relevant models of kidney disease.

With the need for more physiologically relevant assays than two-dimensional (2D) cell cultures, and more clinically relevant models, as well as ethical issues related to animal models, three-dimensional (3D) cell culture systems are increasingly used for biologics research. 3D cell culture allows cells to behave much more like *in vivo*. Within tissues, cells interact not only with the same-cell types but other cell types and with the ECM, which has a significant impact on the response to stimuli and gene expression.[95-98] The context of a cell is important in its behaviour, and 3D culture of cells is much more akin to *in vivo*. Many cell types have been reported to behave differently when cultured in 3D compared to 2D.[95, 99] 3D culture also allows co-culture of cells to create an even more relevant *in vitro* model than 2D culture, and allows examination of crosstalk between cell types that is vital for many cellular processes, including renal glomerular cells in glomerulosclerosis.

Human organ culture (HOC) is another methodology that could provide important insight and clinical relevance in the study of kidney fibrosis and glomerulosclerosis, and this technique was utilised for this thesis. The culture of tissue slices was introduced by Otto Warburg in the study of cancer cell metabolism and has since been used on a variety of organ tissue types, including kidney, both animal and human in origin.[100-105] Complex organ architecture and cell heterogeneity are maintained in organ culture, allowing a more clinically informative study of disease pathogenesis than when cells are culture in isolation on a 2D substrate, especially when human tissue is utilised.

To provide better therapeutic options to patients with CKD there needs to be elucidation of novel targets and clinically relevant models to study cellular mechanisms. 3D culture using human renal cells is a way to do this. My PhD project aimed to use primary human GEC, MC and POD cells in 3D culture (tri-culture) to model glomerulosclerosis *in vitro.* The goal was to enable further understanding of the cellular mechanisms and cross-talk involved in fibrosis of the glomerulus, identify therapeutic targets, and provide a model system to test new treatments. Parallel analysis with HOC of normal kidney tissue

enabled comparison of any findings from the model. The aim being to elucidate the pathogenesis of glomerulosclerosis and inhibit this process.

Chapter 2 – Literature Review

This literature review provides further detail about the key signalling pathways involved in kidney fibrosis and the targets highlighted in these pathways; current animal and HOC models of fibrosis will be discussed further; along with consideration of the use and validity of 3D cell culture models and how this has been used in the study of kidney disease. This will highlight the areas where further work is needed and how this PhD project aimed to contribute towards this.

Cytokines & Growth Factors in Fibrosis

TGF-β & BMP signalling

Canonical TGF-β/BMP signalling is SMAD-mediated and although TGF-β can also signal through non-canonical means, the progression of renal fibrosis via canonical TGF-β signalling is the focus of this report. Human studies have linked TGF-β and its signalling pathways to the pathogenesis of various kidney diseases. Yamamoto *et al*.[28] demonstrated that within the glomerulus and tubulo-interstitium of patients with renal diseases characterised by ECM accumulation, there was a significant increase in TGF-β expression, along with elevated levels of fibronectin EDA+ and plasminogen activator inhibitor-1 (PAI1), which are both induced by TGF-β. Sharma *et al*.[106] tested the aortic, renal vein and urinary levels of TGF-β in patients with T2D versus non-diabetic patients, and found there was a net renal production of TGF-β in diabetic patients, whereas non-diabetic patients had net renal extraction of TGF-β. Diabetic patients also had significantly higher levels of urinary TGF-β. These early research findings linking TGF-β and kidney disease have been confirmed by many other groups in human studies, animal and cell studies,[107-112] and efforts have been made to target TGF-β in renal fibrosis. Border *et al*.[113] demonstrated in the Thy-1 nephritis rat model that anti-TGF-β antiserum suppressed increased ECM production, and attenuated histological indicators of glomerulonephritis. Many others have tested different methods of TGF-β inhibition in model systems with successful results, but the use of TGF-β blocking interventions has not translated into clinical treatment. This is primarily because TGF-β plays many roles, and thus systemic blocking of it is likely to result in serious adverse effects. TGF-β is often referred to as having two sides; pro-fibrotic and anti-inflammatory. Indeed, mice deficient in TGF-β die due to exaggerated inflammatory responses[114], and Wang *et al*.[115] found that transgenic mice that overexpressed LTGF-β are protected via the anti-inflammatory action of TGF-β from progression of renal fibrosis. Furthermore, the loss of TGF-β mediated signalling via SMAD7 has been implicated in inflammatory bowel diseases.[116] Therefore, whilst anti-fibrotics

targeting TGF-β are still in the pipeline, focus has shifted towards targeting downstream of TGF-β to aim at pro-fibrotic effects more specifically.

As outlined earlier SMAD2 and SMAD3 are identified as the mediators of TGF-β receptor binding, whereas SMAD7 is an inhibitor of this. SMAD7 has been highlighted as a mediator of potential interest in the attempt to dampen TGF-β induced fibrosis.[117, 118] Li *et al*.[119] demonstrated that SMAD7 gene transfection and overexpression in normal rat kidney tubular epithelial cells inhibited SMAD2 activation and collagen synthesis and myofibroblast transformation. Lan *et al*.[120] overexpressed SMAD7 in the rat UUO model with gene transfection and found that SMAD2/3 activation was inhibited with decreased tubulo-interstitial myofibroblast accumulation and collagen I and III expression.

SMAD transcriptional co-repressors interact with activated SMADs in the nucleus and form complexes which are transcriptionally inactive and can control SMAD mediated gene transcription and TGF-β mediated responses. Sloan-Kettering Institute proto-oncogene (Ski), Ski-related novel gene, non-Alu-containing (SnoN) and TG-interacting factor) TGIF are three SMAD co-repressors; Yang *et al*.[121] demonstrated in the UUO mouse model Ski and SnoN were progressively reduced in the fibrotic kidney versus normal mice, highlighting this control mechanism on TGF-β in kidney disease and thus identifying these co-repressors as potential targets to block TGF-β mediated fibrosis.

ALK5 activates SMAD2/3 upon phosphorylation via TGF-β bound TGF-βR-II, and thus is central to TGF-β mediated fibrosis. Moon *et al*.[122] used a small molecule ALK5 inhibitor (ALK5i) to prevent the phosphorylation of SMAD3 in the UUO rat model; inhibition resulted in a decrease in levels of TGF-β, collagen I and pSMAD2 mRNA and a reduction of pathogenic morphological features such as tubular atrophy and inflammatory cell infiltration compared to control UUO kidneys. This data implies that there is a therapeutic potential of using TGF-β receptor modulation to inhibit TGF-β mediated fibrosis. However, Moon *et al*. could not fully prevent late stage fibrosis in the UUO mouse using the ALK5i, suggesting that at this late stage TGF-β independent pathways are also involved in the fibrotic response. This combined with the same potential problem of affecting the anti-inflammatory activity of TGF-β as with direct TGF-β inhibition, perhaps suggests that ALK5 inhibition is better used as a tool in understanding the TGF-β mediated and non-TGF-β mediated mechanisms in renal fibrosis.

TGF-β is bound to a LAP, which must be cleaved before TGF-β is active; inhibition of TGF-β activation by LAP cleavage is, therefore, a potential avenue of TGF-β inhibition. Several proteases are known to evoke this cleavage, including plasmin, thrombospondin and matrix metalloproteinase (MMP) 2 and MMP9.[33, 123] Lu *et al*.[124] targeted thrombospondin-dependent TGF-β activation with a peptide antagonist in a T1D mouse model (C57BL/6J-Ins2^{Akita}, Akita mice have a spontaneous point mutation in the Ins2 gene (encoding preproinsulin 2) resulting in misfolding of insulin, which results in pancreatic β-cell failure), which underwent uninephrectomy and T2D mouse model (*db/db*) to find that urinary

TGF-β and phosphorylated SMAD2/3 levels were reduced. However, there was no impact on glomerulosclerosis, suggesting that there could be modulation of TGF-β mediated fibrosis by modifying its activation via LAP cleavage.

BMP7 has an antagonistic action upon TGF-β induced fibrosis, as BMP7 promotes renal repair. Vukicevic *et al*.[125] studied the effect of recombinant BMP7 in acute renal failure in rats after bilateral renal artery occlusion, which preserved kidney function and increased survival rate. Wang *et al*.[38] studied the expression of BMP7 in the STZ-diabetic rat model and demonstrated that after 15 weeks expression halved and BMP receptor expression declined, with an increase in secretion of the BMP antagonist gremlin. Some of these changes could be explained with increased TGF-β levels, but not all. POD loss is a key feature of glomerulosclerosis; Mitu *et al*.[35] demonstrated in murine PODs that high glucose reduced BMP7 secretion and altered POD marker expression, while high glucose and TGF-β increased apoptosis, indicating that BMP7 is a POD survival factor. This suggests BMP7 is an intriguing target, with antagonistic effects on TGF-β, a key mediator in kidney fibrosis, whist promoting renal repair.

The literature strongly supports the role of TGF-β in renal fibrosis. Therefore, the cytokine was used to induce fibrosis in the *in vitro* 3D glomerular model, while BMP7 was used to look for the antagonistic effects the literature reports on TGF-β. ALK5i is of interest to study how much of the fibrotic response is TGF-β dependent, whilst analysis of CTGF in the 3D glomerular model provides insight into its relationship with TGF-β in mediating fibrosis. Much study has been around tubular epithelial cells/ tubulo-interstitium as opposed to glomerular cells and the glomerulus; as such studying TGF-β response in each human glomerular cell type alone in 3D and then together in the 3D glomerular tri-culture model should elucidate how these cells respond, how they differ from one another, and how they communicate together in fibrosis. The literature also suggests potential targets that could be investigated during this PhD to inhibit TGF-β mediated fibrosis without the likely deleterious direct TGF-β inhibition.

CTGF, PDGF-BB, EGF, bFGF & HGF in Fibrosis

CTGF is a growth factor implicated in renal fibrosis, which has a close relationship with TGF-β as a downstream mediator. Murphy *et al*.[126] revealed strong expression of CTGF in primary human mesangial cells in response to high glucose, which was partially suppressed with an anti-TGF-β antibody. Ito *et al*.[127] demonstrated with in situ hybridisation of human renal biopsy samples across several renal diseases that CTGF was intensely upregulated in FSGS, DN, IgA nephropathy, and in the extracapillary and severe mesangial proliferative lesions of crescentic glomerulonephritis. Yokoi *et al*.[128] examined the effects of CTGF antisense oligonucleotide in UUO model rat kidneys. This

attenuated the induction of CTGF, fibronectin and collagen I, with a significant decrease in α-smooth muscle actin (α-SMA) expressing myofibroblasts. A phase I study with an anti-CTGF monoclonal antibody (FG-3019) developed by Fibrogen demonstrated a significant decrease in albuminuria in diabetic patients with kidney disease.[129] Thus CTGF may be a therapeutic target in kidney fibrosis, but elucidation of its relationship with TGF-β and mode of action is required.

PDGFs exist in five dimers (PDGF-AA, PDGF-BB, PGDF-CC, PDGF-DD and PDGF-AB), which signal via three PDGFRs (dimers PDGFR-αα, PDGFR-ββ and PDGFR-αβ). The major mechanism by which PDGFs promote renal fibrosis is the mediation of MC proliferation and activation.[48, 49] Upregulated expression of PDGFs has been described in many animal models of kidney disease, and the kidney tissue of patients with equivalent renal disease. Floege *et al*.[48] have summarised this. PDGF-BB stimulation of human MCs induces proliferation, as observed by Floege *et al*.[130] using ^{3}H-thymidine incorporation. Hudkins *et* al.[131] demonstrated that healthy mice injected with an adenovirus construct encoding PDGF-BB developed mesangial proliferative glomerulonephritis. These and other studies, with the increased expression of PDGF-BB seen in animal models and human disease, identify PDGF-BB as a potential target in the prevention of progressive renal fibrosis. Indeed, Ostendorf *et al*.[132] established that antagonism of PDGF-B using an aptamer in the Thy-1 nephritis rat model reduced interstitial fibrosis and glomerulosclerosis. The small molecule Imatinib, an inhibitor of PDGFR tyrosine kinase activity, has been used in animal models of renal disease with general success, summarised by Kok *et al*.[42] However, as described by Boor *et al*.[49], Imatinib inhibits non-specific PDGFR tyrosine kinase activity and could have adverse effects such as defective wound healing. Taken with the knowledge that Imatinib can inhibit other tyrosine kinases the development of a more specific PDGF inhibitor seems appropriate. PDGF/PDGFR signalling appears to be involved in tubular cell proliferation and regeneration in the acute phase of kidney injury. Nakagawa *et al*.[133] demonstrated in rats that during recovery from ischemic insult, induced by clamping of bilateral renal arteries, Trapidil (a nonspecific PDGF antagonist drug) decreased renal function and increased mortality. PDGF/PDGFR is therefore involved in progression of renal fibrosis and the role of PDGF-BB, in particular, was studied in this thesis.

EGF is one of the three main ligands for ERBB, the others being heparin-binding EGF-like growth factor (HB-EGF) and transforming growth factor-α (TGF-α). Downstream signalling is dependent upon ligand/receptor combination (there being four ERBB), which can activate MAPK/ERK, PI3/Akt and JAK/STAT signalling.[51, 134] EGF, the most intensely studied of the three ligands, has the highest affinity for ERBB. EGF may have a role as a biomarker of kidney disease, evidenced by Jørgensen *et al*.[135] demonstrating partial EGF excretion from plasma in rats using ^{125}I-EGF. Tsau and Chen[52] demonstrated that urinary EGF levels correlated with kidney function in children with chronic kidney

failure, which has also been seen in adults.[136] Terzi *et al*.[137] used a kidney-specific functional inactivation of ERBB to stop renal lesion development post renal injury. POD-specific ERBB knockout mice with STZ-induced T1D were demonstrated by Chen *et al*.[138] to have reduced POD loss and reduced albuminuria compared to WT T1D mice, and reduced TGF-β expression, SMAD2/3 phosphorylation and fibronectin deposition of the glomerulus. Various small molecules have been used in animal models targeting EGF/ERBB signalling; Gefitinib and Erlotinib both reduced fibrosis in Adriamycin®, UUO and hypertension models.[50, 139-141] Study of EGF/ERBB in human disease has highlighted a possible role in sex differences in predisposition to progressive kidney injury by Zhang *et al*.[142], identifying lower ERBB expression in female than male normal adult kidneys. Kim *et al*.[143] identified single nucleotide polymorphisms (SNPs) in both EGF and ERBB genes of the Korean population that appear to associate with risk of ERSD and acute renal transplant rejection.

Like CTGF, EGF signalling interacts with those of TGF-β, which both complicates and provides an opportunity for inhibition of fibrosis. Chen *et al*.[50] demonstrated in a mouse model where proximal tubules are ERBB deficient that ERBB-dependant ERK signalling was involved with TGF-β mediated fibrosis. However, as with targeting PDGF/PDGFR, EGF/ERBB signalling is implicated with renal regeneration and so blockade of this signalling pathway requires specificity.[144, 145] EGF signalling, therefore, plays in the fibrotic melee.

bFGF is involved in renal fibrosis and can behave as a potent mitogen for a number of cell types. Silver *et al*.[146] demonstrated this in human MCs by measuring ^{3}H-thymidine incorporation while Ballermann[147] used the same technique to show the mitogenic effect of bFGF on bovine GECs. The mitogenic effect of bFGF has been demonstrated in rat PODs by Takeuchi *et al*.[148]. The role of bFGF upon fibroblasts, major effector cells during fibrosis, was implicated with TGF-β by Strutz *et al.*[149], who demonstrated that TGF-β evoked proliferation of human renal fibroblasts that was dependent upon bFGF, the mitogenic effect of TGF-β being inhibited using a bFGF neutralising antibody. bFGF has also been implicated by Messmer *et al*.[55] in TNF-α mediated apoptosis of bovine GECs, where bFGF potentiates apoptosis. This was quantified by measuring apoptotic DNA fragmentation by the diphenylamine reaction. GEC apoptosis resulting in the loss of glomerular capillaries is a feature of progressive kidney disease.[18] Animal models have shown the involvement of bFGF in renal fibrosis. Floege *et al*.[150] administered intravenous bFGF to Thy-1 rats and saw induction of glomerular proliferation that appeared to be mostly MCs (PDGF-BB was also administered and demonstrated this same response, along with matrix accumulation). POD injury evoked by bFGF was evidenced by Floege *et al*.[54] using rats with membranous nephropathy, where retraction of foot processes, detachment from the glomerular basement membrane (GBM) and pseudocyst formation was seen with bFGF injection. Rats with membranous nephropathy injected with bFGF established a higher degree of

glomerulosclerosis compared to those without bFGF treatment. However, bFGF induced injury of PODs only occurred in PODs that had previous injury. Strutz *et al*.[53] studied bFGF expression by immunofluorescence (IF), western blot and in situ hybridisation in normal and fibrotic human kidneys and demonstrated that increased bFGF expression correlated with interstitial fibrosis. bFGF has an anti-fibrotic action in non-renal tissue and so specific targeting of this cytokine would be vital to prevent adverse effects of inhibition.[151] bFGF therefore has an intricate role in the development of renal fibrosis.

HGF is distinct from the cytokines discussed until now as it antagonises the fibrotic action of TGF-β. Dai *et al.*[60] used both rat and human MCs, as well as mice which had been uninephrectomised to become a diabetic nephropathy model, to investigate the effects of HGF on TGF-β induced MC activation. Both western blot and IF demonstrated suppression of TGF-β induced α-SMA expression with HGF, which also repressed expression of TGF-β mediated fibronectin and collagen I expression. The abundance of SMAD transcriptional corepressor TGIF in MCs was rapidly upregulated by HGF as a result of stabilisation of the corepressor from degradation, which resulted in suppression of SMAD mediated responses to TGF-β. The diabetic rat kidneys showed that expression of TGIF was downregulated compared to control rats, while HGF treatment induced TGIF expression. Dai *et al*.[60] show HGF can antagonise TGF-β mediated fibrosis through TGIF. Yang *et al*.[59] established that HGF could suppress the activation of renal interstitial myofibroblasts mediated by TGF-β via ERK-1/2 activation. Several animal models of CKD show HGF improves kidney fibrosis. Liu[63] has tabulated this. Lekushi *et al*.[62] showed that HGF can promote apoptosis of myofibroblasts by increasing expression of MMPs via the FAK-ERK-MMP signalling cascade using human MCs and HGF transgenic mice treated with angiotensin II to induce renal fibrosis. mRNA expression of TGF-β1, collagen I and IV were decreased in angiotensin II HGF transgenic mice while MMP-2 and MMP-9 expression was increased, highlighting another mechanism by which HGF appears to modulate renal fibrosis. Patients with acute kidney failure were shown by Taman *et al*.[152] to have increased urinary HGF, which supports the idea of harnessing the anti-fibrotic potential of HGF in the treatment of renal disease. Oka *et al*.[153] used mesothelial sheets (engineered sheets of cells with no scaffold) transplanted onto the kidney surface of UUO rats. Mesothelial cells transfected with HGF before sheet formation and transplantation resulted in strong suppression of myofibroblast induction and collagen expression for 28 days. The cell sheet provided continuous HGF suggesting a strategy for long-term HGF treatment.

Inflammatory Cytokines

Hasegawa *et al*.[154] described a role for TNF-α in the development of DN. Incubation of the GBM from STZ- diabetic rats with thioglycollate-elicited peritoneal macrophages from normal rats induced TNF-α compared with incubations with GBM of non-diabetic rats. Nakamura *et al*.[155] demonstrated increased TNF-α mRNA in the glomeruli of STZ-diabetic rats. Serum markers of TNF-α signalling in both T1D and T2D patients are considerably higher than in non-diabetics.[156-158]. DiPetrillo *et al*.[159] found that treatment with a soluble TNF-α antagonist (anti-TNFR fusion protein) in the STZ-diabetic rat model reduced urinary TNF-α and prevented sodium retention and renal hypertrophy. Awad *et al*.[70] tested a murine anti-TNF-α antibody in Ins2Akita mice and found a reduction in albuminuria, plasma creatinine and macrophage recruitment to the kidney. Experimental models make a case for anti-TNF-α in DN, as was the case with TGF-β, but the multiple effects of TNF-α make the potential advantage of TNF-α blockade less clear; TNFR-I, for example, is predominately thought to promote cell death whilst TNFR-II can oppose this.

TNF-α and TGF-β represent two major pillars of disease, inflammation and fibrosis. SMAD7 transcription can be upregulated by TNF-α, while Hong *et al*.[160] demonstrated the anti-inflammatory activity of TGF-β by induction of SMAD7, which disrupted TRAF2-TAK1-TAB2/3 complex formation and so inhibited TNF-α/NF-κB signalling.[118] This data demonstrates the cross-talk between these pathways are likely to be at play in the loss of homeostasis and the development of inflammation and fibrosis in kidney disease.

As with TGF-β, the literature strongly supports the role of TNF-α in renal diseases pathogenesis. Thus, the 3D glomerular culture system was used to examine the effects the cytokine has alone and in co-treatment with TGF-β.

Other pro-inflammatory cytokines involved in renal disease are IL-1α and IL-1β. These cytokines are ligands of the same receptor, IL-1 receptor (IL-1R), which is present on many kidney and non-kidney cells[161]. Despite signalling through the same receptor complex, IL-1α and IL-1β have several differences, which will not be detailed at length but include secretion, expression and gene regulation; Sims and Smith[77] discuss this further. Lonnemann *et al*.[162] demonstrated IL-1 synthesis in human renal fibroblasts, resulting in production of IL-8 and IL-6; use of a IL-1R antagonist resulted in partial inhibition of IL-8 and IL-6 expression. This was greater using human renal fibroblasts from fibrotic kidneys. PODs have been established by Niemir *et al*.[163] as a source of both IL-1α and IL-β in several human glomerular diseases characterised by intraglomerular inflammation. Renal biopsies examined using IHC and in situ hybridisation demonstrated IL-1α and IL-1β production in PODs of diseased glomeruli, which was higher in early disease states. A central component in the initiation of inflammation is inflammasome activation. Inflammasomes are multimeric protein complexes, which

respond to “danger” signals and evoke an inflammatory response. The nucleotide-binding domain and leucine-rich repeat pyrin domain-containing protein 3 (NLRP3) inflammasome has been implicated in kidney disease, with the maturation and release of IL-1 being controlled by the inflammasome.[79, 164, 165] Shahzad *et al*.[165] demonstrated a role of the NLRP3 inflammasome for the progression of STZ diabetic mice, where blockade of IL-1 signalling using a IL-1R antagonist prevented and even reversed diabetic nephropathy, further implicating IL-1, as well as the NLRP3 inflammasome, in the pathogenesis of CKD. Lemos *et al.*[166] demonstrated crosstalk between the mechanism of inflammation and fibrosis in kidney disease, where IL-1β induces a metabolic switch promoting fibrosis. Fibrotic kidneys from CKD patients underwent RNA sequencing and a metabolic switch from oxidative phosphorylation to glycolysis, controlled by transcription factor MYC, was identified. This switch was modelled using human kidney stromal cells, in *vivo* using murine models of kidney disease as well as human kidney organoids. IL-1β and MYC expression was correlated in this modelling and IL-1β evoked the switch identified in CKD patients, with IL-1β treatment promoting fibrosis. IL-1R inhibition prevented this. This work defines a link between inflammation and fibrosis, which involves IL-1β, where inhibition of this pathway ameliorates fibrosis. Lei *et al*.[167] targeted IL-1β in chronic kidney disease, with expression of IL-β1, identified in kidney biopsies of diabetic patients across the spectrum of disease stage. Lei *et al.*[167] used a IL-1β neutralising antibody in uninephrectomised diabetic db/db mice and observed reduced fibrosis and preserved POD number with the anti-IL-1β antibody. Clearly there is a body of data, which identifies the IL-1 signalling pathway as a therapeutic target in kidney diseases. Inflammation is, however, a vital response against infection and injury so specific targeting is imperative.

Integrin αvβ8

Integrins mediate cell-matrix interactions and can control matrix remodelling in fibrosis. The αvβ8 integrin is of particular interest due to its role in activation of TGF-β.

Five integrins, including αvβ8, bind Arginine – Glycine – Aspartic acid (RGD) ligand sites that are found in fibronectin and vitronectin as well as the TGF-β LAP, with the αv integrin subfamily all demonstrating an ability to bind LAP.[82] The αvβ8 integrin has a higher affinity to the RGD of LAP than other integrins, through this RGD binding αvβ8 controls levels of active TGF-β.[168, 169] MMPs have been implicated in the cleavage of LAP to release active TGF-β. Mu *et al.*[169] demonstrated using epithelial and neuronal human cell lines that TGF-β release from αvβ8 bound LAP was dependent upon membrane type 1 (MT1)-MMP. However, Campbell *et al*.[170] used cryogenic electron microscopy (cryo-EM) to realise a mechanism where αvβ8 bound LAP-TGF-β does not require release of LAP from TGF-β for activation and signalling of TGF-β. Instead, LAP-TGF-β presented by GARP (a transmembrane

protein found on the surface of regulatory T cells) on an opposing cell is activated by αvβ8 binding as a result of structural flexibility in LAP-TGF-β upon RGD binding. αvβ8 expression has been identified primarily the kidney, brain and female reproductive organs.[171] Expression of αvβ8 in MCs was demonstrated by Lakhe-Reddy *et al.*[172] using in situ hybridisation and quantitative reverse transcription PCR (RT-qPCR) on mouse kidneys; expression of αvβ8 was reduced in mouse models of kidney disease. Mice which lack αvβ8 or αvβ6 activity were shown by Aluwihare *et al*.[173] to develop the abnormalities seen in TGF-β knock-out mice, highlighting the requirement of αvβ8 upon TGF-β signalling. αvβ8 appears to be a significant target for renal fibrosis, yet despite interest in targeting αv-RGD integrins, specific integrin inhibitors are lacking, with pan-RGD or pan-αv integrin inhibitors being more commonly used in research. Hatley *et al*.[174] review drug discovery of αv-RGD integrins. Bon *et al.*[175] used a co-culture of human renal proximal tubular epithelial cells and renal fibroblasts to develop a mature ECM with interstitial collagens and demonstrate that anti-integrin blockade inhibited ECM accumulation. Basta *et al*.[176] used anti-RGD integrin inhibitors in a murine model of renal fibrosis where a dose of aristolochic acid I sodium salt evoked injury. Treatment with RGD integrin antagonist reduced collagen deposition and markers of myofibroblasts. Reichart *et al.*[177] reported the design of a cyclic peptide specific for αvβ8, which by radioactive labelling was used to identify αvβ8 expression in mice with subcutaneous tumour xenografts. No further work with this ligand is reported.

The industrial sponsor and collaborator of this project, MedImmune, have developed an anti-αvβ8 antibody, which can be used in the *in vitro* model of human glomerulosclerosis to understand the contribution of αvβ8 to renal fibrosis.

The Study of Fibrosis

Animal Models

The Adriamycin® rodent model is used to model FSGS. Chen *et al*.[178] first described Adriamycin® induced renal injury in mice, where FSGS occurred with enhanced glomerular deposition and matrix expression. The Adriamycin® model is reproducible, evokes renal injury in a matter of days with predictable severity, and accompanying mortality and morbidity are not usually excessive.[84] However, injury can vary with the batch of drug, and doses of 0.5mg/kg above or below that calculated to induce injury can lead to lethal toxicity or no renal injury.[84] Response is also strain dependent, and seemingly sex-dependent, as female rats are less susceptible to renal injury by Adriamycin®.[179]

STZ-diabetic rodent models of type I diabetes is dependent upon glucose transporter expression in β-cells for STZ movement into them. Thus, the general expression of glucose transporters can mean other cell types are affected and animal symptoms may not be strictly hyperglycaemic related.[180]

While the STZ-diabetic rodent models become hyperglycaemic, and the clinical characteristics of DN in humans of microalbuminuria followed by renal function decline and histological characteristics of GBM thickening, MC expansion, and sclerosis are seen in these models, the severity is mild,[86] making comparisons between with human DN more difficult.

The *db/db* mouse model of type II diabetes involves leptin receptor mutations, resulting in humans in MC expansion, glomerular enlargement and albuminuria, although GBM thickening and progressive increases in albuminuria are not consistently seen.[87] Advanced DN hallmarks of nodular glomerulosclerosis, tubular atrophy and tubule-interstitial fibrosis are not seen in this model, and immune complex deposits within the glomerulus are not consistent with DN in humans.[87] Thus, the pathology appears to have some differences with human disease, especially long term features, and the prevalence of such a leptin receptor mutation as a cause of T2D may not be relevant to the majority of cases of the human disease.

Thy-1 nephritis rat model of human IgA nephropathy administers anti-Thy-1 antibody, which is found on rat mesangial cells and induces their cell death. Mosley *et al*.[181] demonstrated necrosis induced mesangiolysis with monocyte infiltration and fibrin deposition, as well as MC proliferation and matrix expansion, which is seen in human IgA nephropathy. However, there are no IgA deposits seen in human IgA nephropathy, and thus the model does not accurately mimic the human disease.[89, 180]

Mice with a COL4A3 knockout are used to mimic human Alport syndrome where mutations are either in COL4A3, COL4A4 and COL4A5. Cosgrove *et al*.[91] demonstrated that these mice develop progressive glomerulonephritis and proteinuria, as seen in the human disease and transmission electron microscopy (TEM) revealed GBM multilaminated thickening and thinning. However, Alport mice have extracapillary crescentic proliferation at an early stage that is not characteristic of human Alport syndrome.[89]

The 5/6 nephrectomy comprises uninephrectomy plus removal of approximately 2/3 of the other kidney to reduce nephron numbers. Either ablation and/or ligation methods are performed to achieve this, thus methodology can affect outcome as renal failure progression is closely related to the amount of tissue removed or infarcted, which is technically difficult to replicate.[89, 180] Hypertension and proteinuria develop, with glomerular hypertrophy in the acute phase, which by 12 weeks develops into glomerulosclerosis and tubular atrophy.[89] This development of hypertension needs to be considered in experimental design, as well as the long timeline for disease progression.

The UUO model is used to induce kidney fibrosis for the study of tubule-interstitial disease. It is most commonly used in rodents but also studied in other animals, where interstitial inflammation and fibrosis develop from 7 days. The surgery is reproducible and not too complex, and the contralateral kidney can be used as a control. However, the absence of functional readouts as compensation by the

unobstructed kidney means there is little change in serum creatinine or proteinuria concentrations.[89, 180]

No animal model can fully recapitulate human renal disease. Models often do not reflect human disease aetiology or fully display all human disease hallmarks, and are privy to selection to minimise experimental variance. Indeed, therapeutic responses or safety evaluation demonstrated in animal models do not necessarily translate into humans. There is a need for a model system that is more clinically relevant for human disease to bridge gaps from basic research to patients; the use of human cells, such as human glomerular cell types, in 3D cultures to form glomerular structures could do just that. Ethically it is important to reduce and eventually stop animal research; this is something the scientific community is striving for with the replacement, reduction and refinement ethos. Working on 3D human model culture systems will facilitate this.

Human Organ Culture Models

HOC provides an ex vivo model of human disease, where complex organ architecture remains intact. As such, HOC has been widely used to examine drug metabolism in a variety of tissue types.[102] In the study of kidney disease HOC has been developed and used to investigate disease pathology and therapeutic targets. Stribos *et al*.[103] prepared precision cut kidney slices from healthy human cortical tissue of tumour nephrectomy patients, using a tissue slicer to obtain pieces of tissue between 4-6mg in weight and 250-300µm in thickness. The HOC was then cultured for up to 72hrs and incubated with TGF-β to model fibrosis. TGF-β resulted in increased gene expression of fibrotic markers such as COL1A1 and FN1 as well as upregulation of PAI1, which acts downstream of TGF-β. Some intrinsic fibrosis was seen with no TGF-β treatment. Jensen *et al*.[182] used the Stribos *et al*.[103] HOC kidney model to examine the effect of prostaglandin E2 receptor 2 (EP2 receptor) agonist butaprost. Butaprost reduced fibrotic gene expression. Bigaeva *et al*.[183] used the HOC model of fibrosis with fibrotic renal tissue from ESRD patients as well as healthy cortical tissue of nephrectomy patients with anti-fibrotic treatments. This was performed alongside culture of precision cut slices of normal murine and UUO murine kidneys. HOC of fibrotic renal tissue displayed increased baseline gene expression of COL1A1, SERPINE1, TNF and IL-1B in comparison to healthy HOC. Anti-fibrotics used in the study by Bigaeva *et al*.[183] were pirfenidone (has anti-TGFβ activity), galunisertib (a TGF-βR-I inhibitor) and imatinib (inhibitor of PDGFR tyrosine kinase activity). While all anti-fibrotics attenuated fibrosis by some degree, measured using both RT-qPCR and IHC, galunisertib had the most pronounced effect and any effects of anti-fibrotics were lessened in HOC from fibrotic renal tissue compared to healthy tissue. This demonstrates the use of HOC in studying fibrosis and its therapeutic targets, and when

Bigaeva *et al*.[183] compared the outcome of *in vivo* animal and human research of the anti-fibrotics tested there were parallels.

Isolated glomeruli have been used to isolate glomerular cells[184, 185], but have also been used as a more specific form of HOC observing glomerulosclerosis. Esposito *et al*.[186] used isolated human glomeruli and treated them with HGF to investigate its anti-fibrotic effect. Both the expression and synthesis of TGF-β and collagen IV were reduced with HGF treatment while gene expression of MMP-2 was downregulated.

HOC requires access to human tissue. This is not straightforward and involves ethical planning and regulation. All researchers cannot access fresh human tissues and availability is scarce and expensive. Animal precision cut kidney slices have been used in many studies into renal fibrosis and efficacy of potential treatments.[187-191] This lacks the direct clinical translation that HOC has, with issues of genetic differences. HOC has limited longevity, Stribos *et al*.[103] reported signs of cellular damage when cultures exceeded 72hrs. Dedifferentiation of cells is also reported; Stribos *et al*.[103] observed a loss in differentiated PODs. A further limitation is the lack of perfusion in the tissue, which may contribute to the limited longevity. Lack of physiological flow limits the translatability of HOC as it can evoke change in tissue microenvironments. Work on methodologies to provide an element of flow is ongoing. Paish *et al.*[192] recently used bioreactors to culture liver HOC for 6 days, with HOC remaining functional to model fibrosis and investigate therapeutics.

The Bradley laboratory is in the privileged position to have access to human renal tissue and routinely works with HOC, therefore it was logical to use this resource to compare effects in HOC and the 3D culture system of glomerulosclerosis.

3D Cell Culture Models

The importance of cellular context in determining cellular events has become apparent by using 3D culture of cells previously cultured in 2D. Weaver *et al*.[99], in the Mina Bissell research group who are pioneers of 3D cell culture, demonstrated in their human breast cancer model that treatment of human mammary epithelial cells in Engelbreth-Holm-Swarm (EHS) matrix extract (Matrigel®) with an inhibitory β1-integrin antibody reversed tumour cells into a normal phenotype. The effect of culturing cells in 3D compared to 2D on protein and gene expression has been demonstrated in cancer cells and is highlighted in discussion of renal 3D cultures below.[96, 98]

There are various methodologies for 3D cell culture. Non-scaffold techniques include hanging drop-plates, where cells form spheroids in the absence of solid substrate. Scaffold techniques involve gels to mimic the ECM. Gel based 3D culture is the method used in this project. Instead of Matrigel® where its biological origin can be a disadvantage, a rat type I collagen-based gel was utilised (full gel

composition and 3D cell culture formation are described in the methods). JP Waters cultured human umbilical vein endothelial cells (HUVECs) and human dermal microvascular endothelial cells (HMVECs) alone and in co-culture[193], as well as primary human GECs and MCs alone and in co-culture in this gel-based 3D system, where endothelial cells form tubule networks with lumen, which pericytes interact with.[194] MCs form nodules that contain collagen VI in response to TGF-β treatment that is SMAD3 dependent, which BMP7 treatment cannot rescue.[194] Loss of GEC branching by TGF-β treatment was shown to be SMAD2 dependent, which BMP7 could reverse.[194] This project stems from this work.

Marx *et al*.[195] cultured rat MCs in type I collagen gels and described a cell phenotype more akin to *in vivo,* which produced collagen IV and V. The resultant network of branching cells with occasional "junctional complexes" have been termed nodules in this report. In culture microvascular endothelial cells form tubule/vascular structures in 3D; Sankar *et al*.[196] demonstrated rat capillary endothelial cells had a different TGF-β receptor profile when cultured in 2D compared to 3D type I collagen culture, with a decrease in cell surface TGFβRII in cells cultured in 3D versus 2D, indicating a change in cell response to TGF-β when cells are in a ECM environment.

The co-culture of cells is a step towards an accurate replication of the *in vivo* environment by allowing cells to interact as they would *in vivo,* and interact with ECM. Byron *et al*.[197] cultured conditionally immortalised human PODs with conditionally immortalised human MCs in 2D in isolation and co-culture to analyse ECM composition and assembly. There was altered composition and organisation in mono-cultures compared to co-cultures, such as increased collagen VI, implying cellular cross-talk in ECM production. The ECM composition of co-cultures was closer to that of the *in vivo* glomerulus than the ECM produced by mono-cultures. This supports the importance of glomerular cell-cell communication for ECM composition; as aberrations in ECM production are a key process of glomerulosclerosis, the culture of all three glomerular cell types in 3D should better replicate that *in vivo*.

Li *et al*.[198] described a 3D culture model of either rat or conditionally immortalised mouse PODs and a mouse microvascular endothelial cell line. A porous membrane coated in collagen IV separated PODs and endothelial cells. This co-culture was suspended in a plate well, and human mesenchymal stem cells could be cultured on the well bottom. Experiments, such as albumin permeability, were performed to model proteinuria. However, individual cell types are still grown in a monolayer, which forces polarity on a cell type that does not replicate 3D culture.

Takasato *et al*.[199] used human induced pluripotent stem (iPS) cells on Matrigel® treated culture dishes to generate kidney organoids with individual nephrons segmented into distal and proximal tubules, early loops of Henle and glomeruli with PODs; gene expression of these organoids was akin to a first

trimester human kidney. These kidney organoids consist of analogous tissue organisation to the human kidney but on the microscale; with powerful applications in drug safety screening, disease modelling, and possible engineering of kidneys for transplantation. However, it would be difficult to unpick the signalling and pathogenic processes in the glomeruli alone in this model.

These renal/renal-related 3D culture systems are more physiological than traditional 2D cultures and more translational than animal models, and ethically and economically beneficial compared to the animal alternative. To the best of my knowledge, there is no 3D glomerular culture model that incorporates primary human GECs, POD sand MCs that can physically interact, mimicking the *in vivo* environment, and thus the work described in this report is novel.

The literature review shows the relevance of TGF-β/BMP and TNF-α signalling tested in the 3D glomerular tri-culture model developed in this PhD project, representing the main pillars of fibrosis and inflammation in renal diseases. Other pro-fibrotic targets include CTGF, PDGF-BB, EGF and bFGF. Pro-inflammatory targets include IL-1α and IL-1β, and anti-fibrotic agents include HGF and αvβ8.

Aims & Objectives

This thesis aims to present an *in vitro* model of human glomerulosclerosis. The hypothesis being that a 3D culture of the three glomerular cell types can model glomerulosclerosis. Providing these cells with a microenvironment and cellular context similar to the *in vivo* situation should allow cells to behave as they would *in vivo*. GECs, PODs and MCs co-cultured in a collagen matrix and used to model human glomerulosclerosis with the treatment of TGF-β. Fibrosis replicated in the 3D tri-culture model with specific characterised read-outs.

This *in vitro* model of human glomerulosclerosis could be used to understand disease pathogenesis. By testing known mediators of glomerulosclerosis, such as TGF-β, the contributions of these mediators can be assessed. Additionally, the cross-talk between glomerular cell types and the importance of such interaction in the development of fibrosis can be determined.

Such investigations could identify targets for the prevention and reversal of fibrosis. These were targeted in the model. In this collaborative Thesis project between the University of Cambridge and MedImmune, an anti-αvβ8 antibody, a CVRM therapeutic developed by MedImmune, was utilised to assess its effectiveness and demonstrate the potential role of the model in drug development.

Alongside this glomerular cell work, renal tissue work was performed with the objectives of investigating a potential source of glomerular cells for the model system, as well as creating HOC where glomerulosclerosis could be studied and compared with the 3D tri-culture model.

Chapter 3 – Methods

Cell Culture

2D Cell Culture

Human foetal glomerular endothelial cells (fGECs) were cultured in Endothelial Cell Medium (ECM); a 500ml basal medium containing 25ml foetal bovine serum (FBS), 5ml endothelial cell growth supplement (ECGS) and 5ml penicillin/streptomycin solution (P/S). Human foetal mesangial cells (fMCs) were cultured in Mesangial Cell Medium (MCM); a 500ml basal medium containing 10ml FBS, 5ml mesangial cell growth supplement (MsCGS) and 5ml P/S (human fGECs, human fMCs along with their respective media and supplements were from ScienCell Research Laboratories, CA, USA). There were two sources of foetal human podocytes (fPODs). Celprogen human fPODs were cultured in human POD cell culture complete media with serum (Celprogen, CA, USA). Lonza human fPODs (Lonza, Switzerland) were cultured in 500ml of RPMI 1640 R8758 (Sigma, MO, USA) containing 50ml FBS F7524 (Sigma, MO, USA), 5ml of insulin, Apo-transferrin and sodium selenite (ITS) in ITS mix (100x; Gibco™ by Thermo Fisher, UK) and 5ml P/S (Sigma, MO, USA). Media composition for Lonza fPODs came from the literature.[184, 185, 200] All cells were grown on tissue culture (TC) treated plasticware (Corning Incorporated, NY, USA). Cells were maintained in a 37°C incubator (95% air, 5% CO_2) and used in experiments between passage 0 and passage 6 (p0-p6).

3D Cell Culture

Either in tri-culture or mono-culture human fPODs, fGECs and fMCs were suspended within rat tail type I collagen (1.5mg/ml; Corning Incorporated, NY, USA), human plasma fibronectin (90µg/ml; Merck Millipore, MA, USA), 1.5mg/ml $NaHCO_3$, 25Mm HEPES and M199 medium (10x; Sigma, MO, USA) at 4°C. Gel was pH adjusted with 0.1M HCl (Fisher Scientific, UK) to pH 7.4. The cell/gel suspension was pipetted into plasticware of choice, either 48 well plates (Corning Incorporated, NY, USA) or tissue culture µ-Slide Angiogenesis slides (ibidi®, Germany) in a volume of 320µl or 10µl per well, respectively. Mono-cultures of fGECs, fMCs, aMCs and fPODs had $0.5x10^6$ cells per well. For tri-culture, renal glomerular cells were used at a ratio of 16:3:1 (fGECs: fPODs: fMCs), 320,000-384,000 fGECs, 60,000-72,000 fPODs and 20,000-24,000 fMCs per 320µl. Cell/gel suspension was polymerised at 37°C for 20 minutes, after which 500µl (48 well plates) or 40µl (µ-Slide Angiogenesis) of media was pipetted on top of the gel. Tri-culture media was composed of 100ml RMPI 1640 (Gibco™ by Thermo Fisher, UK), 2mls FBS, 1ml penicillin/streptomycin, 1ml insulin (1mg/ml), Apo-transferrin (1mg/ml), sodium selenite (3.4 µM) (in ITS mix) and 1ml ECGS (supplements all from ScienCell Research Laboratories, CA, USA). Cultures were maintained for 24hrs in a 37°C incubator (95% air, 5% CO_2). Cells were used in experiments between p0-p6.

Glomeruli Isolation & HOC

Glomeruli Isolation

Mouse

Female BALB/c and C57BL/6J mouse kidneys were treated with collagenase (Sigma, MO, USA) for various time periods, or untreated, were placed in 60mmx150mm dishes (C60s) (Corning Incorporated, NY, USA). Kidneys were decapsulated and cut up using scissors. The kidneys were then pushed through a 100µm sieve and passed through 70µm and 40µm sieves (Falcon™, by Thermo Fisher, UK). Basal media, RMPI 1640 (Gibco™ by Sigma, MO, USA), was used for kidney filtrate sieving. The 40µm sieve was upturned and supplement media (500ml RMPI 1640, 50ml FBS, 5ml ITS and 5ml Antibiotic-Antimycotic (100x) (all Gibco™ by Thermo Fisher, UK)) was passed through to remove isolated glomeruli from sieve and into culture plasticware, which was either 6-well plates (Corning Incorporated, NY, USA), 8-well slides (Thermo Fisher, UK) or tissue culture µ-Slide Angiogenesis slides (ibidi®, Germany). Glomeruli were cultured for up to 13 days for podocyte outgrowth. Glomeruli cultures were maintained in a 37°C incubator (95% air, 5% CO_2).

Human

All experiments using human tissue were performed with the written informed consent of patients and the approval of the local Ethical Committee and Addenbrooke's Hospital Tissue Bank. Fresh kidney cortex tissue was obtained from unused cadaveric kidneys harvested for transplantation (from the Cambridge Biorepository for Translational Medicine (CBTM), University of Cambridge, Cambridge University Hospitals (CUH)) NHS Foundation Trust). Tissue was transferred to sterile petri dish on ice and covered in basal media (RMPI 1640 R8758 (Sigma, MO, USA)) and any kidney capsule was removed using disposable scalpels (Fisher Scientific, UK). Tissue was cut into small pieces, approximately 1-2mm^3, and then chopped finely using large scalpel blade (PM40, Swann-Morton, UK). Kidney tissue was then pushed through a 425µM steel sieve (Endecotts, UK) and washed using basal media. Kidney tissue filtrate was then passed through 180µM and 125µM steel sieves (Endecotts, UK), washed using culture media (500ml RPMI 1640 R8758 (Sigma, MO, USA) containing 50ml FBS F7524 (Sigma, MO, USA), 5ml of insulin, Apo-transferrin and sodium selenite (ITS) in ITS mix (100x; Gibco™ by Thermo Fisher, UK) and 5ml P/S (Sigma, MO, USA)). Isolated glomeruli were transferred from the 125µM sieve to TC treated plasticware (Corning Incorporated, NY, USA) and cultured for up to 7 days, maintained in a 37°C incubator (95% air, 5% CO_2). These glomeruli isolation procedures came from the literature along with some collaboration with the Jaakko Patrakka group of the Karolinska Institute.[184, 185] All experiments using human tissue were performed with written informed consent and with ethical, Human Research Authority and Addenbrooke's Hospital Tissue Bank approvals.

Culture Protocols

Haemocytometer and trypan blue (Sigma, MO, USA) were used for all cell and glomeruli counts. Mycoplasma testing was performed by culturing approximately 10,000 cells in antibiotic-free media for 5 days, the cell supernatant was taken and spun at 300 xg for 5 minutes to remove any debris. A 100µl sample was taken and tested using the MycoAlert™ Mycoplasma detection assay from Lonza (Lonza, Switzerland).

HOC

Patient kidney tissue (two sources; normal kidney tissue from the Human Research Tissue Bank (HTRB), Addenbrooke's Hospital & National Institute for Health Research (NIHR) Cambridge Biomedical Research Centre (BRC) and normal kidney cortex from the CBTM, University of Cambridge, NHS CUH) was collected and processed as rapidly as able to reduce any deterioration of the tissue. A "time zero" (T0) sample of tissue was taken at HOC commencement as a control for tissue characteristics before any culture or treatment of tissue. Any excess blood was removed using a sterile phosphate-buffered saline (PBS) wash (Thermo Fisher, MA, USA). Tissue was dissected into <1 mm^3 pieces using two sterilized carbon steel single-edged razor blades (T585; Agar Scientific, UK). Three tissue pieces were placed in 200µl of tissue culture medium in a sterile 96-well plate (Corning Incorporated, NY, USA), containing; 500ml M199 M7528 (Sigma, MO, USA), 50ml heat-inactivated foetal calf serum (FCS), 5ml L-glutamine and 5ml P/S (FCS, L-glutamine and P/S from Thermo Fisher, MA, USA). HOC were maintained in a 37°C incubator (95% air, 5% CO_2) for either 6hrs or 24hrs. This HOC methodology came from an established protocol in the Bradley laboratory.[105]

Stimulation Assays

For stimulations; 10 ng/ml TGF-β, 25ng/ml CTGF (Life Technologies Ltd (Thermo Fisher, MA, USA), 10ng/ml FGF, 30ng/ml HGF,10ng/ml IL-1α, 10ng/ml IL-1β, 10ng/ml PDGF-BB, 25ng/ml EGF, 75µg/ml 1D11 (anti-TGF-β antibody), 80ng/ml LTGF-β, 15µg/ml αvβ8 (anti-αvβ8 integrin antibody; MedImmune, UK), 15µg/ml NIP228 (isotype control antibody; MedImmune, UK), 10 ng/ml TNFα, 100 ng/ml BMP7, 2µM/3.5µg/ml ALK5i (compound 616456; TGF-β RI Kinase Inhibitor V (Merck Millipore, MA, USA)) and 8mg/ml CTGF neutralising antibody (CTGF nAb (ab109606, Abcam, Cambridge, UK) alone or in combination, were added to media either in HOC, media placed on top of 3D culture gels or media of 2D cell cultures in C60s (Corning Incorporated, NY, USA) ; before either 6hr or 24hr incubation. TGF-β, FGF, IL-1α, IL-1β, 1D11, LTGF-β, TNF-α and BMP7 from R&D Systems (Bio-Techne Ltd, MN, USA). CTGF, HGF, PDGF-BB and EGF from Life Technologies Ltd (Thermo Fisher, MA, USA). Control treatment was media alone. Replicate samples for treatments and time points were

used for reproducibility. For 2D cell cultures treatments were run in duplicate, for 3D cultures treatments were run in duplicate at a minimum and in HOC treatments were run in triplicate at a minimum.

RNA Extraction

2D

RNA was extracted from glomerular renal cells grown on tissue-culture treated C60s (Corning Incorporated, NY, USA) using RLT lysis buffer (Qiagen, Germany) and β-mercaptoethanol (Sigma, MO, USA), (10µl β-mercaptoethanol per 1ml RLT; 600µl used per culture dish). Cells were scraped and then sample added to spin column of UltraClean® Tissue and Cells RNA Isolation Kit (MO BIO, CA, USA) and manufacturer's protocol followed, incorporating DNase digest step (On-Spin Column DNase I Kit; MO BIO, CA, USA). RNA was quantified by a NanoDrop 1000 Spectrophotometer (Thermo Fisher, MA, USA) before reverse transcription with a High Capacity cDNA Reverse Transcription kit (Thermo Fisher, MA, USA) following the manufacturer's protocol. Stored at -80°C.

3D

RNA was extracted from 3D culture gels by two methods. First, TRIzol® (Invitrogen, CA, USA) extraction, 1ml of TRIzol® reagent was used per 320µl culture gel. After vortexing, 15-minute incubation at room temperature gels and further vortexing, culture gels had dissolved. Chloroform (VWR International, PA, USA), 200µl per 1ml TRIzol®, was added and shaken for approximately 15 seconds. Then, incubated for 2 minutes at room temperature followed by centrifugation for 15 minutes at 12000 xg at 4°C. The RNA containing clear aqueous phase was taken off and half of this volume of 100% Ethanol (Sigma, MO, USA) added. Sample was then added to a spin column of UltraClean® Tissue and Cells RNA Isolation Kit (MO BIO, CA, USA) and manufacturer's protocol followed, incorporating DNase digest step (On-Spin Column DNase I Kit; MO BIO, CA, USA). The second method of RNA extraction from 3D cultures was using RNeasy Fibrous Tissue Mini Kit (Qiagen, Germany), where the kit protocol was followed. Extracted RNA was quantified by a NanoDrop 1000 Spectrophotometer (Thermo Fisher, MA, USA) and assessed for quality by a 2100 Bioanalyzer with an Agilent RNA 6000 Nano Kit (Agilent, CA, USA) before reverse transcription with a High Capacity cDNA Reverse Transcription kit (Thermo Fisher, MA, USA) following the manufacturer's protocol. Stored at -80°C.

Glomeruli

Glomeruli were immersed in RLT lysis buffer (Qiagen, Germany) for RNA extraction and stored at -20˚C until processed using RNeasy Plus Mini Kit (Qiagen, Germany) following the manufacturer's protocol. Extracted RNA was quantified by a NanoDrop 1000 Spectrophotometer (Thermo Fisher, MA, USA) and assessed for quality by a 2100 Bioanalyzer with an Agilent RNA 6000 Nano Kit (Agilent, CA, USA) before reverse transcription with a High Capacity cDNA Reverse Transcription kit (Thermo Fisher, MA, USA) following the manufacturer's protocol. Stored at -80ºC.

HOC

RNA was extracted from HOCs by first immersing tissue in RNA*later*™ (Thermo Fisher, MA, USA), and storage at +4˚C overnight, before RNA extraction or long term storage at -80˚C until processing. RNA extraction started by blotting excess RNA*later*™ (Thermo Fisher, MA, USA) from tissue and finely dicing tissue on ice using a razor blade (T585; Agar Scientific, UK), before placing diced tissue in lysis buffer from RNeasy Fibrous Tissue Mini Kit (Qiagen, Germany). Tissue was homogenised using a TissueRuptor (Qiagen, Germany), at this point, the sample was processed using the RNeasy Fibrous Tissue Mini Kit (Qiagen, Germany) following the manufacturer's protocol. Extracted RNA was quantified by a NanoDrop 1000 Spectrophotometer (Thermo Fisher, MA, USA) and assessed for quality by a 2100 Bioanalyzer with an Agilent RNA 6000 Nano Kit (Agilent, CA, USA) before reverse transcription with a High Capacity cDNA Reverse Transcription kit (Thermo Fisher, MA, USA) following the manufacturer's protocol and storage at - 80ºC.

Protein Extraction

Protein was extracted from glomerular renal cells grown on tissue-culture treated C60s (Corning Incorporated, NY, USA) using RIPA buffer (Thermo Fisher, MA, USA) and protease inhibitor cocktail tablets (Roche, UK) (7ml RIPA buffer per 1 tablet; 450µl per culture dish). Cells were scraped and sample vortexed for 30 seconds, returned to ice for 2-3 minutes and then vortexed again; this was repeated for 15 minutes. Samples then centrifuged at 1200 RPM for 2 minutes. Protein concentration was quantified by bicinchoninic acid assay (BCA assay) (Thermo Fisher, MA, USA), using a BioRad Model 680 microplate reader (BioRad, CA, USA) and protein stored at -20ºC.

RT-qPCR

RT-qPCR reactions were prepared using cDNA diluted 1:10 with RNase free water (Sigma, MO, USA); 4.5µl was added per well to a MicroAmp® Optical 96-Well Reaction Plate (Thermo Fisher, MA, USA). Master Mix was composed of SYBR® Green JumpStart™ Taq ReadyMix™ (Sigma, MO, USA), ROX

Reference Dye (Thermo Fisher, MA, USA), Quantitect Primers (Qiagen, Germany) and RNase free water (Sigma, MO, USA), to make a total of 10.5µl per well. Therefore, the total reaction volume was 15µl. Reaction plate was covered with MicroAmp® Optical Adhesive Film (Thermo Fisher, MA, USA) and amplified on StepOnePlus™ Instrument (Thermo Fisher, MA, USA), using the comparative CT (ΔΔCT) method for analysis. Quantitect primers used were: COL1A1, COL3A1, COL4A1, COL6A1, ACTA2, FN1, LAMB2, SMAD2, SMAD3, CTGF, SERPINE1, TGM2, CCL2, TGFB1, ITGAV, ITGB8, CDH1, CLDN1, CTNNB1, CXCL8, BMP7, NPHS2 and housekeeping gene (HK gene) GAPDH. Data was conveyed as the fold-change relative to the control.

Western Blot

Extracted and quantified protein samples were added to 4 x Laemmli sample buffer at between 20µg and 40µg. Samples were run by sodium dodecyl sulfate polyacrylamide gel electrophoresis (SDS-PAGE) electrophoresis, using a BioRad Mini-PROTEAN® Tetra Cell system with a BioRad Model 200/2.0 Power Supply (both BioRad, CA, USA). Gels were transferred to a 0.2µm nitrocellulose membrane (BioRad, CA, USA) using a Trans-Blot SD Semi-Dry Transfer Cell (BioRad, CA, USA). Membranes were blocked using either 5% non-fat dry milk powder or bovine serum albumin (BSA) (both Sigma, MO, USA), dependent on antibody, in 1 x Tris-buffered saline (TBS)-Tween 20 (0.1%) for 1hr at room temperature. Once blocked membranes were incubated with primary antibodies overnight at 4ºC and incubated with either a goat anti-rabbit or a goat anti-mouse horseradish peroxidase (HRP) conjugated secondary antibody (Dako, Denmark) for 1hr at room temperature. Protein bands were detected using chemiluminescence by SuperSignal West Dura and SuperSignal West Pico (both Thermo Fisher, MA, USA). X-ray film RX NIF sheets (Fujifilm, Japan) was developed using a Konica Medical Film Processor SRX-101A (Konica Minolta, Japan). Primary antibodies used were rabbit anti-pSMAD2, rabbit anti-pSMAD1/5, rabbit anti-pSMAD3, rabbit anti-tSMAD3, rabbit anti-collagen I/III and rabbit anti-β-Actin (pSMAD2, tSMAD2 and tSMAD3 (Cell Signalling Technology, MA, USA); pSMAD3 (Abcam, UK) and β-Actin (Sigma, MO, USA)). Membranes stored at -20ºC.

Western blots were analysed by densitometry using Image J software (U. S. National Institutes of Health, MD, USA) to quantify changes in protein expression normalised to β-Actin.

Imaging

Immunofluorescence (IF)

2D

Human glomerular cells were grown in mono-culture in either C60s (Corning Incorporated, NY, USA), 96 Well Clear Flat Bottom Polystyrene TC-Treated Microplates (Corning Incorporated, NY, USA) or tissue culture µ-Slide Angiogenesis slides (ibidi®, Germany). After 24hrs incubation, culture media was removed, and cells were fixed with Methanol (Thermo Fisher, MA, USA) chilled to -20ºC for 5 minutes at -20˚C. Following this, cells were permeabilized using Dulbecco's Phosphate-Buffered Saline $(DPBS)^{++}$ with 0.1% Tween 20 (both reagents from Thermo Fisher, MA, USA), and blocked for 1hr with 1% BSA (Sigma, MO, USA) in DPBS++ with 0.1% Tween 20. Incubation with primary antibody was overnight at 4ºC in a humidified environment, followed by incubation with NorthernLights™ fluorescent secondary antibodies (either donkey anti-mouse or donkey anti-rabbit labelled with either fluorochrome 557, 498 or 493; (R&D Systems (Bio-Techne Ltd, MN, USA)), or Alexa Fluor® 488 chicken anti-rabbit (Thermo Fisher, MA, USA) for 1hr at room temperature, protected from light. VECTASHIELD® Hard▪Set™ Mounting Medium (Vector Laboratories, UK) was added before cells were imaged on a Leica TCS SP5 confocal microscope (NIHR Cambridge BRC Cell Phenotyping Hub (Leica Microsystems, Germany)). Primary antibodies used were mouse anti-collagen IV, mouse anti-α tubulin, rabbit anti-avβ8 (Calico CAL16 (Calico Biolabs Inc., CA, USA)); POD markers: rabbit anti-WT1, rabbit anti-podocin, rabbit anti-Ezrin, rabbit anti-Synaptopodin, rabbit anti-CD2AP, rabbit anti-Nephrin, rabbit anti-GLEPP-1, rabbit anti-podocalaxyin; MC markers: rabbit anti-Thy1, rabbit anti-NG2, rabbit anti-α-SMA, rabbit anti-fibronectin and rabbit anti-PDGFR-β; GEC markers: mouse anti-CD31 and rabbit anti-vWF (Cell Signalling Technology, MA, USA or Abcam, UK). Controls run included no primary antibody, no secondary antibody, no primary or secondary antibody and isotype controls. Treated cells were stored at 4ºC in the dark.

3D

3D cultures in tissue culture µ-Slide Angiogenesis slides (ibidi®, Germany) for 24hrs were stained for antibodies using the same method as described above or human glomerular cells were fluorescently labelled before suspension in gel mix. PODs were labelled with PKH26 dye (Sigma, MO, USA), following the manufacturer's protocol. MCs were labelled with a Celltracker™ Blue CMAC dye (Thermo Fisher, MA, USA, following the manufacturer's protocol. GECs were either transfected with green fluorescent protein (GFP) using a lentiviral vector containing the human polypeptide chain elongation factor-1 (EF-1) promoter by using 10µl virus in 4000µl media per approximately 300,000 GECs. Cells were counted and plated into 6-well TC treated plates (Corning Incorporated, NY, USA), left in culture 24hrs and then culture medium was replaced, and cells were treated with lentivirus for 48hrs. Or, GECs were

whole mount stained using fluorescein-labelled *Ulex europaeus* agglutinin I (ULEX) (Vector Laboratories, UK). ULEX staining was performed by fixing the 3D mono-culture GEC or tri-culture gel after 24hrs incubation using 4% paraformaldehyde (PFA) for either an hour for 320µl gels or 20 minutes for 40µl gels. Gels were then incubated overnight at 4°C in the dark with ULEX in a 1:250 dilution (8µg/ml) with $DPBS^{++}$ (Thermo Fisher, MA, USA). 3D cultures were either followed in real time or after fixation (ULEX staining) by confocal microscopy, Leica TCS SP5 confocal microscope (NIHR Cambridge BRC Cell Phenotyping Hub (Leica Microsystems, Germany)).

Glomeruli

Mouse and human glomeruli IF staining followed the same protocol as outlined for 2D cultures. Human glomeruli required cytospin centrifugation (Shandon Cytospin 2; Shandon Scientific Company Limited, UK)) prior to staining as they would not attach to TC treated plasticware. Human glomeruli were spun down at 1000 RPM for 5 minutes, re-suspended in an appropriate volume of culture media to allow for 200µl per sample deposition. The cytospin was run at 800 RPM for 5 minutes, after which glass slides (Thermo Scientific™ Shandon™ Polysine Slides; Thermo Fisher, MA, USA) were air-dried for 5 minutes before submersion in Methanol (Thermo Fisher, MA, USA) chilled to -20°C for 5 minutes at -20˚C for fixation.

Immunohistochemistry (IHC)

Human Kidney

For IHC, normal human kidney sections were immersed in a fixative of 4% PFA in 0.1M PIPES at pH 7.4 overnight at 4˚C. Sections were stained for αvβ8. 4% paraffin-wax embedded sections were dewaxed in xylene (X/0250/17; Thermo Fisher, MA, USA) for 15 minutes at room temperature and dehydrated in descending series of ethanol solution (VWR International, PA, USA) 100, 90, 70% for 5 minutes in each at room temperature. They were then thoroughly rinsed in running tap water, rinsed in MilliQ water and subjected to high pressure antigen retrieval using a pressure cooker and 0.1M sodium citrate buffer pH 6.0 for 2 minutes. The slides were then left under running tap water to cool for 20 minutes. Then, endogenous peroxidase activity was quenched using 0.6% H_2O_2 solution (23615.261; VWR International, PA, USA) in absolute methanol for 30 minutes at room temperature. Sections were washed thoroughly under running tap water for 10 minutes, then rinsed in PBST (PBS containing 0.01% Tween-20) 2 x 3 minutes in a coplin jar on a shaker. Sections were circled with a hydrophobic Mini PAP Pen (008877; Invitrogen, CA, USA) to retain solution. Blocking of non-specific antibody binding was performed by incubating slides in blocking buffer (containing 10% FCS in 0.001% PBST) for 30 minutes at room temperature in a humidified chamber. Excess blocking buffer was removed and immediately

sections were incubated with primary antibody, rabbit anti-human αvβ8 integrin (ab237705; Abcam, UK) at 1:100 dilution, at 4°C overnight. After thorough rinsing in PBST, sections were further incubated with anti-rabbit-IgG HRP linked secondary antibody (7074S; Cell Signalling Technology, MA, USA) 1:100 at room temperature for 1hr. Antibody binding sites were visualised microscopically using a vortexed mixture of SIGMAFAST DAB (3'3 diaminobenzidine,) and $UREAH_20_2$ (by dissolving 1 tablet of each in 1 ml PBS) (D4168; Sigma, MO, USA). DAB incubation varied from 2-10 minutes. Slides were then washed thoroughly in running tap water and counterstained with Harris's modified hematoxylin haematoxylin solution (HH532; Sigma, MO, USA) for approximately 90 seconds and thoroughly washed in running tap water "*blueing*". Slides were then dehydrated in an ascending series of ethanol (70, 90 and 100%), then cleared in xylene for 5 minutes. They were then coverslipped in DPX solution (06522; Sigma, MO, USA). Images were taken using Leitz Laborlux 12 microscopy with Infinity 2 camera.

Scanning Electron Microscopy (SEM) & Transmission Electron Microscopy (TEM)

SEM of 2D human glomerular cells was performed by rinsing cells cultured in T25 tissue-culture flasks with normal saline (0.9% NaCl) solution twice after culture flask had equilibrated to room temperature. Approximately 4ml of fixative consisting of 2% glutaraldehyde and 2% formaldehyde in 0.05M sodium cacodylate buffer at pH 7.4 was added per T25 tissue-culture flask and incubated for 4hrs at 4°C. Glomerular cells were then scraped in the fixative and aspirated into tubes, after which cells were rinsed by centrifugation at 15000 RPM with 0.1M cacodylate buffer up to 5 times until a packed pellet was formed. Excess buffer was removed immediately after centrifugation to prevent re-suspension of cells. Cell pellets were kept at 4°C for a maximum of 2 days until transferred to the Cambridge Advanced Imaging Centre (CAIC) for SEM. TEM of 3D human glomerular cells was performed by washing 3D culture gels with normal saline, then gels were placed in the fixative described above for 4hrs at 4°C and again washed with normal saline. Samples were transferred to the CAIC for TEM.

Image Quantification

3D tri-culture gels and 3D MC culture gels nodule formation was quantified by taking six random fields of view per gel under phase contrast microscope and manually counting the number of nodules. HALO analysis software (Indica Labs, NM, USA) at MedImmune was also trialled for quantification of collagen IV deposition in 3D tri-cultures, where software measured the amount of collagen IV positive staining relative to nuclei staining, as well as the intensity of collagen IV staining.

Statistical Analysis

Differences between treatments on gene expression, protein expression and nodule number were analysed using either an unpaired two-tailed t-test or an Ordinary one-way ANOVA with Tukey's multiple comparison post-tests to test pairwise differences, using GraphPad Prism Version 6.05 for Windows (GraphPad Software, CA, USA).

Chapter 4 – Results: Characterisation of Glomerular Cell Types

Celprogen Podocyte Characterisation

Characterisation of fPODs (Celprogen, CA, USA) was performed to check morphology and expression of phenotypic markers, and then to understand responses of fPODs to cytokines in both 2D and 3D culture before incorporating fPODs with the other glomerular renal cell types. fMCs and fGECs used in this work had been previously studied in both 2D and 3D, in both mono- and co-culture.[193, 194, 201]

Characterisation by Imaging

2D Cultures

IF staining of 2D Celprogen fPOD cultures was performed for POD phenotypic markers (Figure 1). Markers used for this were; ezrin, Wilms' tumour protein (WT-1), synaptopodin, podocin and nephrin. The staining shows (Figure 1) that the Celprogen fPODs used did express all the phenotypic markers of mature PODs described above when cultured in 2D. Ezrin staining (Figure 1 B) formed a ring-like pattern around Celprogen fPOD nuclei. Staining for WT-1 (Figure 1 C) was nuclear; while staining of synaptopodin, podocin and nephrin was cytoplasmic (Figure 1 D-F). Some extracellular membrane staining for nephrin could be seen (Figure 1 F). Staining for tubulin (Figure 1 A) was also performed to assess Celprogen fPOD cell morphology.

IF staining of 2D Celprogen fPOD and 2D fMC cell cultures was performed in parallel for phenotypic POD and MC markers to determine their specificity (Figure 2). These markers were ezrin and podocin for PODs. For MCs markers used were Thy1 and NG2. fPODs expressed ezrin (Figure 2 E) and podocin (Figure 2 C) in the same pattern as seen in Figure 1. fMCs showed negligible IF compared to Celprogen fPODs. Staining for the MC markers showed no expression of Thy1 in Celprogen fPODs, whereas nuclear expression of Thy1 was seen in fMCs in 2D (Figure 2 G and H). MC marker NG2 expression in the fMCs was mainly cytoplasmic and weak, Celprogen fPODs had weaker expression with more nuclear in localisation (Figure 2 I and J). IF staining of the fMCs was weak for MC markers but still present. Tubulin staining of Celprogen fPODs and fMCs (Figure 2 A and B) showed the morphological differences between cell types, Celprogen fPODs had distinct processes and fMCs more spread-out tubulin filaments.

SEM (Figure 3) and TEM imaging (Figure 4) of 2D Celprogen fPOD cells were performed for morphological characterisation of this cell type, where foot-like processes (Figure 3 D and Figure 4) and slit-diaphragm like structures (Figure 4 D) were visible.

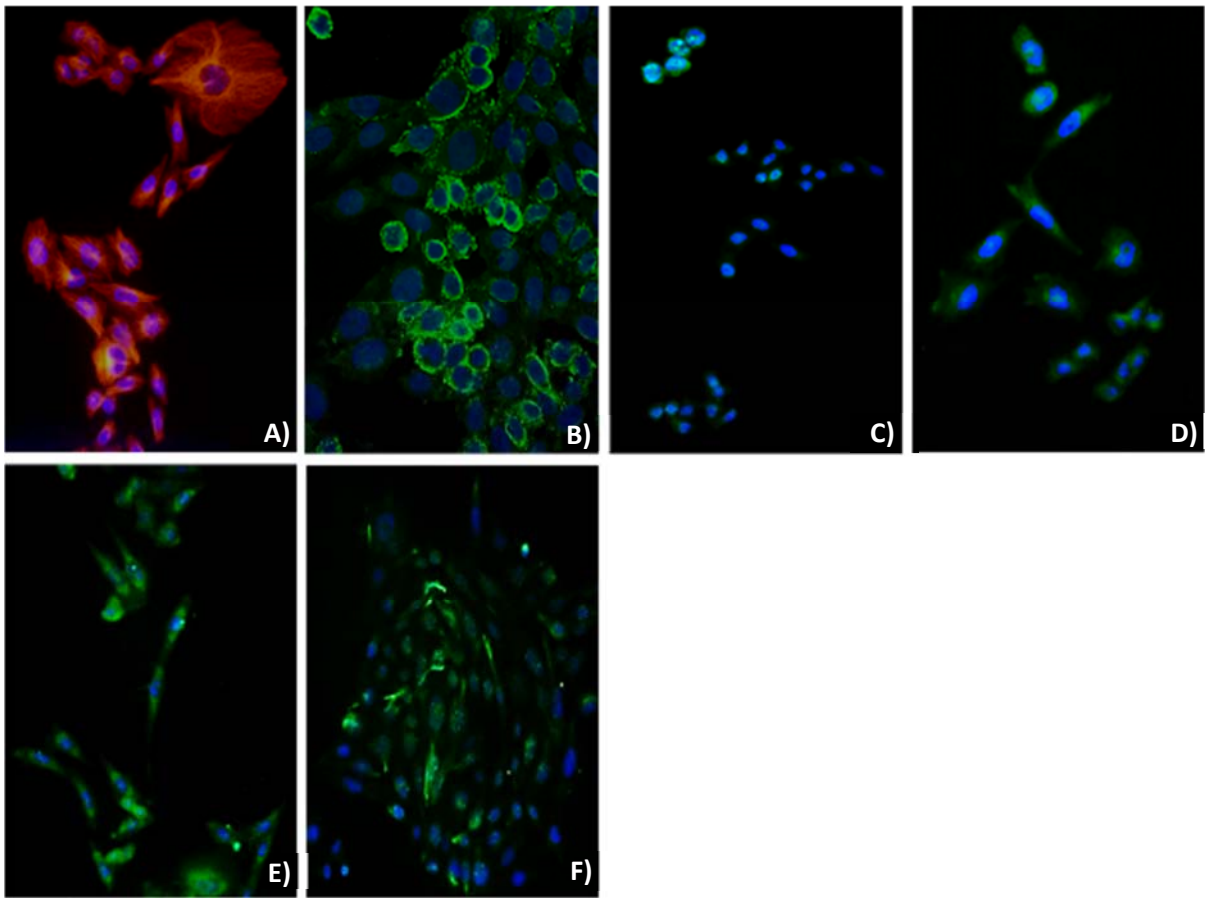

Figure 1. IF staining of 2D Celprogen fPODs.

Staining for (A) tubulin (red) and phenotypic markers (green); (B) ezrin, (C) WT-1, (D) synaptopodin, (E) podocin and (F) nephrin. Nuclei counterstained with DAPI (blue). 20X magnification.

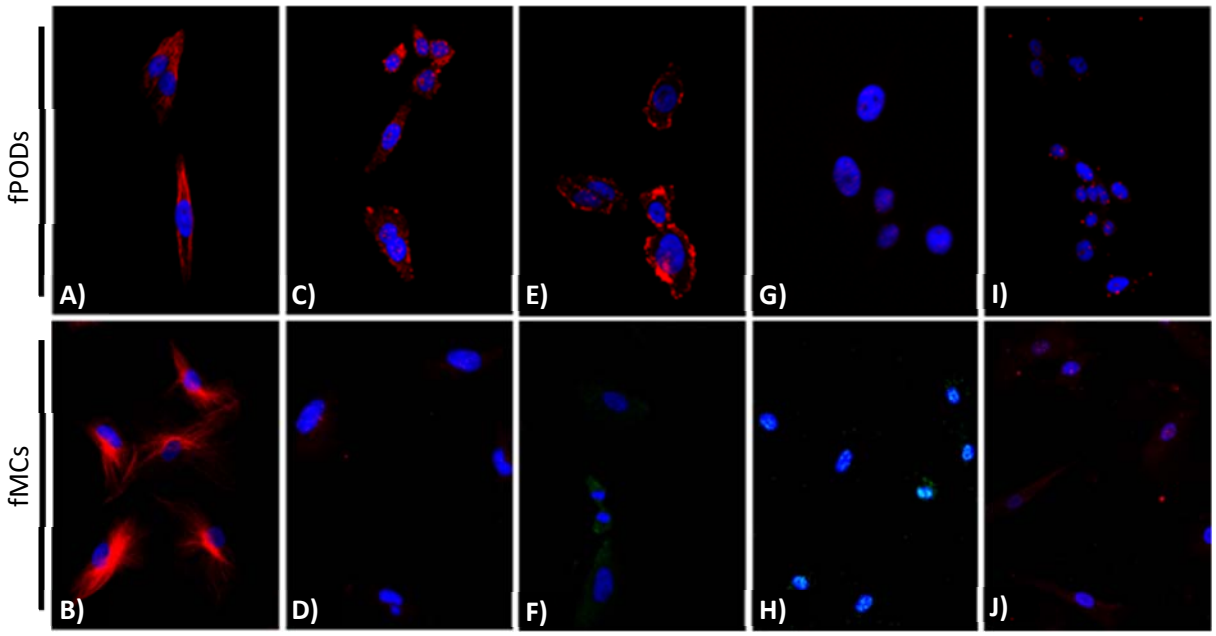

Figure 2. IF staining of 2D Celprogen fPODs and fMCs.

Staining (red) of 2D cultures of Celprogen fPODs (A, C, E, G and I) and fMCs (B, D, F, H and J) for tubulin (A and B), podocin (C and D), ezrin (E and F), Thy1 (G, H), and NG2 (I and J). Nuclei counterstained with DAPI (blue). 20X magnification.

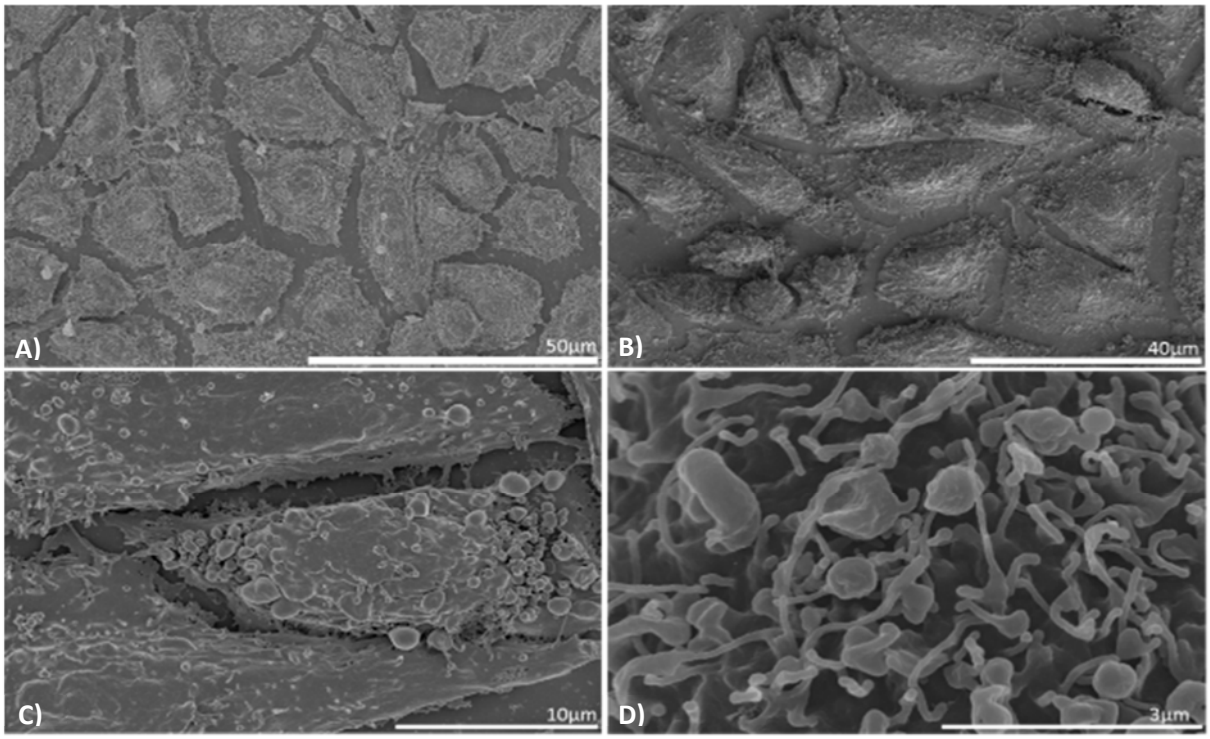

Figure 3. SEM images of 2D Celprogen fPODs.

(A, B) overview of 2D fPOD cultures, showing a raised central body with some arborisation and interaction with neighbouring cells. (C) a higher magnification SEM image with enhanced detail of interactions between cells and their morphology. (D) SEM image with higher magnification showing the fine detail of foot-like processes of 2D fPODs.

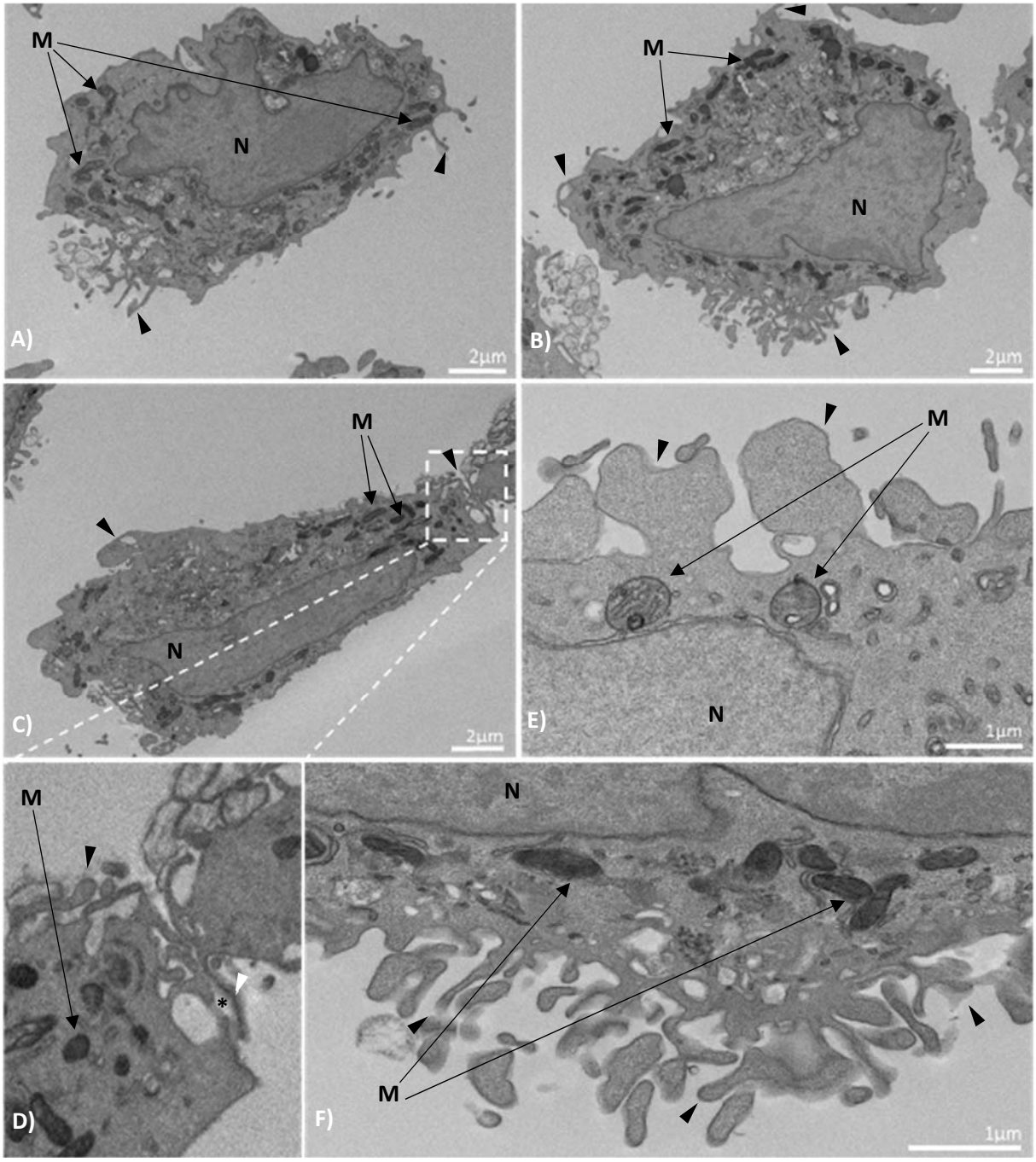

Figure 4. TEM images of 2D Celprogen fPODs.

(A-C) low power images show overall morphology of cells with nuclei (N), mitochondria (M) and foot like processes (black arrows). (D) 150X magnification of section in image (C) where a junction 20 40nm wide between processes of two 2D fPOD cells (asterisk) can be seen with electron dense material (white arrow) characteristic of a slit diaphragm. (E - F) higher power images of foot-like processes (black arrows) of 2D fPODs, with nuclei (N) and mitochondria (M) labelled.

3D Cultures

IF staining of 3D cultures was performed on Celprogen fPODs as well as fMCs and fGECs where POD markers ezrin, podocin, synaptopodin and nephrin were stained to assess expression of these phenotypic markers in 3D cultures (Figure 5). α-SMA, a MC phenotypic marker, was also stained for. Positive staining for ezrin (Figure 5 A) in Celprogen fPODs grown in 3D displayed the same pattern as that in 2D (Figure 1 B), with positive staining in a ring around the fPOD nuclei. Ezrin staining was negative in both fMCs and fGECs (Figure 5 B and C). Podocin staining could be seen in all the glomerular cell types cultured in 3D, with Celprogen fPODs pattern of staining being a ring around the cell nuclei (Figure 5 D), which differed from 2D Celprogen fPOD culture staining (Figure 1 E). Both fMCs and fGECs had positive cytoplasmic podocin staining (Figure 5 E and F). Staining for synaptopodin was weakly positive in Celprogen fPOD cytoplasm, with points of stronger staining along fPOD cell membranes (Figure 5 G). However, there were also spots of background staining. This pattern of staining differed from 2D Celprogen fPOD culture staining (Figure 1 D). Weak staining for synaptopodin could be seen in fMCs (Figure 5 H), through the cell cytoplasm, while fGECs showed no staining (Figure 5 I). Weak patchy staining for nephrin could be seen in all the glomerular cell types, suggesting this was background more than positive staining. Nephrin staining of Celprogen fPODs in 2D (Figure 1 F) was stronger with a pattern of membrane staining. Positive α-SMA staining was seen in fMCs (Figure 5 N), with no staining seen in either Celprogen fPODs or fGECs (Figure 5 M and O).

SEM of 3D Celprogen fPOD cultures (Figure 6) was performed for morphological characterisation of the glomerular cell type in 3D culture matrix. Foot-like processes and the interaction of these processes between multiple fPOD cells was seen.

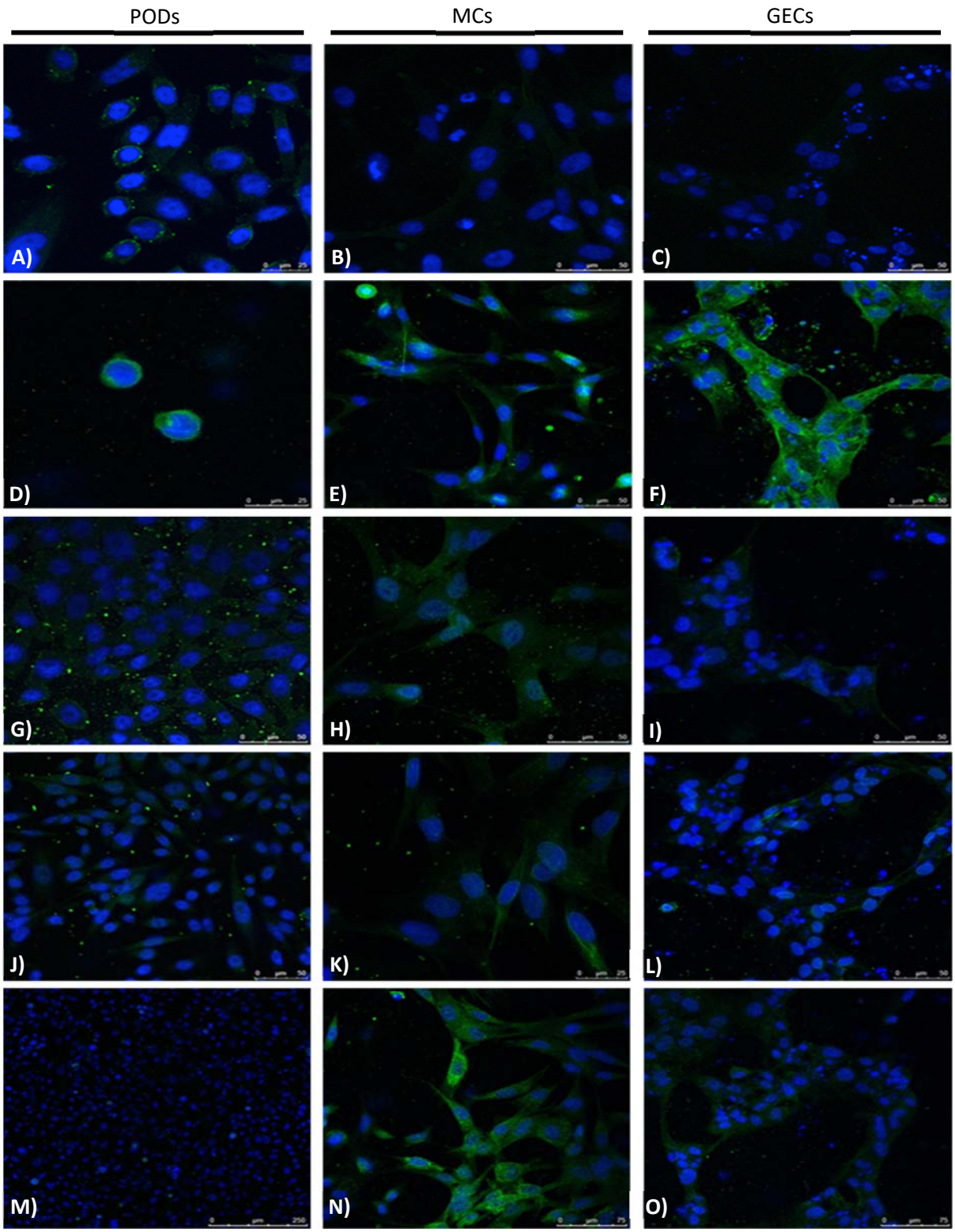

Figure 5. IF staining of 3D Celprogen fPODs, fMCs and fGECs.

Staining (green) of 3D Celprogen fPODs (A, D, G, J and M), fMCs (B, E, H, K and N) and fGECs (C, F, I, L and O). Phenotypic markers stained for were ezrin (A, B and C), podocin (D, E and F), synaptopodin (G, H and I), nephrin (J, K and L) and α-SMA (M, N and O). Nuclei counterstained with DAPI (blue). 20X magnification.

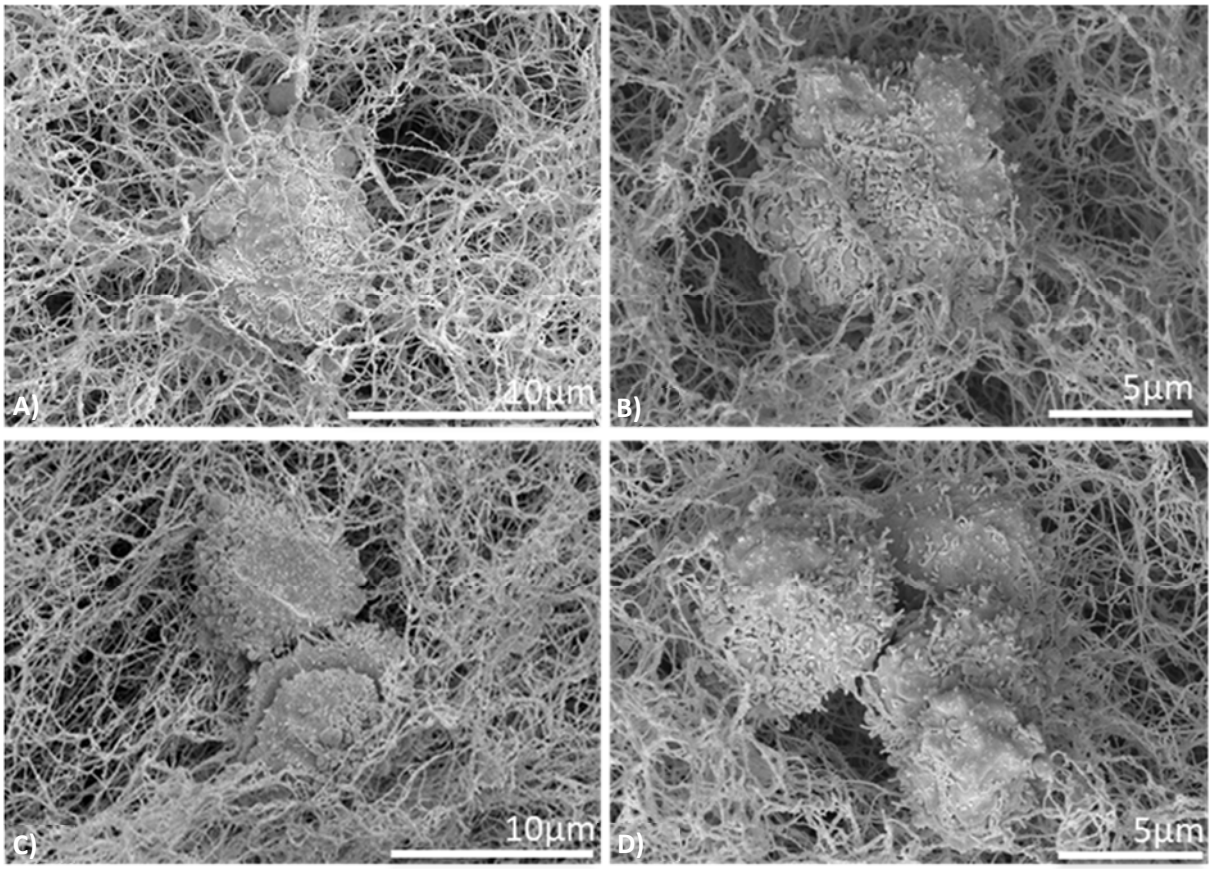

Figure 6. SEM images of 3D Celprogen fPODs.

(A and B) overview of single 3D fPODs within gel matrix, showing cell morphology with foot-like processes on the cell surface. (C and D) SEM images showing interactions between fPODs and their morphology within the 3D matrix.

Characterisation by RT-qPCR

2D Cultures

Celprogen fPODs were cultured in 2D and treated with either TGF-β or BMP7 alone or in combination for either 6hrs or 24hrs. The effect of TGF-β upon these cells and any antagonism evoked by BMP7 was examined. Gene expression of CTGF and SMAD3 was assessed. Average CT values were generally good, suggestive of a good degree of expression in these samples. With the 6hr timepoint (Figure 7) CTGF expression was significantly increased with both TGF-β treatment alone and in combination with BMP7. BMP7 alone did not change CTGF expression compared to control values. SMAD3 expression was not significantly altered by any of the treatments. At the 24hr timepoint (Figure 8) CTGF expression appears to have followed the pattern seen with the 6hr timepoint (Figure 7), however, the average fold-change in CTGF expression after these treatments was higher with the 24hr timepoint. SMAD3 expression was not significantly altered by any of the treatments compared to control.

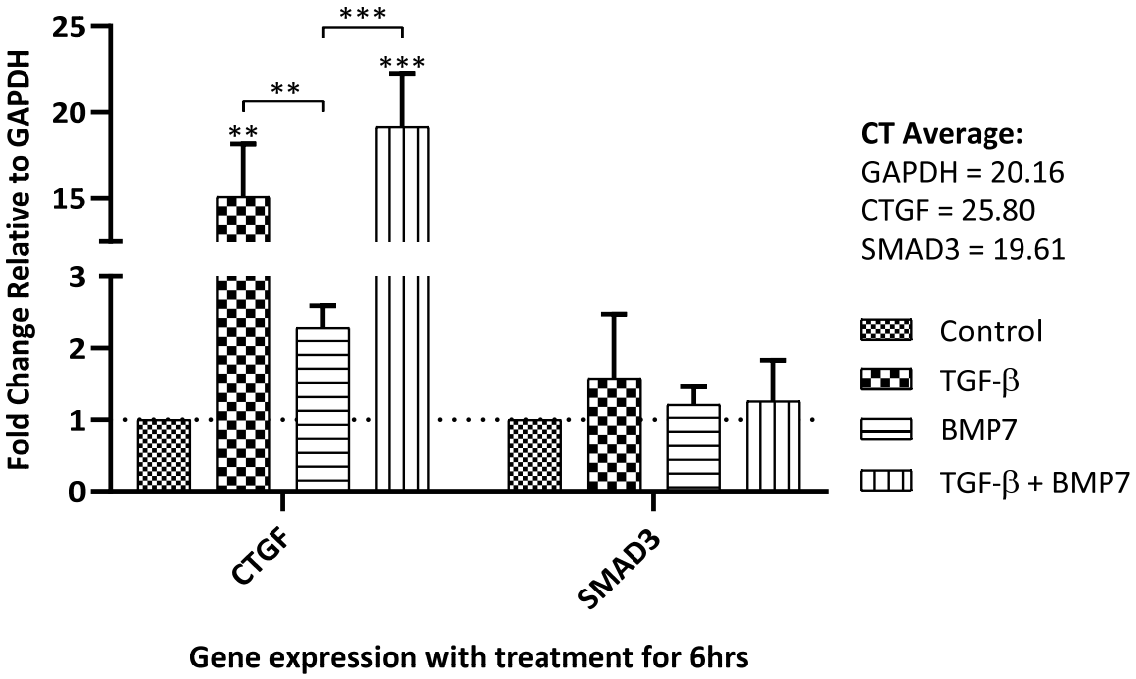

Figure 7. RT-qPCR of 2D fPOD Celprogen samples, 6hr treatment.

ΔΔCT analysis to study the relative fold change of the gene of interest against housekeeping gene GAPDH, with either TGF-β and/or BMP7 treatment for 6hrs. N=4 (CTGF) and N=2 (SMAD3). SEM error bars, One-way ANOVA; CTGF p-value 0.0001 (***); SMAD3 p-value 0.8974 (ns); followed by Tukey's multiple comparison post-tests. CT averages of each gene for reference.

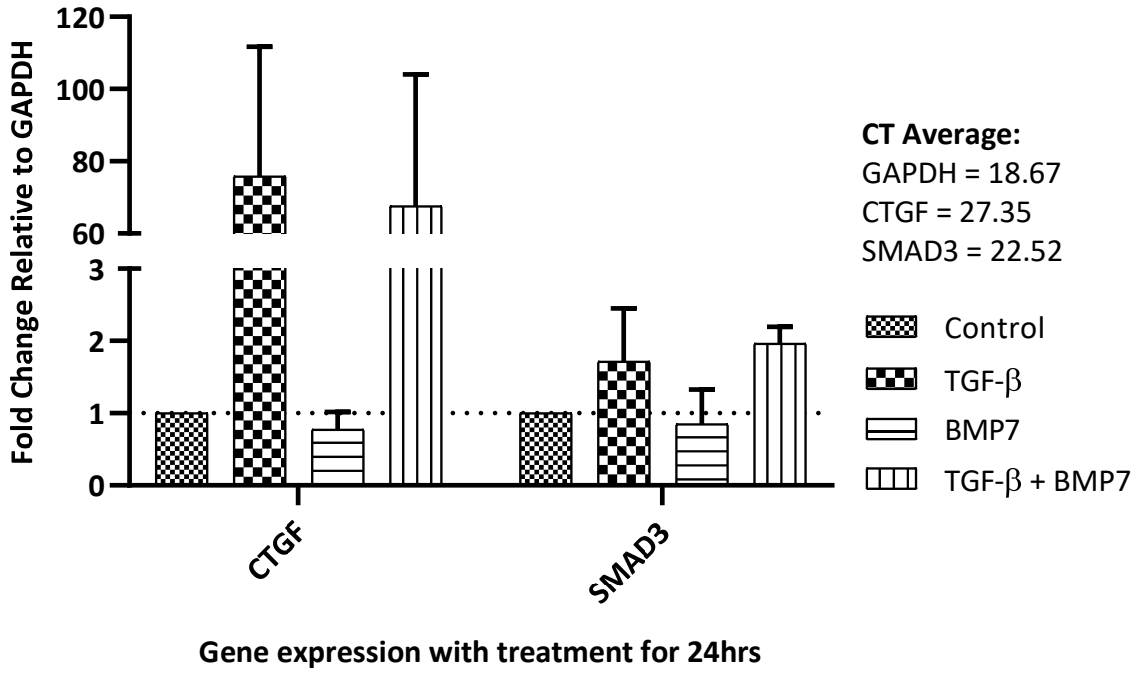

Figure 8. RT-qPCR of 2D fPOD Celprogen samples, 24hr treatment.

ΔΔCT analysis to study the relative fold change of the gene of interest against housekeeping gene GAPDH, with either TGF-β and/or BMP7 treatment for 24hrs. N=3 (CTGF) and N=2 (SMAD3). SEM error bars, One-way ANOVA; CTGF p-value 0.1263 (ns); SMAD3 p-value 0.3560 (ns). CT averages of each gene for reference.

3D Cultures

Celprogen fPODs were cultured in 3D gels for 24hrs with TGF-β and BMP7 alone and in combination. Gene expression of SMAD3, CTGF and SERPINE1 was analysed (Figure 9). Average CT values suggested a good level of gene expression in these samples. SMAD3 expression was unaltered by treatments. CTGF expression was significantly increased with TGF-β treatment alone and in combination with BMP7, whilst BMP7 did not alter CTGF expression. This followed the pattern of expression seen with 2D Celprogen fPODs with these treatments both at 6hr (Figure 7) and 24hr (Figure 8) time points, with an average fold-change much higher in Celprogen fPODs cultured in 3D. SERPINE1 expression was significantly different across treatments, with a trend of increased expression with TGF-β treatment alone and in combination with BMP7.

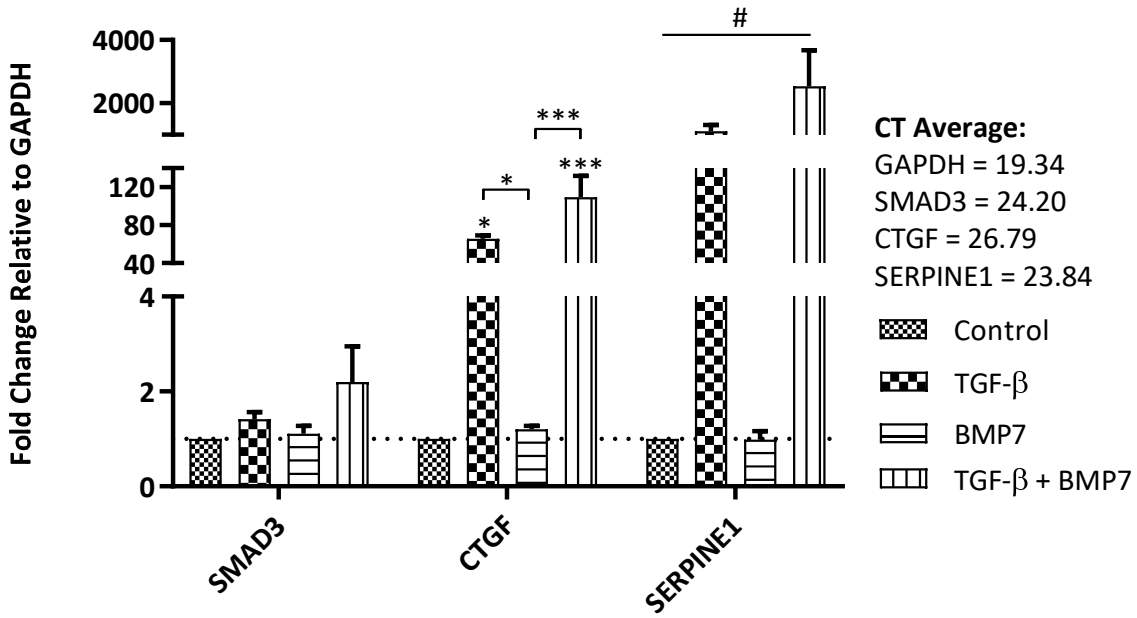

Figure 9. RT-qPCR of 3D fPOD Celprogen samples.

ΔΔCT analysis to study the relative fold change of the gene of interest against housekeeping gene GAPDH with either TGF-β and/or BMP7 treatment for 24hrs. N=3. SEM error bars, One-way ANOVA; SMAD3 p-value 0.2074 (ns); CTGF p-value 0.0003 (***); SERPINE1 p-value 0.0442 (#); followed by Tukey's multiple comparison post-tests. CT averages of each gene for reference.

Characterisation by Western Blot

No good methodology for extraction of protein from 3D gels had been optimised as with RNA extraction. TRIzol® did not result in good quantities of protein. Therefore, only 2D Celprogen fPOD cultures were used for western blot analysis. SMAD phosphorylation was analysed by western blot as this signalling pathway is central to TGF-β mediated fibrosis.

Previous work investigated whether BMP7 had an antagonistic effect upon canonical TGF-β SMAD2/SMAD3 signalling at a protein level in fMCs and fGECs.[194, 201] The effects of BMP7 on Celprogen fPODs was investigated. Celprogen fPODs were grown in 2D, treated with either TGF-β and/or BMP7. Treatment with TGF-β and the co-treatment induced a significant increase in pSMAD2 protein expression (Figure 10) compared to control expression levels. This was significantly higher than expression levels with BMP7 treatment, which remained at control values. There was a non-significant decrease in pSMAD2 expression when 2D Celprogen fPODs had been treated with both TGF-β and BMP7, compared with those treated with TGF-β alone.

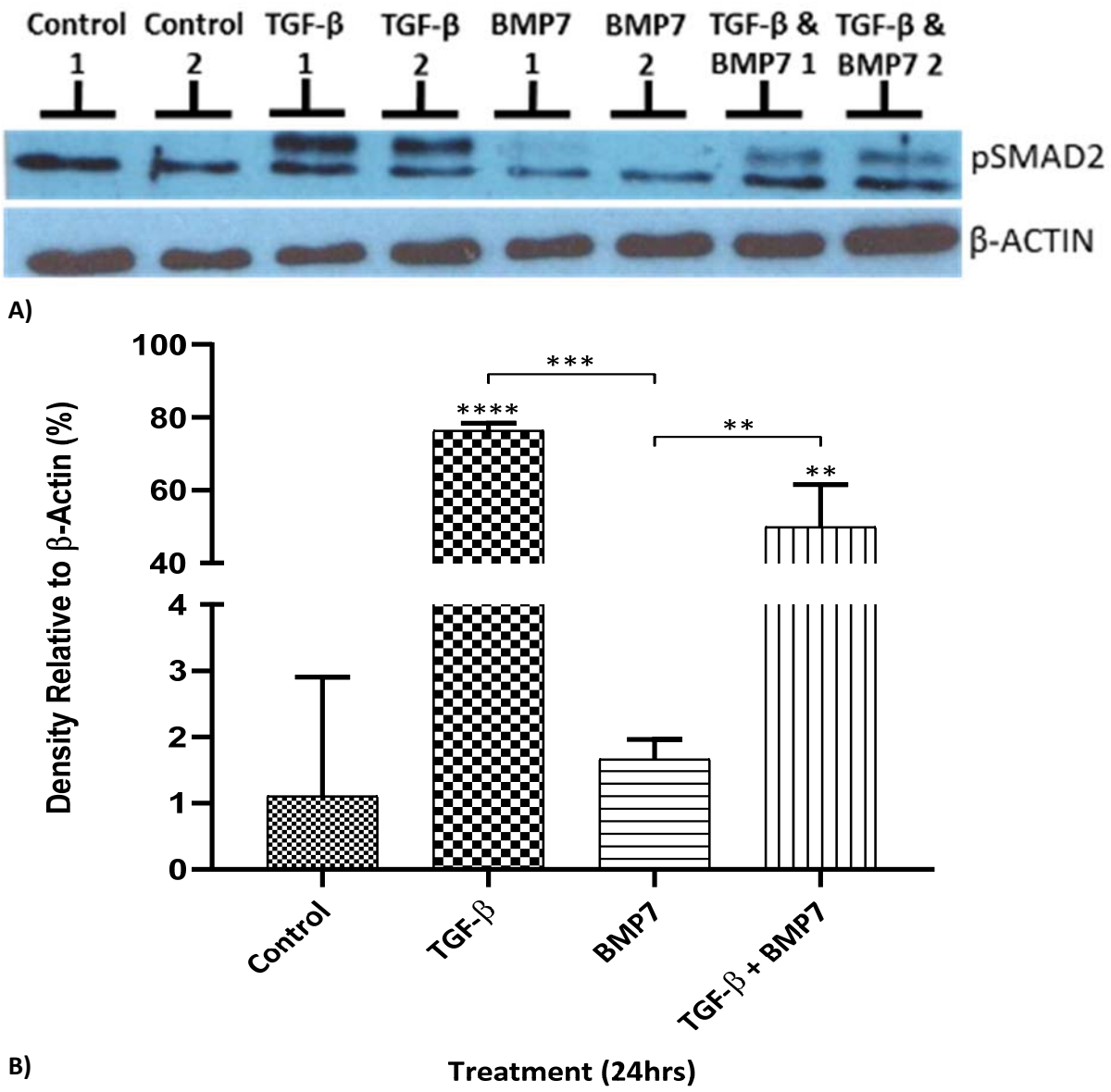

Figure 10. Western Blot of 2D fPOD Celprogen samples, pSMAD2 expression.

Western Blot (A) of 2D fPOD Celprogen samples run for pSMAD2 expression. The top band was pSMAD2 expression and β-actin the bottom band. Results were analysed by calculating the percentage density of protein bands relative to β actin expression (B). N=3. SEM error bars, One-way ANOVA; p-value < 0.0001 (****); followed by Tukey's multiple comparison post-tests.

An antibody which detected both pSMAD2 and pSMAD3 expression (Figure 11) mimicked the pattern of expression seen with the pSMAD2 probe (Figure 10); where TGF-β induced a significant increase in expression compared to control, that was significantly greater than expression evoked by BMP7 treatment.

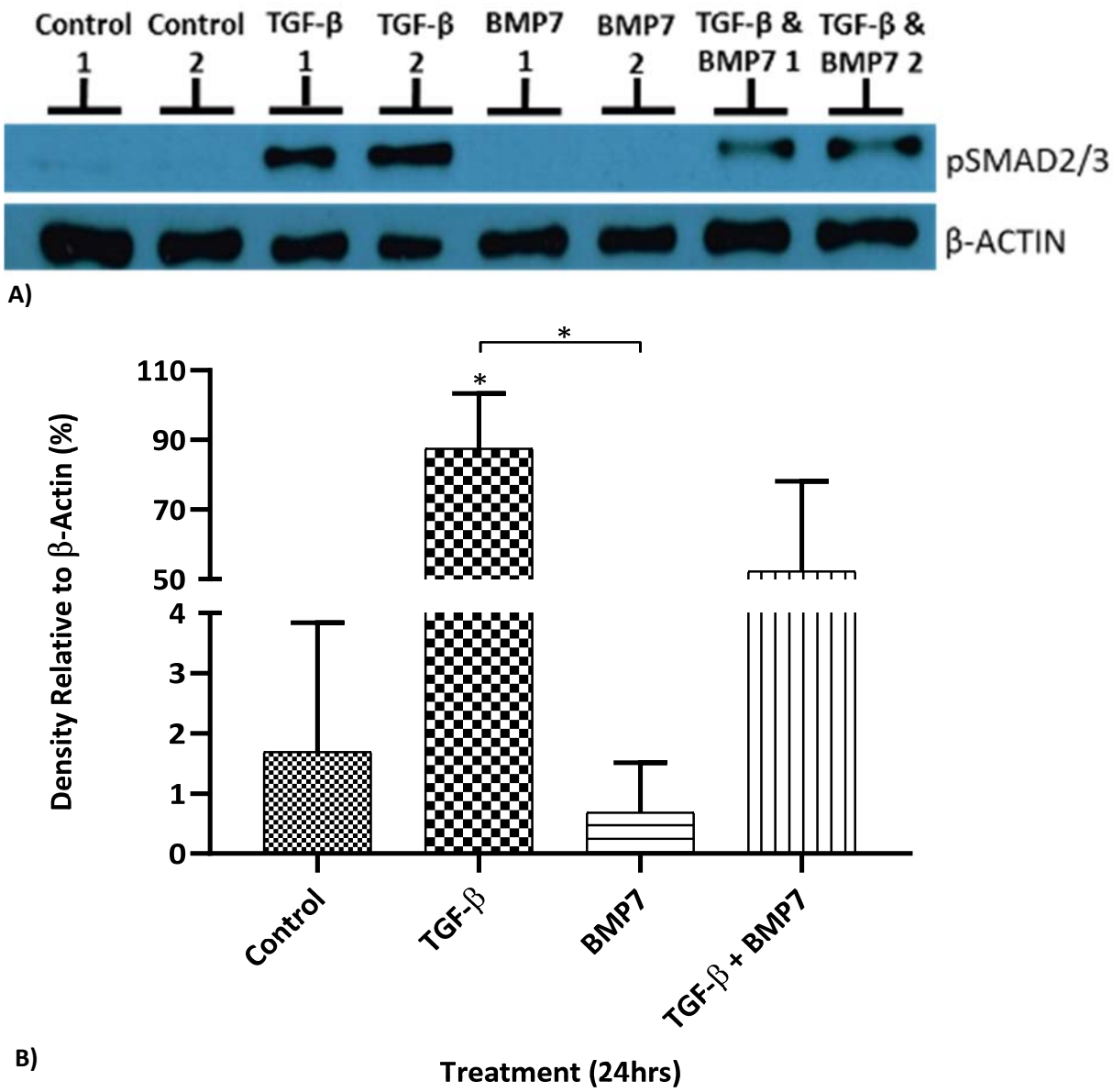

Figure 11. Western Blot of 2D fPOD Celprogen samples, pSMAD2/3 expression.

Western Blot (A) of 2D fPOD Celprogen samples run for pSMAD2/3 expression. The top band was pSMAD2/3 expression and β-actin the bottom band. Results were analysed by calculating the percentage density of protein bands relative to β actin expression (B). N=3. SEM error bars, One-way ANOVA; p-value 0.0094 (**); followed by Tukey's multiple comparison post-tests.

Expression of pSMAD3 (Figure 12) in 2D Celprogen fPODs was significantly increased across all treatment groups compared to controls; this, along with the patterns of expression of the pSMAD2 alone probe (Figure 10) and pSMAD2/3 probe (Figure 11) suggests that the antibody for pSMAD2/3 detects pSMAD2 preferentially. This data suggests that in 2D Celprogen fPODs BMP7 can evoke SMAD3 phosphorylation, co-treatment, however, does not result in additive expression levels indicating redundancy in SMAD3 phosphorylation.

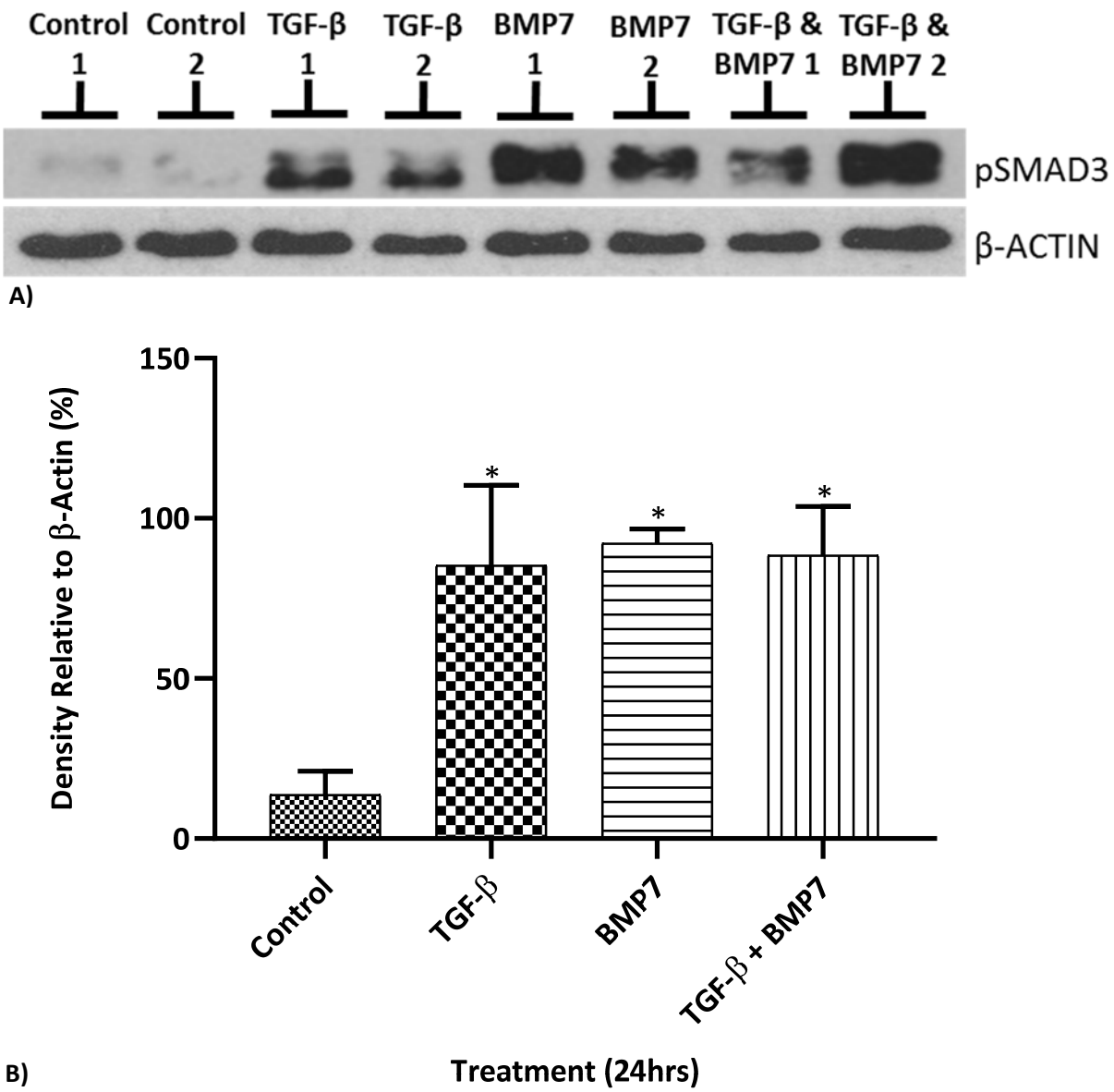

Figure 12. Western Blot of 2D fPOD Celprogen samples, pSMAD3 expression.

Western Blot (A) of 2D fPOD Celprogen samples run for pSMAD3 expression. The top band was pSMAD3 expression and β-actin the bottom band. Results were analysed by calculating the percentage density of protein bands relative to β actin expression (B). N=3. SEM error bars, One-way ANOVA; p-value 0.0189 (*); followed by Tukey's multiple comparison post-tests.

Expression of tSMAD3 (Figure 13) was significantly decreased with TGF-β treatment and co-treatment in 2D Celprogen fPODs, while BMP7 did not alter tSMAD3 expression from control values. Suggesting BMP7 did not affect TGF-β negative feedback mechanisms, regarding tSMAD3 protein levels.

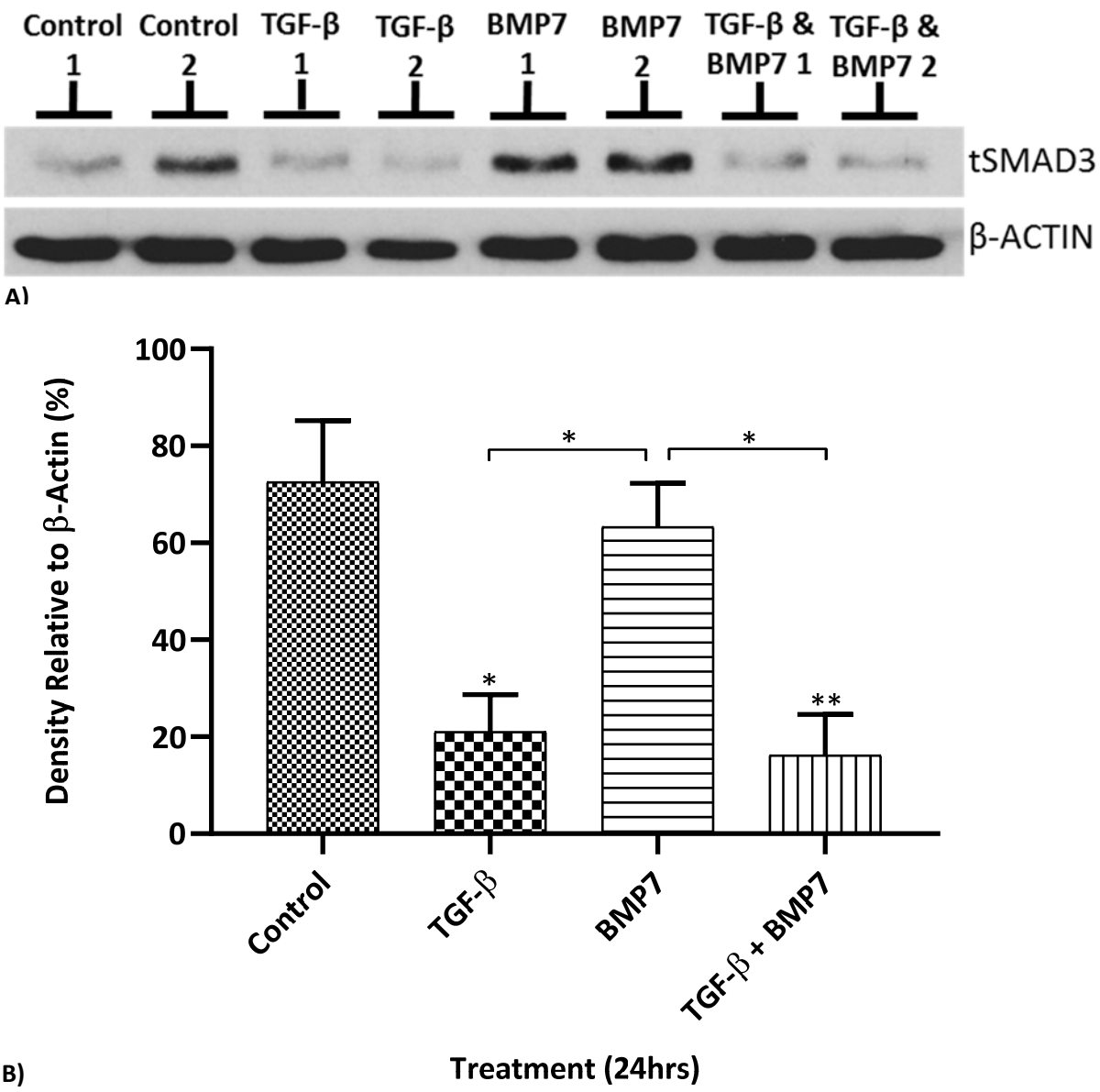

Figure 13. Western Blot of 2D fPOD Celprogen samples, tSMAD3 expression.

Western Blot (A) of 2D fPOD Celprogen samples run for tSMAD3 expression. The top band was tSMAD3 expression and β-actin the bottom band. Results were analysed by calculating the percentage density of protein bands relative to β actin expression (B). N=4. SEM error bars, One-way ANOVA; p value 0.0022 (**); followed by Tukey's multiple comparison post-tests.

Expression of pSMAD1/5 (Figure 14) in 2D Celprogen fPODs was significantly increased with BMP7 and co-treatment compared to controls, TGF-β treatment did not alter expression levels. This data suggests that exogenous TGF-β did not affect canonical BMP7 signalling.

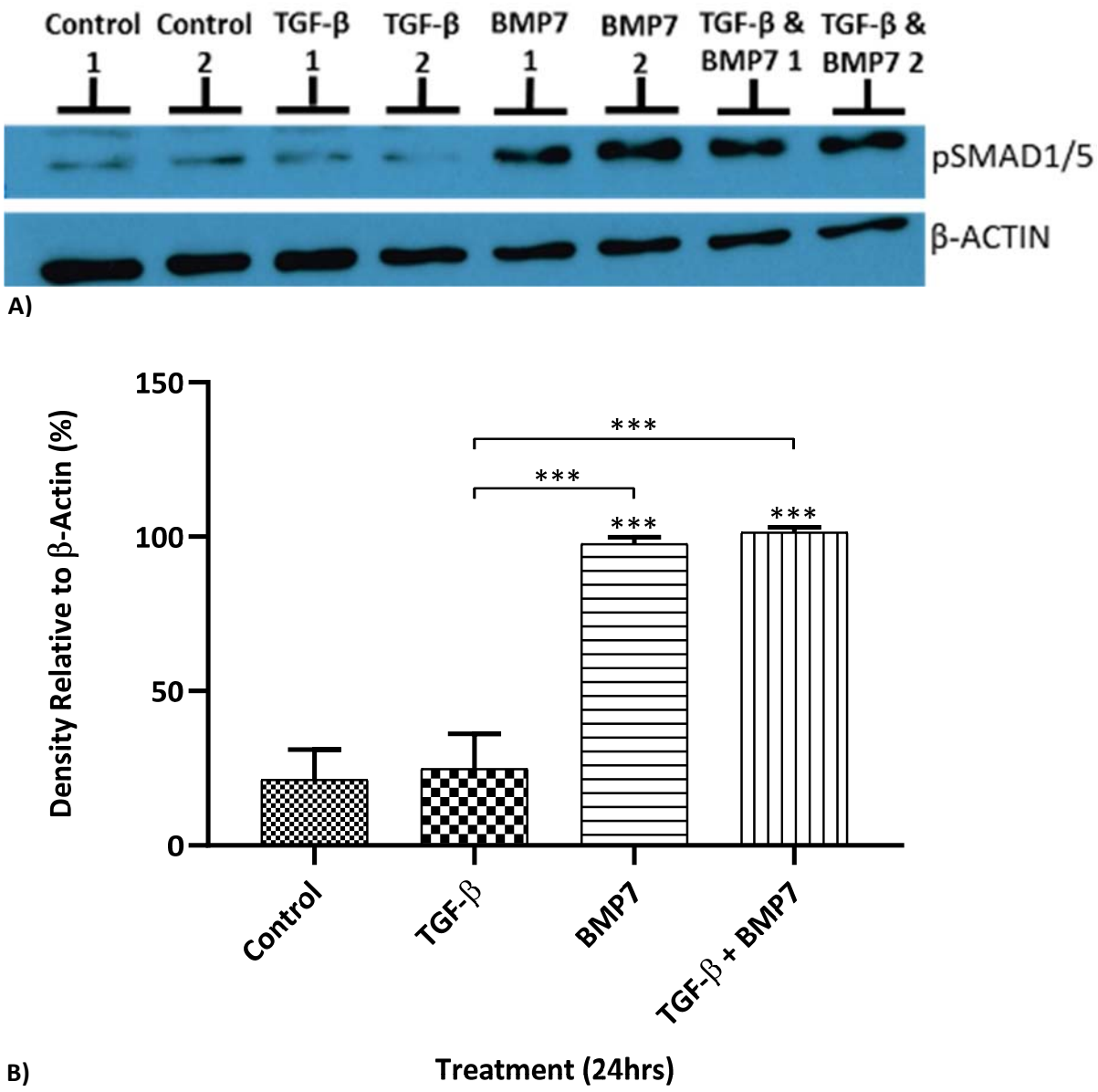

Figure 14. Western Blot of 2D fPOD Celprogen samples, pSMAD1/5 expression.

Western Blot (A) of 2D fPOD Celprogen samples run for pSMAD1/5 expression. The top band was pSMAD1/5 expression and β-actin the bottom band. Results were analysed by calculating the percentage density of protein bands relative to β actin expression (B). N=3. SEM error bars, One-way ANOVA; p value <0.0001 (****); followed by Tukey's multiple comparison post-tests.

2D Celprogen fPOD western blot data showed that SMAD2 phosphorylation was induced by TGF-β and not BMP7, while BMP7 did not affect this activation when treated in conjunction with TGF-β. SMAD3 phosphorylation however was induced by both TGF-β and BMP7 in 2D Celprogen fPODs, and this was also the case with co-treatment. Total SMAD3 expression in 2D Celprogen fPODs was downregulated by TGF-β and co-treatment, suggesting degradation, while no downregulation was seen with BMP7

stimulation, implying that TGF-β stimulates degradation via negative feedback, which is not changed by exogenous BMP7 and not seen with BMP7 treatment. Expression of pSMAD1/5 was significantly increased with BMP7 and co-treatment, not with TGF-β treatment, in 2D Celprogen fPODs, demonstrating that BMP7 induces SMAD1/5 phosphorylation whilst TGF-β does not and does not affect induction in 2D PODs.

Once Celprogen fPODs had been characterised with phenotypic markers, morphological observations and study of both gene and protein expression responses to cytokines, they were used with primary human fGECs and fMCs in 3D gel culture to assess the structures formed in triculture.

Further Characterisation of Subsequent lots of Celprogen fPODs

Subsequent lots of fPODs were purchased by both MedImmune and the Bradley laboratory, which tested negative for mycoplasma at the University of Cambridge (Table 1). Short Tandem Repeat (STR) profiling by MedImmune of their independently purchased Celprogen fPODs highlighted no human genomic DNA (gDNA) was present, instead Chinese hamster ovary (CHO) cell gDNA was found. Vials of Celprogen fPODs at the Bradley laboratory were then tested for CHO DNA by RT-qPCR using CHO primers (Table 2). Of the three lots of Celprogen fPOD cells that had been cultured, 2 lots (lot. 1314181-10 and lot. 1314181-28) appeared to contain a high number of CHO cells. Whilst the third lot (lot. 1314181-24) appeared to have CHO cells present at a low level.

Table 1. Mycoplasma testing of Celprogen fPOD.

Both lots of fPODs tested, along with Celprogen fPOD media and M199 medium used for 3D culture gels were negative for mycoplasma contamination. The level of ATP in a sample measured both before (read 1) and after the addition of the MycoAlert™ Substrate (read 2), the ratio indicates the presence or absence of mycoplasma.

Sample	Read 1	Read 2	Read 2/Read 1	Result (<0.9 = negative)
Celprogen fPOD Lot. 1314181-28 passage 1	3219	899	0.28	Negative
Celprogen fPOD Lot. 1314181-10 passage 5	2607	714	0.27	Negative
Celprogen fPOD Media Lot. 1702018211-03 Expiry. FEB18	114	56	0.49	Negative
M199 Media Lot. RNBC4375 Expiry. DEC13	5378	1048	0.19	Negative

3D tri-cultures had been created using Celprogen fPODs, both optimising the procedure for creating glomerular renal cell 3D tri-cultures, as well as generating data with different cytokines. To test any effect CHO cells may have had on this data another source of human fPODs was identified and these cells were characterised and tested in the same manner as the Celprogen fPODs, with some of the Celprogen fPOD 3D tri-culture experiments repeated with the new fPODs.

Table 2.RT-qPCR testing three lots of Celprogen fPODs at different passage points.

Lot. 1314181-10 and lot. 1314181-28 had low CT values for CHO primers and high CT values for human primers; indicating CHO cells. Lot. 1314181-24 had higher CT values for CHO primers while having lower CT values for human primers; indicating possible low presence of CHO cells. No signal was detected in any RT-qPCR run with Human NPHS2 primers. CHO NPHS2 primers did produce CT values; these were high, indicating CHO cells were not CHO POD cells. (- = no CT value produced.)

Sample		Human Primers CT Values			Chinese Hamster Primers CT Values		
		GAPDH	BA	NPHS2	GAPDH	BA	NPHS2
Lot. 1314181-10 Received JUN 2014	p2 03DEC14	26.9	30.0	-	19.5	20.2	33.3
	p5 12FEB15	27.1	30.8	-	19.9	21.3	32.0
	p7 31MAR15	24.3	28.8	-	19.0	18.6	30.9
	p8 09APR15	28.6	31.3	-	21.6	21.8	30.0
Lot. 1314181-24 Received MAR 2015	p2 19AUG15	17.6	20.9	-	-	-	32.9
	p3 28APR15	15.7	17.9	-	-	33.6	33.2
	p5 17JUL15	19.3	22.3	-	-	37.5	31.7
	p6 21MAY15	15.9	16.7	-	-	32.7	30.9
	p7 13MAY15	16.2	19.0	-	-	32.7	32.2
Lot. 1314181-28 Received AUG 2015	p2 19AUG15	26.5	30.5	-	18.7	17.2	32.6
	p3 28APR15	30.1	30.2	-	21.5	19.2	33.2
	p5 17JUL15	24.9	28.1	-	18.7	16.7	33.2
	p6 21MAY15	16.9	18.8	-	20.5	18.9	34.0
	p7 13MAY15	25.4	27.3	-	18.5	16.9	33.3

Lonza Podocyte Characterisation

Lonza fPODs were characterised in the same way as Celprogen fPODs; assessing the morphology and expression of phenotypic markers, as well as response to cytokines in both 2D and 3D.

Characterisation by Imaging

2D Cultures

Using bright-field microscope images (Figure 15) Lonza fPODs displayed the typical cobblestone morphology, with several fPODs exhibiting flattening and arborisation.

IF staining for phenotypic markers (Figure 16) showed weak cytoplasmic nephrin staining (Figure 16 A-B) staining and cytoplasmic staining of podocin (Figure 16 C-D). Synaptopodin staining (Figure 16 E-F) was mainly nuclear, with some positive cytoplasmic staining. Ezrin staining (Figure 16 G-H) was ring-like around the nuclei, and podocalyxin (Figure 16 K-L) was weakly cytoplasmic. GLEPP1 staining (Figure 16 M-N) was nuclear. CD2AP (Figure 16 I-J) and WT1 (Figure 16 O-P) staining were negative. No staining of an endothelial cell marker (CD31, Figure 16 Q-R), was detected. There was some weak nuclear and cytoplasmic αSMA (Figure 16 S-T) staining; there was no PDGFR-β (Figure 16 U-V) staining. The staining patterns compare well with those seen in 2D Celprogen fPODs (Figure 1-2) where ezrin staining is seen around the cell nucleus, with podocin, nephrin and synaptopodin exhibiting cytoplasmic staining. Staining differs slightly between the two fPOD cultures with synaptopodin exhibiting some nuclear staining in 2D Lonza fPOD cultures. Therefore, both fPOD exhibit phenotypic markers of PODs.

TEM imaging (Figure 17-18) of 2D Lonza fPOD cells was performed for morphological characterisation of this cell type, where foot-like processes and secondary foot-like processes (Figure 17 H) were visible. This TEM imaging confirmed that the two fPOD cultures had similar morphology, demonstrating foot-like processes. The impact of TGF-β treatment upon the structure of 2D Lonza fPODs under TEM was also imaged (Figure 18), where ultrastructural damage with membrane rupture and vacuolisation could be seen in some cells.

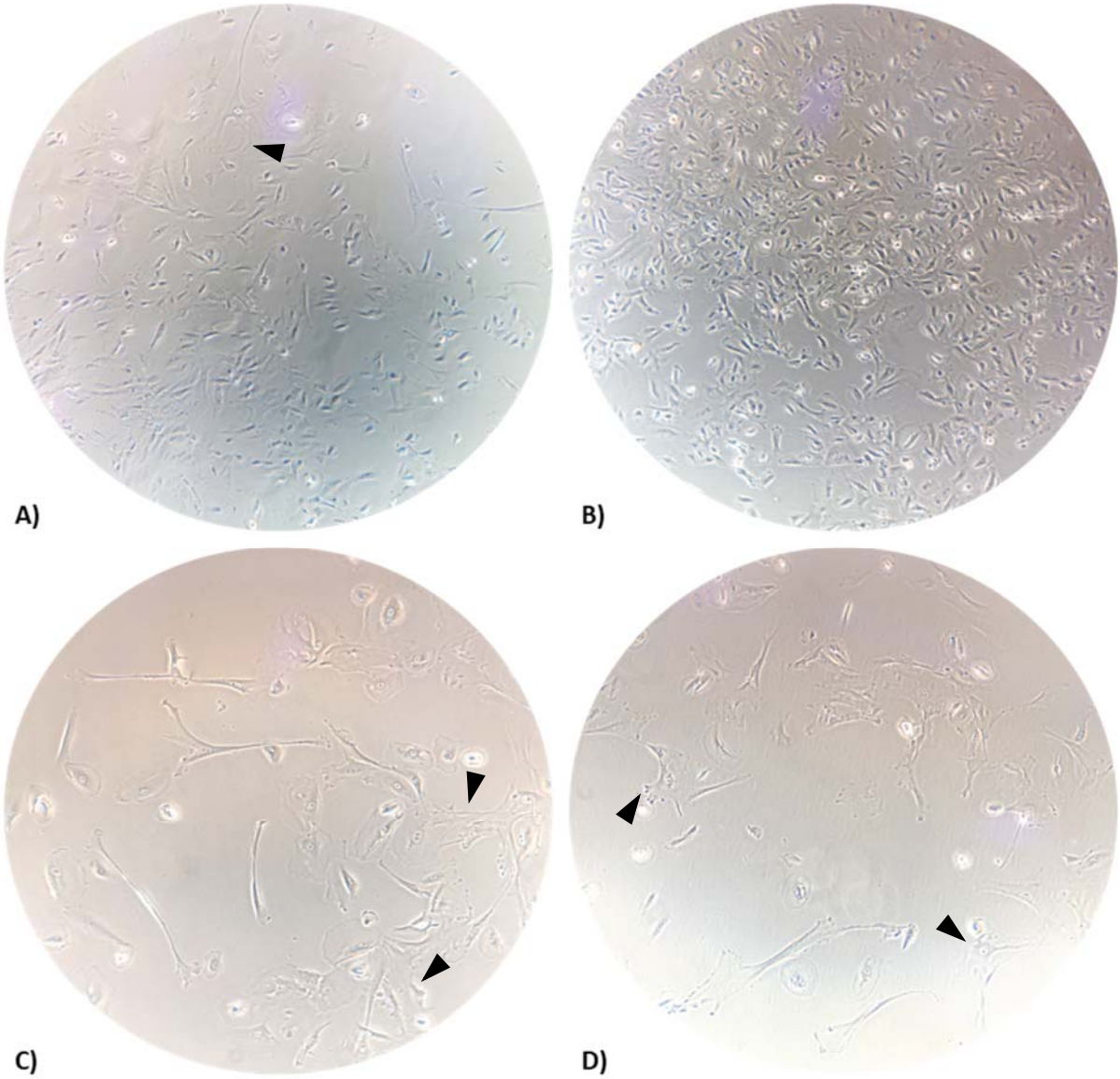

Figure 15. Bright field images of 2D Lonza fPODs.

Lonza fPODs displayed both the typical cobblestone morphology, along with some exhibiting flattening and arborisation (black arrows). A and B, 5X magnification; C and D, 20X magnification.

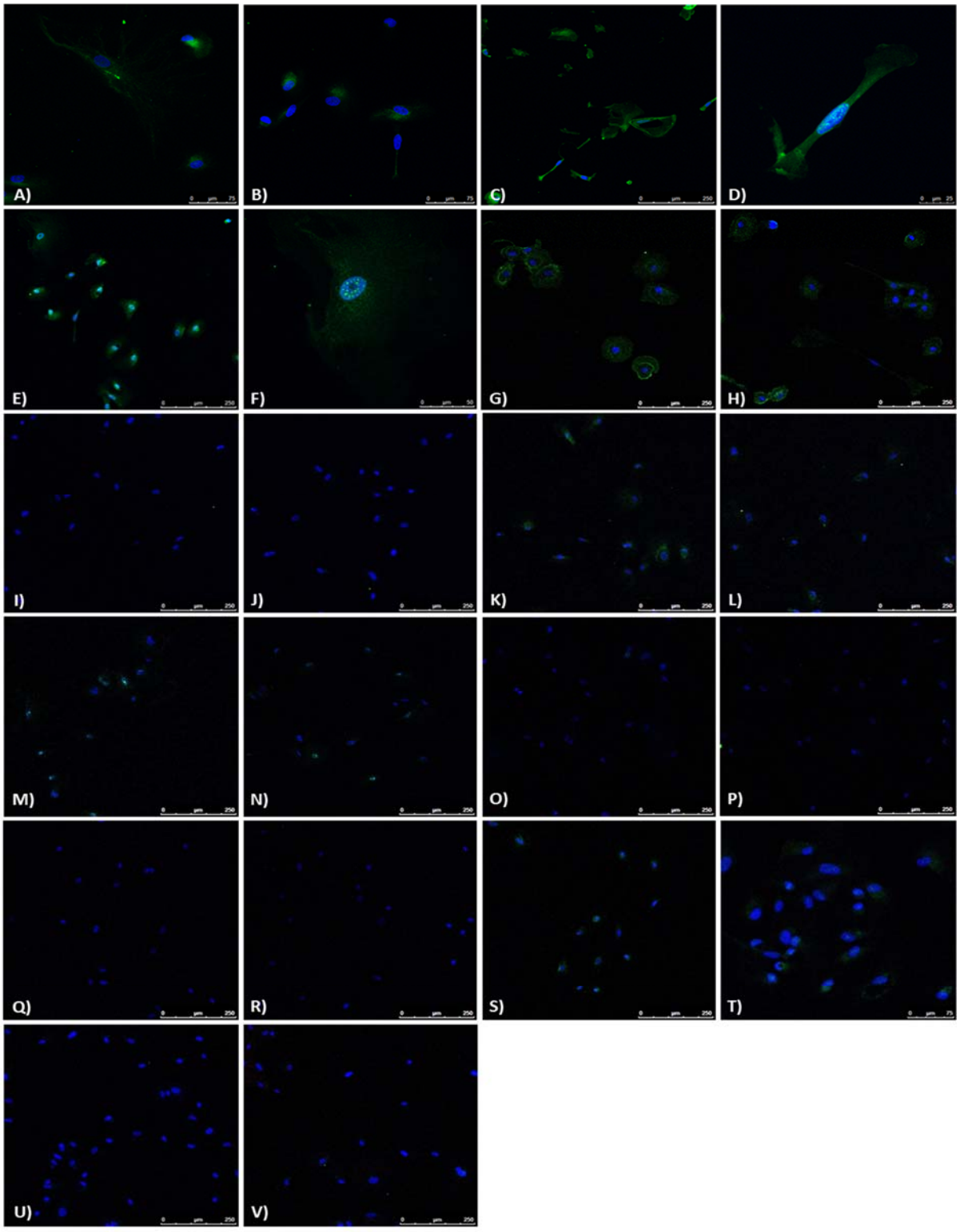

Figure 16. IF of 2D Lonza fPODs for phenotypic markers.

IF (green) of 2D Lonza fPODs for phenotypic markers of PODs, as well as markers for endothelial cells and MCs. Nephrin (A-B), podocin (C D), synaptopodin (E-F), ezrin (G-H), CD2AP (I-J), podocalyxin (K-L), GLEPP1 (M-N), WT1 (O-P), CD31 (Q-R), αSMA (S-T) and PDGFR-β (U-V). Nuclei counterstained with DAPI (blue). 20X magnification.

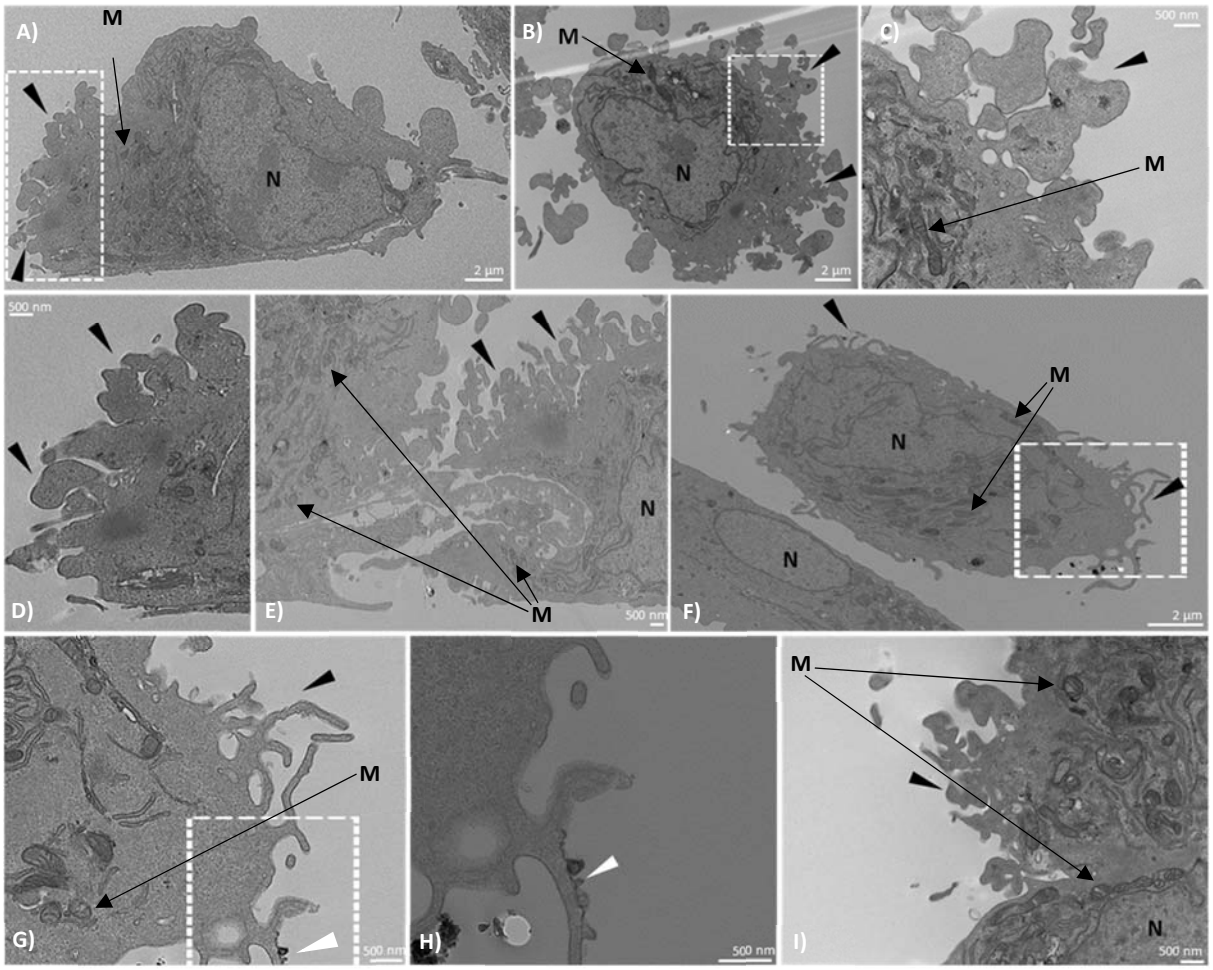

Figure 17. TEM images of 2D Lonza fPODs.

(A, B and F) low power images show overall morphology of cells with nuclei (N), mitochondria (M) and foot like processes (black arrows). (D) is the magnification of section in image (A), (C) is the magnification of section in image (B) and (G) is the magnification of section in image (F) where foot-like processes can be seen clearly, with nuclei (N) and mitochondria (M) labelled. (H) is a higher power image of the section in image (G) where secondary foot-like processes (white arrows) can be seen, with nuclei (N) and mitochondria (M) labelled.

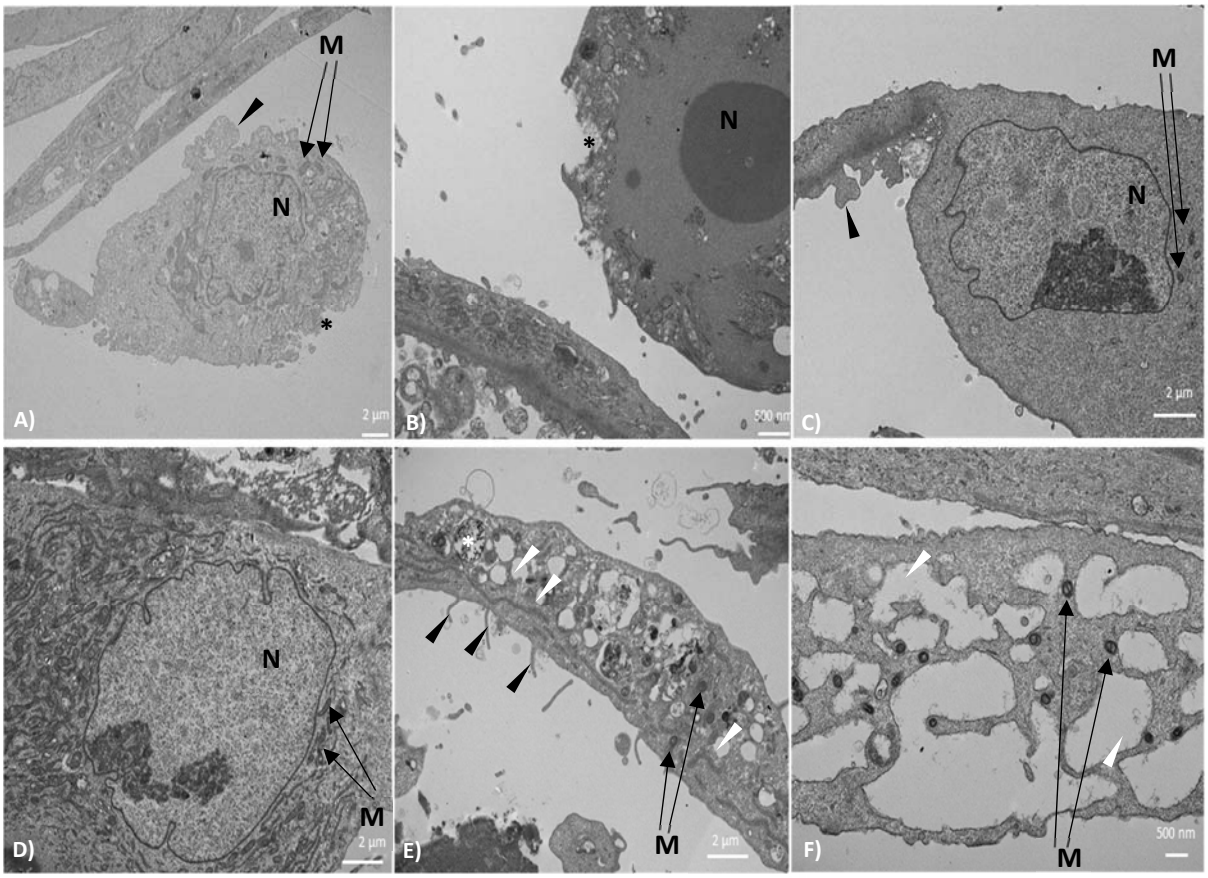

Figure 18. TEM images of 2D Lonza fPODs treated with TGF-β.

(A, C, D and E) low power images show overall morphology of cells with nuclei (N), mitochondria (M) and foot like processes (black arrows); TGF-β treatment appeared to result in necrotic damage to the cellular ultrastructure of the cells with extracellular membrane rupture (black asterisk) and intensive cytoplasmic vacuolisation (white arrows). (M) a higher power image of the cytoplasmic vacuolisation seen in some TGF-β treated Lonza fPOD cells. Evidence of secondary lysosomes (white asterisk), where electron dense bodies contained within a membrane, can be seen (E). (F) is a higher power image where substantial cytoplasmic vacuolisation (white arrows) can be seen, with mitochondria (M) labelled. While TGF-β treatment clearly caused cellular damage of 2D Lonza fPOD cultures, cells were not all affected in the same way.

3D Cultures

IF staining of 3D cultures was performed on Lonza fPODs (Figure 19) for the same phenotypic markers as studied when these cells were cultured in 2D (Figure 16). Nephrin (Figure 19 A-B), podocin (Figure 19 C-D), synaptopodin (Figure 19 E-F) staining was strongly cytoplasmic; this mimicked the pattern seen in 2D cultures (Figure 16 A-F), with staining stronger in the 3D cultures. Strong cytoplasmic staining could be seen for ezrin (Figure 19 G-H) which differed from both the pattern seen in 2D Lonza fPODs (Figure 16 G-H) and patterns seen in Celprogen fPODs (Figure 1-2, 5), where ring staining around the cell nucleus had been seen. There was also weakly positive staining for CD2AP (Figure 19 I-J), staining for which was negative in 2D Lonza fPODs (Figure 16 I-J). Podocalyxin (Figure 19 K-L) and GLEPP1 (Figure 19 M-N) staining was diffused within the cytoplasm of 3D Lonza fPODs, as opposed to the nuclear staining of GLEPP1 in 2D Lonza fPODS (Figure 16 M-N), this staining was stronger than that seen in 2D Lonza fPODs (Figure 16 K-N). Staining for WT1 (Figure 19 O-P) was negative, as was the case for 2D Lonza fPOD cultures (Figure 16 O-P). As with 2D Lonza fPOD cultures, the endothelial marker CD31 was used and no staining was detected. MC phenotypic markers, αSMA (Figure 19 S-T) and PDGFR-β (Figure 19 U-V) were again used. There was some weak cytoplasmic αSMA (Figure 19 S-T) staining; there was no PDGFR-β (Figure 19 U-V) staining.

In comparison to 3D Celprogen fPOD culture staining (Figure 5), staining of the POD phenotypic markers used on both cultures (ezrin, podocin, synaptopodin and nephrin) appeared stronger in the 3D Lonza fPODs (Figure 19). There was no ring pattern around cell nuclei for ezrin and podocin in 3D Lonza fPODs (Figure 19 C-D and G-H), as was seen with 3D Celprogen fPODs (Figure 5 A and D).

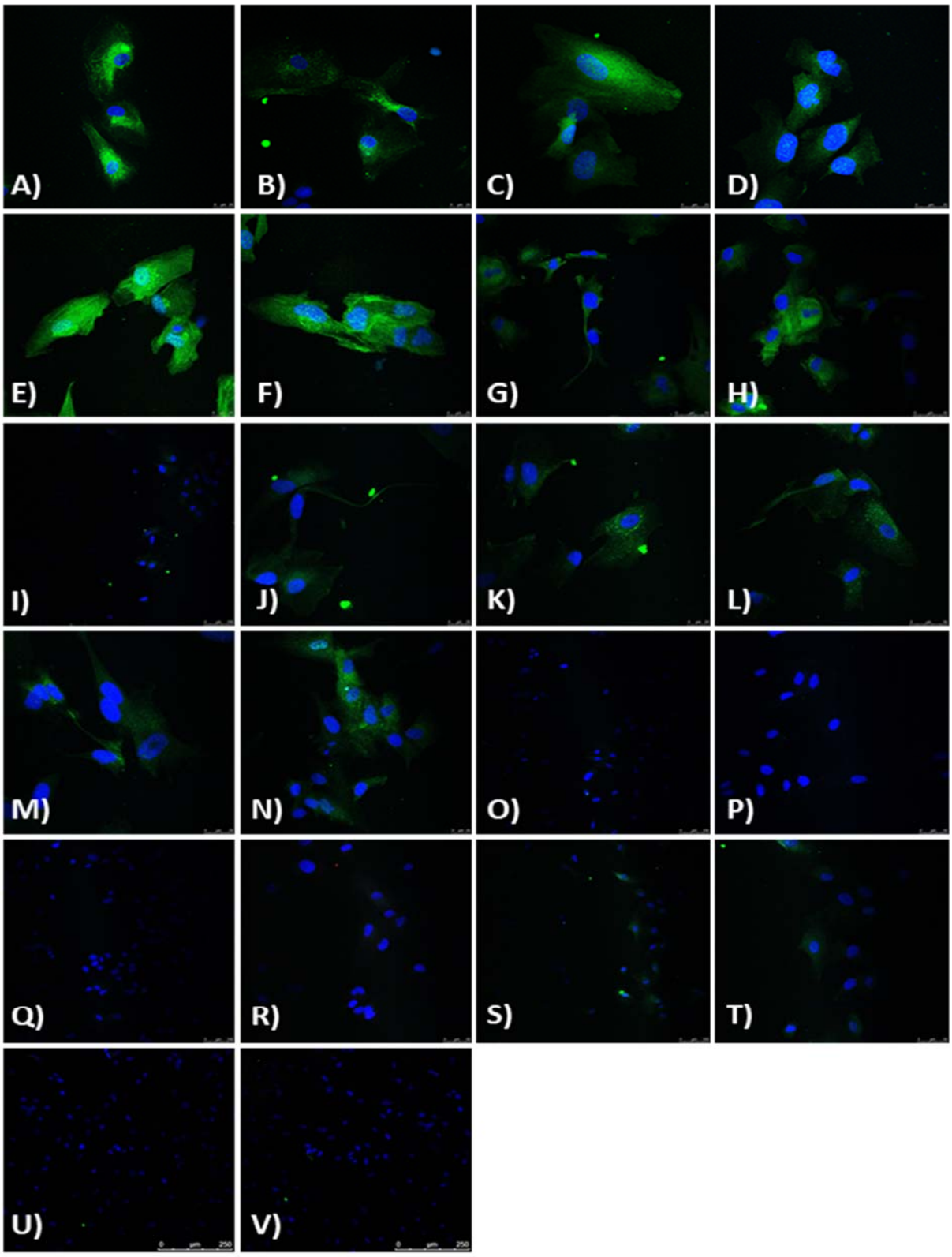

Figure 19. IF of 3D Lonza fPODs for phenotypic markers.

IF (green) of 3D Lonza fPODs for phenotypic markers of PODs, as well as markers for endothelial cells and MCs. Nephrin (A-B), podocin (C D), synaptopodin (E-F), ezrin (G-H), CD2AP (I-J), podocalyxin (K-L), GLEPP1 (M-N), WT1 (O-P), CD31 (Q-R), αSMA (S-T) and PDGFR-β (U-V). Nuclei counterstained with DAPI (blue). 20X magnification.

Characterisation by RT-qPCR

2D Cultures

Lonza fPODs were cultured in 2D and treated with either TGF-β and/or BMP7 for 24hrs, as was the case with Celprogen fPODs, to assess and compare gene expression responses to the treatments. A panel of genes was studied; CTGF, SMAD3, SERPINE1 and TGFB1. CT averages were high for all genes, and so indicated a good level of RNA expression in these samples. There is no statistical significance to this data set as it at N=1. The expression of TGF-β signalling genes (Figure 20) were tested. Expression of CTGF appeared to increase with TGF-β treatment alone and when used in combination with BMP7, while BMP7 alone appeared to not affect CTGF expression. The pattern of CTGF expression with these treatments followed that seen in both 2D (Figure 7-8) and 3D (Figure 9) Celprogen fPODs. SMAD3 expression trended downwards with both TGF-β treatment and co-treatment, while BMP7 appeared to have little effect upon expression of SMAD3 compared to control values.

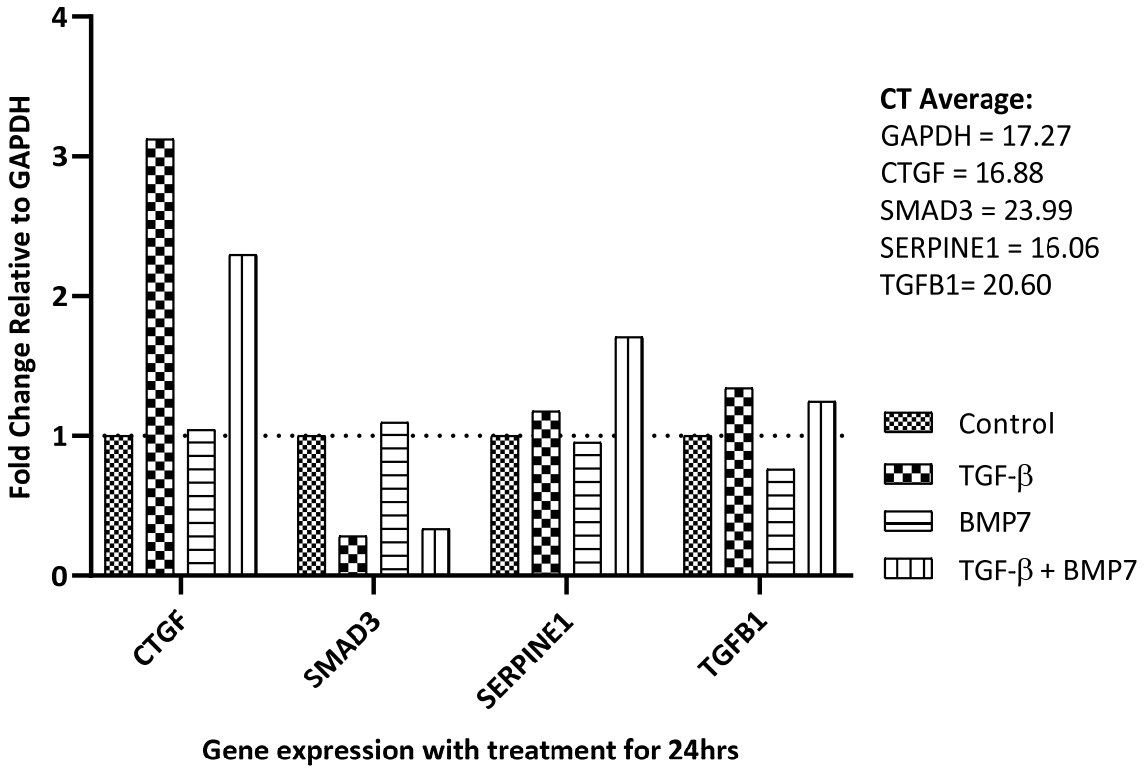

Figure 20. RT-qPCR of 2D fPOD Lonza samples, TGF-β signalling genes.

ΔΔCT analysis to study the relative fold change of the gene of interest against housekeeping gene GAPDH with either TGF-β and/or BMP7 treatment for 24hrs. N=1. CT averages of each gene for reference.

SERPINE1 expression seemed to slightly increase with TGF-β expression, increasing to a greater extent with co-treatment, while BMP7 treatment appeared to not affect expression compare to control value. This pattern of expression mimics that seen with 3D Celprogen fPODs (Figure 9) treated with the same stimulations, yet with much lower average fold-change values. Expression of TGFB1 was upregulated somewhat with both TGF-β treatment and co-treatment, while BMP7 appeared to result in a slight downregulation in TGFB1 expression.

3D Cultures

Lonza fPODs were cultured in 3D and treated with either TGF-β and/or BMP7 for 24hrs, as was the case with Celprogen fPODs, to assess and compare gene expression responses to the treatments. A panel of genes was studied; CTGF, SMAD3, SERPINE1 and TGFB1. CT averages were high for all genes, and so indicated a good level of RNA expression in these samples. Expression of TGF-β signalling genes (Figure 21) were examined. Expression of CTGF appeared to increase with both TGF-β and co-treatment, while BMP7 appeared to result in a decrease in expression of CTGF. This followed the pattern of expression seen in 2D Lonza fPODs (Figure 20) as well as that seen in both 2D and 3D Celprogen fPODs (Figure 7-9), with TGF-β and co-treatment resulting in increased CTGF expression. Expression of SMAD3 appeared to decrease with TGF-β and co-treatment, while BMP7 appeared to cause a very slight increase in SMAD3 expression. This echoed the expression pattern seen with these treatments upon SMAD3 expression in 2D Lonza fPODs (Figure 20). SERPINE1 expression was significantly increased with both TGF-β and co-treatment compared to control values, while BMP7 treatment resulted in a small non-significant increase in SERPINE1 expression. This generally mimicked the pattern of expression seen in 2D Lonza fPODs (Figure 20) and that seen with 3D Celprogen fPODs (Figure 9) treated with the same stimulations, where co-treatment resulted in the higher fold-change increase in SERPINE1 expression. TGFB1 expression was significantly increased with TGF-β treatment compared to control values, while co-treatment resulted in a slight non-significant increase in expression. BMP7 treatment caused a slight decrease in TGFB1 expression. This followed the same pattern of expression seen with 2D Lonza fPODs (Figure 20).

Lonza fPODs had been characterised in the same manner as Celprogen fPODs, with phenotypic markers, morphological observations and assessment of response to cytokine insults in both 2D and 3D. Showing convincing similarity to Celprogen fPODs, they were used along with primary human fGECs and fMCs in 3D gel culture to assess the structures formed when these three glomerular cell types were cultured together in this format.

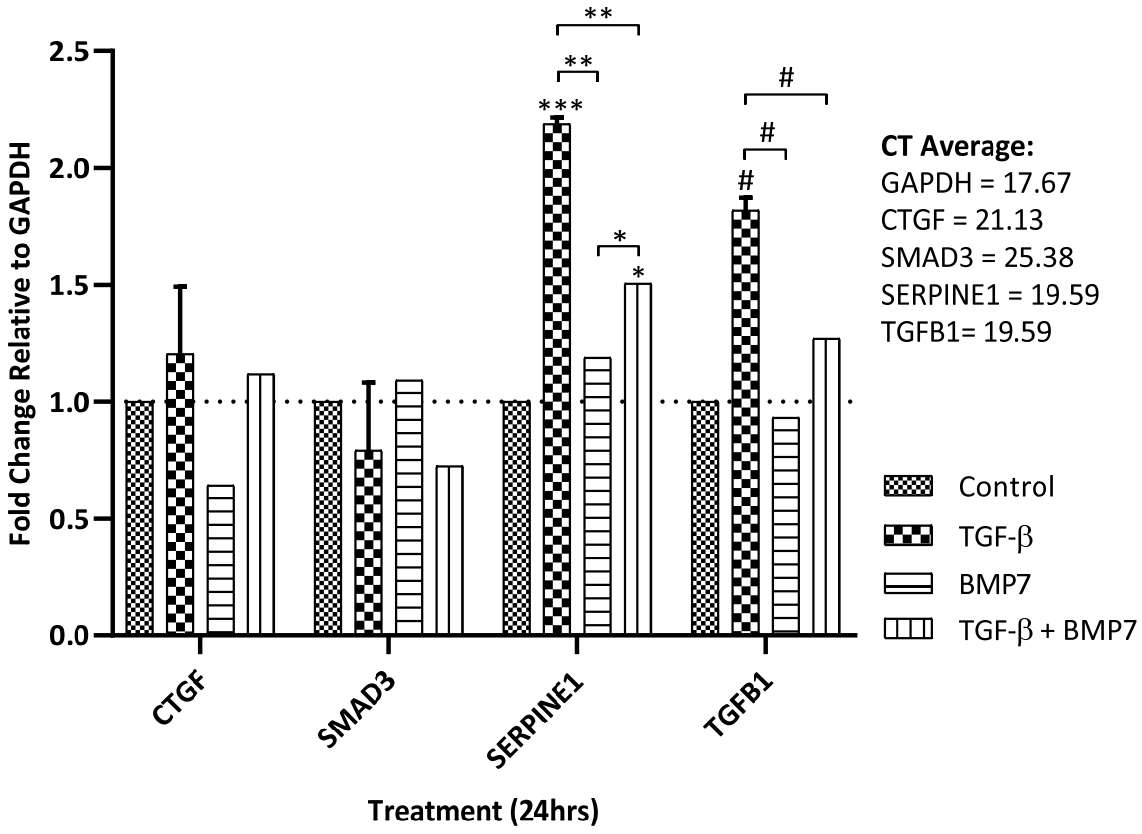

Figure 21. RT-qPCR of 3D fPOD Lonza samples, TGF-β signalling genes.

ΔΔCT analysis to study the relative fold-change of the gene of interest against housekeeping gene GAPDH with either TGF-β and/or BMP7 treatment for 24hrs. N=2 (Control & TGF-β) and N=1 (BMP7 & co-treatment). SEM error bars, One-way ANOVA; CTGF p-value 0.5659 (ns); SMAD3 p-value 0.7497 (ns); SERPINE1 p-value 0.0015 (**) and TGFB1 p-value 0.0100 (**). CT averages of each gene for reference.

Chapter 5 – Results: 3D Tri-culture Development & Characterisation

In this chapter, the results of the development of the 3D tri-culture system and how it was characterised shall be detailed. 3D tri-cultures were first developed using Celprogen fPODs, therefore the data presented in this chapter comes from 3D tri-cultures using these cells.

3D Tri-culture Development

Several factors involved with 3D culture of multiple cell types had to be evaluated and optimised to successfully culture the three glomerular cell types together in 3D. The results of the key areas of optimisation are outlined below.

3D tri-cultures were imaged using both brightfield and fluorescent imaging of each cell type to help assess the effects of factors optimised throughout development of the system. fMCs were labelled blue using a Celltracker™ Blue CMAC dye, fPODs were labelled red using a cell membrane PKH26 dye. fGECs were initially labelled green using fluorescein-labelled ULEX, to acquire better images fGECs were instead transfected with GFP.

Gel Matrix & Polyglycolic Acid Mesh (PGA) Mesh

To culture cells in 3D they must be dispersed within a matrix, which can also include a mesh to reinforce the matrix. The gel matrix used in this work followed from previous methods reported in the literature.[193, 194] The matrix consisted of rat tail type I collagen, human plasma fibronectin, $NaHCO_3$, HEPES and M199 medium. The rat tail type I collagen concentrations altered slightly by batch, and so quantities needed adjusting accordingly. A PGA mesh had been used previously to strengthen the gel matrix against contraction by cells, especially from highly contractile cell types such as fMCs. The need for PGA mesh for 3D tri-cultures was assessed (Table 3), and it was determined there was no need to continue using a PGA mesh.

Glomerular Cell Numbers & Ratios

In the development of the 3D tri-culture, a key factor for consideration and optimisation was the number of each glomerular cell type seeded in the 3D gel, taking account of the ratio of each cell type and the total cell number per 3D culture gel. In mono-culture the total number of cells used per 3D culture gel was $0.5x10^6$, which provided enough RNA for RT-qPCR analysis whilst preventing over-confluence and gel contraction. This provided a potential maximum total number of glomerular cells to work with for 3D tri-cultures.

Initial experiments took account of the proportionate number of each cell type *in vivo,* ensuring that sufficient numbers of fGECs were available to form cord microvessel networks, based on monoculture

experiments, and that fMCs are limited because of their highly contractile nature. Therefore, initially, a ratio of 20 fGECs: 4 fPODs: 1 fMC was chosen, where 500,000 fGECs, 90,000 fPODs and 24,000 fMCs were used (Table 3). This meant a total of 615,000 cells per 3D culture gel, and this resulted in the overcrowding of the culture gel, where all cell types appeared to be unhealthy (Figure 22 A-B and Table 3). Total cell numbers were twice reduced by approximately 6% (Table 3), which improved the viability of glomerular cells and the structures formed to some extent.

A larger reduction in total cell number of 30% was introduced, along with lowering the numbers of fGECs and fPODs to aid this reduction further, altering the glomerular cell type ratio to 16 fGECs: 3 fPODs: 1 fMC (Figure 23-28, Table 3). This resulted in a 3D tri-culture where all cell types appeared healthy, with fGECs forming cord microvessel networks with branches and lumen (Figure 23-28, Table 3). fPODs interacted closely with the fGEC networks, with foot-like processes of the fPODs engaging, while fMCs were spread through the 3D matrix (Figure 23-28, Table 3). With some further optimisation balancing quantities of RNA obtainable from 3D tri-cultures versus cell viability in the 3D culture system, the minimum total number of cells per culture gel was determined as 400,000 whilst the maximum was 480,000 cells; with the glomerular cell type ratio of 16 fGECs: 3 fPODs: 1 fMC (Table 3). These total cell numbers were used for all 3D tri-culture work using Celprogen fPODs. It was noted upon introduction of Lonza fPODs that 3D tri-culture gels were more contractile, therefore the total cell number was kept at the minimum total number of cells (400,000) when using Lonza fPODs.

Tri-culture Media

To culture the three glomerular cell types in 3D, a media which was appropriate for the needs of each cell type was required. The medium for each individual cell type had been designed for the optimal growth of that specific cell type, and the results of media optimisation are detailed in Table 3.

Initially, an equal mix of medium for each individual cells type was used on the 3D tri-culture system (a third of each medium type). The obvious issue here was fMCs took over the culture (Figure 22 C-D and Table 3). The next mixture tried was an equal mix of just the Celprogen fPOD and fGEC mediums, here the fMCs did not outgrow the culture, yet it became apparent that the fGECs were not growing satisfactorily, failing to form the many tube/cord-like structures seen when these cells are grown in 3D mono-culture (Figure 22 E-F and Table 3). Therefore, pure endothelial cell media was used on the 3D tri-culture model and the fGECs did grow and form structures as anticipated and the fMCs growth was under control. However, the Celprogen fPODs did not appear to be very healthy, appearing very rounded without formation of any foot-like process as observed in mono-cultures (Figure 22 G-H and Table 3). These issues in balancing the needs of each individual cell type of the tri-culture from the purchased complete mediums led to formulating a specific medium for the 3D tri-culture system.

Initially, a medium (tri-culture medium version 1(V1)) was formulated which consisted of RMPI 1640, the basal medium the literature suggests for POD cell culture.[184, 185, 202] ECGS (1%) was used as the fGECs appeared to require this growth factor to survive and form tubular structures. Penicillin/Streptomycin (P/S 1%) was used, a standard concentration of antibiotics used in cell culture. FBS (10%) was used, a higher concentration than used in either fMC or fGEC culture mediums but at the concentration advised by the literature for POD culture medium.[184, 185, 202] As neither MsCGS nor ITS was included the higher FBS concentration was hypothesised to combat this; however, it appeared that this increase in FBS led to MCs overgrowing the culture (Figure 22 I-J and Table 3). Therefore, tri-culture medium version 2 (V2) was composed, consisting of the same basal medium as used in V1 (RPMI 1640) as well as the same concentrations of ECGS and P/S. In this formulation, ITS (1%) was used, which is the literature recommended supplement in POD medium but also allows for a lower FBS concentration.[184, 185, 202] This meant that FBS could be used at 2%, which is the concentration used in fMC medium but much lower than in both fGEC and fPOD mediums. This medium composition supported the growth and survival of all the tri-culture cell types, maintaining the approximate ratio of each cell type and therefore was used for all further work on the model system (Figure 23-28, Table 3).

Table 3. 3D Tri-culture factor optimisation.

Optimised factors were: use of PGA mesh, total number of cells per 3D culture gel, glomerular cell ratio and media type used. Final experimental set up was no PGA mesh, a minimum total cell number of 4.00x105 and maximum of 4.80x105, a glomerular cell ratio of 16:3:1 and culture with tri-culture media V2.

3D Tri-culture Optimisation Experiment	Factor for Optimisation															Result
	PGA Mesh		Total Cell Number (x10^5)						Glomerular Cell Ratio		Media Type					
	+	-	6.15	5.76	5.48	3.90	4.00	4.80	20:4:1	16:3:1	1/3 fPOD, 1/3 fGEC & 1/3 fMC Mediums	1/2 fPOD & 1/2 fGEC Mediums	fGEC Media	Tri-culture media V1	Tri-culture media V2	
1	X		X						X		X					Too many cells, cell health poor, few microvessels.
2	X			X					X		X					Too many cells, cell health poor, few microvessels.
3	X				X				X		X					Too many cells, cell health poor, few microvessels.
4	X					X				X	X					fMCs took over 3D culture.
5	X						X			X		X				Few microvessels formed. Good quantity of RNA extracted.
6	X						X			X			X			Celprogen fPODs unhealthy.
7	X						X			X				X		fMCs took over 3D culture.
8	X						X			X					X	Microvessel networks, fPODs interacted, fMCs throughout.
9	X							X		X					X	As experiment 8, max total cell number system tolerated.
10		X					X			X					X	Absence of PGA mesh did not affect 3D tri-culture.
11		X						X		X					X	Absence of PGA mesh did not affect 3D tri-culture.

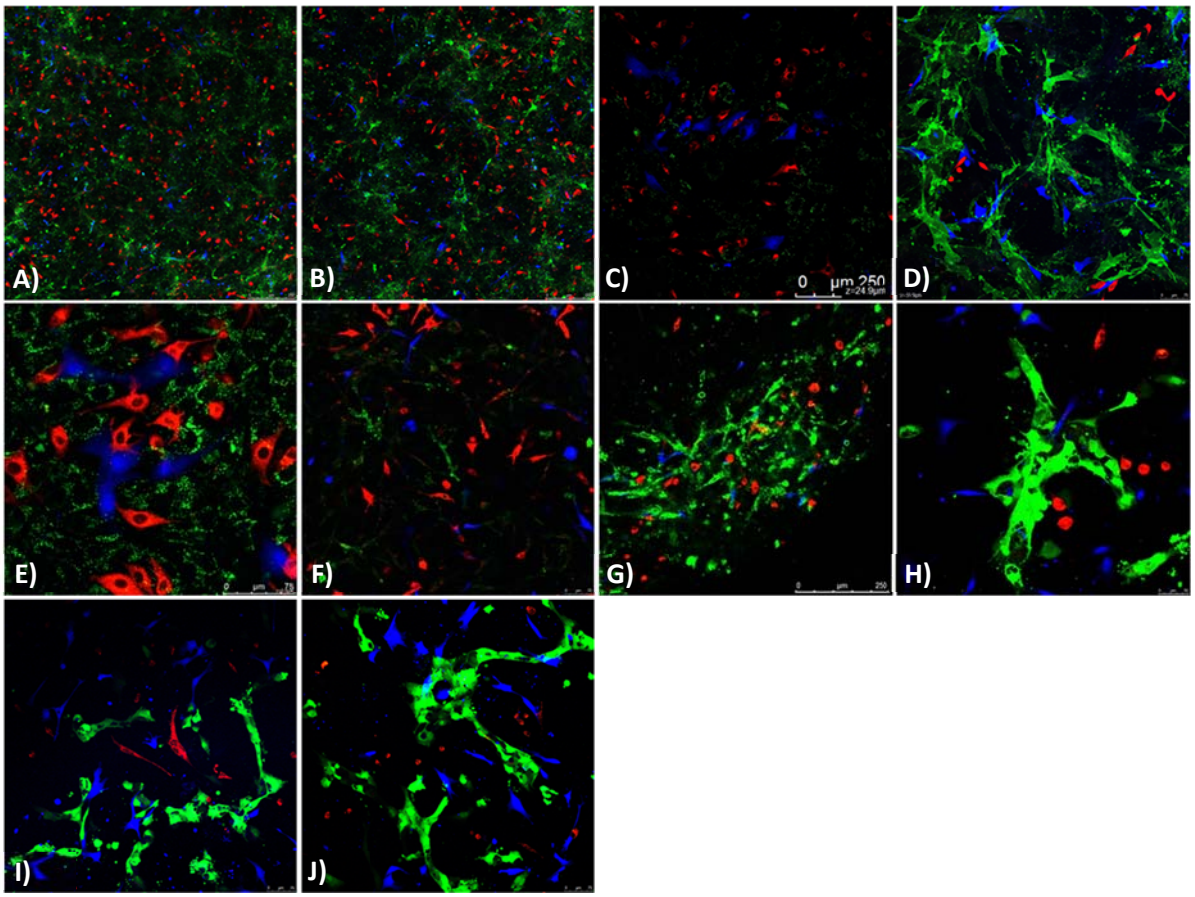

Figure 22. IF imaging of 3D tri-culture factor optimisation.

fGECs (green; A-G Ulex, H-J GFP), Celprogen fPODs (red) and fMCs (blue). Early culture total cell numbers were too high and so 3D cultures were overcrowded (A-B). In optimisation of the media used for 3D tri-cultures, both using equal volumes of each individual media type (C-D), and the higher FBS concentration in tri-culture media V1 (I-J) lead to fMCs overtaking the cultures. Use of equal amounts of fGEC and Celprogen fPOD media (E-F) resulted in fGEC not forming microvessel networks as seen previously both in 3D mono-culture and 3D tri-culture. fGEC culture media alone (G-H) on 3D tri-cultures resulted in poor Celprogen fPOD health, where cells were rounded in shape with no foot-like processes formed. (A-C and G) 10x magnification, (D-F and H-J) 20x magnification.

3D Tri-culture Techniques & Read-out Characterisation

Imaging

3D tri-cultures were imaged (Figure 23 and Figure 24) using fluorescent labelling of each cell type. fMCs were labelled blue using a Celltracker™ Blue CMAC dye, fPODs were labelled red using a cell membrane PKH26 dye. fGECs were initially labelled green using fluorescein-labelled ULEX (Figure 23), to acquire better images fGECs were instead transfected with GFP (Figure 24). The formation of vascular structures by the fGECs and their close interaction fPODs was demonstrated. fMCs are interspersed between fGECs or fPODs in 3D tri-cultures. These cellular interactions formed in the 3D tri-cultures mimic the cellular interactions of the glomerulus. To visualise fibrosis fluorescently labelled 3D tri-cultures treated with TGF-β (Figure 25) were analysed qualitatively. With TGF-β treatment increased cellular debris was noted, along with truncated fGEC vascular-like structures, which had fewer loops. The number of fMCs appeared increased in comparison to control 3D tri-cultures, whilst the number of fPODs decreased, and their morphology became more rounded with fewer fPODs interacting closely with the fGECs vascular-like structures. These responses to treatment with TGF-β are consistent with some of those seen in glomerulosclerosis *in vivo*.

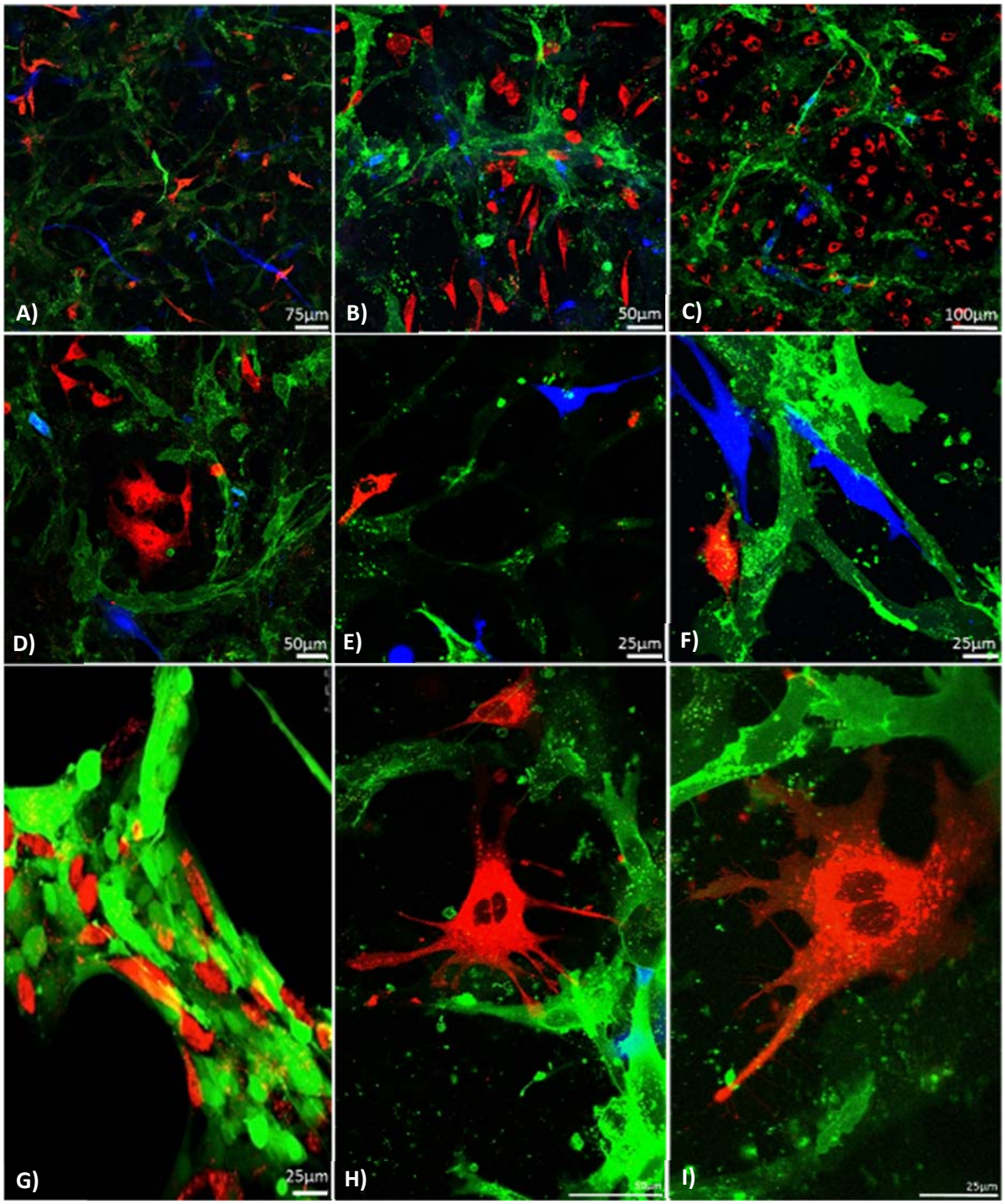

Figure 23. Imaging of fluorescently labelled 3D tri-cultures, Ulex.

fGECs (green, Ulex), Celprogen fPODs (red), and fMCs (blue) could be seen to interact closely. fGECs formed vascular-like structures with branching; long processes were formed by fPODs which extended and associated with the fGEC structures (G-I). fMCs could be seen to interact with both cell types (A-F). These images show that when grown in 3D co-culture these glomerular cell types interact and form structures like those is seen *in vivo*. (A-C) 10x magnification, (D-G) 20x magnification, (H-I) 63x magnification.

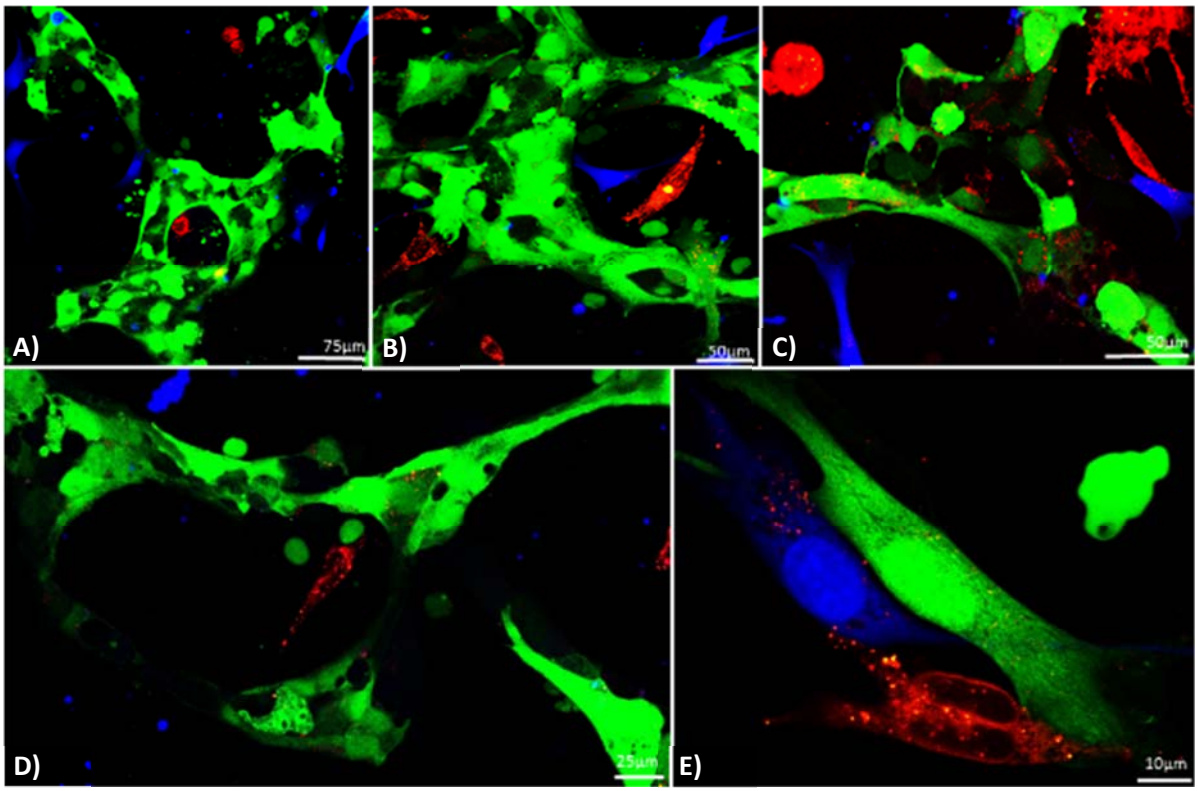

Figure 24. Imaging of fluorescently labelled 3D tri-cultures, GFP.

Celprogen fPODs (red) and fMCs (blue) were labelled in the same manner as Figure 23. fGECs (green) were transfected with GFP. GFP transfection provided better visualisation of the vascular-like structures that fGECs formed, such as branching, loops and vacuoles. The same close physical interaction between the three glomerular cell types was observed as in Figure 23. (A-D) 20x magnification, (E) 63x magnification.

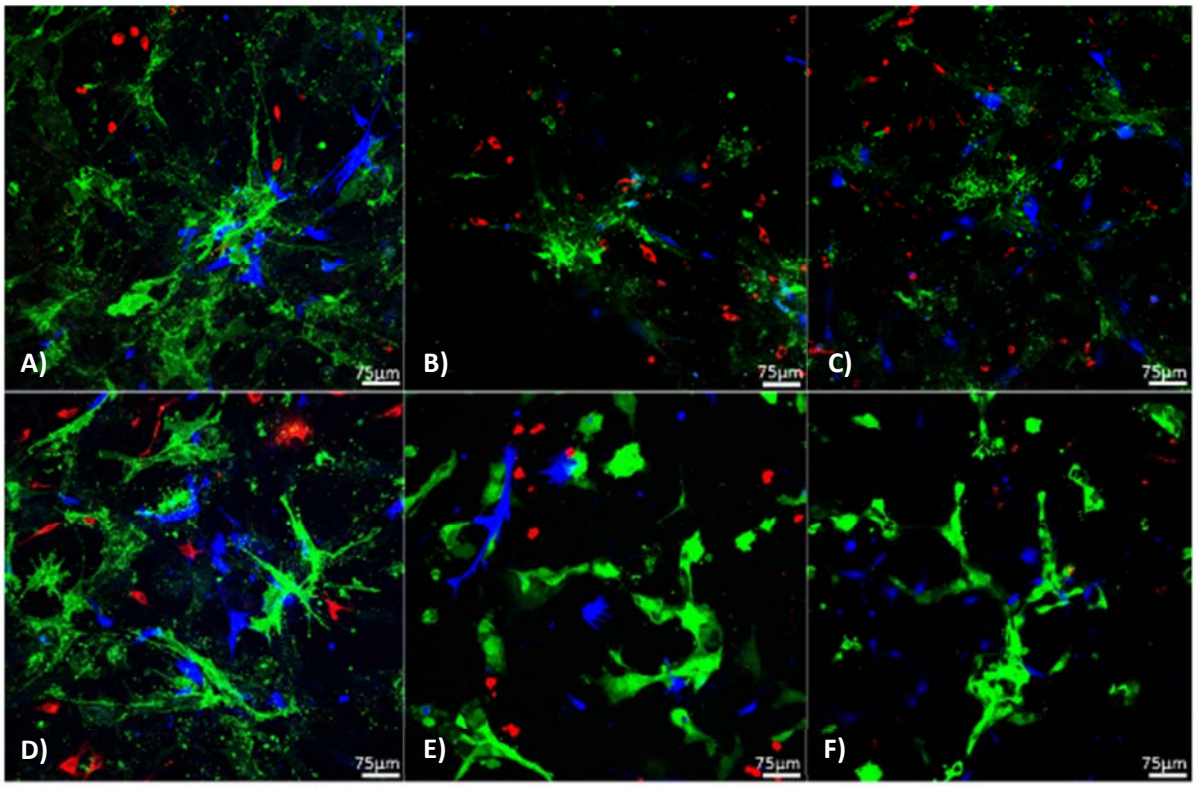

Figure 25. Imaging of fluorescently labelled 3D tri-culture treated with TGF-β.

Labelled in the same manner as Figure 24. Celprogen fPODs (red), fMCs (blue) and fGECs (green). In comparison to control 3D tri-cultures (Figure 23 and Figure 24), greater cell debris could be seen, along with greater numbers of fMCs. Celprogen fPODs became more rounded in morphology. 20x magnification.

Nodule Counts

One method of quantifying fibrosis in the 3D tri-culture system developed was counting the number of nodules formed. Previous work demonstrated that when culturing fMCs in 3D mono-culture, TGF-β treatments promoted the formation of nodules, which consisted of cells and ECM proteins; an analogous fibrotic response to fMC expansion and ECM deposition seen in glomerulosclerosis [201]. Upon formation of 3D tri-cultures and treatment with TGF-β for 24hrs such nodule formation was observed in this system also (Figure 26). Following the methodology of the previous works on quantifying nodules, this was performed by taking random images of each 3D tri-culture at 20x magnification using a bright field microscope and manually counting the number of nodules. A basal number of nodules could be seen in the 3D tri-culture system that significantly increased in number with TGF-β treatments (Figure 26). This supported the use of nodule number as a read-out of fibrosis in the 3D tri-culture model system.

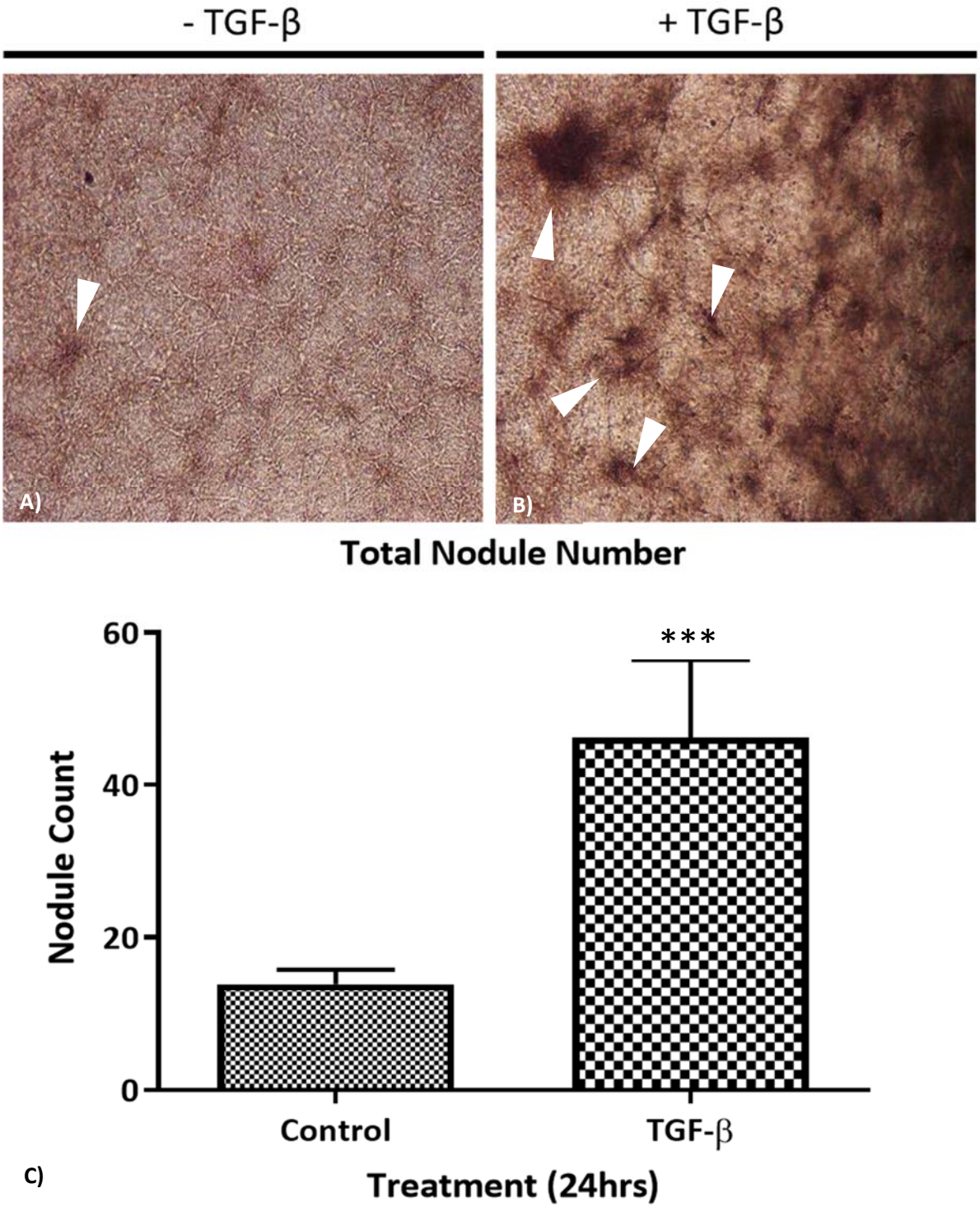

Figure 26. Nodule quantification in 3D tri-cultures.

Bright field images of nodules (white arrows) within 3D tri-cultures with (B) and without (A) TGF-β treatment for 24hrs. Graph (C) quantifies total nodule number counts with both control 3D tri-cultures and those which were treated with TGF-β for 24hrs. (A-B) 20x magnification. (C) N=4, SEM error bars, unpaired two-tailed t-test p-value 0.008; <0.001 (***)

To investigate this read-out further, human glomerular cells grown in 3D tri-culture were treated with either TGF-β and/or BMP7 (Figure 27). As expected, TGF-β treatment induced a significant increase in nodule formation. BMP7 treatment did not change nodule number from basal levels and did not affect TGF-β induced nodule formation. Demonstrating that BMP7 treatment could not prevent TGF-β evoked fibrosis in the 3D tri-culture, consistent with published data on fMCs cultured in 3D, where BMP7 treatment was also unable to prevent TGF-β induced nodule formation.[201]

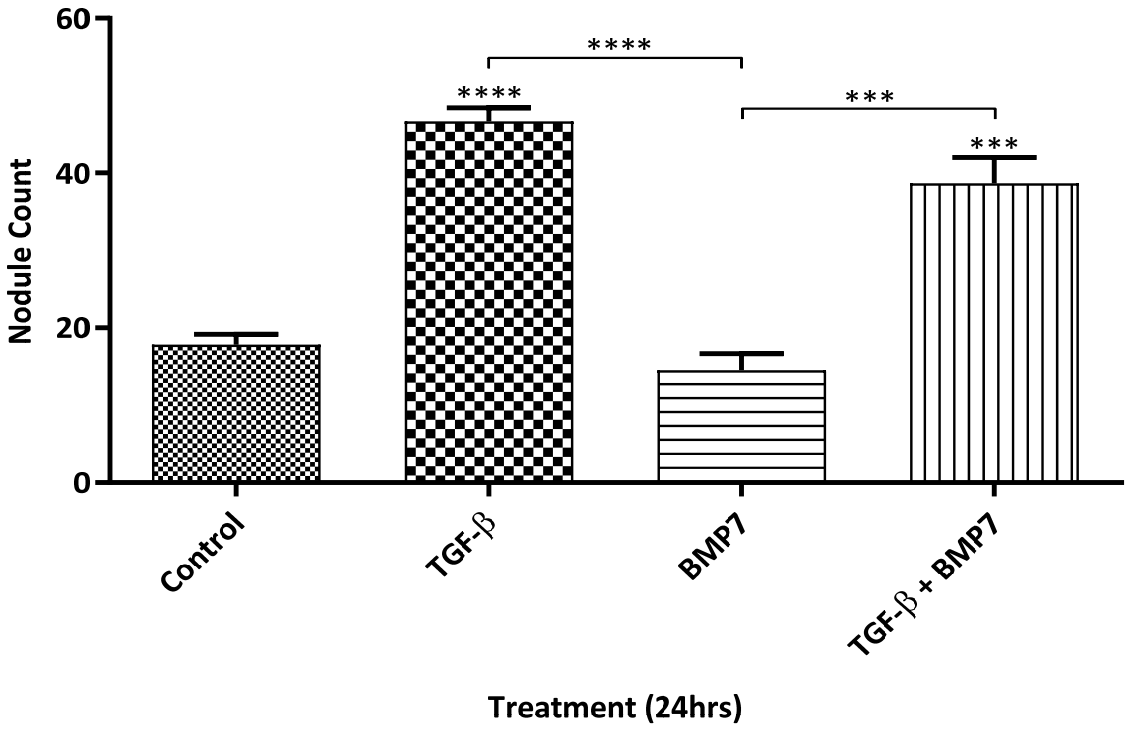

Figure 27. Nodule count of 3D tri-cultures treated with either TGF-β and/or BMP7.

Graph quantifying total nodule number counts in 3D tri-cultures treated with either TGF-β and/or BMP7 for 24hrs. N=3, SEM error bars, One-way ANOVA p-value 0.008; <0.0001 (****) followed by Tukey's multiple comparison post-test.

Preliminary work was made on developing a more high-throughput method for counting and quantifying nodule counts by using IF staining in 3D tri-cultures for collagen IV (Figure 28). Collagen IV being a contributor to nodules formed in previous reports.[201] Confocal images were analysed using HALO software, which measured the amount of collagen IV positive staining relative to nuclear DAPI staining, as well as the intensity of collagen IV staining (Figure 28). Five random images of an untreated and TGF-β treated 3D tri-culture gel were taken; this initial work picked up no difference in quantity or intensity of collagen IV staining between untreated and TGF-β treated 3D tri-cultures.

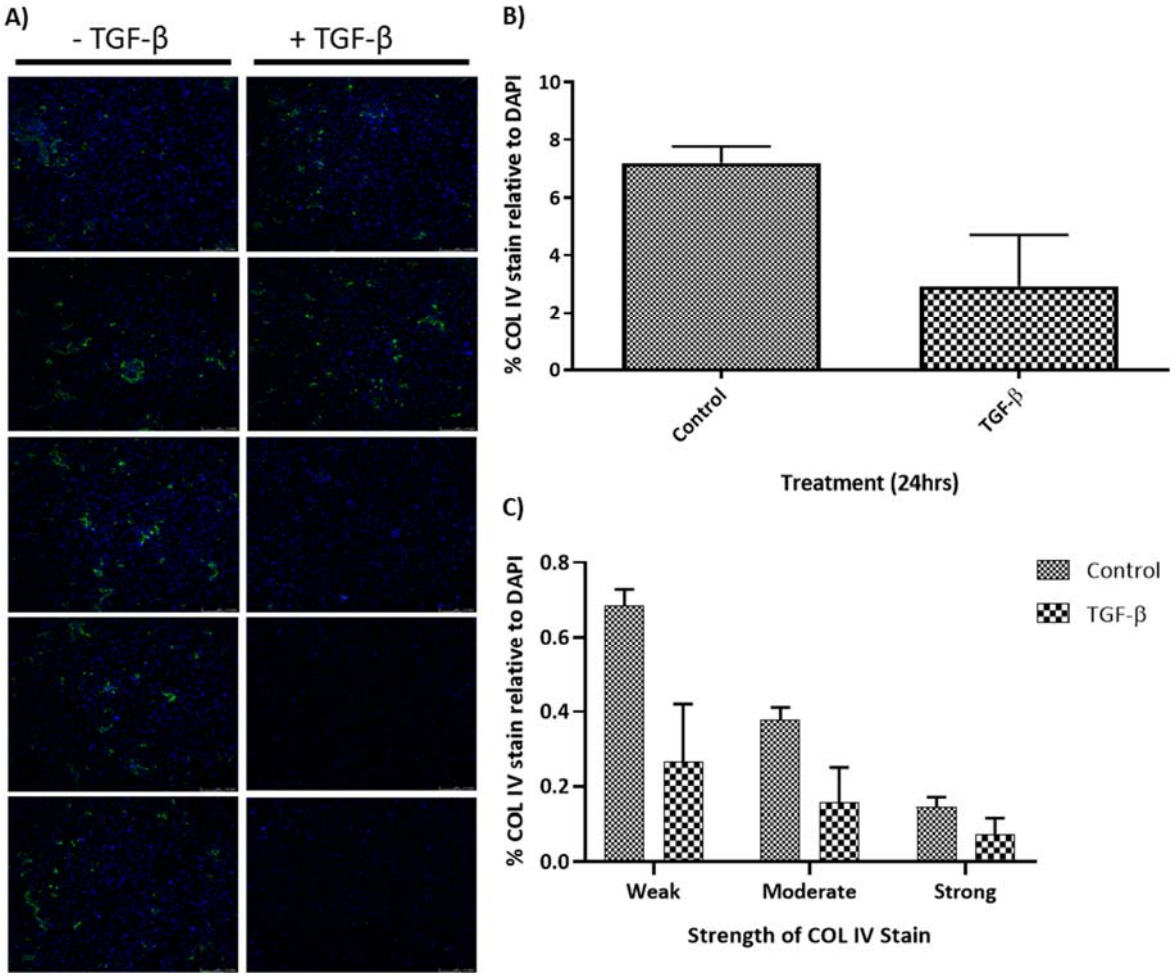

Figure 28. Preliminary HALO analysis for nodule quantification in 3D tri-cultures.

Five confocal images (A) were taken of collagen IV IF staining (green) within 3D tri-cultures both with and without TGF-β treatment for 24hrs. HALO analysis software was used to determine both the amount (B) of collagen IV staining relative to nuclear staining (blue, DAPI) and the intensity of that collagen IV staining (C). (A) 10x magnification. (B-C) N=1, SEM error bars.

RT-qPCR

Fibrosis, as well as other processes involved in kidney diseases, such as inflammation, were assessed using RT-qPCR to measure expression with known mediators. With the extraction of RNA being more

complex in 3D gel cultures as gel degradation is required, the methodology for RNA extraction from 3D tri-cultures required several rounds of optimisation to ensure both enough quantity and quality of RNA for RT-qPCR analysis of gene expression. This also changed with the different facilities available in MedImmune and Cambridge University laboratories.

Once the method of RNA extraction from 3D culture gels had been optimised, 3D tri-cultures treated with either TGF-β and/or BMP7 were analysed for changes in gene expression using RT-qPCR. This experimental set up also further explored the potential antagonism of TGF-β BMP7 could elicit in the 3D tri-culture system, with nodule counts (Figure 27) demonstrating that TGF-β induced nodule formation in the 3D tri-culture was not prevented by BMP7. Gene expression of COL1A1, COL4A1, CTGF, SMAD3, and PAI1 was analysed (Figure 29) to investigate genes involved in fibrotic, TGF-β signalling and inflammatory response. Expression of COL1A1 (Figure 29) was significantly different across treatments, with a similar non-statistically significant increase in expression with TGF-β treatment alone and in combination with BMP7. While BMP7 treatment appeared to have little effect, suggesting that BMP7 has no effect upon TGF-β induced COL1A1 expression in the 3D tri-culture model.COL4A1 expression (Figure 29) followed the same trend as COL1A1, demonstrating a pro-fibrotic effect of TGF β in 3D tri-culture that BMP7 did not affect. These data link with nodule data shown earlier where BMP7 treatment did not affect TGF-β stimulated nodule formation in 3D tri-culture (Figure 31).SMAD3 expression (Figure 29) significantly decreased with both TGF-β and co-treatments, whilst BMP7 treatment did not change SMAD3 expression from control levels. BMP7, therefore, had no effect upon TGF-β mediated downregulation of SMAD3 expression in 3D tri-culture. Expression of CTGF (Figure 29) was significantly increased with co-treatment compared to control expression levels. TGF-β treatment alone demonstrated a non-statistically significant increase in CTGF expression. BMP7 treatment did not change CTGF expression from control values, indicating BMP7 did not affect TGF-β mediated CTGF expression in 3D tri-culture. Expression of PAI1 (Figure 29) followed the same pattern as CTGF expression with treatments, however, the average fold-changes recorded were much higher for PAI1. Again, BMP7 appeared to have little effect upon TGF-β mediated gene expression.

These data demonstrate the opposing effects of TGF-β and BMP7, where TGF-β evoked increased expression of COL1A1, COL4A1, CTGF, and PAI1. While SMAD3 expression was decreased. BMP7 evoked no change in expression in these genes implicated in fibrosis; despite sharing a common signalling pathway.

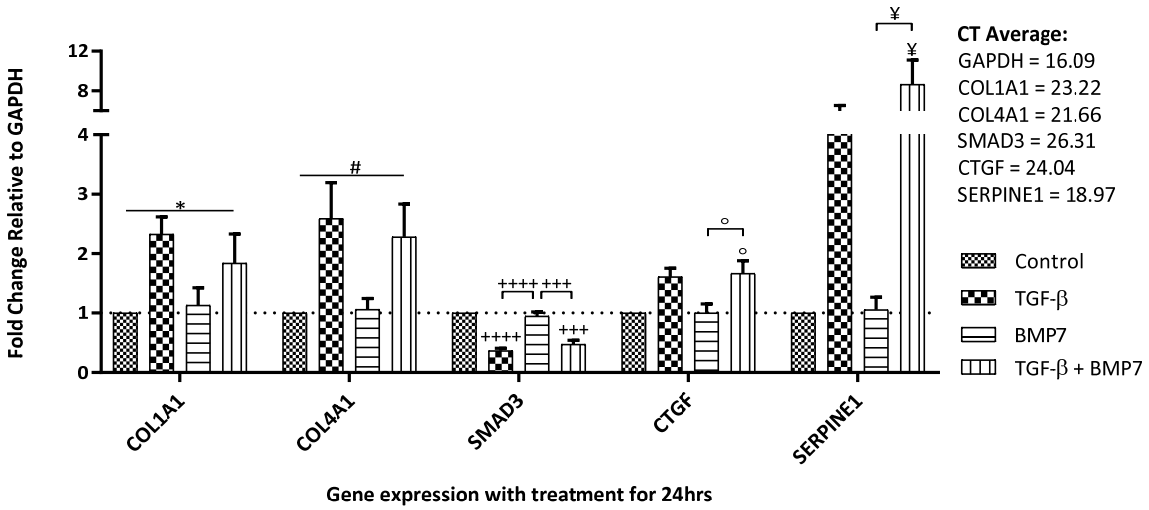

Figure 29. RT-qPCR performed on 3D tri-cultures treated with TGF-β and/or BMP7 for 24hrs.
ΔΔCT analysis to look at the relative fold-change of the gene of interest against housekeeping gene GAPDH with either TGF-β and/or BMP7 treatment for 24hrs. N=3 (COL1A1 & COL4A1), N=4 (CTGF, SMAD3 & PAI1), SEM error bars, One-way ANOVA; COL1A1 p-value 0.0406 (*); COL4A1 p-value 0.0380 (#); SMAD3 p-value < 0.0001(++++); CTGF p-value 0.0093 (°°); PAI1 p value 0.0055 (¥¥); followed by Tukey's multiple comparison post-tests. CT averages of each gene for reference.

The results detailed in this chapter outline the development and optimisation of the 3D tri-culture model, as well as the read-outs developed to examine fibrosis in the system. These results demonstrate that in the 3D tri-culture system TGF-β can induce fibrosis that can be measured using nodule counts and analysis of gene expression using RT-qPCR. IF can be used to visualise the 3D tri-culture system and how the three glomerular cell types interact. This was used to further employ the 3D tri-culture model to investigate cytokines and potential targets of glomerulosclerosis.

Chapter 6 – Results: 3D Tri-culture Model, Cytokines & Growth Factors

Following the development and optimisation of the 3D tri-culture system and read-outs of fibrosis, the culture system was used to study several cytokines and growth factors implicated in glomerulosclerosis. The cytokines and growth factors chosen for this work have been discussed in the literature review. This chapter will be separated into sections for each cytokine/combination of cytokines.

3D tri-cultures were first developed with Celprogen fPODs. However, upon detection of CHO cells in Celprogen fPOD cultures, Lonza fPODs were validated and used as an alternative. The specific fPOD type used has been specified throughout.

TGF-β & TNF-α

Human glomerular cells grown in 3D tri-culture were treated with either TGF-β and/or TNF-α. Examining if TNF-α treatment evoked an inflammatory response, how these cytokines interacted in combination, and in particular if TNF-α modulated TGF-β mediated nodule formation. Read-outs of nodule formation and gene expression were used in these experiments.

Nodule Counts

3D tri-cultures were treated with either TGF-β and/or TNF-α for 24hrs before nodule counts. Due to gel contractions, no nodule counts were made for Lonza fPOD 3D tri-cultures.

Nodule counts of Celprogen fPOD 3D tri-cultures (Figure 30) demonstrated the previously documented significant increase in nodule number with TGF-β. TNF-α treatment had no effect upon nodule count alone or in combination with TGF-β, implying TNF-α did not affect fibrosis in terms of upregulated ECM production.

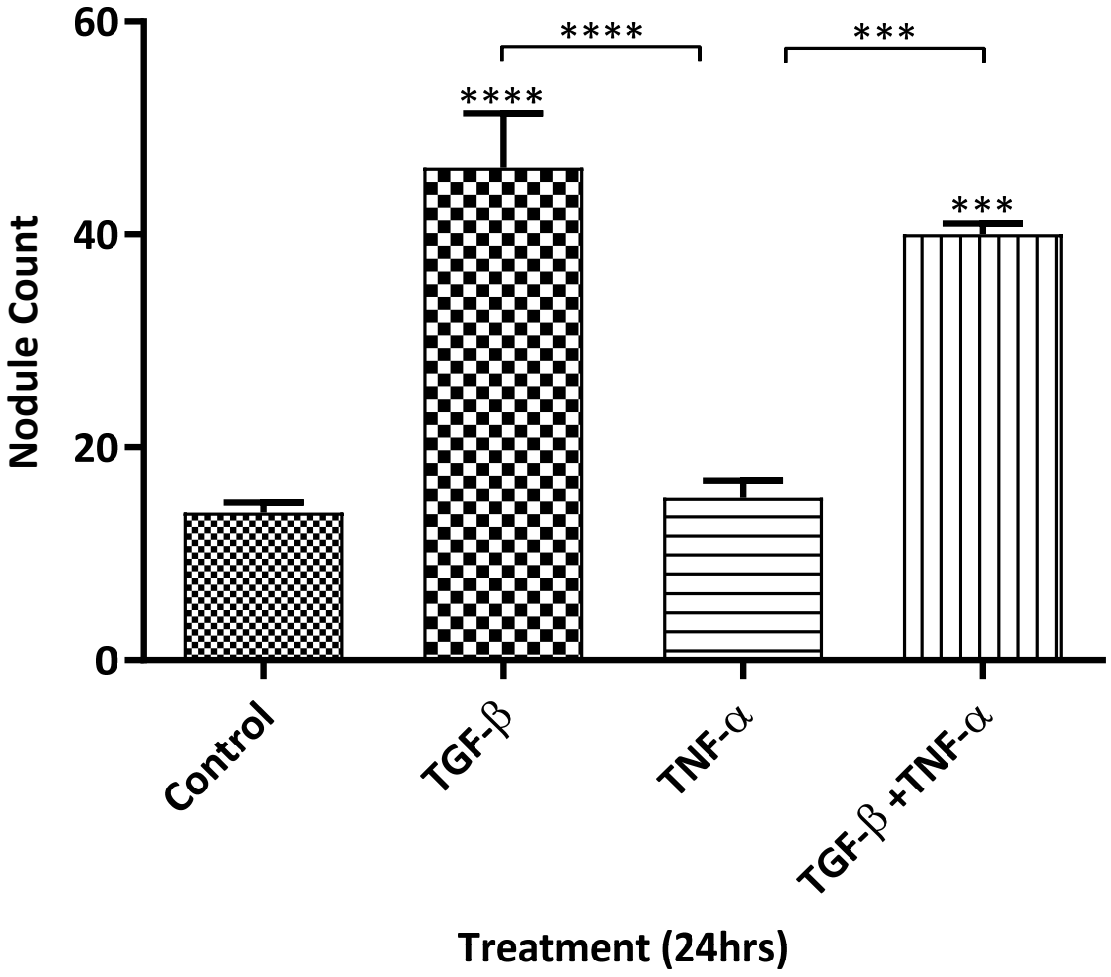

Figure 30. Nodule counts with TGF-β and TNF-α treatments in Celprogen fPOD 3D tri-cultures.

Celprogen 3D tri-cultures were treated with either TGF-β and/or TNF-α for 24hrs before nodule counts. TGF-β evoked a significant increase in nodule number compared to control. N=4, SEM error bars, One-way ANOVA p-value <0.0001 (****), followed by Tukey's multiple comparison post-tests.

RT-qPCR

The effects of TGF-β and TNF-α treatments in the 3D tri-culture model were further investigated by examination of gene expression. Gene expression of ECM proteins, mediators, and downstream effectors of TGF-β, along with gene expression of inflammatory proteins were investigated.

Celprogen fPOD 3D tri-cultures

COL1A1 expression (Figure 31) increased without statistical significance to almost a 3 fold-change average value with TGF-β treatment compared to control, which was significantly higher than the COL1A1 expression evoked by TNF-α treatment that decreased below control values without statistical significance. Co-treatment did not evoke a change in COL1A1 expression from control values, indicating the overall effect of TGF-β mediated increased COL1A1 expression is prevented by TNF-α. Comparing the average CT value for COL1A1 to GAPDH, as well as the other genes investigated, demonstrate that COL1A1 has the highest average CT value at 28.31, indicating that COL1A1 expression overall was lower than other genes tested.

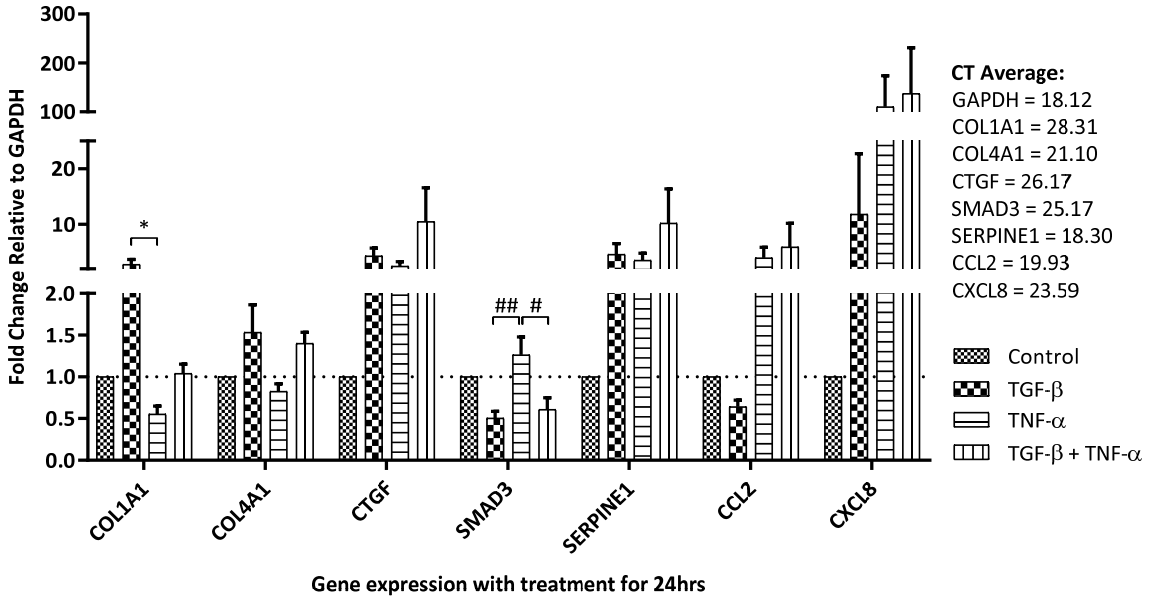

Figure 31. Gene expression with TGF-β and TNF-α treatments in Celprogen fPOD 3D tri-cultures.

RT-qPCR performed on Celprogen fPOD 3D tri-cultures treated with TGF-β and/or TNF-α for 24hrs. ΔΔCT analysis to look at the relative fold-change of the gene of interest against housekeeping gene GAPDH. N=4, SEM error bars, One-way ANOVA; COL1A1 p-value 0.0164 (*); COL4A1 p-value 0.0589 (ns); CTGF p-value 0.2127 (ns); SMAD3 p-value 0.0060 (**); SERPINE1 p-value 0.2940 (ns); CCL2 p-value 0.3566 (ns); CXCL8 p-value 0.2699 (ns); followed by Tukey's multiple comparison post-tests. CT averages of each gene for reference.

Expression of COL4A1 (Figure 31) increased without statistical significance with TGF-β and co-treatments to a similar fold-change value. Data suggestive of that COL4A1 expression is unaffected by TNF-α. Expression of both CTGF and SERPINE1 (Figure 31) was observed to increase without reaching statistical significance with all treatments, mostly with co-treatment. Expression of SMAD3 (Figure 31) was significantly increased by TNF-α treatment compared to TGF-β and co-treatments, which both followed a trend of downregulation from control that did not reach statistical significance. Expression of CCL2 (Figure 31) increased without statistical significance with both TNF-α and co-treatment, with co-treatment eliciting the higher average fold-change. TGF-β induced a non-statistically significant decrease in CCL2 expression. This data suggests that in 3D tri-culture TGF-β and TNF-α may evoke an additive increase in CCL2 expression which *in vivo* would likely result in an inflammatory response. CXCL8 expression (Figure 31) increased without statistical significance with all treatments, increasing in fold-change average from TGF-β to TNF-α and co-treatment.

These Celprogen fPOD 3D tri-culture data display the differential effects TGF-β and TNF-α have upon expression levels of these genes implicated in fibrosis and that when used together they can have an inhibitory effect upon the other or have a potentially cooperative effect. TGF-β mediated COL1A1 expression is prevented by TNF-α yet this is not the case with COL4A1 and tying this information with nodule data (Figure 30) suggests COL4A1, not COL1A1 is likely the major contributor of nodule formation.

Lonza fPOD 3D tri-cultures

3D tri-cultures using Lonza fPODs were used to repeat the TGF-β and TNF-α experiment outlined above in Celprogen fPOD 3D tri-cultures to validate this data post detection of CHO contamination. A larger panel of genes was examined in these experiments, separated into broad categories of ECM genes, TGF-β signalling genes, and other genes of interest.

The average CT values of ECM genes demonstrated good amounts of target gene RNA in these samples (Figure 32). Expression of COL1A1 (Figure 32) significantly increased with treatment with TGF-β, while treatment with TNF-α and co-treatment did not change expression from control values. This increase in expression with TGF-β reproducing the trend seen in Celprogen fPOD 3D tri-cultures (Figure 31), which was prevented by co-treatment with TNF-α. No change in COL3A1 expression (Figure 32) expression was seen with any treatment. Expression of COL4A1 (Figure 32) was not significantly changed with any treatments, although the general pattern followed that seen with Celprogen fPOD 3D tri-cultures (Figure 31). No statistical significance in changed ACTA2 expression was seen across treatments (Figure 32), but SEM was large between replicates. A trend could be seen, where expression appeared increased with either TGF-β treatment alone or in combination

with TNF-α. Similarly, no statistical significance in changes of FN1 expression was seen, but there was a trend to increased FN1 expression with TGF-β treatment and co-treatment. Expression of LAMB2 (Figure 32) was the final ECM studied in these experiments, which demonstrated a significant increase in LAMB2 expression with co-treatment. Overall the data presented in Figure 32 broadly demonstrates the general pattern of increased ECM gene expression with TGF-β treatment, which TNF-α had little effect upon. The exceptions being COL1A1 where TNF-α attenuated the effect of TGF-β and LAMB2, where TNF-α appeared to be the main driver for increased LAMB2 expression.

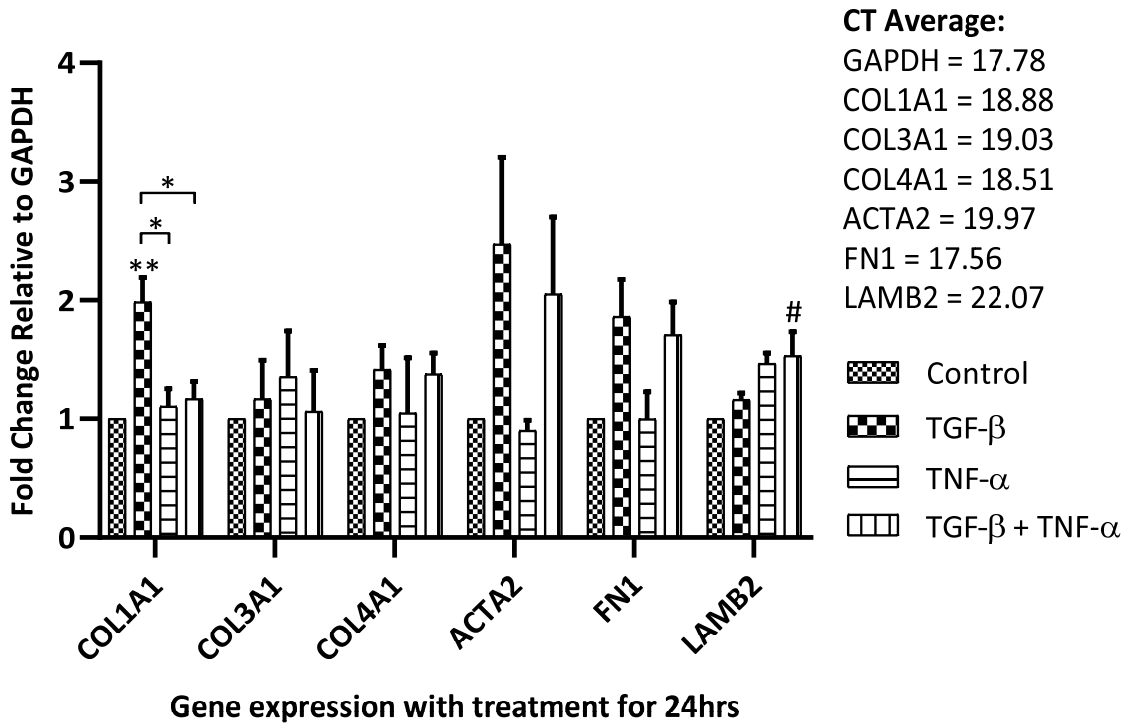

Figure 32. ECM gene expression with TGF-β and TNF-α treatments in Lonza fPOD 3D tri-cultures.
RT-qPCR performed on Lonza fPOD 3D tri-cultures treated with TGF-β and/or TNF-α for 24hrs. ΔΔCT analysis to look at the relative fold-change of the gene of interest against housekeeping gene GAPDH. N=3, SEM error bars, One-way ANOVA; COL1A1 p-value 0.0055 (**); COL3A1 p-value 0.8540 (ns); COL4A1 p-value 0.6061 (ns); ACTA2 p-value 0.1335 (ns); FN1 p-value 0.0612 (ns); LAMB2 p-value 0.0328 (*); followed by Tukey's multiple comparison post-tests. CT averages of each gene for reference.

Genes involved in TGF-β signalling or downstream mediators of TGF-β (Figure 33) were examined. The average CT values of these genes were generally demonstrative of good amounts of target gene RNA in these samples, except BMP7, where the high value indicated that BMP7 was not expressed to a great extent in these samples. CTGF expression (Figure 33) was significantly upregulated with TGF-β alone and in co-treatment compared to treatment with TNF-α alone. This differs from the pattern of expression seen in Celprogen fPOD 3D tri-cultures (Figure 31), where all treatments resulted in a non-significant trend of increased CTGF expression.

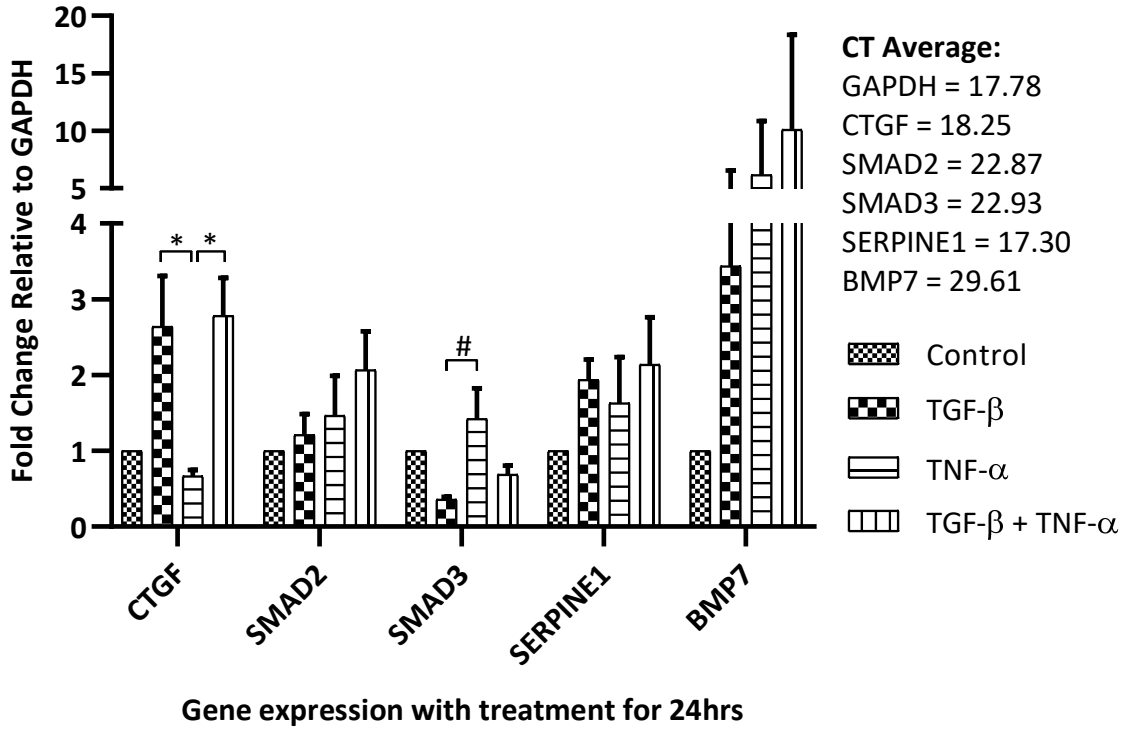

Figure 33. TGF-β signalling gene expression with TGF-β and TNF-α treatments in Lonza fPOD 3D tri-cultures.

RT-qPCR performed on Lonza fPOD 3D tri-cultures treated with TGF-β and/or TNF-α for 24hrs. ΔΔCT analysis to look at the relative fold-change of the gene of interest against housekeeping gene GAPDH. N=3, SEM error bars, One-way ANOVA; CTGF p-value 0.0138 (*); SMAD2 p-value 0.3117 (ns); SMAD3 p-value 0.0357 (*); SERPINE1 p-value 0.3735 (ns); BMP7 p-value 0.6263 (ns); followed by Tukey's multiple comparison post-tests. CT averages of each gene for reference.

SMAD2 expression (Figure 33) remained statistically unchanged across all treatments. A trend of increased expression with TNF-α treatment alone and in combination with TGF-β could be seen, however, differences in replicate values gave no statistical significance to this. Expression of SMAD3 (Figure 33) was significantly decreased with TGF-β treatment compared to treatment with TNF-α. The pattern of SMAD3 expression with treatments followed that seen in Celprogen fPOD 3D

tri-cultures (Figure 31), where TGF-β alone and in co-treatment evoked a downregulation in SMAD3 expression. Expression of SERPINE1 (Figure 33) did not demonstrate any statistically significant change in expression across any treatment. All treatments did appear to upregulate SERPINE1 expression to some degree, mimicking the data obtained from Celprogen fPOD 3D tri-cultures (Figure 31). BMP7 expression (Figure 33) remained statistically unaffected with any treatment. However, it did appear that all treatments could evoke some upregulation in BMP7 gene expression.

Overall the data presented in Figure 33 demonstrates that both TGF-β and TNF-α treatments in the 3D tri-culture were having some impact upon downstream mediators of TGF-β. TGF-β evoked a significant increase in CTGF expression, while both TGF-β and TNF-α demonstrated a trend to evoked SERPINE1 and BMP7 expression to some degree, which did not reach significance. SMAD3 expression was downregulated by TGF-β, which co-treatment with TNF-α could not prevent.

Inflammatory genes CCL2 and CXCL8 were also investigated; alongside TGM2 and CTNNB1, both of which are implicated in fibrosis development and progression (Figure 34). The average CT values of these genes were demonstrative of good amounts of target gene RNA in these samples. Expression of CCL2 (Figure 34) was not changed with any statistical significance with any treatment. The data appears to demonstrate some degree of CCL2 upregulation with TGF-β and TNF-α treatments. TGM2 expression (Figure 34) was significantly decreased with TGF-β treatment alone and in combination with TNF-α compared to control values, while TNF-α treatment alone did not affect TGM2 expression. Expression of CTNNB1 (Figure 34) was not significantly altered with any treatment in these experiments. There did appear to be some small degree of upregulation evoked by TGF-β and TNF-α treatments. Expression of CXCL8 (Figure 34) was significantly increased with co-treatment of TGF-β and TNF-α in the 3D tri-culture. Treatment with TNF-α alone appeared to evoke an increase in CXCL8 expression, but this was not statistically significant. This data partially replicates that seen with Celprogen fPOD 3D tri-cultures (Figure 31) where both TNF-α treatment alone and in combination with TGF-β appeared to evoke an increase in CXCL8 expression.

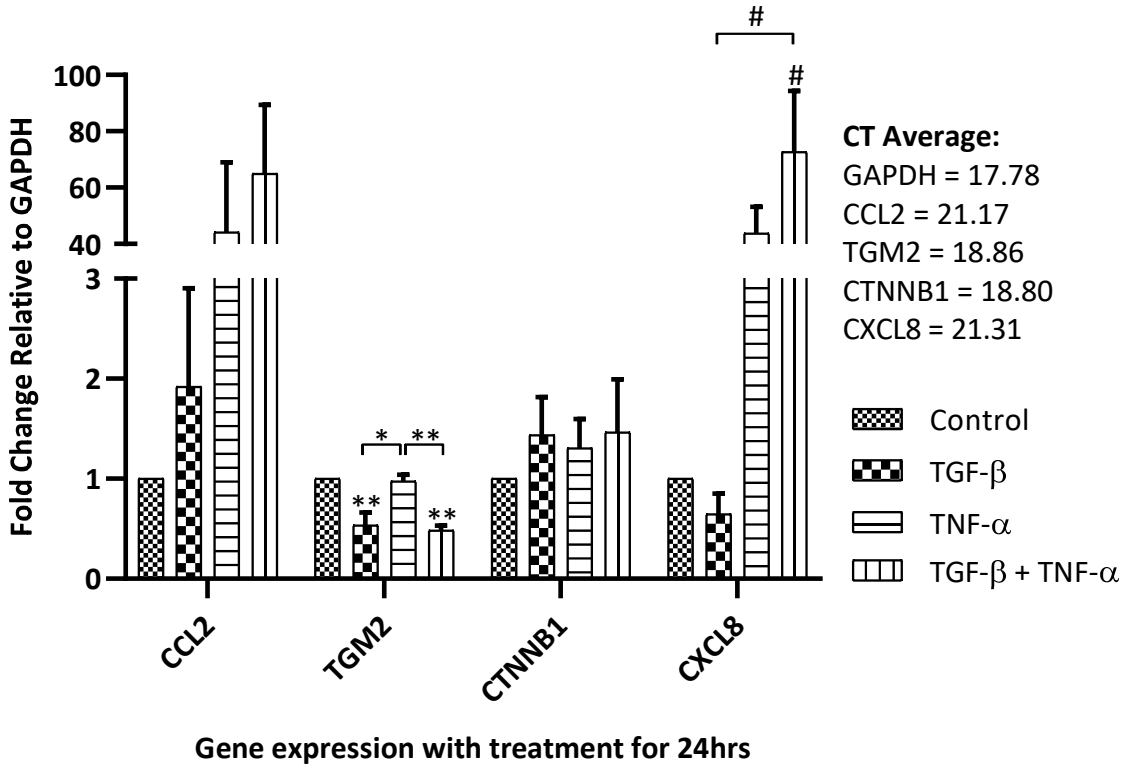

Figure 34. Expression of other genes of interest in Lonza fPOD 3D tri-cultures treated with TGF-β and TNF-α.

RT-qPCR performed on Lonza fPOD 3D tri-cultures treated with TGF-β and/or TNF-α for 24hrs. ΔΔCT analysis to look at the relative fold-change of the gene of interest against housekeeping gene GAPDH. N=3, SEM error bars, One-way ANOVA; CCL2 p-value 0.0771 (ns); TGM2 p-value 0.0017 (**); CTNNB1 p-value 0.7864 (ns); CXCL8 p-value 0.0062 (**); followed by Tukey's multiple comparison post-tests. CT averages of each gene for reference.

Overall, TGF-β and TNF-α can have additive effects upon gene expression in the 3D tri-culture system (Figure 34). The cytokines appear to have some cooperative, additive effect in terms of inflammatory genes, CCL2 and CXCL8. Whereas TGM2 is downregulated by TGF-β treatment and unaffected by TNF-α.

The nodule and RT-qPCR data presented in Figure 30-Figure 34 where cytokines TGF-β and TNF-α were used in the 3D tri-culture model demonstrates opposing, cooperative and additive effects between these two cytokines, which represent fibrosis and inflammation. In general, the response of 3D tri-cultures containing either Celprogen fPODs or Lonza fPODs was consistent. ECM genes were mostly upregulated by TGF-β while TNF-α had little effect. The exception being that in co-treatment, TNF-α prevented the TGF-β evoked upregulation of COL1A1 expression (Figure 31-43). Tying this data to nodule data (Figure 30), where TNF-α did not affect TGF-β induced nodule formation,

suggesting COL1A1 is not a major contributor to nodule formation, and COL4A1 may be. Downstream mediators of TGF-β responded to TGF-β treatment in the 3D tri-culture model, and overall remained unaffected by TNF-α treatment. Co-treatment did appear to result in some cooperative action between the two cytokines promoting greater responses in gene expression, with BMP7 expression for example (Figure 31 and Figure 33). In terms of inflammatory genes CCL2 and CXCL8, co-treatment appeared cooperative and additive in promoting expression (Figure 31 and Figure 34). Average CT values provided a rough idea of overall expression levels in 3D tri-culture samples, genes were overall well expressed, with values slightly higher in Celprogen fPOD 3D tri-cultures than Lonza fPOD 3D tri-cultures.

TGF-β, CTGF nAb & ALK5i

The 3D tri-culture model was treated with either TGF-β, CTGF nAb and/or ALK5i. BMP7 treatment was unable to inhibit TGF-β evoked fibrosis in the system, so other potential targets were explored. A CTGF nAb was tested to understand the contribution that TGF-β induced CTGF had in promoting fibrosis in the culture system, along with examining the effect of ALK5 inhibition to prevent the majority of TGF-β signalling. ALK5 inhibition had been shown to prevent TGF-β induced nodule formation in 3D fMC cultures.[201] Read-outs of nodule formation and gene expression were used in these experiments. Only 3D tri-cultures using Celprogen fPODs were used in these experiments.

Nodule Counts

3D tri-cultures were treated with either TGF-β, CTGF nAb, and/or ALK5i for 24hrs before nodule counts. Nodule counts (Figure 35) demonstrated the expected increase in nodule number with TGF-β treatment, and while both CTGF nAb and ALK5i treatments did appear to reduce TGF-β evoked nodule formation, both CTGF nAb and ALK5i used in combination were required to significantly reduce nodule formation induced by TGF-β to control values. This data demonstrates a difference from that of 3D fMCs, where ALK5i was sufficient to prevent TGF-β induced nodule formation. This suggests the interplay between the three glomerular cell types in the 3D tri-culture model was playing a role here with the synergistic relationship between CTGF and TGF-β.

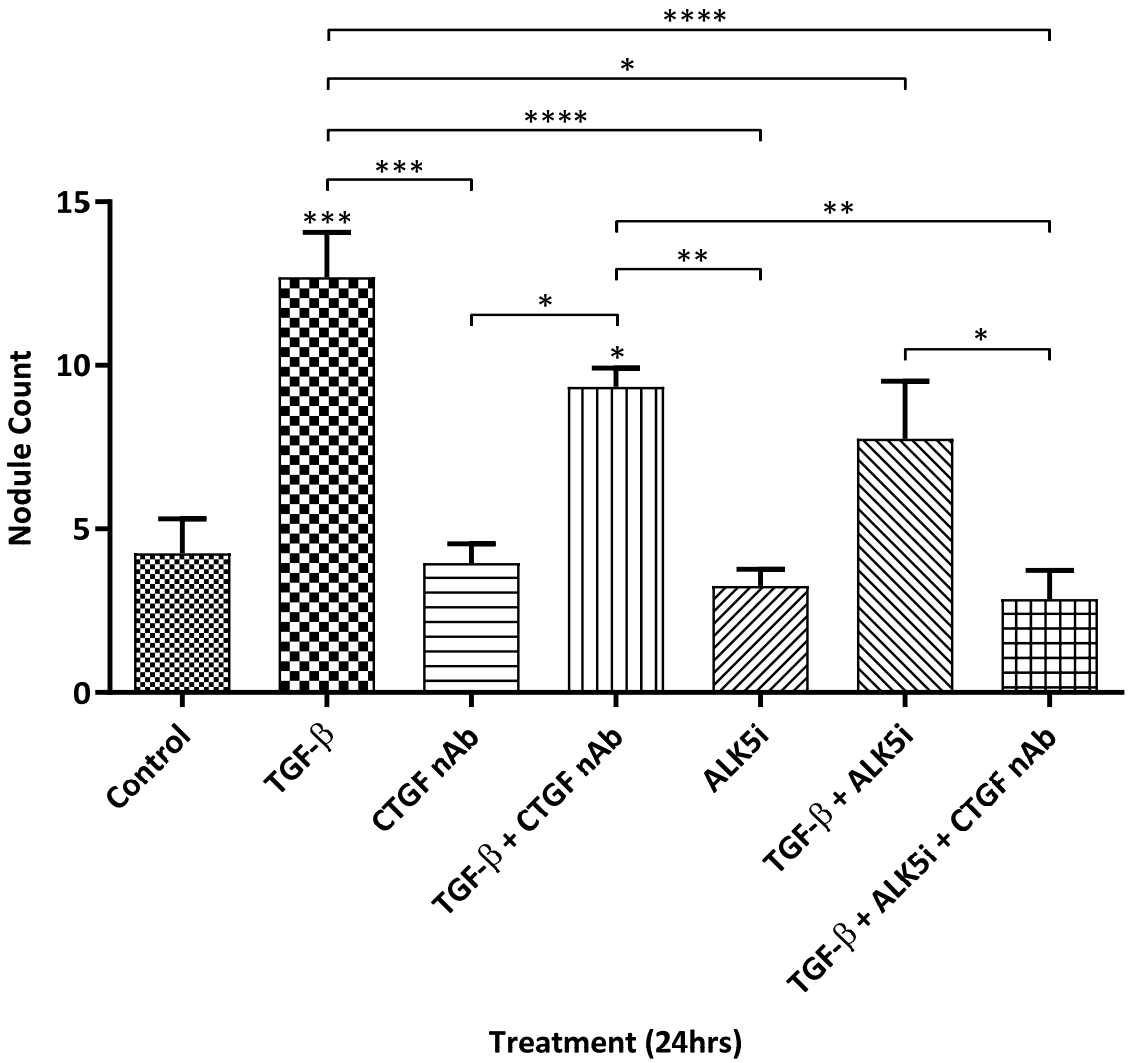

Figure 35. Nodule counts with TGF-β, CTGF nAb and ALK5i treatments in Celprogen fPOD 3D tri-cultures.

Celprogen fPOD 3D tri-cultures were treated with either TGF-β, CTGF nAb, and/or ALK5i for 24hrs before nodule counts. TGF-β evoked a significant increase in nodule number, which was prevented by co-treatments of CTGF nAb and ALK5i. N=4, SEM error bars, One-way ANOVA p-value <0.0001 (****), followed by Tukey's multiple comparison post-tests.

RT-qPCR

The effects of CTGF nAb and ALK5i upon TGF-β treatment in the 3D tri-culture model were further investigated by examination of gene expression. Gene expression of COL1A1, COL4A1 and CTGF itself were examined (Figure 36). The average CT values of COL1A1 and COL4A1 demonstrated reasonable expression levels within these samples. However, the average CT value CTGF was 27.61 in these samples, indicating that CTGF was not highly expressed. COL1A1 expression (Figure 36) was significantly increased with TGF-β treatment, this was also true for TGF-β treatment with CTGF nAb; indicating that endogenous CTGF was not necessary for the exogenous TGF-β mediated response of increased COL1A1 expression. ALK5i treatment significantly decreased TGF-β stimulated COL1A1 expression. Treatment of TGF-β, CTGF nAb and ALK5i together did not change COL1A1 expression from control values.

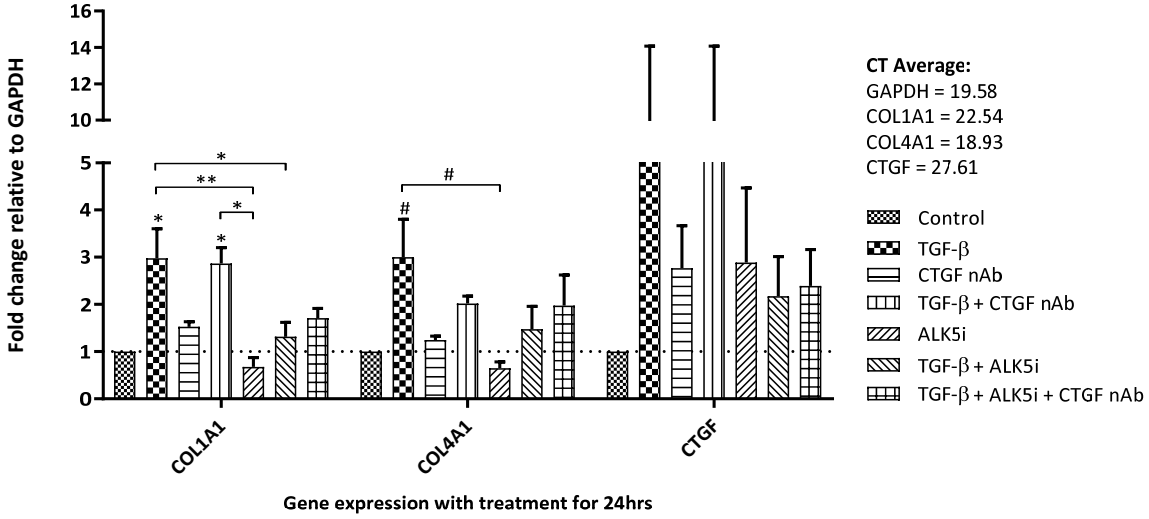

Figure 36. Gene expression with TGF-β, CTGF nAb and ALK5i treatments in Celprogen fPOD 3D tri-cultures.

RT-qPCR performed on Celprogen fPOD 3D tri-cultures treated with TGF-β, CTGF nAb and/or ALK5i for 24hrs. ΔΔCT analysis to look at the relative fold-change of the gene of interest against housekeeping gene GAPDH. N=5 (Control, TGF-β, CTGF nAb & TGF-β + CTGF nAb), N=4 (TGF-β + ALK5i), N=3 (ALK5i & TGF-β + ALK5i + CTGF nAb), SEM error bars, One-way ANOVA; COL1A1 p-value 0.0024 (**); COL4A1 p-value 0.0182 (*); CTGF p-value 0.2236 (ns); followed by Tukey's multiple comparison post-tests. CT averages of each gene for reference.

This data demonstrates the significance ALK5 has in TGF-β mediated COL1A1 expression, the relevance of this is limited however in light of data presented earlier that COL1A1 is likely not a major contributor to nodule formation in the 3D tri-culture system. Expression of COL4A1 (Figure 36) was significantly increased almost 3-fold with TGF-β treatment, which was significantly higher than the

expression levels of COL4A1 evoked by ALK5i treatment alone. Thus, highlighting the important role of ALK5 in COL4A1 expression. Co-treatment of TGF-β and ALK5i decreased COL4A1 expression without statistical significance. CTGF nAb treatments resulted in COL4A1 expression that did not significantly increase above control values. Neither CTGF nAb or ALK5i treatment in combination with TGF-β stimulation resulted in a significant decrease in COL4A1 expression compared to TGF-β treatment alone, it suggests there is potentially another driver in COL4A1 expression in 3D tri-culture. CTGF expression (Figure 36) increased without statistical significance with TGF-β treatment, when CTGF nAb was used in combination with TGF-β this expression level decreased without statistical significance but not to control values; indicating that endogenous CTGF inhibition is not sufficient to inhibit CTGF expression levels induced by TGF-β. ALK5i treatments demonstrate that TGF-β signalling mediated by ALK5 is necessary for a portion of CTGF expression.

This data demonstrates the pivotal role of ALK5 mediated TGF-β signalling in increased expression levels of COL1A1, COL4A1, and CTGF, genes implicated in the fibrotic process. CTGF appears to play a role in COL4A1 expression levels, as CTGF neutralisation treatments resulted in COL4A1 expression levels which did not significantly increase, unlike COL1A1 where CTGF nAb did not alter TGF-β induced expression.

Nodule and RT-qPCR data presented in Figure 35-Figure 36 highlights the importance of both ALK5 and CTGF in the development of fibrotic response in the 3D tri-culture model. Blockade of both was required to inhibit TGF-β induced nodule formation, while the effects upon a small selection of fibrotic genes were more complex. This indicated other pro-fibrotic mediators were involved, highlighting the need for further investigation. Average CT values generally demonstrated good expression levels within these data; expression of CTGF appeared low.

TGF-β, TNF-α & CTGF nAb

The 3D tri-culture model was treated with either TGF-β, TNF-α and/or CTGF nAb. Presented data has demonstrated that TNF-α could attenuate the TGF-β mediated increase in COL1A1 gene expression in the 3D tri-culture system, but not COL4A1. The data also showed a trend towards CTGF nAb lessening TGF-β mediated COL4A1 gene expression, but this was not statistically significant. Nodule numbers were unaffected by TNF-α treatment, suggesting COL4A1 and not COL1A1 was a major contributor to nodules formed with TGF-β treatment. In light of this, an experiment was designed to test the CTGF nAb alongside TGF-β, TNF-α and co-treatments to determine whether TNF-α treatment and CTGF neutralisation in combination could ameliorate TGF-β nodule formation. Only 3D tri-cultures using Celprogen fPODs were used in these experiments.

Nodule Counts

3D tri-cultures were treated with either TGF-β, TNF-α, and/or CTGF nAb for 24hrs before nodule counts. As anticipated nodule counts (Figure 37) TGF-β induced the significant increase in nodule number seen in all previous experiments. As with previous data, TNF-α treatment did not evoke nodule formation and did not significantly reduce TGF-β evoked nodule formation. CTGF nAb treatment did significantly decrease TGF-β evoked nodule formation, however not to control values. Unlike data presented earlier, CTGF nAb treatment alone significantly increased nodule counts compared to control values and TNF-α treatment reduced this response to control values.

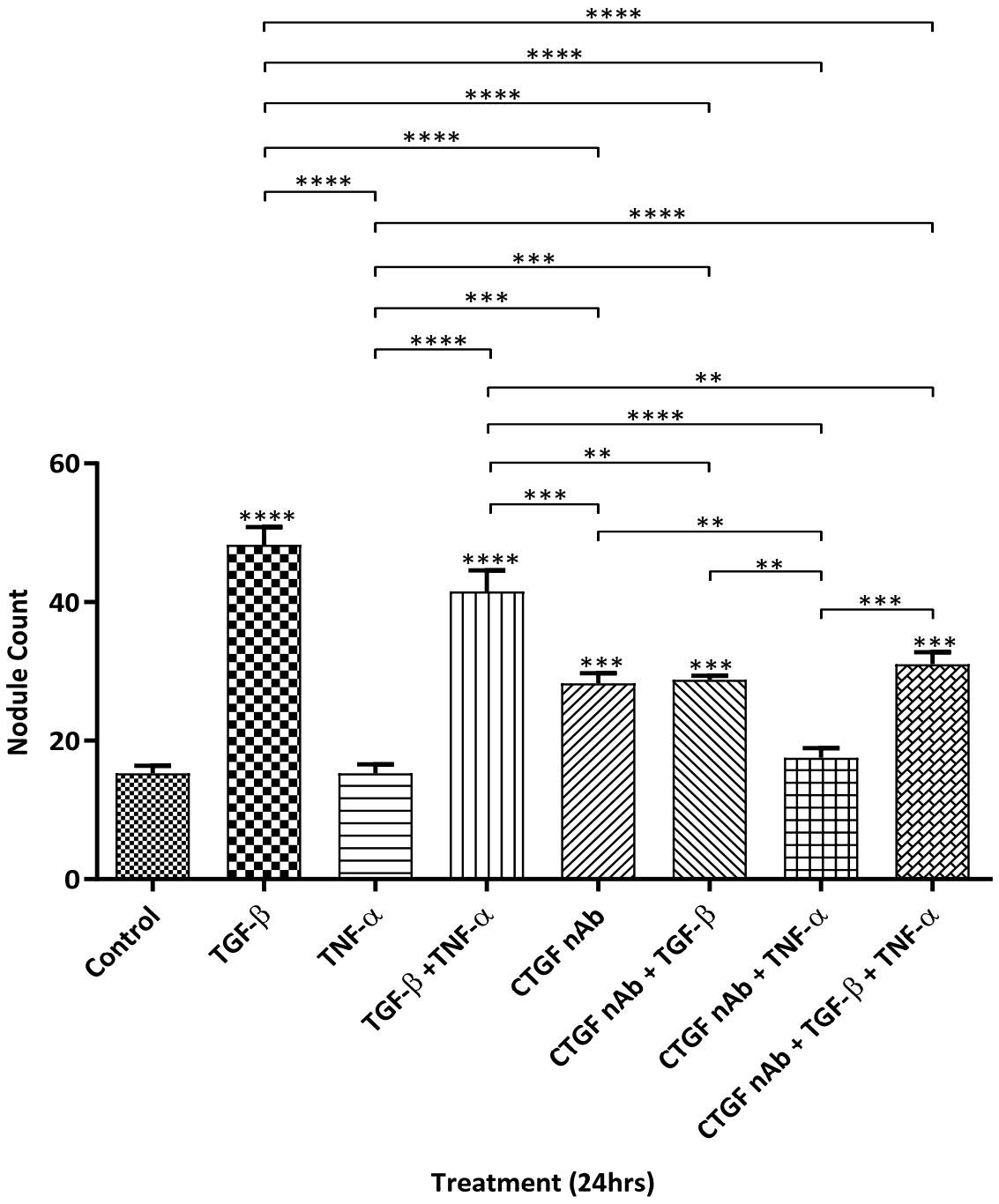

Figure 37. Nodule counts with TGF-β, TNF-α and CTGF nAb treatments in Celprogen fPOD 3D tri- cultures.

Celprogen fPOD 3D tri-cultures were treated with either TGF-β, TNF-α, and/or CTGF nAb for 24hrs before nodule counts. TGF-β evoked a significant increase in nodule number, which was somewhat reduced by co-treatments of TNF-α and CTGF nAb. N=2, SEM error bars, One-way ANOVA p-value <0.0001 (****), followed by Tukey's multiple comparison post-tests.

RT-qPCR

The effects of CTGF nAb and TNF-α upon TGF-β treatment in the 3D tri-culture model were further investigated by examination of gene expression. The panel of genes examined in these experiments can be separated into the broad categories outlined earlier of ECM genes, TGF-β signalling genes and other genes of interest.

ECM genes will be discussed first (Figure 38), the average CT value of these genes was suggestive of reasonable expression in these samples. COL1A1, COL3A1 and COL4A1 expression (Figure 38) did not change with any statistical significance with any treatment compared to control. There was wide variation in repeated samples. Expression of ACTA2 (Figure 38) was significantly increased with TGF-β and CTGF nAb co-treatment. TGF-β increased in ACTA2 expression, but this was not statistically significant, while CTGF nAb treatment alone did not significantly alter ACTA2 expression from control values, suggesting that CTGF nAb did not affect TGF-β induced ACTA2 upregulation. Increased ACTA2 expression with TGF-β treatment has been demonstrated in earlier experiments.

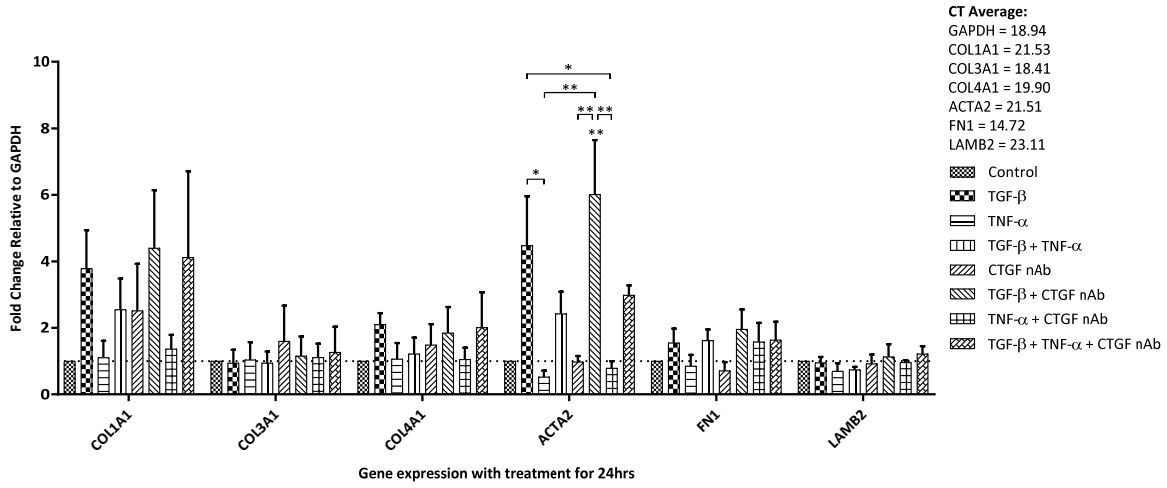

Figure 38. ECM gene expression with TGF-β, TNF-α, and CTGF nAb treatments in Celprogen fPOD 3D tri-cultures.

RT-qPCR performed on Celprogen fPOD 3D tri-cultures treated with TGF-β, TNF-α and/or CTGF nAb for 24hrs. ΔΔCT analysis to look at the relative fold-change of the gene of interest against housekeeping gene GAPDH. N=2, SEM error bars, One-way ANOVA; COL1A1 p-value 0.4173 (ns); COL3A1 p-value 0.9944 (ns); COL4A1 p-value 0.7575 (ns); ACTA2 p-value 0.0006 (***); FN1 p-value 0.3848 (ns); LAMB2 p-value 0.6296 (ns); followed by Tukey's multiple comparison post-tests. CT averages of each gene for reference.

FN1 expression (Figure 38) was statistically unchanged with any treatment, a slight trend of increased expression with TGF-β treatment could be seen, which neither TNF-α or CTGF nAb appeared to affect. Data presented earlier also demonstrated a trend of increased FN1 expression with TGF-β

treatment. Neither TNF-α and CTGF nAb alone did not appear to alter ACTA2 expression from control values. Expression of LAMB2 (Figure 38) was unaffected across any treatment in this experiment.

Overall the data presented in Figure 38 demonstrates that TGF-β generally evokes the expected upregulation in ECM genes. TNF-α did appear to have some effect upon ACTA2 upregulation evoked by TGF-β, while CTGF nAb appeared to have little effect upon ECM genes.

TGF-β signalling genes were investigated next (Figure 39), the average CT value of these genes was suggestive of a good level of expression in these samples. SMAD2 expression (Figure 39) was not statistically changed with any treatment type, however, some trends with treatments could be seen. Both TGF-β and TNF-α appeared to evoke SMAD2 expression while co-treatment of these cytokines appeared to downregulate expression. This differs from data presented earlier where SMAD2 appeared to be slightly evoked with this co-treatment. CTGF nAb treatment alone appeared to downregulate SMAD2 expression, CTGF nAb appears to have an inhibitory effect upon TNF-α evoked SMAD2 expression but not that evoked by TGF-β. Treatment with TGF-β, TNF-α and CTGF nAb resulted in the highest average fold-change value for SMAD2 expression, suggesting any inhibitory effect of CTGF nAb upon TNF-α is lost when in combination with TGF-β.

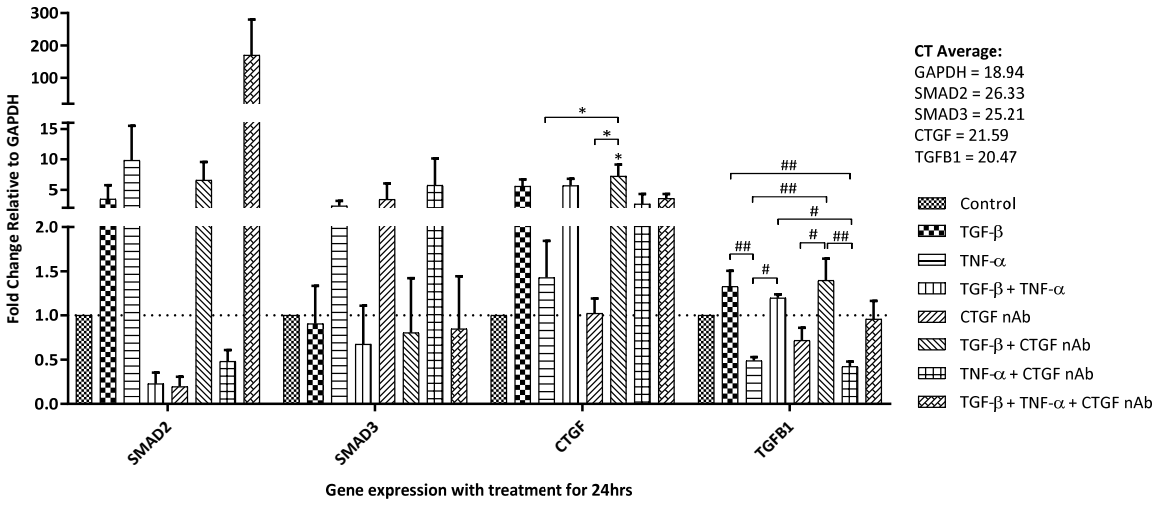

Figure 39. TGF-β signalling gene expression with TGF-β, TNF-α and CTGF nAb treatments in Celprogen fPOD 3D tri cultures.

RT-qPCR performed on Celprogen fPOD 3D tri-cultures treated with TGF-β, TNF-α and/or CTGF nAb for 24hrs. ΔΔCT analysis to look at the relative fold-change of the gene of interest against housekeeping gene GAPDH. N=2, SEM error bars, One-way ANOVA; SMAD2 p-value 0.0726 (ns); SMAD3 p-value 0.5111 (ns); CTGF p-value 0.0018 (**); TGFB1 p-value 0.0002 (***); followed by Tukey's multiple comparison post-tests. CT averages of each gene for reference.

Expression of SMAD3 (Figure 39) was not significantly altered with any treatment group. All treatments including TGF-β did not appear to alter SMAD3 expression from control values. Previously

presented data had demonstrated TGF-β resulting in some downregulation of SMAD3. CTGF expression (Figure 39) was significantly increased with TGF-β and CTGF nAb co-treatment compared to control values and CTGF expression was significantly higher with this treatment than that of TNF-α alone as well as CTGF nAb alone. This data appears to reproduce that of earlier data where CTGF expression was upregulated by TGF-β treatments while TNF-α had no effect. TGFB1 expression (Figure 39) was significantly decreased with TNF-α treatment compared to TGF-β treatment, TGF-β and TNF-α co-treatment and TGF-β and CTGF nAb co-treatment. TGFB1 expression was also significantly decreased with TNF-α and CTGF nAb co-treatment compared with TGF-β treatment, TGF-β and TNF-α co-treatment and TGF-β and CTGF nAb co-treatment. When the 3D tri-culture model was treated with TGF-β, TNF-α and CTGF nAb together, TGFB1 expression remained at control values, suggesting some interplay preventing the both TGF-β evoking TGFB1 expression and TNF-α downregulating TGFB1 expression when these treatments were used in combination.

Finally, other genes of interest which are implicated in fibrosis and inflammation were studied (Figure 40). The average CT value of these genes was suggestive of reasonable expression in these samples, except CDH1, with a value of 32.89, demonstrating low expression. Expression of SERPINE1 (Figure 40) was not altered with any statistical significance with any treatment. TGM2 expression (Figure 40) remained statistically unchanged across treatments. This differs from previous data where TGF-β treatment alone and in combination with TNF-α resulted in a significant downregulation of TGM2 expression. Expression of CCL2 (Figure 40) was significantly increased with TNF-α alone and in co-treatment with TGF-β as well as TGF-β and CTGF nAb compared to control values. Co-treatment with TNF-α and CTGF nAb also resulted in an apparent increase in CCL2 expression, without statistical significance. Treatments of TGF-β or CTGF nAb alone or together did not alter expression from control values. Therefore, TNF-α appeared to evoke CCL2 expression in the 3D tri-culture model and neither TGF-β or CTGF nAb impacted upon this. This does replicate some data presented earlier where TGF-β treatment did not affect CCL2 expression while TNF-α treatment evoked upregulation. CDH1 expression (Figure 40) was significantly decreased compared to control values, with all treatments except treatment with CTGF nAb. When all treatments were used in combination the greatest decrease in CDH1 expression was observed. TGF-β and TNF-α in combination did not result in a greater decrease in expression than when used in isolation, suggesting it was the addition of CTGF nAb that evoked the greater decrease in CDH1 expression in the TGF-β, TNF-α and CTGF nAb stimulation. Expression of CLDN1 (Figure 40) was significantly decreased with TGF-β treatment and TGF-β and TNF-α co-treatment compared to TNF-α and CTGF nAb co-treatment. There was a non-statistically significant decrease in CLDN1 expression with TGF-β and CTGF nAb treatment. Together the data suggest TGF-β drives a decrease in CLDN1 expression, while TNF-α and CTGF nAb treatments appeared to have little effect upon expression.

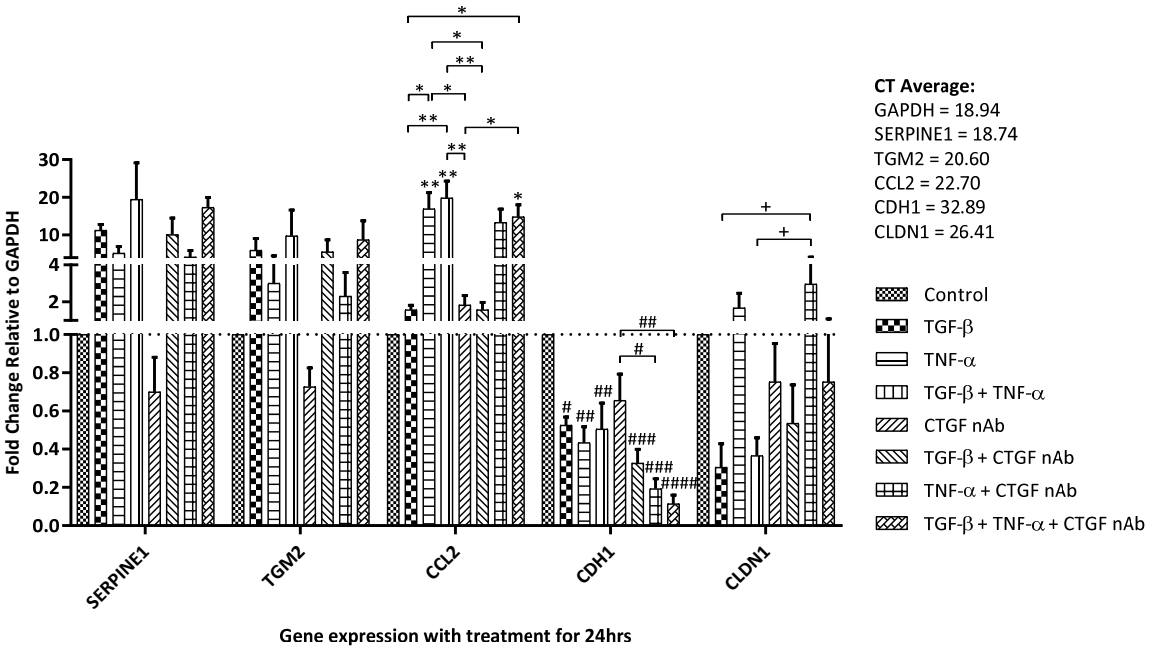

Figure 40. Expression of other genes of interest in Celprogen fPOD 3D tri-cultures treated with TGF-β, TNF-α, and CTGF nAb.

RT-qPCR performed on Celprogen fPOD 3D tri-cultures treated with TGF-β, TNF-α and/or CTGF nAb for 24hrs. ΔΔCT analysis to look at the relative fold-change of the gene of interest against housekeeping gene GAPDH. N=2, SEM error bars, One-way ANOVA; SERPINE1 p-value 0.0667 (ns); TGM2 p-value 0.4667 (ns); CCL2 p-value <0.0001 (****); CDH1 p-value <0.0001 (****); CLDN1 p-value 0.0273 (*); followed by Tukey's multiple comparison post-tests. CT averages of each gene for reference.

Nodule and RT-qPCR data presented in Figure 37-Figure 40 demonstrates again the differential roles of TGF-β and TNF-α that can also be cooperative. The data also again determines the impact of inhibiting CTGF in the 3D tri-culture model. The combination of TNF-α and CTGF nAb did not reduce TGF-β induced nodule formation to control values, with TNF-α having no effect compared to when CTGF nAb was used alone. In terms of ECM gene expression, it appeared CTGF nAb treatment had little effect while TNF-α could suppress some increased gene expression evoked by TGF-β. TGF-β signalling genes affected by TGF-β treatment were generally unchanged when a co-treatment of either TNF-α and/or CTGF nAb was used. The other genes of interest examined demonstrated the differential effects the combinations of treatments could have upon gene expression. Generally, the data presented here mimicked that presented in earlier figures, however, there were some discrepancies, to be discussed later. The CT averages of this data set were good; except for CDH1. CTGF nAb in the 3D tri-culture system had further added to awareness of the role CTGF plays in

fibrosis in the system and the synergy it appears to have with TGF-β, highlighting CTGF for further investigation in the model system of glomerulosclerosis.

TGF-β & CTGF

To further assess the role CTGF plays in fibrosis an experimental set-up was designed where treatment of CTGF either alone or in combination with TGF-β was tested, whereas previously inhibition of CTGF had been used. Only 3D tri-cultures using Celprogen fPODs were used in these experiments.

Nodule Counts

3D tri-cultures were treated with either TGF-β and/or CTGF for 24hrs before nodule counts. As anticipated following previous data, TGF-β treatment evoked a significant increase in nodule counts (Figure 41). CTGF treatment also resulted in a significant increase in nodules. Co-treatment of TGF-β and CTGF evoked a significant increase in nodule number, this increase was no greater than that achieved when each cytokine was used separately, suggesting there was no additive effect upon nodule number.

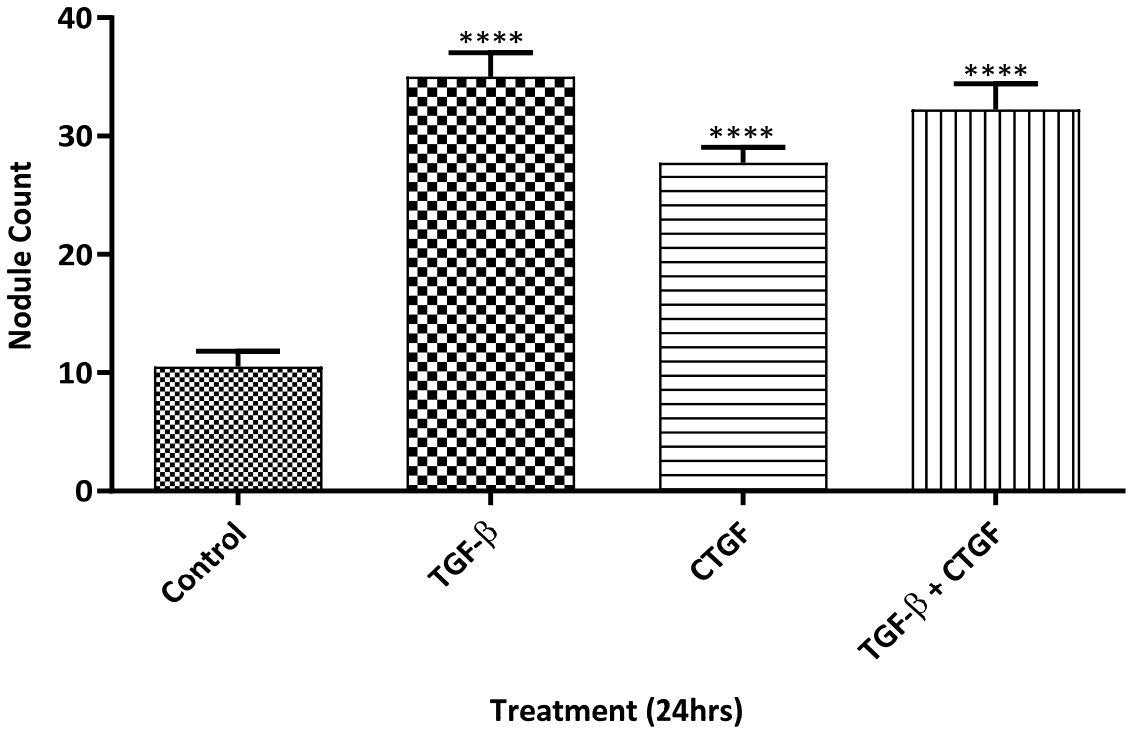

Figure 41. Nodule counts with TGF-β and CTGF treatments in Celprogen fPOD 3D tri-cultures.
Celprogen fPOD 3D tri-cultures were treated with either TGF-β and/or CTGF for 24hrs before nodule counts. TGF-β evoked a significant increase in nodule number as did CTGF and co-treatments. N=2, SEM error bars, One-way ANOVA p-value <0.0001 (****), followed by Tukey's multiple comparison post-tests.

RT-qPCR

The effects of CTGF treatment alone and in combination with TGF-β treatment in the 3D tri-culture model were further investigated by examination of gene expression. The panel of genes examined in these experiments can be separated into two of the broad categories outlined earlier of ECM genes and other genes of interest.

ECM genes will be discussed first (Figure 42). The average CT value of these genes was suggestive of reasonable expression in these samples, except LAMB2, with a value of 27.90, demonstrating lower expression of LAMB2. COL1A1 expression (Figure 42) did not change with any statistical significance. Previous data presented has consistently demonstrated that TGF-β treatment evoked an upregulation in COL1A1 expression. Expression of COL3A1 (Figure 42) was not altered with any statistical significance with any treatment type, previous data demonstrated TGF-β treatment did not alter COL3A1 expression. COL4A1 expression (Figure 42) also did not change with any statistical significance with any treatment. There was a trend of increased COL4A1 expression with TGF-β treatment while CTGF treatment appeared to not change the average fold-change in COL4A1 expression. Earlier data demonstrated that TGF-β induced upregulation in COL4A1 expression.

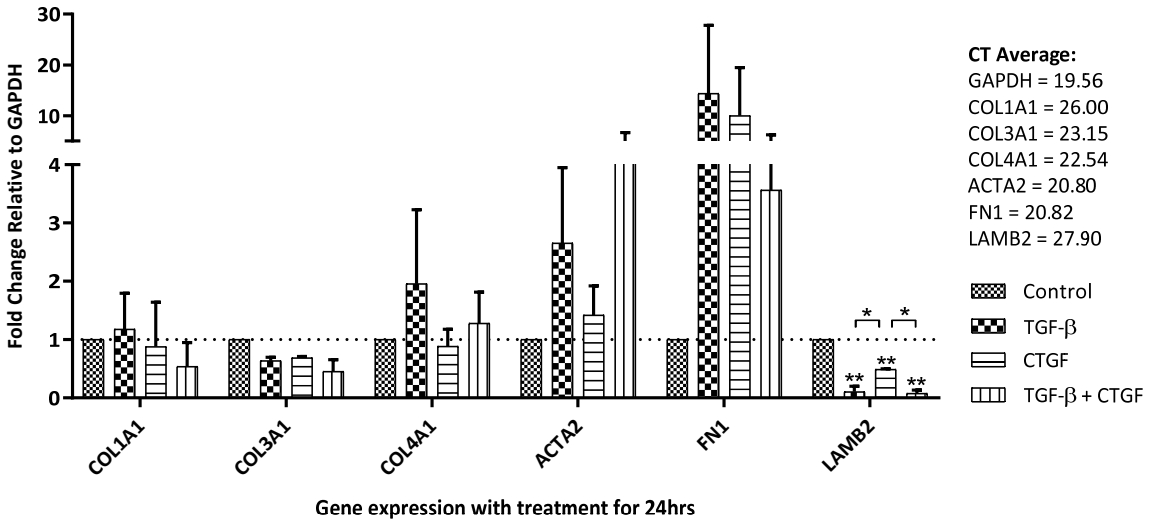

Figure 42. ECM gene expression with TGF-β and CTGF treatments in Celprogen fPOD 3D tri-cultures. RT-qPCR performed on Celprogen fPOD 3D tri-cultures treated with TGF-β and/or CTGF for 24hrs. ΔΔCT analysis to look at the relative fold-change of the gene of interest against housekeeping gene GAPDH. N=2, SEM error bars, One-way ANOVA; COL1A1 p-value 0.8533 (ns); COL3A1 p-value 0.0896 (ns); COL4A1 p-value 0.7204 (ns); ACTA2 p-value 0.4802 (ns); FN1 p-value 0.6819 (ns); LAMB2 p-value 0.0008 (***); followed by Tukey's multiple comparison post-tests. CT averages of each gene for reference.

Expression of ACTA2 (Figure 42) did not alter with any treatment with any statistical significance. However, there were some trends to note, one of an increased fold-change average with TGF-β treatment alone and in combination with CTGF. The average fold-change evoked by TGF-β and CTGF co-treatment was greater than that of TGF-β alone, implying some additive effect. Earlier presented data demonstrated that TGF-β treatment resulted in increased ACTA2 expression. FN1 expression (Figure 42) did not alter with any statistical significance across any treatment type; however, the data does appear to show an increase in FN1 expression with all treatment types compared to control values. Previous data demonstrated that TGF-β treatment increased FN1 expression in the 3D tri-culture model, fitting with this data set. Expression of LAMB2 (Figure 42) was significantly decreased with all treatments compared to control values. TGF-β treatment alone and in combination with CTGF evoked a downregulation in LAMB2 expression significantly lower than that evoked by CTGF treatment alone. This suggests that TGF-β more powerfully downregulates LAMB2 than CTGF. Previous data demonstrated that TGF-β did not appear to affect LAMB2 expression.

Other genes of interest which are implicated in fibrosis and inflammation were studied (Figure 43). The average CT value of these genes was suggestive of reasonable expression in these samples, with the SMAD2 and CCL2 demonstrative of lower levels of expression. SMAD2 expression (Figure 43) did not change with statistical significance, however, expression did appear to trend upwards with all treatments. No statistical significance or repeated pattern for SMAD2 expression had been seen in earlier data. Expression of SMAD3 (Figure 43) remained unchanged with any statistical significance across any treatment. SMAD3 expression decreased with TGF-β treatment in data presented earlier. CTGF expression (Figure 43) did not change with significance with any treatment type. There was an apparent trend of upregulation in CTGF expression with TGF-β treatment alone and in co-treatment CTGF, this pattern has been demonstrated in earlier data also. Expression of SERPINE1 (Figure 43) was not changed with any statistical significance, yet there was an increased average fold-change value with TGF-β treatment alone and in combination with CTGF treatment. Earlier data has also demonstrated that TGF-β treatment would evoke SERPINE1 expression in the 3D tri-culture model.

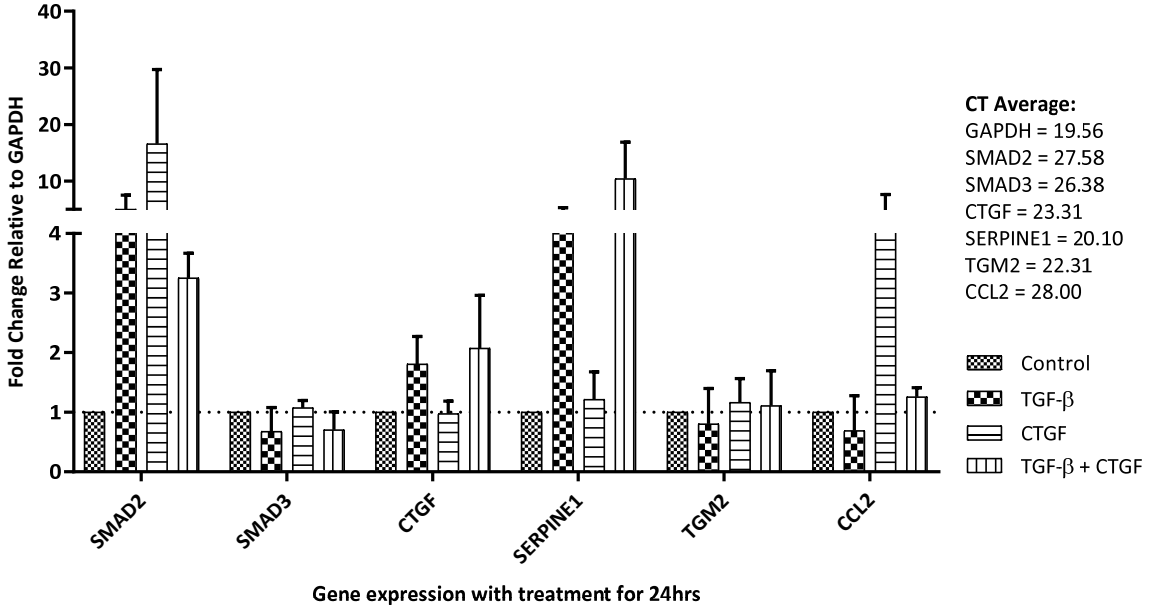

Figure 43. Expression of other genes of interest in Celprogen fPOD 3D tri-cultures treated with TGF-β and CTGF.

RT-qPCR performed on Celprogen fPOD 3D tri-cultures treated with TGF-β and/or CTGF for 24hrs. ΔΔCT analysis to look at the relative fold-change of the gene of interest against housekeeping gene GAPDH. N=2, SEM error bars, One-way ANOVA; SMAD2 p-value 0.4528 (ns); SMAD3 p-value 0.6455 (ns); CTGF p-value 0.4163 (ns); SERPINE1 p-value 0.2858 (ns); TGM2 p-value 0.9440 (ns); CCL2 p-value 0.4980 (ns); followed by Tukey's multiple comparison post-tests. CT averages of each gene for reference.

Expression of TGM2 (Figure 43) did not alter with any statistical significance with either TGF-β and/or CTGF treatment. Data presented earlier demonstrated TGF-β could evoke a statistically significant decrease in TGM2 expression in the 3D tri-culture model.

CCL2 expression (Figure 43) did not change with statistical significance with any treatment. There was an apparent trend of increased CCL2 expression with CTGF treatment. The average fold-change for CCL2 with co-treatment remained at control values, suggesting TGF-β inhibited CTGF evoked CCL2 expression.

Nodule and RT-qPCR data presented in Figure 41-Figure 43 demonstrated that while both evoke an increase in nodule number and therefore promoting fibrosis in the 3D tri-culture system, TGF-β and CTGF appear to have similar and divergent effects upon fibrotic and inflammatory genes. For example, CTGF treatment did not evoke COL4A1 expression as TGF-β appeared to, yet both cytokines evoked FN1 expression. This data set did not achieve much statistical significance. Likely due to it being at N=2, with replicates in each experiment. The CT averages were generally good and

reasonable for analysis. A comparison of this data set where exogenous CTGF is added and the previous data sets where endogenous CTGF is inhibited with CTGF nAb treatment will be made, more appropriately, in the discussion. This data still further highlights the complicated interplay of TGF-β and CTGF in glomerulosclerosis; yet, it is widely accepted that there are many other cytokines at play in the development and progression of the disease. The effects of these in the 3D tri-culture model were to be investigated next.

TGF-β, bFGF, IL-1α, PDGF-BB & HGF

Additional cytokines demonstrated to be involved in the processes of glomerulosclerosis were tested in the 3D tri-culture model to explore the role they play in the system. Those additional cytokines being bFGF, IL-1α, PDGF-BB and HGF. Only 3D tri-cultures using Celprogen fPODs were used in these experiments.

Nodule Counts

3D tri-cultures were treated with either TGF-β, bFGF, IL-1α, PDGF-BB, or HGF for 24hrs before nodule counts. As anticipated following previous data, TGF-β treatment evoked a significant increase in nodule counts (Figure 44). bFGF, IL-1α, and PDGF-BB treatments also significantly increased nodule numbers compared to control values, however, TGF-β evoked significantly greater nodule numbers. HGF treatment did not alter nodule numbers from control values.

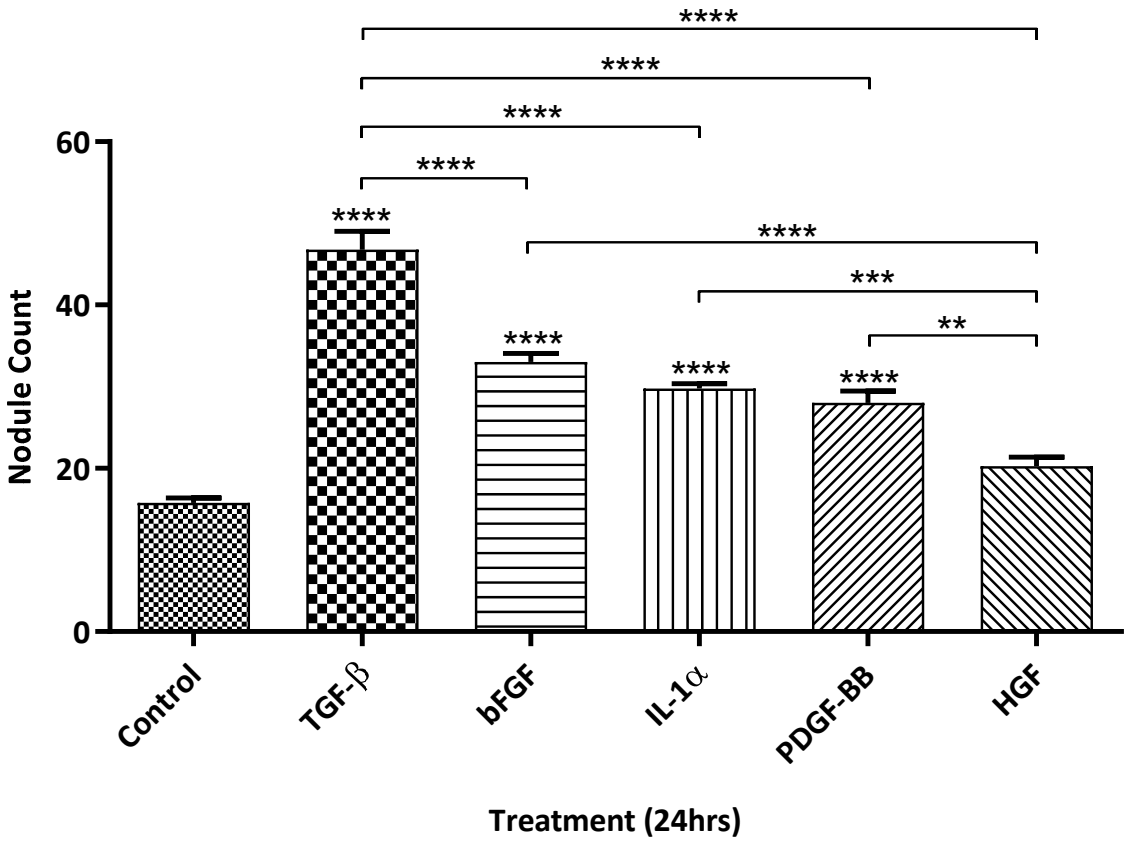

Figure 44. Nodule counts with TGF-β, bFGF, IL-1α, PDGF-BB and HGF treatments in Celprogen fPOD 3D tri-cultures.

Celprogen fPOD 3D tri-cultures were treated with either TGF-β, bFGF, IL-1α, PDGF-BB, or HGF for 24hrs before nodule counts. TGF-β, bFGF, IL-1α and PDGF-BB evoked a significant increase in nodule number. N=2, SEM error bars, One-way ANOVA p-value <0.0001 (****), followed by Tukey's multiple comparison post-tests.

RT-qPCR

The effects of either TGF-β, bFGF, IL-1α, PDGF-BB or HGF treatments in the 3D tri-culture model were further investigated by examination of gene expression. The panel of genes examined in these experiments can be separated into two of the broad categories outlined earlier of ECM genes and other genes of interest.

ECM genes will be discussed first (Figure 45), the average CT value of these genes was suggestive of reasonable expression in these samples. COL1A1 (Figure 45) expression did not change with any statistical significance with any treatment, however, there were some trends in the data. All treatments appeared to increase the average fold-change in COL1A1 expression, the greatest increase was with TGF-β treatment. Previously presented data has also shown increased COL1A1 expression with TGF-β treatments.

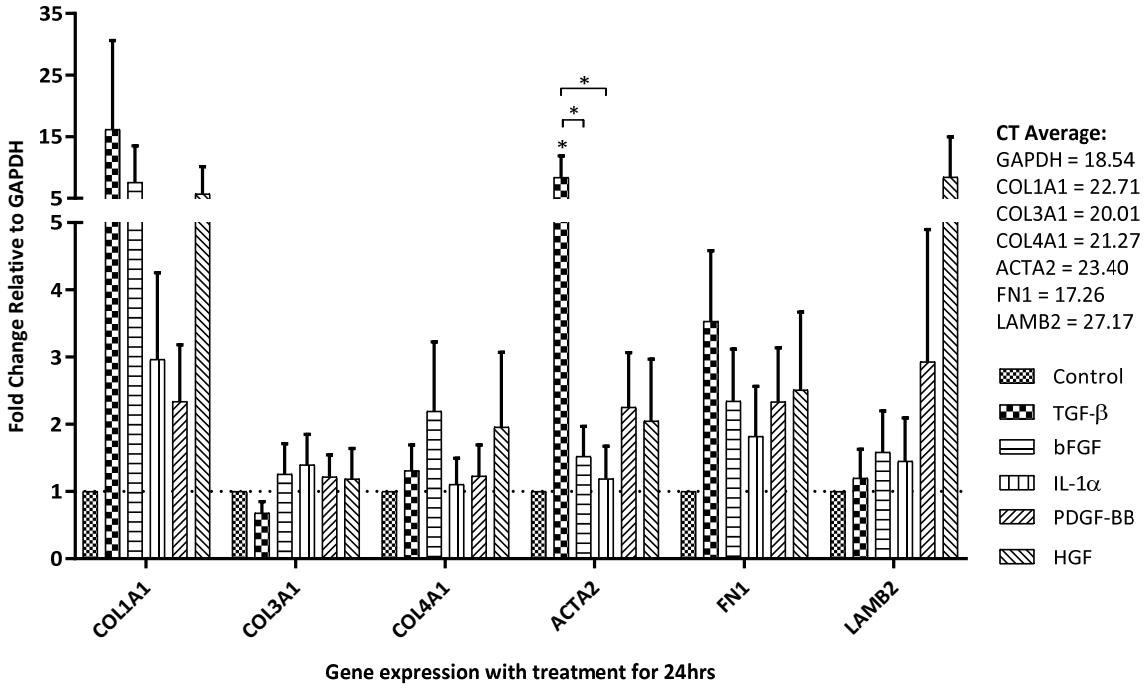

Figure 45. ECM gene expression with TGF-β, bFGF, IL-1α, PDGF-BB and HGF treatments in Celprogen fPOD 3D tri-cultures.

RT-qPCR performed on Celprogen fPOD 3D tri-cultures treated with TGF-β, bFGF, IL-1α, PDGF-BB or HGF for 24hrs. ΔΔCT analysis to look at the relative fold-change of the gene of interest against housekeeping gene GAPDH. N=2, SEM error bars, One-way ANOVA; COL1A1 p-value 0.6319 (ns); COL3A1 p-value 0.7656 (ns); COL4A1 p-value 0.7651 (ns); ACTA2 p-value 0.0156 (*); FN1 p-value 0.4438 (ns); LAMB2 p-value 0.4148 (ns); followed by Tukey's multiple comparison post-tests. CT averages of each gene for reference.

COL3A1 expression (Figure 45) was not altered with any treatment with statistical significance. Data presented earlier has no change in expression with TGF-β treatment. Expression of COL4A1 (Figure 45) did not change with statistical significance across any treatment type. There were some patterns of expression where TGF-β, bFGF and HGF appeared to evoke some increase in COL4A1 expression, while IL-1α and PDGF-BB expression did not appear to change expression from control values. Earlier presented data has demonstrated TGF-β treatment would evoke COL4A1 expression in the 3D tri-culture model. Expression of ACTA2 (Figure 45) was significantly increased with TGF-β treatment, evoking a level of expression that was significantly greater than that seen with either bFGF or IL-1α treatments. bFGF, PDGF-BB and HGF treatments all appeared to induce some increase in ACTA2 expression, which did not reach significance. Earlier data also demonstrated that TGF-β treatment evoked ACTA2 expression in the 3D tri-culture model. FN1 expression (Figure 45) did not alter with any statistical significance with any treatment group. All treatments did appear to increase FN1 expression, TGF-β evoked the highest increase in average fold-change compared to control values. Previously presented data also demonstrated that TGF-β evoked an increase in FN1 expression in the glomerular model. Expression of LAMB2 (Figure 45) was not changed with any statistical significance with any treatment type. PDGF-BB and HGF appeared to evoke some increase in expression. Data presented earlier has demonstrated TGF-β treatment had no effect on LAMB2 expression and could also decrease LAMB2 expression.

Other genes of interest (Figure 46) were also investigated. The average CT value of these genes was generally suggestive of reasonable expression in these samples, the value for SMAD2 however demonstrated a low level of expression. Expression of SMAD2 (Figure 46) was examined, being at N=1, statistical analysis could not be performed. Data presented so far has demonstrated that TGF-β treatment would generally evoke an increase in SMAD2 expression. SMAD3 expression (Figure 46) remained statistically unchanged with any treatment type. Earlier data indicated SMAD3 expression was downregulated with TGF-β treatment in the 3D tri-culture system.

Expression of CTGF (Figure 46) was significantly increased with TGF-β treatment compared to all other treatment groups. Earlier data had also demonstrated that TGF-β treatment evoked an increase in CTGF expression.

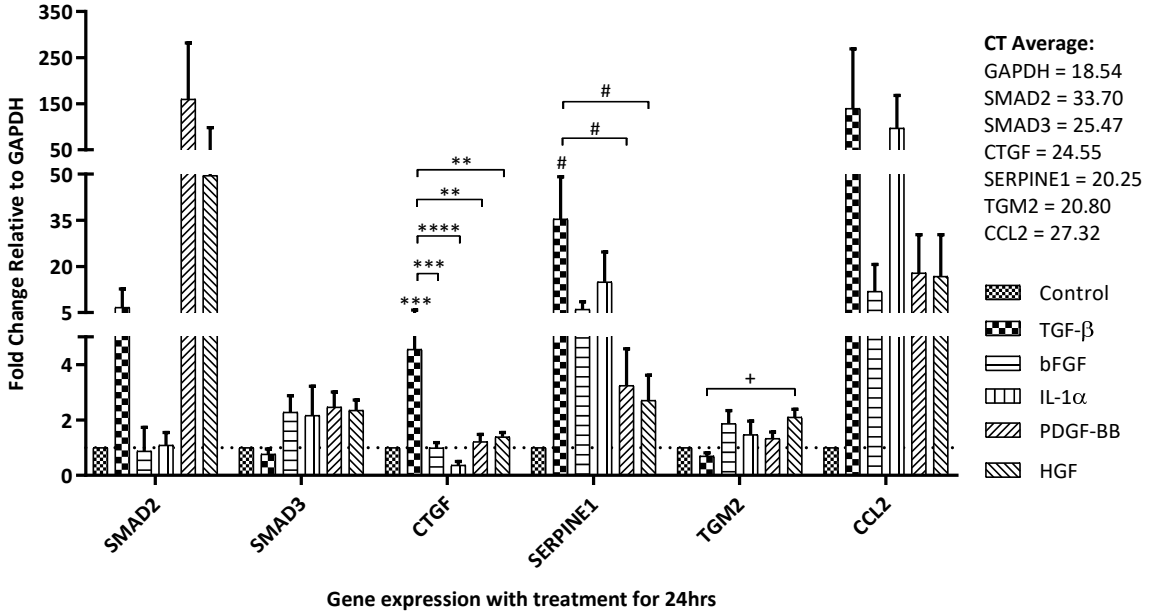

Figure 46. Expression of other genes of interest in Celprogen fPOD 3D tri-cultures treated with TGF-β, bFGF, IL-1α, PDGF-BB, and HGF.

RT-qPCR performed on Celprogen fPOD 3D tri-cultures treated with TGF-β, bFGF, IL-1α, PDGF-BB or HGF for 24hrs. ΔΔCT analysis to look at the relative fold-change of the gene of interest against housekeeping gene GAPDH. N=2 (SMAD2 N=1), SEM error bars, One-way ANOVA; SMAD2 p-value 0.3466 (ns); SMAD3 p-value 0.1528 (ns); CTGF p-value <0.0001 (****); SERPINE1 p-value 0.0118 (*); TGM2 p-value 0.0392 (*); CCL2 p-value 0.5047 (ns); followed by Tukey's multiple comparison post-tests. CT averages of each gene for reference.

Expression of SERPINE1 (Figure 46) was significantly increased with TGF-β treatment compared to control values and those of PDGF-BB and HGF treatments. bFGF, IL-1α, PDGF-BB and HGF treatments also all appeared to evoke an increase in SERPINE1 expression compared to control values, without achieving statistical significance. Previously presented data has demonstrated that TGF-β would evoke increased SERPINE1 expression in the 3D tri-culture. TGM2 expression (Figure 46) changed with some statistical significance across treatment types. TGF-β appeared to evoke a slight decrease in TGM2 expression, while all other treatments appeared to increase TGM2 expression to some degree. Previous data also demonstrated that TGF-β would generally result in a decrease in TGM2 expression in the 3D tri-culture model. Expression of CCL2 (Figure 46) was not altered with any statistical significance with any treatment group. All treatments did appear to evoke an increase in CCL2 expression, without reaching significance. Earlier presented data had shown that TGF-β treatment generally evoked a decrease in CCL2 expression.

Nodule and RT-qPCR data presented in Figure 44-Figure 46 demonstrated cytokines other than TGF-β could evoke fibrotic response in the 3D tri-culture model. The extent of fibrotic response varied across treatment type and the gene investigated. The CT averages were generally good for analysis, except for SMAD2 where the average CT was high at 33.70 and so conclusions will be measured. This data establishes further that a multitude of cytokine involved in and capable of fibrosis, further investigation into these cytokines and additional cytokines followed.

TGF-β, CTGF, IL-1α, IL-1β, PDGF-BB, EGF, bFGF & HGF

The panel of cytokines tested in the 3D tri-culture model was expanded to include IL-1β and EGF, both understood to play roles in the development and progression of renal fibrosis and inflammation. CTGF was also used in this experimental set-up to enable more straightforward comparison between treatment types. Only 3D tri-cultures using Celprogen fPODs were used in these experiments.

Nodule Counts

3D tri-cultures were treated with either TGF-β, CTGF, IL-1α, IL-1β, PDGF-BB, EGF, bFGF, or HGF for 24hrs before nodule counts (Figure 47). As expected considering previous data, TGF-β treatment stimulated a significant increase in nodule formation compared to control values. The number of nodules counted with TGF-β treatment was significantly higher than that with treatments of IL-1α, IL-1β or HGF. Data presented earlier demonstrated that CTGF, bFGF, IL-1α and PDGF-BB could all evoke a significant increase in nodule formation in the 3D tri-culture model. There did appear to be a trend of increased nodule numbers with these treatments, as well as with IL-1β and EGF treatments, without any statistical significance. As earlier data also established, HGF treatment did not change nodule count from control values.

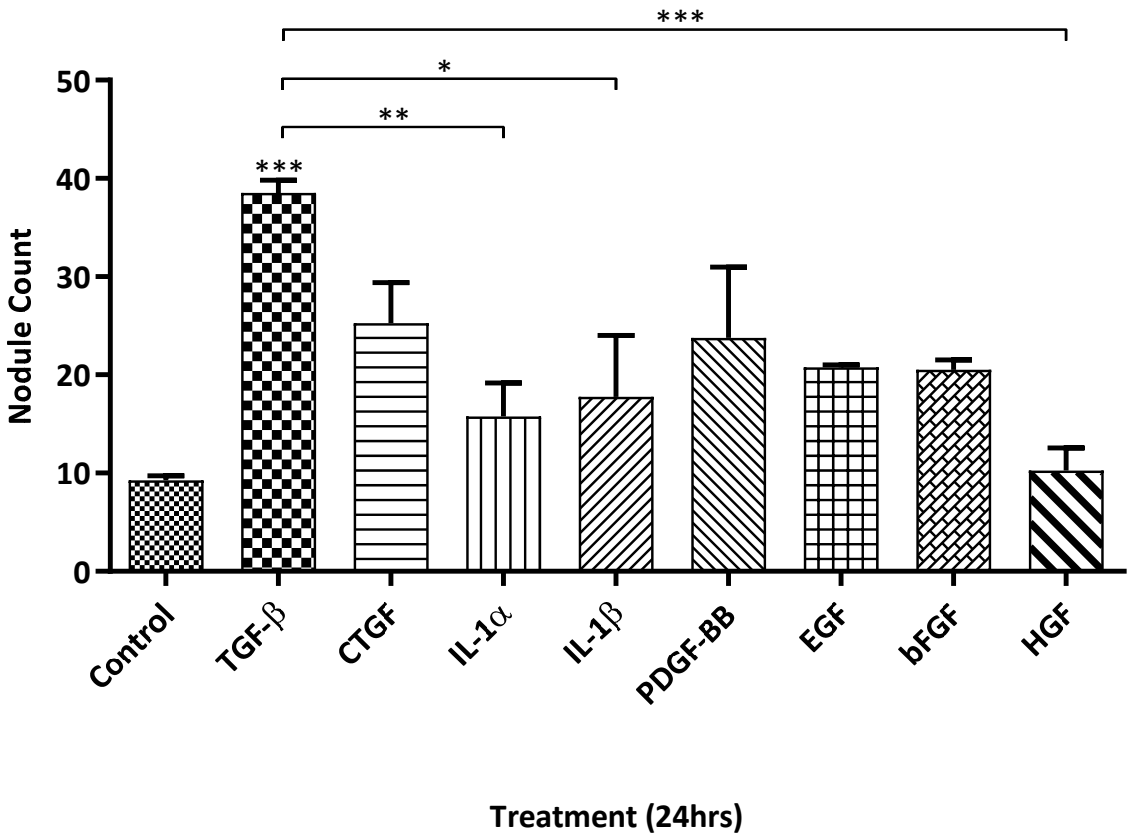

Figure 47. Nodule counts with TGF-β, CTGF, IL-1α, IL-1β, PDGF-BB, EGF, bFGF and HGF treatments in Celprogen fPOD 3D tri-cultures.

Celprogen fPOD 3D tri-cultures were treated with TGF-β, CTGF, IL-1α, IL-1β, PDGF-BB, EGF, bFGF, or HGF for 24hrs before nodule counts. TGF-β evoked a significant increase in nodule number. N=4, SEM error bars, One-way ANOVA p-value 0.0004 (***), followed by Tukey's multiple comparison post-tests.

RT-qPCR

The effects of either TGF-β, CTGF, IL-1α, IL-1β, PDGF-BB, EGF, bFGF or HGF treatments in the 3D tri-culture model were further investigated by examination of gene expression. The panel of genes examined in these experiments can be separated into the three broad categories outlined earlier of ECM genes, TGF-β signalling genes and other genes of interest.

ECM genes (Figure 48) will be discussed first. The average CT value of these genes was suggestive of reasonable expression in these samples. COL1A1 expression (Figure 48) significantly increased with TGF-β treatment in the 3D tri-culture model, as had been demonstrated with earlier data. Only PDGF-BB appeared to also induce an increase in COL1A1 expression, without reaching significance. Therefore all other cytokines did not appear to alter COL1A1 expression from control values. Earlier data mainly fits with these results, except for bFGF, IL-1α and HGF treatments which had demonstrated some upregulation of COL1A1 expression in the 3D tri-culture model.

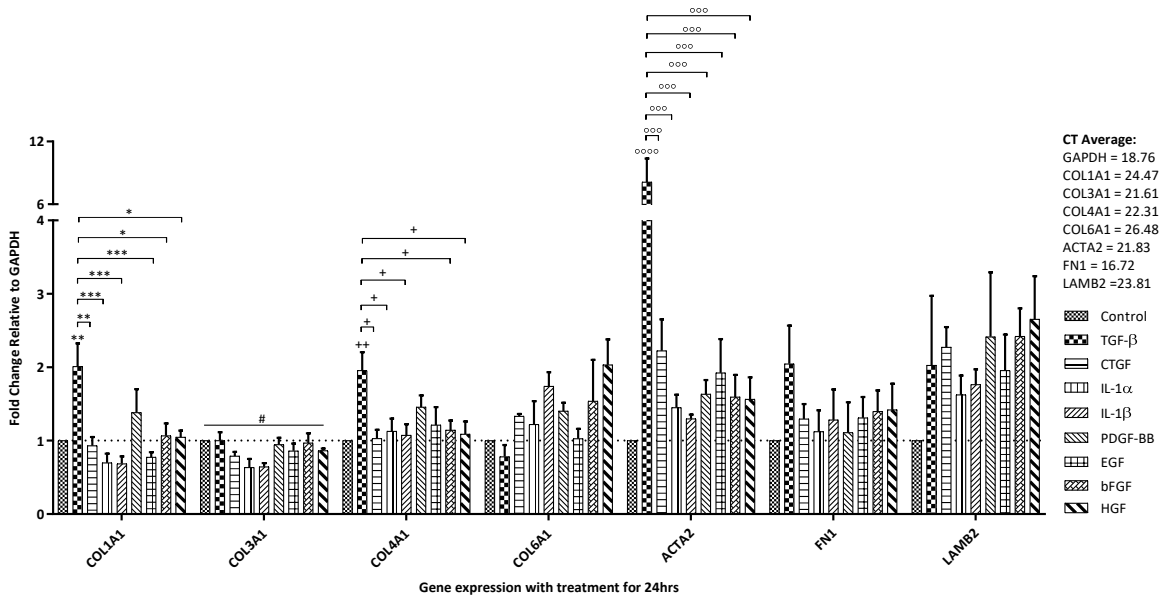

Figure 48. ECM gene expression with TGF-β, CTGF, IL-1α, IL-1β, PDGF-BB, EGF, bFGF and HGF treatments in Celprogen fPOD 3D tri-cultures.

RT-qPCR performed on Celprogen fPOD 3D tri-cultures treated with TGF-β, CTGF, IL-1α, IL-1β, PDGF-BB, EGF, bFGF or HGF for 24hrs. ΔΔCT analysis to look at the relative fold-change of the gene of interest against housekeeping gene GAPDH. N=2(COL6A1, ACTA2, FN1 & LAMB2), N=4(COL1A1, COL3A1 & COL4A1), SEM error bars, One-way ANOVA; COL1A1 p-value <0.0001 (****); COL3A1 p-value 0.0225 (*); COL4A1 p-value 0.0065 (**); COL6A1 p-value 0.1322 (ns); ACTA2 p-value <0.0001 (****); FN1 p-value 0.5722 (ns); LAMB2 p-value 0.5610 (ns); followed by Tukey's multiple comparison post-tests. CT averages of each gene for reference.

Expression of COL3A1 (Figure 48) was altered with statistical significance across treatment groups. TGF-β, PDGF-BB and bFGF treatments did not appear to alter COL3A1 expression from control values, while all other treatments appeared to evoke some degree of COL3A1 downregulation. COL4A1 expression (Figure 48) was significantly upregulated with TGF-β treatment compared to control values as well as treatments with CTGF, IL-1α, IL-1β, bFGF and HGF. This correlates with earlier presented data has demonstrated that COL4A1 expression was increased with TGF-β treatment, and CTGF having no effect upon COL4A1 expression. Expression of COL6A1 (Figure 48) was not changed with any statistical significance across any treatment type. ACTA2 expression (Figure 48) was significantly increased with TGF-β treatment compared to all other treatment groups. Each cytokine treatment did also appear to evoke some increase in ACTA2 expression without reaching statistical significance. Prior data had also demonstrated these patterns of increased ACTA2 expression. Expression of FN1 (Figure 48) did not alter with any statistical significance across treatment groups. There did appear to some increase in FN1 expression across all treatments, the greatest being with TGF-β treatment. Earlier data compares well with this, as it demonstrated that all tested cytokines could evoke an increase in FN1 expression. LAMB2 expression (Figure 48) was unchanged with any statistical significance with any treatment type. Data presented earlier demonstrated that TGF-β and CTGF treatments could significantly decrease LAMB2 expression in the 3D tri-culture model.

TGF-β signalling genes were investigated next (Figure 49). The average CT value of these genes was suggestive of good expression in these samples, except for BMP7 expression where an average CT value of 35.88 indicated low expression of this gene. SMAD2 expression (Figure 49) was not significantly altered with any treatment type. Expression of SMAD3 (Figure 49) did not alter with any statistical significance, yet TGF-β appeared to evoke some downregulation in SMAD3 expression, a pattern that has been demonstrated with earlier data.

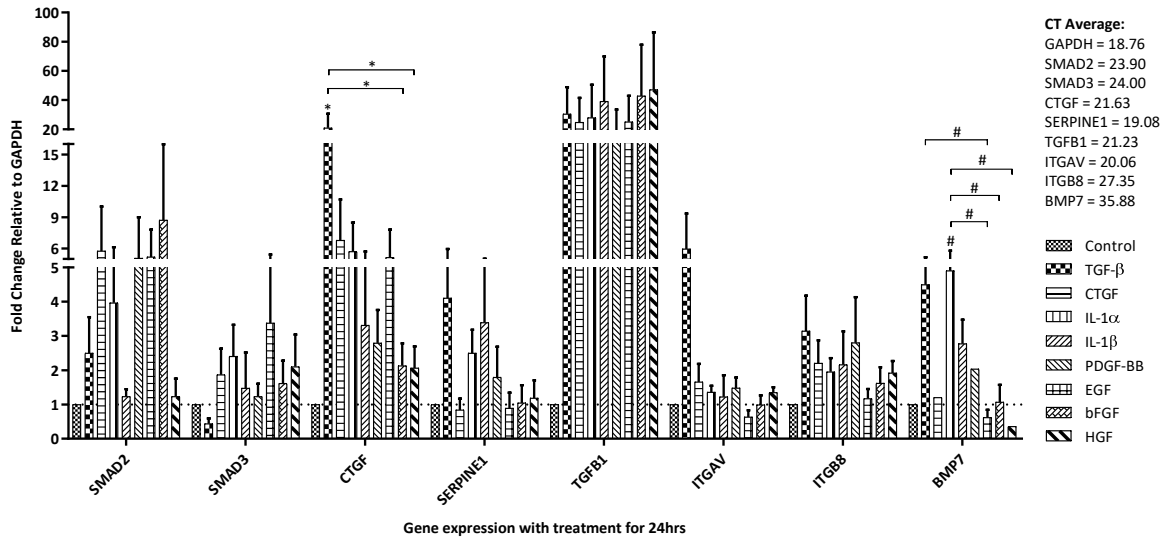

Figure 49. TGF-β signalling gene expression with TGF-β, CTGF, IL-1α, IL-1β, PDGF-BB, EGF, bFGF and HGF treatments in Celprogen fPOD 3D tri-cultures.

RT-qPCR performed on Celprogen fPOD 3D tri-cultures treated with TGF-β, CTGF, IL-1α, IL-1β, PDGF-BB, EGF, bFGF or HGF for 24hrs. ΔΔCT analysis to look at the relative fold-change of the gene of interest against housekeeping gene GAPDH. N=2, SEM error bars, One-way ANOVA; SMAD2 p-value 0.7868 (ns); SMAD3 p-value 0.5771 (ns); CTGF p-value 0.0360 (*); SERPINE1 p-value 0.1181 (ns); TGFB1 p-value 0.9448 (ns); ITGAV p-value 0.1145 (ns); ITGB8 p-value 0.3884 (ns); BMP7 p-value 0.0117 (*); followed by Tukey's multiple comparison post-tests. CT averages of each gene for reference.

As anticipated, CTGF expression (Figure 49) was significantly increased with TGF-β treatment, a pattern demonstrated by previous data. All other cytokine treatments appeared to increase CTGF expression to some degree, without achieving significance, with TGF-β treatment having evoked a significantly greater increase than bFGF and HGF treatments. Expression of SERPINE1 (Figure 49) did not change with any statistical significance across any treatment group. There were some trends in expression with treatments; TGF-β, IL-1α, IL-1β, and PDGF-BB treatments all appeared to increase SERPINE1 expression to some degree, while all other treatments had no effect. Earlier data had demonstrated that TGF-β treatment could significantly increase SERPINE1 expression in the 3D tri-culture model. TGFB1 expression (Figure 49) was not changed with statistical significance with any treatment. Expression of ITGAV (Figure 49) did not alter with any statistical significance across any treatment group. There did appear to be an increase with TGF-β treatment which did not reach significance. ITGB8 expression (Figure 49) also remained unchanged with any statistical significance.

Expression of BMP7 (Figure 49) was significantly increased with IL-1α treatment compared to control values and those evoked by EGF, bFGF and HGF treatments. Previously presented data also demonstrated TGF-β may evoke BMP7 expression.

Finally, other genes of interest in the processes of fibrosis and inflammation involved in glomerulosclerosis were examined (Figure 50). The average CT value of these genes was suggestive of reasonable expression in these samples, apart from genes CDH1 and CLDN1 where expression appeared low. Expression of TGM2 (Figure 50) remained unchanged with any statistical significance across treatments. Data presented earlier had shown that TGF-β generally evoked a decrease in TGM2 expression. CCL2 expression (Figure 50) was significantly increased with IL-1α and IL-1β treatments compared to control values. Previous data also demonstrated an increase in CCL2 expression with IL-1α treatment.

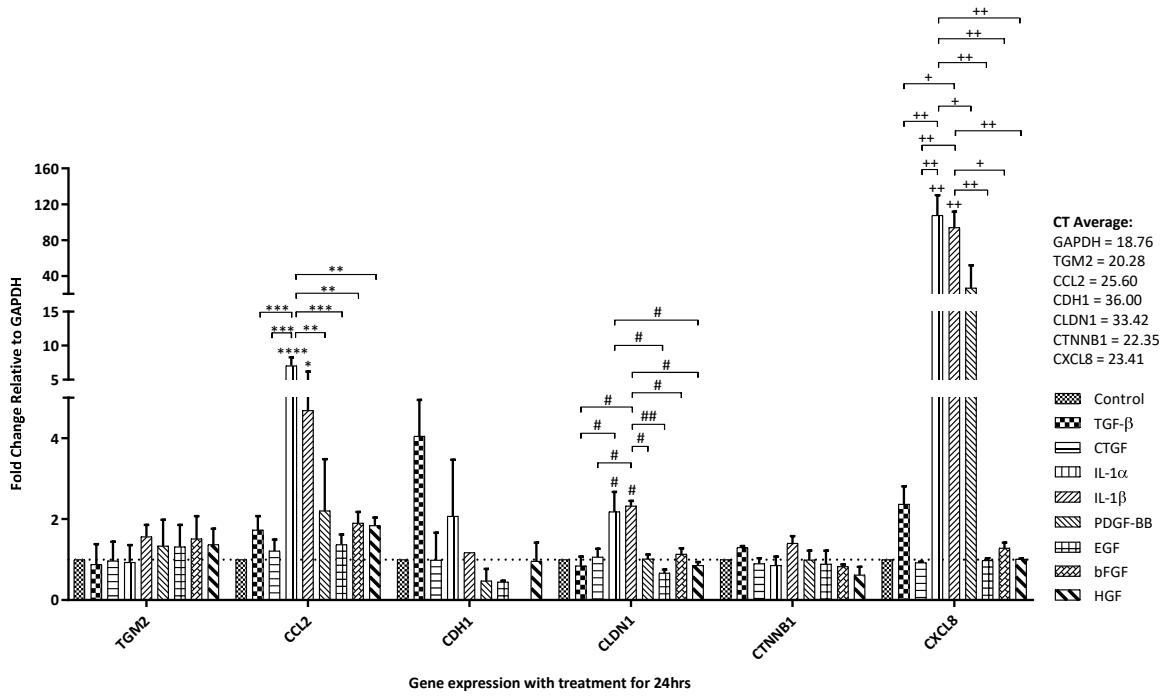

Figure 50. Expression of other genes of interest in Celprogen fPOD 3D tri-cultures treated with TGF-β, CTGF, IL-1α, IL-1β, PDGF-BB, EGF, bFGF, and HGF treatments.

RT-qPCR performed on Celprogen fPOD 3D tri-cultures treated with TGF-β, CTGF, IL-1α, IL-1β, PDGF-BB, EGF, bFGF or HGF for 24hrs. ΔΔCT analysis to look at the relative fold-change of the gene of interest against housekeeping gene GAPDH. N=2, SEM error bars, One-way ANOVA; TGM2 p-value 0.9477 (ns); CCL2 p-value 0.0001 (***); CDH1 p-value 0.0994 (ns); CLDN1 p-value 0.0026 (**); CTNNB1 p-value 0.2122 (ns); CXCL8 p-value 0.0006 (***); followed by Tukey's multiple comparison post-tests. CT averages of each gene for reference.

Expression of CDH1 (Figure 50) was not changed with statistical significance with any treatment type. There was some upregulation in CDH1 expression with TGF-β and IL-1α treatments and some downregulation with PDGF-BB and EGF treatments, which did not achieve significance. No value for bFGF treatment was attained. Earlier data demonstrated that TGF-β treatment could evoke a significant decrease in CDH1 expression in the 3D tri-culture model. CLDN1 expression (Figure 50) was significantly upregulated with IL-1α and IL-1β treatments. Data presented earlier had shown that TGF-β appeared to result in some downregulation of CLDN1 expression. Expression of CTNNB1 (Figure 50) was unchanged with any statistical significance across all treatment groups. Expression of CXCL8 (Figure 50) was significantly increased with IL-1α and IL-1β treatments. Treatment of TGF-β also appeared to evoke CXCL8 expression, without statistical significance. Earlier data had demonstrated that TGF-β may evoke upregulation in CXCL8 expression.

Nodule and RT-qPCR data presented in Figure 47-Figure 50 further demonstrated that other cytokines than TGF-β could evoke some fibrotic response in the 3D tri-culture model, with others evoking inflammatory responses. The extent of fibrotic or inflammatory gene response varied across treatment type and the gene investigated. The CT averages were generally good and reasonable for making fair analysis from the data, except for BMP7, CDH1 and CLDN1 where the average CT values were high at 35.88, 36.00 and 33.42, respectively. Conclusions from these genes will therefore be measured. This data establishes further that there is a multitude of cytokines involved in and capable of evoking fibrosis.

The data presented in this chapter validates the 3D tri-culture model as capable of modelling glomerulosclerosis in the read-out responses when treated with a variety of cytokines known to be involved in the human disease. Increases in nodule numbers along with significant changes in expression levels of genes implicated in both fibrosis and inflammation establishes the 3D tri-culture as both a model for glomerulosclerosis to investigate the effect of cytokines alone and in combination, as well as a tool to examine methods inhibiting and preventing both fibrosis and inflammation. In this chapter, methods used to try and inhibit fibrosis in the 3D tri-culture included treatments of proposed anti-fibrotic cytokines BMP7 and HGF, as well as the inhibitions of ALK5 and CTGF. These measures were successful in varying degrees and would have some practical limitations for clinical use with the specificity in targeting. The next chapter will explore results from a potential target in the inhibition and prevention of renal fibrosis, used in the 3D tri-culture model, which appears to have the necessary targeted specificity.

Chapter 7 – Results: 3D Tri-culture Model & αvβ8

This chapter will present data from the 3D tri-culture model where the integrin αvβ8 has been targeted with a neutralising antibody developed by MedImmune. The integrin αvβ8 has been introduced as an interesting potential target in the development and prevention of fibrosis, background data to support this theory shall be presented in the first part of this chapter to provide some context to testing this treatment in the 3D tri-culture model. This will be followed by nodule count and RT-qPCR data from the 3D tri-culture model, where 3D tri-cultures using either Celprogen fPODs or Lonza fPODs had been used.

Background Data for αvβ8

The data presented here is data that was produced in the workup of validating the targeting of αvβ8 for treatment of renal fibrosis specifically.

An important aspect of this work was to identify where αvβ8 is localised in the human kidney, the literature establishes that expression of the integrin is primarily in the kidney but not fully identifying in which cell types.[171] IF was utilised to investigate expression of αvβ8 in the glomerular cell types used in the 3D tri-culture model and IHC was used to study expression in human renal tissue.

Glomerular Cell IF for αvβ8

The glomerular cell types used in the 3D tri-culture model; Celprogen fPODs, fMCs and fGECs were grown in 2D and an anti-αvβ8 antibody was used to identify αvβ8 expression in these cell types (Figure 51). An anti-α-tubulin antibody was also utilised to inform the cytoskeletal structures of the glomerular cell types (Figure 51). Staining for αvβ8 appeared across all three glomerular cell types, with the strongest staining seen in Celprogen fPODs (Figure 51). There appeared to be a distinctive pattern of nuclear membrane staining for αvβ8 in Celprogen fPODs (Figure 51).

This initial work was suggestive of αvβ8 being primarily localised to PODs. Following this, expression patterns of αvβ8 in human renal tissue were investigated.

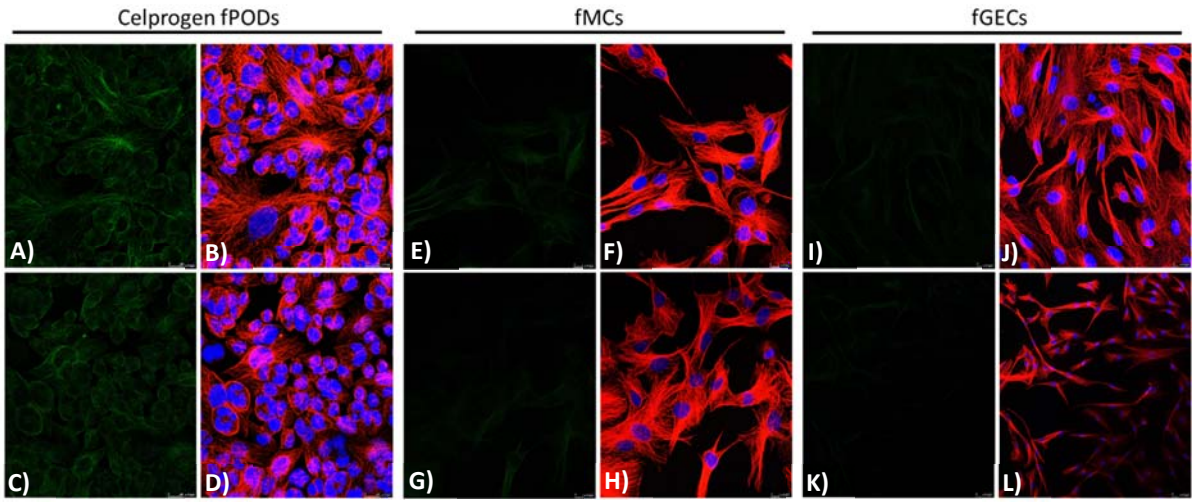

Figure 51.IF analysis for αvβ8 expression in 2D glomerular cell cultures.

IF of 2D glomerular cell types for αvβ8 (green; A, C, E, G, I and K) and α-tubulin (red; B, D, F, H, J and L). Nuclei were counterstained with DAPI (blue). 20X magnification.

Human Tissue IHC for αvβ8

To further understand where αvβ8 was localised in the kidney and so better elucidate and validate the use of inhibiting αvβ8 as a treatment for renal fibrosis, IHC was performed on human renal tissue by Dr Rafia Al-Lamki (Figure 52). The IHC experiment detected positive staining for αvβ8 in both tubular cells and glomeruli (Figure 52). There was stronger staining evident in glomeruli which was generally diffuse in nature, with indications of more acute staining localised to where PODs would be situated.

This data, coupled with the IF data presented above is suggestive of αvβ8 being localised to the glomeruli and more specifically to PODs. This lends support to firstly the theory that targeting of αvβ8 in renal fibrosis allows for a degree of specificity which is unachievable with other targets. Secondly, this data demonstrates clear justification for the validity of using the 3D tri-culture model to study and assess the use of an anti-αvβ8 antibody; with the αvβ8 integrin having been identified as present in glomerular cell types, specifically PODs. The data subsequently presented is that of using the anti-αvβ8 antibody developed by MedImmune in the 3D tri-culture model.

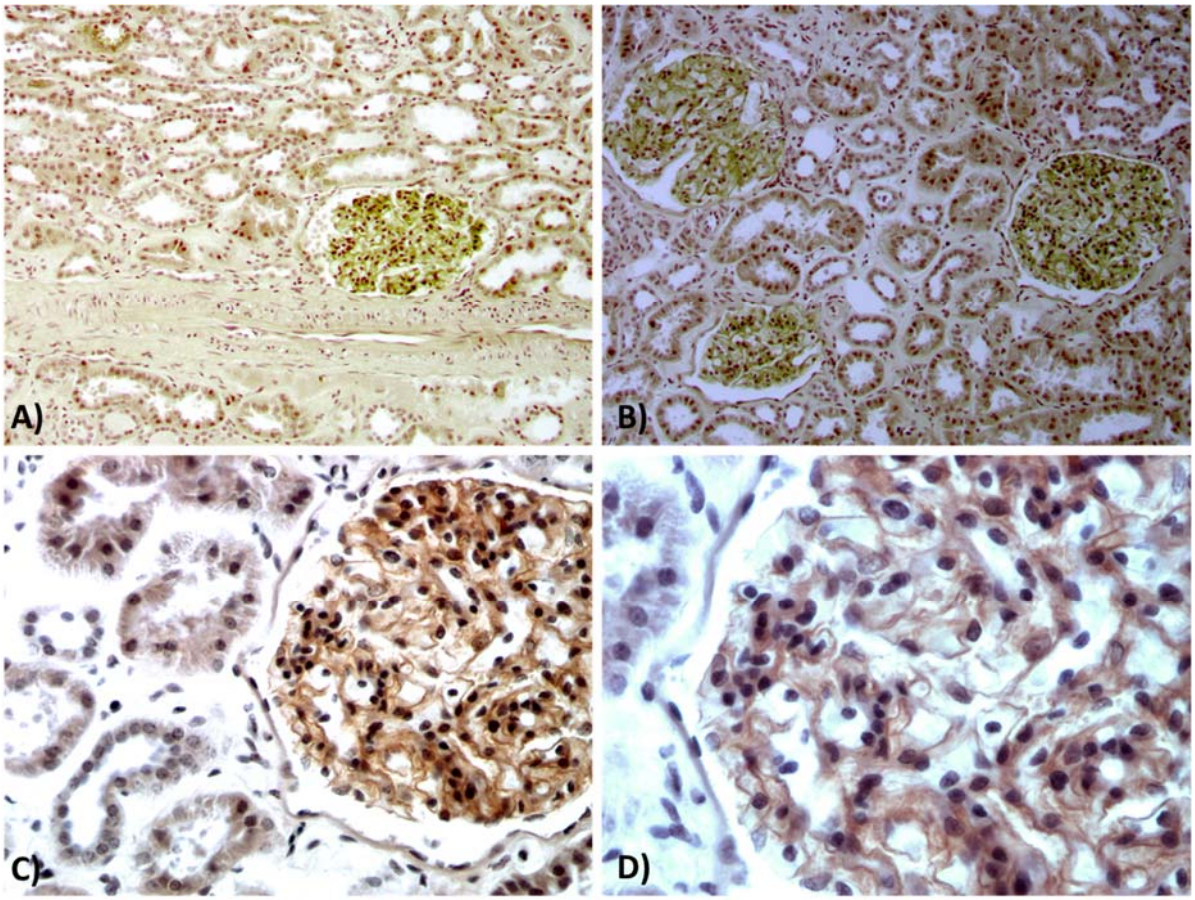

Figure 52. IHC Staining for αvβ8 in human normal kidney tissue.

IHC for αvβ8 in human normal kidney tissue using HRP/DAB. Positive staining could be seen in tubular cells and glomeruli. A-B 20X magnification and C-D 40X magnification. Credit: Dr Rafia Al-Lamki.

Anti-αvβ8 in 3D Tri-culture

The anti-αvβ8 antibody was tested in the 3D tri-culture model to assess how inhibition of the αvβ8 affected fibrosis induced in the system with use of either TGF-β or CTGF, which have both demonstrated to evoke some fibrotic response akin to glomerulosclerosis. As with previous data, the results of this will be presented as nodule counts and RT-qPCR data. Both Celprogen fPODs and Lonza fPODs were used in 3D tri-cultures where the anti-αvβ8 antibody was used. The results below shall be presented in two sections, one where Celprogen fPODs were utilised and one where Lonza fPODs were.

Nodule Counts

Celprogen fPOD 3D tri-cultures

3D tri-cultures were treated with either TGF-β or CTGF alone or in combination with the αvβ8 antibody or control antibody NIP228, for 24hrs before nodule counts (Figure 53). As anticipated, in light of earlier data, TGF-β and CTGF treatments evoked a significant increase in nodule formation in the 3D tri-culture model (Figure 53). Co-treatment with the anti-αvβ8 antibody resulted in a partial inhibition of nodule formation evoked by TGF-β and CTGF treatments (Figure 53). The control antibody, NIP228, hand no effect up nodule counts (Figure 53).

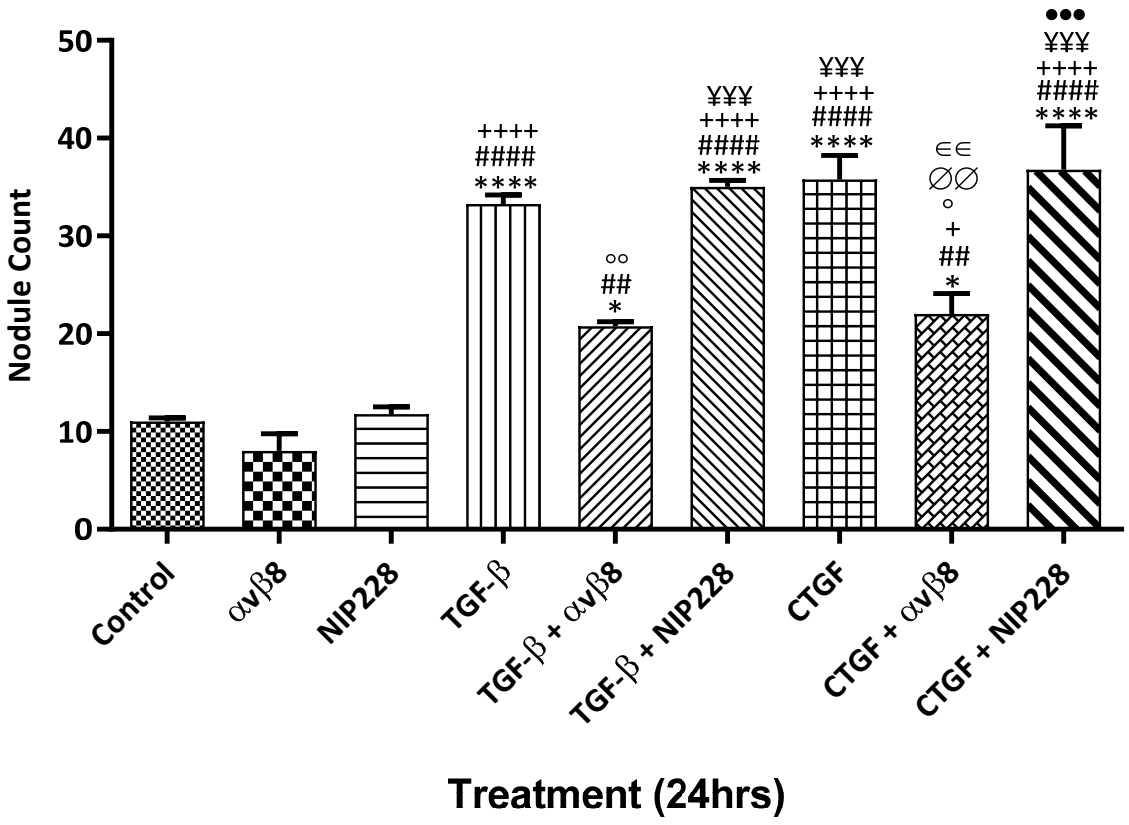

Figure 53. Nodule counts with TGF-β, CTGF, anti-αvβ8 antibody and NIP228 antibody treatments in Celprogen fPOD 3D tri-cultures.

Celprogen fPOD 3D tri-cultures were treated with either TGF-β, CTGF, anti-αvβ8 antibody or NIP228 antibody alone or in combination for 24hrs prior to nodule counts. N=2, SEM error bars, One-way ANOVA p-value <0.0001 (****), followed by Tukey's multiple comparison (Control = *; αvβ8 = #; NIP228 = +; TGF-β = °; TGF-β + αvβ8 = ¥; TGF-β + NIP228 = ∅; CTGF = ∈; CTGF + αvβ8 = •).

Lonza fPOD 3D tri-cultures

As above 3D tri-cultures were treated with either TGF-β or CTGF alone or in combination with the anti-αvβ8 antibody or control antibody NIP228, for 24hrs before nodule counts (Figure 54). Two further treatments were used either alone or in combination with other treatments. These additional treatments were LTGF-β and 1D11, an anti-TGF-β antibody (Figure 54). This data is at N=1 and therefore no statistical analysis was achieved. There appeared to be increased nodule formation with TGF-β and CTGF treatments, in line with previous data (Figure 54). LTGF-β treatment also appeared to evoke increased nodule formation, while 1D11 appeared to cause some small reduction in nodule numbers (Figure 54). Co-treatments of either 1D11 or anti-αvβ8 looked to reduce nodule formation evoked by TGF-β, CTGF and LTGF-β treatments; suggesting both 1D11 and anti-αvβ8 were affecting a common pathway (Figure 54). Treatment with the anti-αvβ8 antibody appeared to evoke some

increase in nodule number (Figure 54). NIP228 also appeared to have some effect upon nodule formation in the 3D tri-culture model in this data set, seemingly evoking some increased nodule formation when used in isolation and apparent inhibition of CTGF, LTGF-β and αvβ8 evoked increased in nodule numbers (Figure 54).

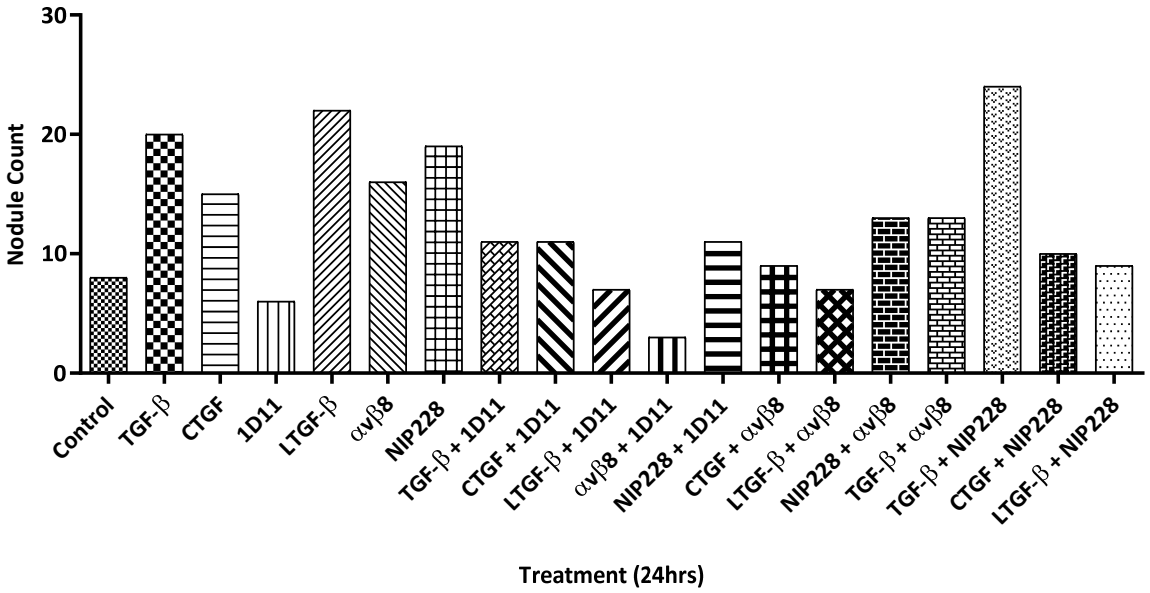

Figure 54. Nodule counts with TGF-β, CTGF, 1D11, LTGF-β, anti-αvβ8 antibody and NIP228 antibody treatments in Lonza fPOD 3D tri-cultures.

Lonza fPOD 3D tri-cultures were treated with either TGF-β, CTGF, 1D11, LTGF-β, anti-αvβ8 antibody, or NIP228 antibody alone or in combination for 24hrs before nodule counts. N=1.

The nodule data from 3D tri-cultures presented in Figure 53-Figure 54 both demonstrate the repeatedly established response of increased nodule counts with TGF-β treatment. CTGF and LTGF-β treatments also evoked this response. Both data sets depicted that anti-αvβ8 antibody treatment could partially inhibit the increased nodule formation evoked by whichever cytokine. The effect of the anti-αvβ8 antibody treatment was mirrored with 1D11 treatment, the anti-TGF-β treatment, suggesting that the anti-αvβ8 was preventing TGF-β activity

RT-qPCR

The effects of the anti-αvβ8 antibody in the 3D tri-culture system were further investigated by examination of gene expression. As with nodule data, RT-qPCR data will be separated by 3D tri-cultures using either Celprogen fPOD or Lonza fPOD.

Celprogen fPOD 3D tri-cultures

3D tri-cultures were treated with either TGF-β or CTGF alone or in combination with the anti-αvβ8 antibody or control antibody NIP228 for 24hrs. The panel of genes examined in these experiments can be separated into the broad categories outlined earlier of ECM genes and TGF-β signalling genes. ECM genes will be discussed first (Figure 55), CT averages for these genes were suggestive of a good expression level. COL1A1 expression (Figure 55) was significantly increased from control values by NIP228 and TGF-β co-treatment. All other treatments appeared to evoke some increase in COL1A1 expression, without statistical significance. TGF-β and CTGF treatments evoked a similar increase in COL1A1 expression, which co-treatment with anti-αvβ8 antibody had no apparent effect upon. Earlier data had demonstrated an increase in COL1A1 expression could be evoked with TGF-β treatment in the 3D tri-culture model.

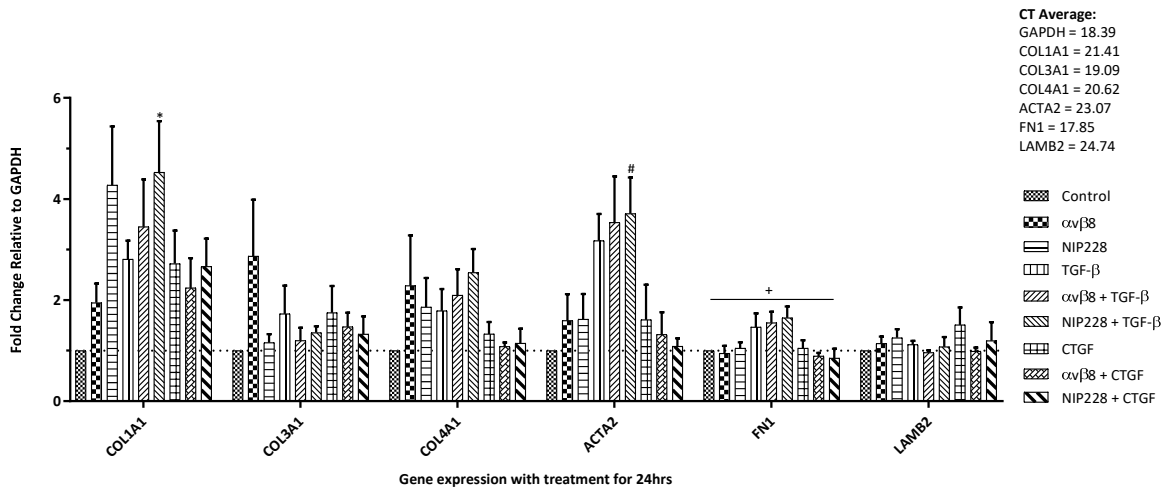

Figure 55. ECM gene expression with anti-αvβ8 antibody, NIP228 antibody, TGF-β and CTGF treatments in Celprogen fPOD 3D tri-cultures.

RT-qPCR performed on Celprogen fPOD 3D tri-cultures treated with anti-αvβ8 antibody, NIP228 antibody, TGF-β and CTGF for 24hrs. ΔΔCT analysis to look at the relative fold-change of the gene of interest against housekeeping gene GAPDH. N=2, SEM error bars, One-way ANOVA; COL1A1 p-value 0.0417 (*); COL3A1 p-value 0.2859 (ns); COL4A1 p-value 0.2633 (ns); ACTA2 p-value 0.0048 (**); FN1 p-value 0.0131 (*); LAMB2 p-value 0.6469 (ns); followed by Tukey's multiple comparison post-tests. CT averages of each gene for reference.

Expression of COL3A1 (Figure 55) was not changed with any statistical significance with any treatment group. Earlier data demonstrated a similar outcome. COL4A1 expression (Figure 55) did not alter with any treatment type with statistical significance. TGF-β treatment seemed to result in increased COL4A1 expression, as demonstrated in the 3D tri-culture model with previous data. Expression of ACTA2 (Figure 55) was significantly increased by co-treatment of NIP228 and TGF-β compared to control values. Treatments with TGF-β alone and in combination with anti-αvβ8 evoked a similar, non-statistically significant, increase in ACTA2 expression. This suggests that it is TGF-β which is promoting ACTA2 expression, fitting with earlier data. CTGF appeared to induce a slight increase in ACTA2 expression, as seen with earlier data, that both anti-αvβ8 and NIP228 appeared to somewhat inhibit. FN1 expression (Figure 55) showed a statistically significant change across treatment groups. TGF-β treatment appeared to evoke an increase in FN1 expression which neither the NIP228 or anti-αvβ8 antibodies had any effect upon. No other treatments appeared to alter FN1 expression from control values. Earlier data had demonstrated increased FN1 expression with TGF-β and CTGF treatments. Expression of LAMB2 (Figure 55) remained unchanged with any statistical significance across any treatment type.

TGF-β signalling genes (Figure 56) examined shall be discussed next. CT averages for these genes were suggestive of a good expression level, except SMAD2, where expression was lower, with an average CT value of 28.46. SMAD2 expression (Figure 56) remained statistically unchanged across all treatments. There were, however, some trends in expression with treatments. All treatments appeared to evoke some increase in SMAD2 expression. Earlier data had demonstrated that both TGF-β and CTGF treatments may evoke increased SMAD2 expression. Expression of SMAD3 (Figure 56) did not change with any statistical significance across any treatment type; there did appear to be some increase in SMAD3 expression with the anti-αvβ8 antibody. Previous data demonstrated TGF-β could downregulate SMAD3 expression. CTGF expression (Figure 56) remained unchanged with any statistical significance with any treatment group. Yet, as had been anticipated in light of earlier data, TGF-β appeared to upregulate CTGF expression, which did not reach statistical significance. Expression of SERPINE1 (Figure 56) did not change with any statistical significance with any treatment. TGF-β evoked some increase in SERPINE1 expression which did not reach significance. Previous data had demonstrated that TGF-β could upregulate SERPINE1 expression. TGFB1 expression (Figure 56) was significantly higher with anti-αvβ8 and TGF-β co-treatment than with CTGF treatment alone or in combination with an anti-αvβ8 antibody treatment. Earlier data demonstrated TGF-β and CTGF treatments increased TGFB1 expression.

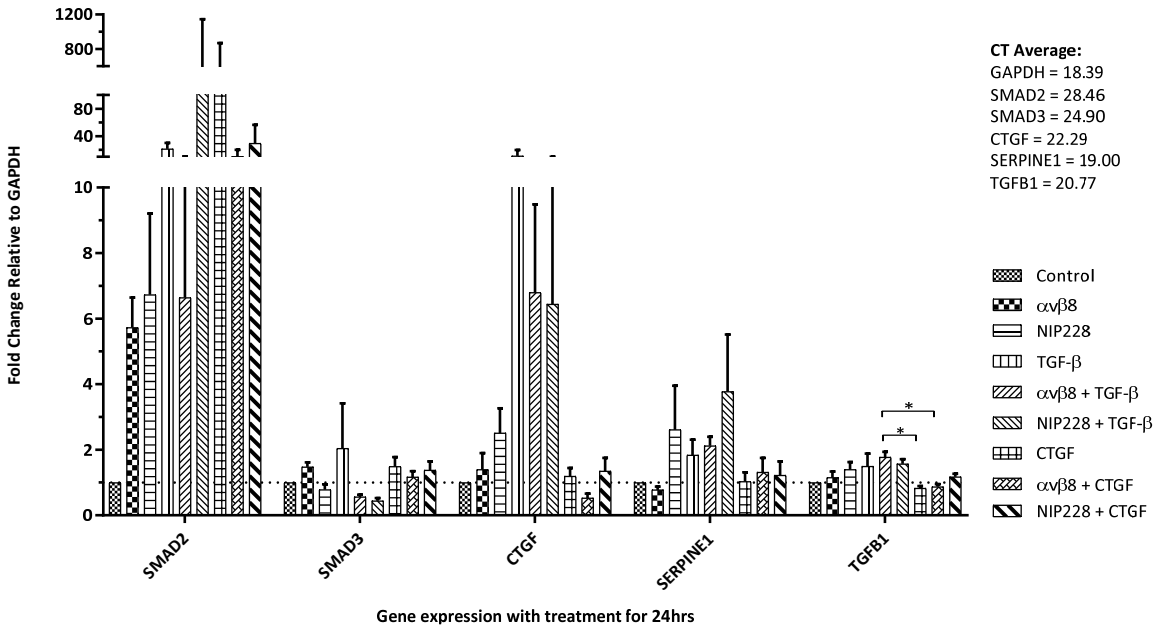

Figure 56. TGF-β signalling gene expression with anti-αvβ8 antibody, NIP228 antibody, TGF-β, and CTGF treatments in Celprogen fPOD 3D tri-cultures.

RT-qPCR was performed on Celprogen fPOD 3D tri-cultures treated with anti-αvβ8 antibody, NIP228 antibody, TGF β, and CTGF for 24hrs. ΔΔCT analysis to look at the relative fold-change of the gene of interest against housekeeping gene GAPDH. N=2, SEM error bars, One-way ANOVA; SMAD2 p value 0.5298 (ns); SMAD3 p-value 0.0511 (ns); CTGF p-value 0.1274 (ns); SERPINE1 p-value 0.2016 (ns); TGFB1 p-value 0.0121 (*); followed by Tukey's multiple comparison post-tests. CT averages of each gene for reference.

Lonza fPOD 3D tri-cultures

COL1A1 expression (Figure 57) remained unchanged with any statistical significance with any treatment. TGF-β appeared to evoke increased COL1A1 expression, as anticipated considering earlier data. The average CT value for COL1A1 was 18.44 in these samples, demonstrating a high level of expression.

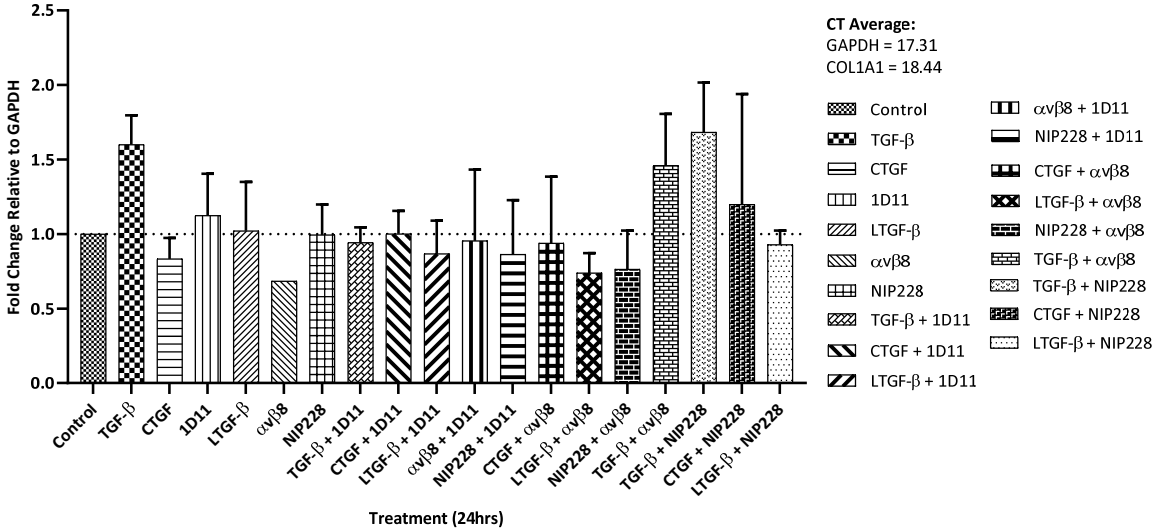

Figure 57. COL1A1 expression in Lonza fPOD 3D tri-cultures treated with TGF-β, CTGF, 1D11 antibody, LTGF-β, anti-αvβ8 antibody, and NIP228 antibody treatments.

RT-qPCR performed on Lonza fPOD 3D tri-cultures treated with TGF-β, CTGF, 1D11 antibody, LTGF-β, anti-αvβ8 antibody, and NIP228 antibody for 24hrs. ΔΔCT analysis to look at the relative fold-change of the gene of interest against housekeeping gene GAPDH. N=2 (N=1, anti-αvβ8 antibody), SEM error bars, One-way ANOVA; COL1A1 p-value 0.7457 (ns), followed by Tukey's multiple comparison post-tests. Gene CT averages for reference.

The data set for expression of COL4A1 (Figure 58) was at N1 so no statistical analysis was possible and so data trends are reported. TGF-β treatment appeared to evoke an increase in COL4A1 expression, consistent with previous data sets. The 1D11 antibody partially inhibited some of the TGF-β mediated upregulation of COL4A1 expression; while the anti-αvβ8 and NIP228 antibody treatments reduced TGF-β mediated expression below control values, resulting in downregulation of COL4A1. CTGF treatment did not alter COL4A1 expression from control values, in line with earlier data. LTGF-β appeared to evoke some increase in COL4A1 expression, which co-treatment with 1D11 brought to control values. LTGF-β with co-treatment of either anti-αvβ8 or NIP228 antibody resulted in overall downregulation in COL4A1 expression. No CT data was attained for the anti-αvβ8 antibody treatment group in this data set. The average CT value for COL4A1 expression was 17.66, therefore demonstrating a high level of expression in these samples.

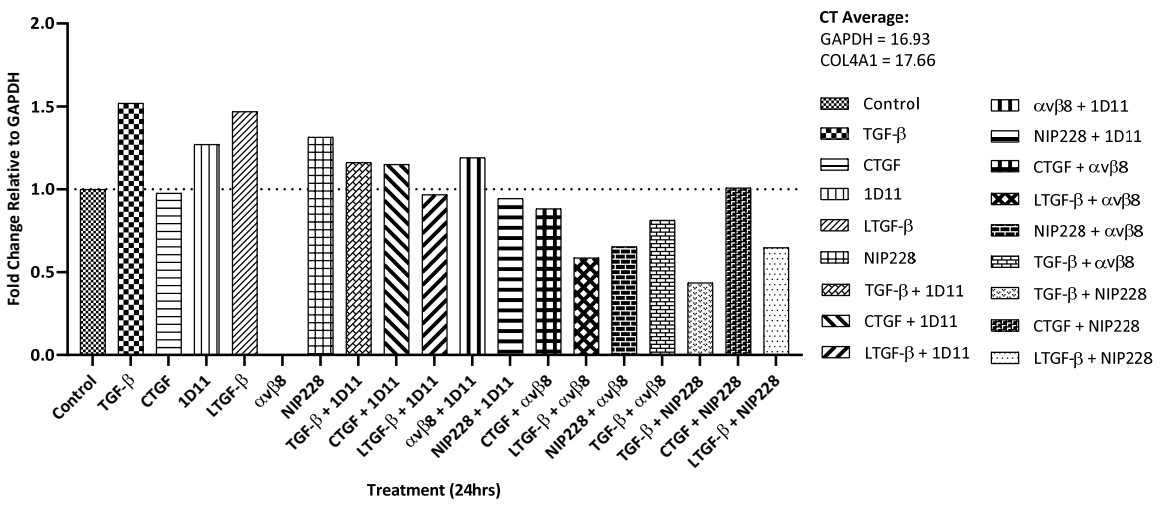

Figure 58. COL4A1 expression in Lonza fPOD 3D tri-cultures treated with TGF-β, CTGF, 1D11 antibody, LTGF-β, anti-αvβ8 antibody, and NIP228 antibody treatments.

RT-qPCR performed on Lonza fPOD 3D tri-cultures treated with TGF-β, CTGF, 1D11 antibody, LTGF-β, anti-αvβ8 antibody, and NIP228 antibody for 24hrs. ΔΔCT analysis to look at the relative fold-change of the gene of interest against housekeeping gene GAPDH. N=1. Gene CT averages for reference.

Expression of ACTA2 (Figure 59) was not changed with any statistical significance across any treatment group. Some trends in data were noted, TGF-β treatment appeared to induce an increase in ACTA2 expression, following patterns of earlier data. 1D11 appeared to reduce TGF-β mediated ACTA2 expression, while the anti-αvβ8 antibody had little effect. CTGF treatment seemed to evoke a slight increase in ACTA2 expression, data presented earlier had demonstrated that CTGF could evoke increased ACTA2 expression. Co-treatment of 1D11 with CTGF did not change ACTA2 expression from that with CTGF treatment alone. LTGF-β treatment appeared to result in ACTA2 upregulation, with 1D11 co-treatment inhibiting this to some degree. Co-treatment of anti-αvβ8 antibody with LTGF-β resulted in complete inhibition of LTGF-β evoked ACTA2 expression, bringing expression below control values. The average CT value for ACTA2 was 21.62, which demonstrates a good level of expression for ACTA2 RNA in these samples.

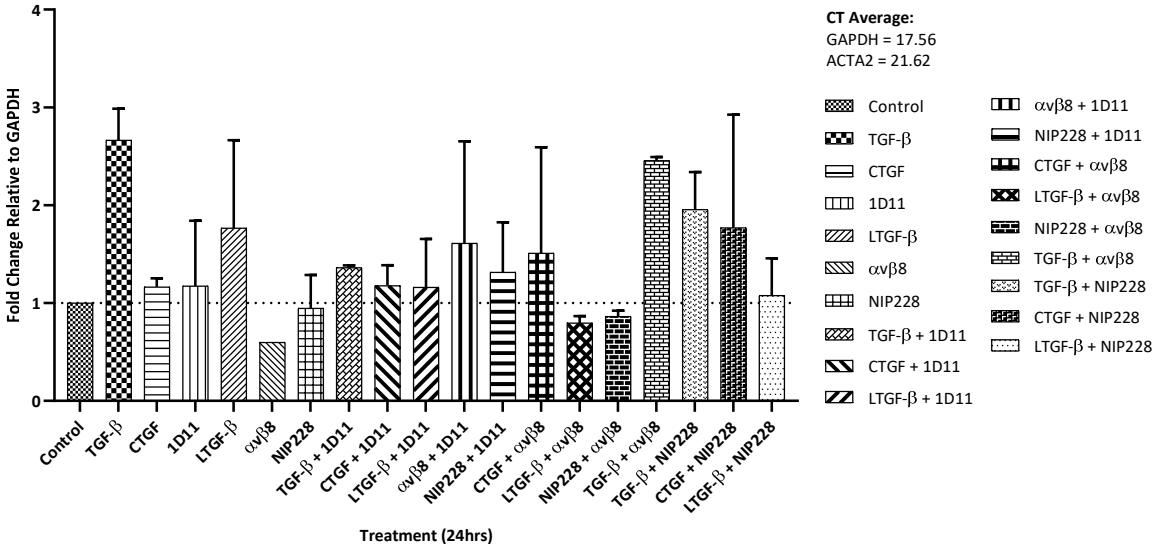

Figure 59. ACTA2 expression in Lonza fPOD 3D tri-cultures treated with TGF-β, CTGF, 1D11 antibody, LTGF-β, anti-αvβ8 antibody, and NIP228 antibody treatments.

RT-qPCR performed on Lonza fPOD 3D tri-cultures treated with TGF-β, CTGF, 1D11 antibody, LTGF-β, anti-αvβ8 antibody, and NIP228 antibody for 24hrs. ΔΔCT analysis to look at the relative fold-change of the gene of interest against housekeeping gene GAPDH. N=2 (N=1, anti-αvβ8 antibody), SEM error bars, One-way ANOVA; ACTA2 p-value 0.6363 (ns), followed by Tukey's multiple comparison post-tests. Gene CT averages for reference.

FN1 expression (Figure 60) was altered with statistical significance across the treatment groups. TGF-β treatment appeared to induce an increase in FN1 expression, which 1D11 inhibited when used in co-treatment. Co-treatments of either anti-αvβ8 or NIP228 antibody with TGF-β did not change FN1 expression evoked by TGF-β. Earlier data had also demonstrated that TGF-β could cause increased FN1 expression. CTGF treatment seemed to result in slightly increased FN1 expression, earlier data established CTGF could increase FN1 expression. Neither 1D11 or anti-αvβ8 antibody treatments affected CTGF treatment with FN1 expression. Treatment of LTGF-β resulted in a slight increase in FN1 expression, which anti-αvβ8 antibody reduced to control values when used in co-treatment. 1D11 and anti-αvβ8 antibody treatments, when used alone, appeared to result in some downregulation in FN1 expression. NIP228 treatment used alone did not alter FN1 expression from control values. The CT average value for FN1 in these samples was 17.26, which demonstrate there was a high level of expression in these samples.

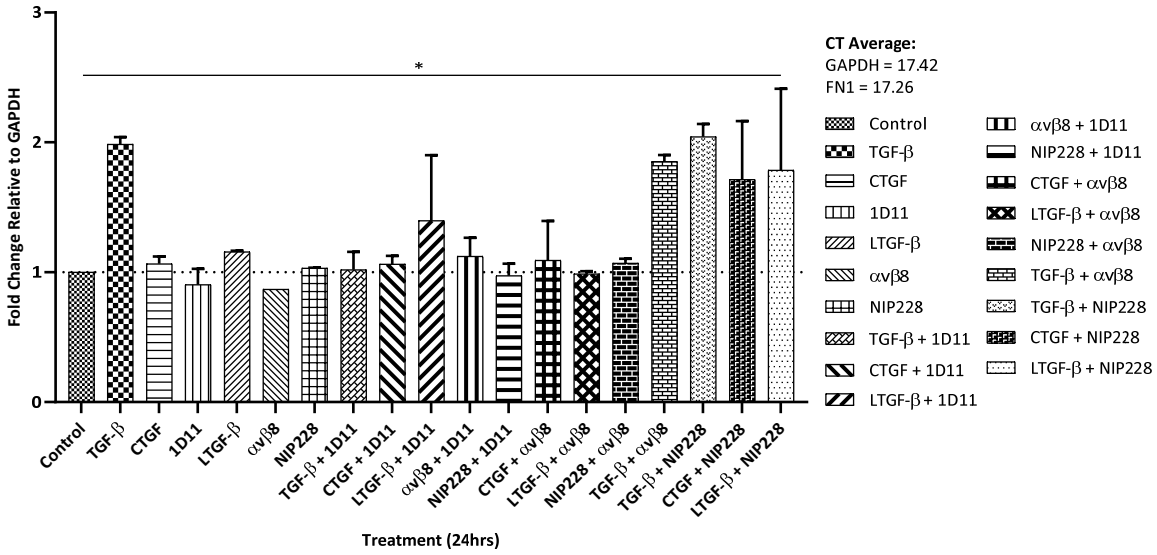

Figure 60. FN1 expression in Lonza fPOD 3D tri-cultures treated with TGF-β, CTGF, 1D11 antibody, LTGF-β, anti-αvβ8 antibody, and NIP228 antibody treatments.

RT-qPCR performed on Lonza fPOD 3D tri-cultures treated with TGF-β, CTGF, 1D11 antibody, LTGF-β, anti-αvβ8 antibody, and NIP228 antibody for 24hrs. ΔΔCT analysis to look at the relative fold-change of the gene of interest against housekeeping gene GAPDH. N=2 (N=1, anti-αvβ8 antibody), SEM error bars, One-way ANOVA; FN1 p-value 0.0238 (*), followed by Tukey's multiple comparison post-tests. Gene CT averages for reference.

CTGF expression (Figure 61) was significantly increased with TGF-β treatment alone and when in combination with the anti-αvβ8 antibody. Co-treatment of 1D11 with TGF-β significantly reduced this increase. Earlier data established TGF-β treatment evoked increased CTGF expression in the 3D tri-culture model. CTGF treatment appeared to evoke some increased CTGF expression, which co-treatments with anti-αvβ8 and NIP228 antibodies seemed to exacerbate. CTGF co-treatment with 1D11 brought CTGF expression to control values. Earlier data had shown CTGF treatment did not change CTGF expression. Treatment with LTGF-β appeared to increase CTGF expression; which 1D11, anti-αvβ8, and NIP228 antibody co-treatments brought to control expression levels. Treatments of either anti-αvβ8 or NIP228 antibodies resulted in some increased CTGF expression. The average CT value for CTGF expression was 18.13, demonstrating a high level of expression for CTGF RNA.

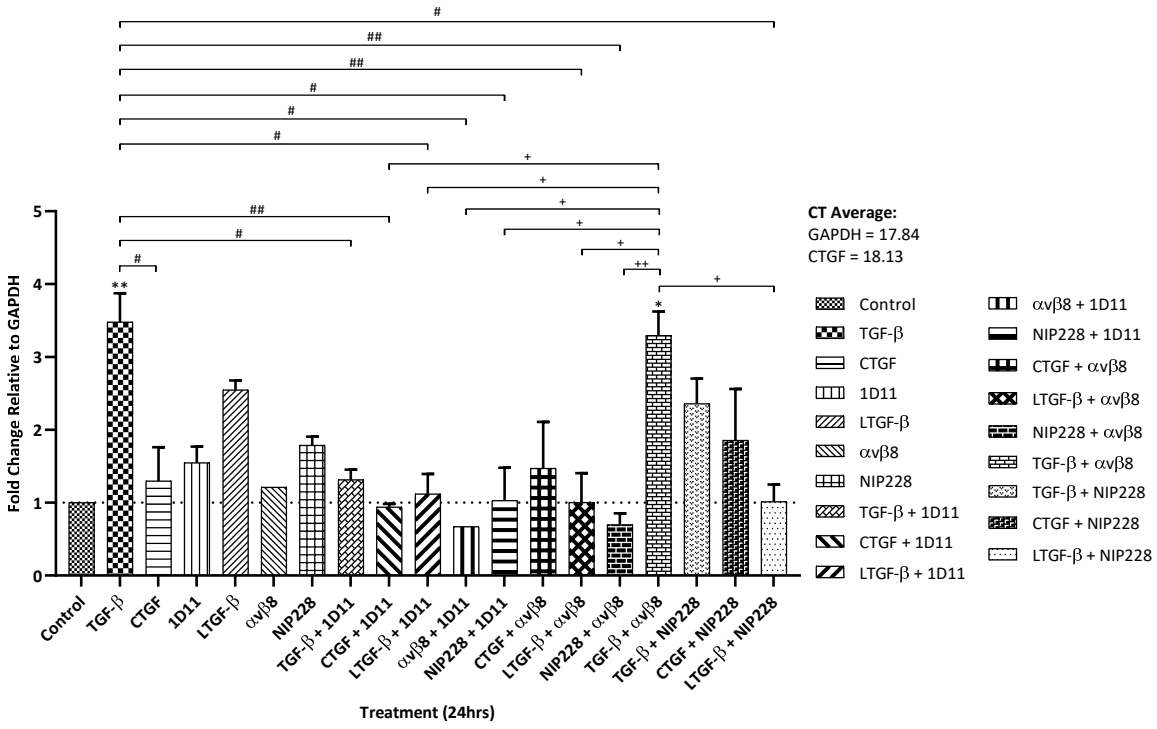

Figure 61. CTGF expression in Lonza fPOD 3D tri-cultures treated with TGF-β, CTGF, 1D11 antibody, LTGF-β, anti-αvβ8 antibody, and NIP228 antibody treatments.

RT-qPCR performed on Lonza fPOD 3D tri-cultures treated with TGF-β, CTGF, 1D11 antibody, LTGF-β, anti-αvβ8 antibody, and NIP228 antibody for 24hrs. ΔΔCT analysis to look at the relative fold-change of the gene of interest against housekeeping gene GAPDH. N=2 (N=1 anti-αvβ8 antibody), SEM error bars, One-way ANOVA; CTGF p-value 0.0007 (***), followed by Tukey's multiple comparison post-tests. Gene CT averages for reference.

Expression of SERPINE1 (Figure 62) was significantly increased with TGF-β treatment, in-line with earlier data. Co-treatment of 1D11 with TGF-β brought SERPINE1 expression back to control values, while anti-αvβ8 and NIP228 antibodies did not. CTGF treatment did not change SERPINE1 expression, previous data demonstrated this response also. Treatment with LTGF-β resulted in a non-significant increase in SERPINE1 expression, which both 1D11 and anti-αvβ8 antibody co-treatments inhibited to below control values of expression. The average CT value for SERPINE1 expression in these samples was 17.15, indicating a high level of expression.

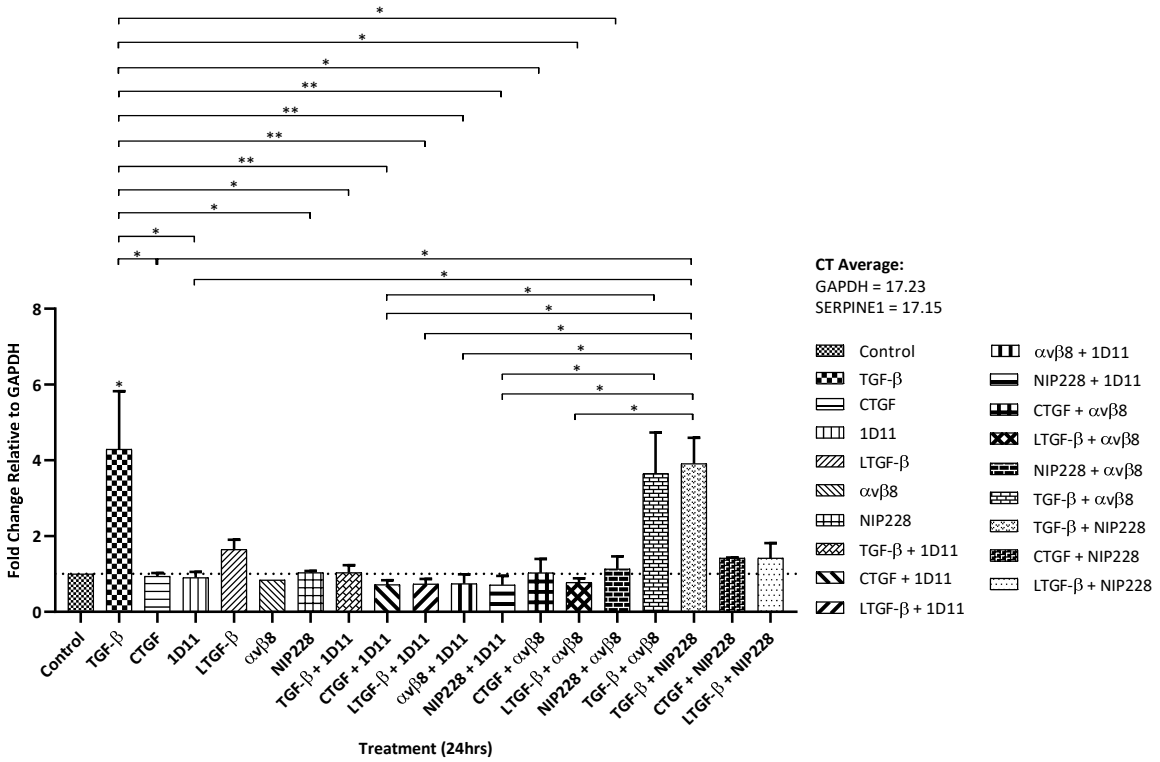

Figure 62. SERPINE1 expression in Lonza fPOD 3D tri-cultures treated with TGF-β, CTGF, 1D11 antibody, LTGF-β, anti-αvβ8 antibody, and NIP228 antibody treatments.

RT-qPCR performed on Lonza fPOD 3D tri-cultures treated with TGF-β, CTGF, 1D11 antibody, LTGF-β, anti-αvβ8 antibody, and NIP228 antibody for 24hrs. ΔΔCT analysis to look at the relative fold-change of the gene of interest against housekeeping gene GAPDH. N=2 (N=1, anti-αvβ8 antibody), SEM error bars, One-way ANOVA; SERPINE1 p-value 0.0007 (***), followed by Tukey's multiple comparison post-tests. Gene CT averages for reference.

Nodule and RT-qPCR data presented in Figure 53-Figure 62 establishes that the targeting of αvβ8 to reduce TGF-β mediated fibrosis is valid, particularly when LTGF-β was used in the system, as responses mediated by exogenous TGF-β often remained unaffected by anti-αvβ8 antibody. LTGF-β did not consistently evoke a fibrotic response, failing to induce FN1 and SERPINE1 expression(Figure 60 and Figure 62), limiting the window of opportunity for anti-αvβ8 antibody to effect. Yet, LTGF-β induced CTGF and COL4A1 upregulation (Figure 58 and Figure 61) was attenuated with αvβ8 inhibition. This early data needs further work to fully validate αvβ8 as an effective target. CT averages in these data sets were all good. To further validate the 3D tri-culture model and its findings, including data involving the targeting of αvβ8 in the inhibition of TGF-β mediated fibrosis, the use of human tissue was explored.

Chapter 8 – Results: Glomeruli Isolation & HOC

Preceding chapters have described the development and use of the 3D tri-culture model. To explore and validate the results of this work, human renal tissue was utilised. There were two ways in which human renal tissue was used, firstly in the isolation of glomeruli as a potential source of PODs and secondly to create HOC to reproduce 3D tri-culture experimental treatments to examine whether responses aligned. This chapter will be divided into glomeruli isolation work and HOC data. The glomeruli isolation section shall be presented first.

Glomeruli Isolation

The initial goal of this glomeruli isolation work was to explore the possibility of isolating PODs for use in the 3D tri-culture model after the identification of CHO contamination in Celprogen fPODs and the apparent lack of commercially available PODs for purchase. The isolation of glomeruli from renal tissue is established in the literature, with some variances in methodologies. Therefore, some optimisation work was required in the set-up of this work. Both the literature and collaboration with the Jaakko Patrakka group of the Karolinska Institute were used in the work-up of the final protocol described in the methods chapter.[184, 185] Glomeruli isolation involves the passing of renal tissue through sieves of varying sizes to separate the glomeruli from the rest of the tissue. The premise of glomerular isolation for POD isolation is that cultured isolated glomeruli will adhere to plasticware and there will be glomerular cell outgrowth, that initially will be PODs.

Mouse kidneys were used to become accustomed to techniques in the glomeruli isolation procedure. This was to ensure that the valuable and limited resource of human renal tissue was not wasted. Mouse isolation work shall be presented first, followed by human data.

Mouse Glomeruli Isolation

The fine detail of the mouse glomeruli isolation procedures is covered in the methods chapter, only the main point of optimisation shall be covered here. Three separate mouse glomeruli isolation experiments were performed, with a key point of optimisation being the use of collagenase. Light microscope images (Figure 63) were taken of the final filtrate containing glomeruli, where a five minute collagenase treatment was compared to no collagenase treatment.

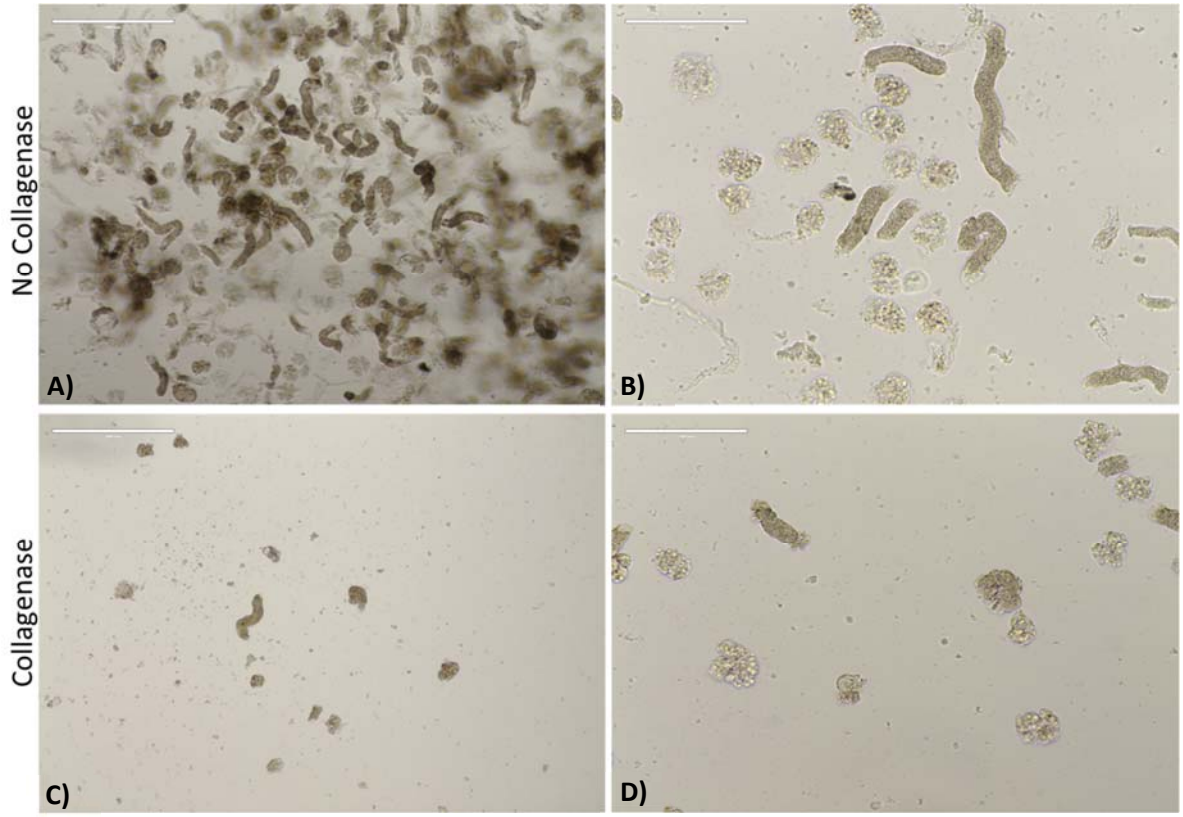

Figure 63. Bright field images of isolated mouse glomeruli.

Bright field images of final filtrate following glomeruli isolation protocol on mouse kidneys. Two experimental procedures followed one with a five minute collagenase treatment (C-D) and one with no collagenase treatment (A-B). (A and C) 10X magnification and (B and D) 20x magnification.

The collagenase treatment reduced the number of tubule sections and glomeruli within the final filtrate (Figure 63). After isolation glomeruli were cultured for various time points before fixation for IF of glomerular cell markers to assess the nature of cellular outgrowth. Isolated mouse glomeruli were fixed and stained for IF at days 6 (Figure 64), 9 (Figure 65), and 13 (Figure 66). Cellular outgrowth is purported to begin between days 7-10 and after day 12 other glomerular cell types, such as MCs may appear and take over the culture. POD markers used were podocin, podocalyxin, nephrin, and GLEPP1. MC markers were αSMA and fibronectin. GEC markers were CD31 and vWF.

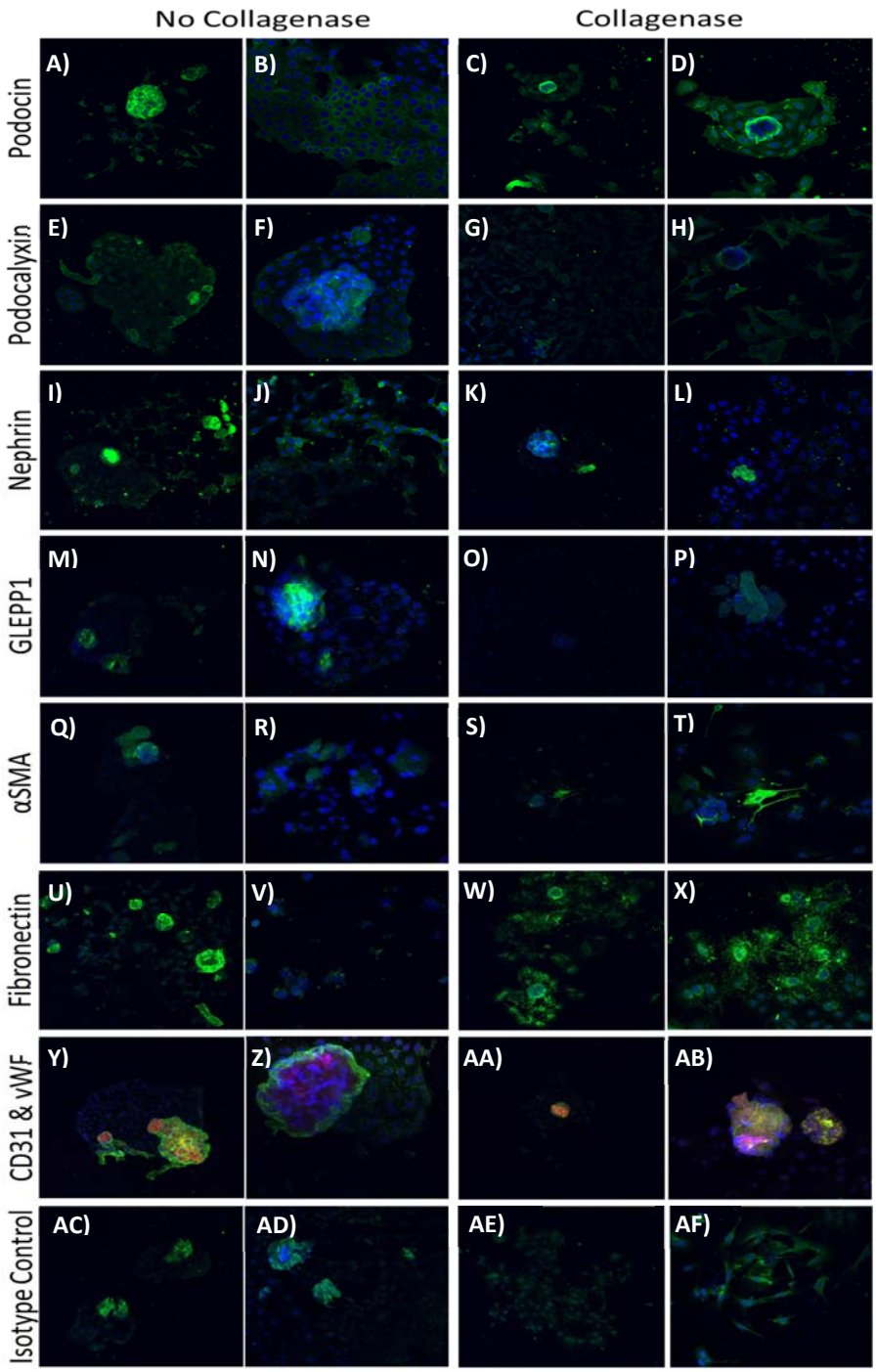

Figure 64. IF of isolated mouse glomeruli on day 6.

IF of isolated mouse glomeruli on day 6 of culture where mouse kidneys had either 5 minutes treatment with collagenase or no collagenase treatment during the isolation procedure. Glomerular cell markers were used to examine the nature of any cellular outgrowth. For PODs, this was podocin (green, A-D), podocalyxin (green, E-H), nephrin (green, I-L), GLEPP1 (green, M-P). For MCs, αSMA (green, Q-T) and fibronectin (green, U-X). For GECs CD31 (green, Y-AB) and vWF (red, Y-AB). Isotype control (green, AC-AF). Nuclei were counterstained with DAPI (blue). 10X magnification (A,C,E,G,I,K,M,O,Q,S,U,W,Y,AA,AC and AE) and 20X magnification (B,D,F,H,J,L,N,P,R,T,V,X,Z,AB,AD,AF).

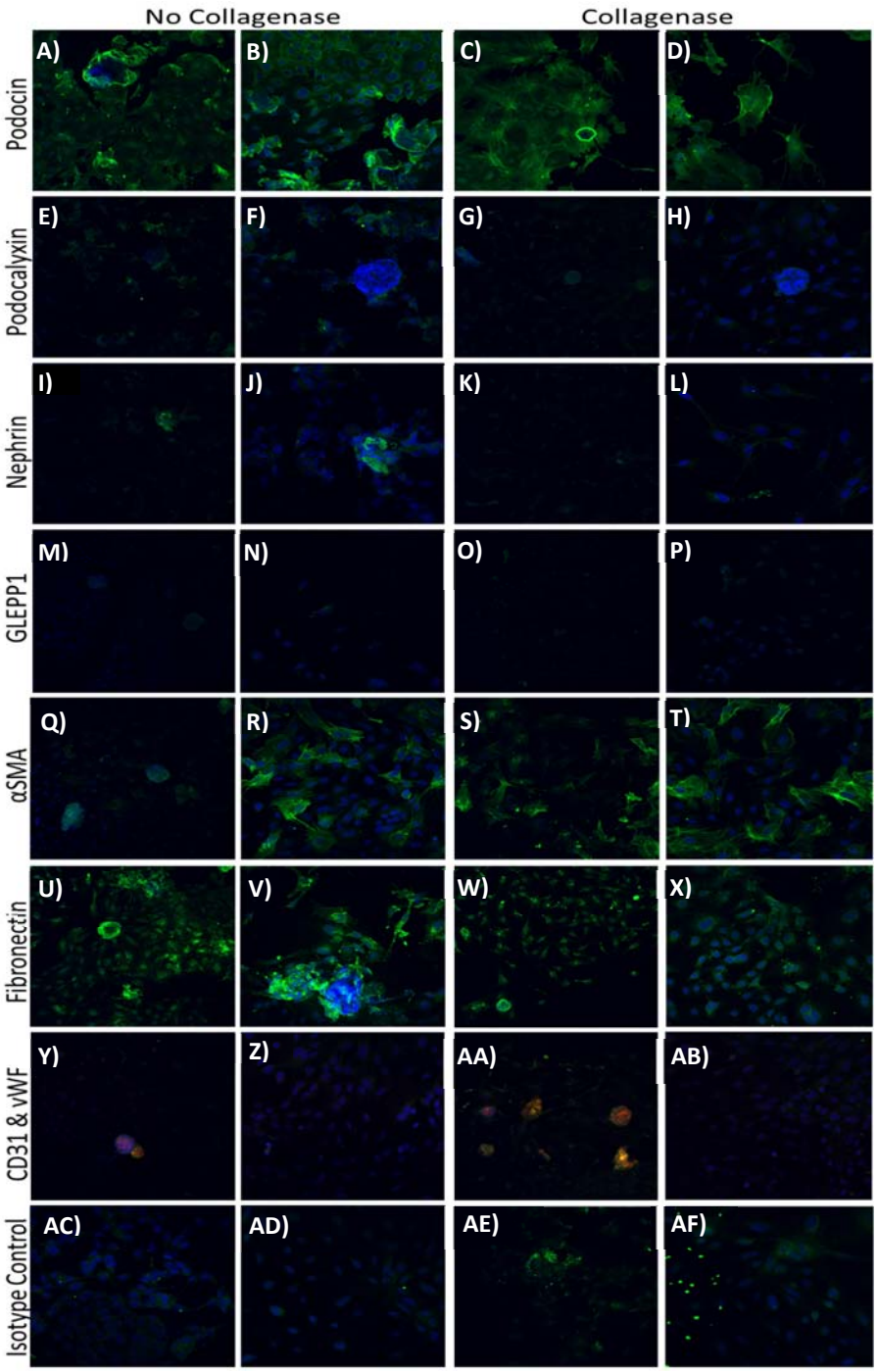

Figure 65. IF of isolated mouse glomeruli on day 9.

IF of isolated mouse glomeruli on day 9 of culture where mouse kidneys had either 5 minutes treatment with collagenase or no collagenase treatment during the isolation procedure. Glomerular cell markers were used to examine the nature of any cellular outgrowth. For PODs, this was podocin (green, A-D), podocalyxin (green, E-H), nephrin (green, I-L), GLEPP1 (green, M-P). For MCs, αSMA (green, Q-T) and fibronectin (green, U-X). For GECs CD31 (green, Y-AB) and vWF (red, Y-AB). Isotype control (green, AC-AF). Nuclei were counterstained with DAPI (blue). 10X magnification (A,C,E,G,I,K,M,O,Q,S,U,W,Y,AA,AC and AE) and 20X magnification (B,D,F,H,J,L,N,P,R,T,V,X,Z,AB,AD,AF).

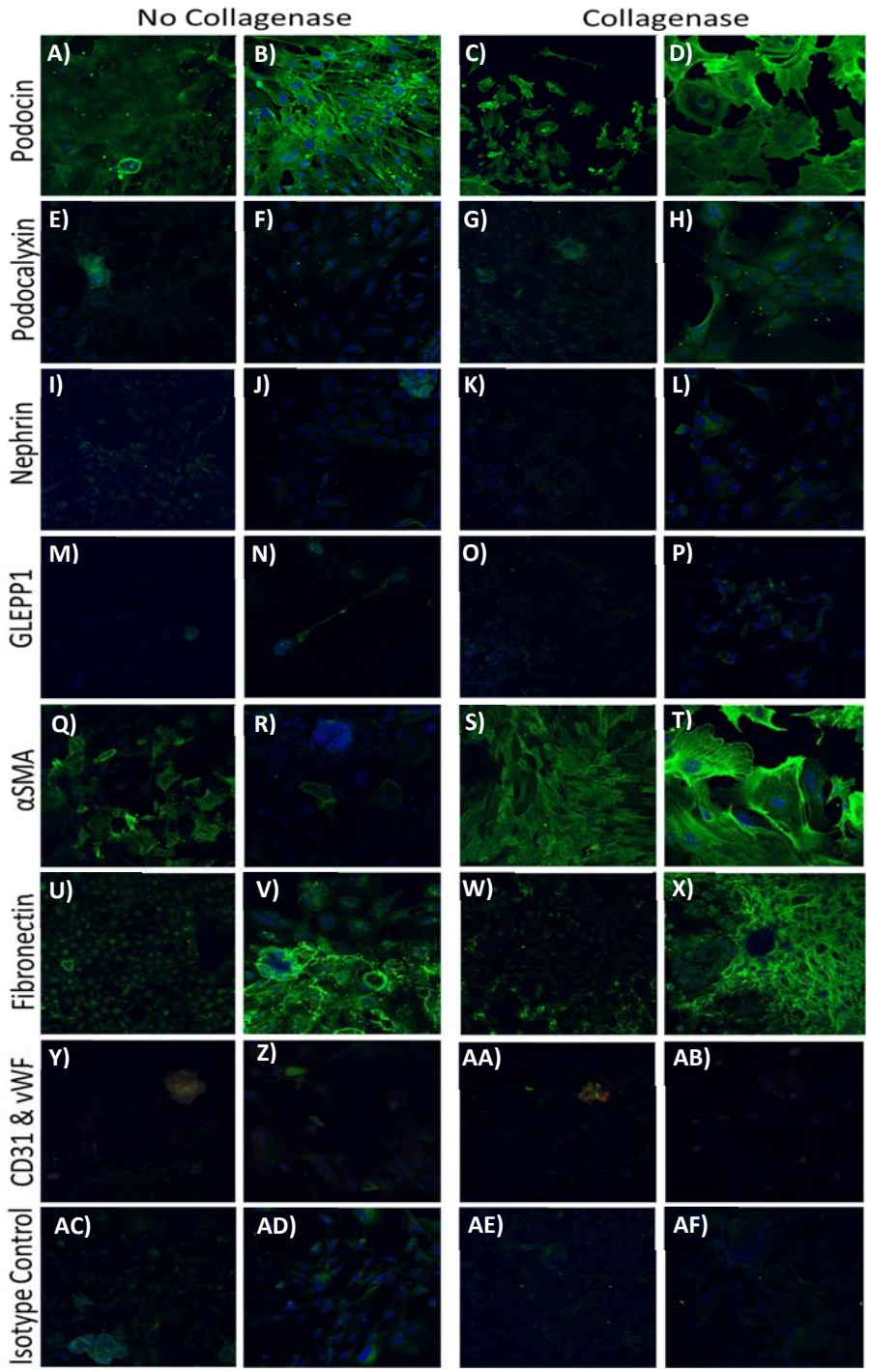

Figure 66. IF of isolated mouse glomeruli on day 13.

IF of isolated mouse glomeruli on day 13 of culture where mouse kidneys had either 5 minutes treatment with collagenase or no collagenase treatment during the isolation procedure. Glomerular cell markers were used to examine the nature of any cellular outgrowth. For PODs, this was podocin (green, A-D), podocalyxin (green, E-H), nephrin (green, I-L), GLEPP1 (green, M-P). For MCs, αSMA (green, Q-T) and fibronectin (green, U-X). For GECs CD31 (green, Y-AB) and vWF (red, Y-AB). Isotype control (green, AC-AF). Nuclei were counterstained with DAPI (blue). 10X magnification (A,C,E,G,I,K,M,O,Q,S,U,W,Y,AA,AC and AE) and 20X magnification (B,D,F,H,J,L,N,P,R,T,V,X,Z,AB,AD,AF).

Comparing the IF data overall, mouse glomeruli attached to plasticware with cellular outgrowth that progressed over time. Generally, there was increased POD marker expression in the outgrown glomerular cells by day 13 than earlier timepoints, the exception being nephrin (Figure 64 - Figure 66). Nephrin expression was lost over time in culture. Expression of endothelial markers CD31 and vWF remained in glomeruli structures and weakened over time, suggesting there was no outgrowth of GECs in these cultures (Figure 64 - Figure 66). Expression of MC markers, αSMA, and fibronectin, increased over time. By day 13, there was strong positive staining for both markers in outgrown glomerular cells (Figure 66). Taken with the positive POD marker staining, this suggested that there was a heterogeneous population of outgrown glomerular cells in these cultures. The use of collagenase in the isolation procedure did not appear to have any impact upon the culturing of glomeruli (Figure 64 - Figure 66), collagenase treatment did appear to reduce the number of tubule fragments, as well as glomeruli, left in filtrate (Figure 63). This would make it easier to have cleaner cultures by being able to more easily separate glomeruli from any tubule contamination, signifying that it is advantageous to use collagenase treatment in the mouse glomeruli isolation procedure. The specific identification of glomeruli outgrowth populations is difficult, the light microscope imaging of the glomeruli containing filtrate at the end of the isolation procedure also showed some tubule fragments, and so the presence of tubular cells was also likely. Further work and method optimisation would be needed to isolate and identifying homogenous POD populations from these cultures. However, the goal was to isolate human POD cells and so this optimisation for mouse was not necessary.

Human Glomeruli Isolation

Once accustomed to glomeruli isolation in mice, work began on human glomeruli isolation. Only renal cortex tissue was used in the human glomeruli isolation procedures, compared to whole kidneys used in mouse glomeruli isolations. This enabled precise targeting for glomeruli isolation. The method for human glomeruli isolation differed from the mouse glomeruli isolation in the sieve sizes used, detailed in the methods section. The media differed slightly, as expected when using tissue from different species. No collagenase treatments were used in this preliminary work. Figure 67 demonstrates bright-field images of both human glomeruli in the final filtrate of the isolation procedure (Figure 67, A) and of human glomeruli that had been in culture for 3 days (Figure 67, B-D). The number of glomeruli isolated from six pieces of ~2cm^3 human renal cortex tissue was roughly counted at 133,000 glomeruli by haemocytometer, where clumps of glomeruli were present. Nyengaard and Bendtsen[203] reported on average 617,000 glomeruli in mature human kidneys, suggesting the isolation procedure was successful by achieving approximately 133,000 glomeruli from the cortex tissue available.

It became apparent very quickly that human glomeruli would not attach to the plasticware, therefore in culture glomeruli would disintegrate and no cellular outgrowth could occur (Figure 67).

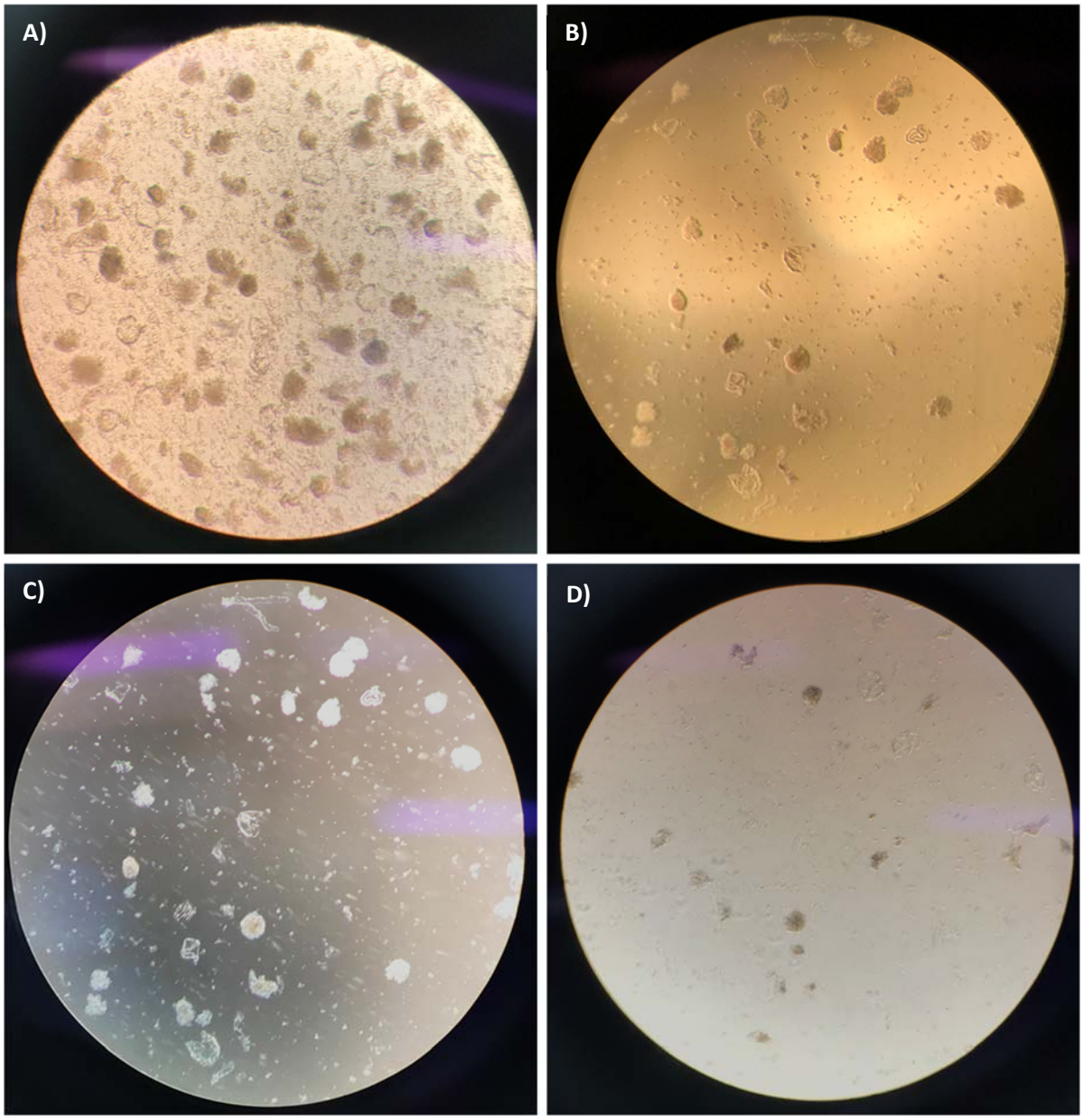

Figure 67. Bright field images of isolated human glomeruli.

Bright field images of (A) final filtrate following glomeruli isolation protocol on human renal cortex tissue and (B-D) isolated glomeruli cultures at day 3. 4X magnification

Higher magnification images of day 3 cultured isolated human glomeruli (Figure 68) established there had been successful isolation of human glomeruli from renal tissue, and glomeruli were in varying states of decapsulation. Human glomeruli were cultured for up to 7 days, nevertheless, glomeruli did not attach to plasticware. This was regardless of the level of decapsulation seen.

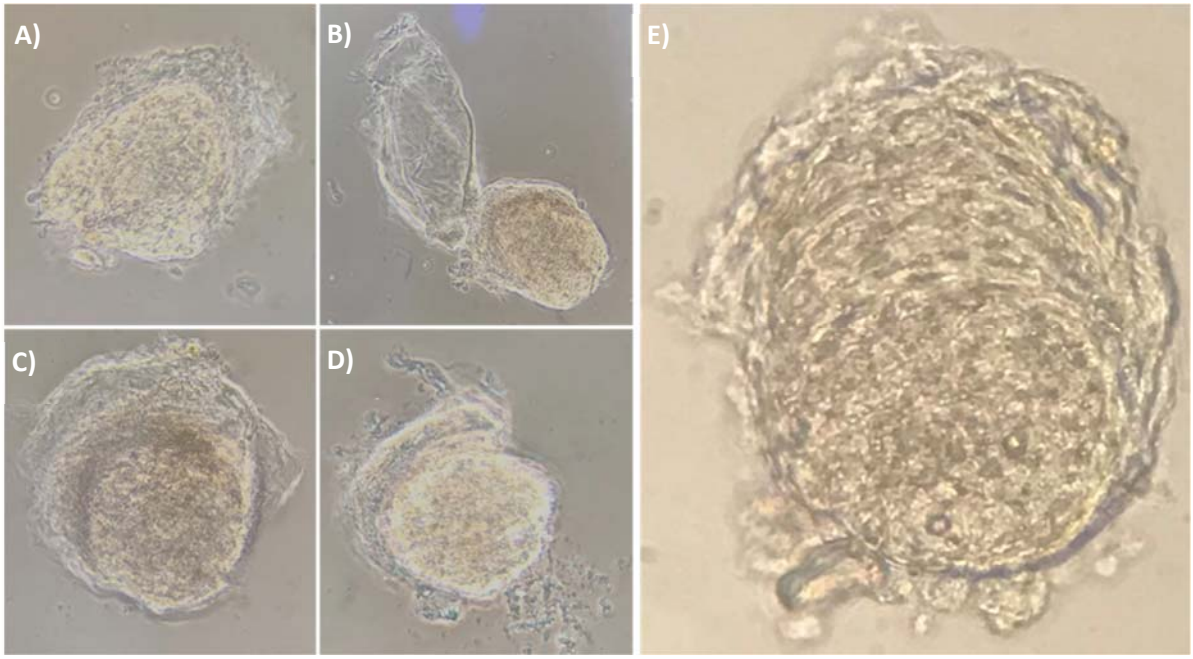

Figure 68. Bright field images of isolated human glomeruli in culture.

Bright field images of isolated human glomeruli in culture on day 3. Glomeruli demonstrate varying degrees of decapsulation (A - E). 40X magnification.

As human glomeruli could not be cultured, cellular outgrowth could not occur and be examined. Therefore, to utilise the isolated human glomeruli some glomeruli were used for IF by using cytospin where the effectiveness of IF antibodies of glomerular cell markers could be examined in human glomeruli (Figure 69). Isolated human glomeruli also underwent RNA extraction to examine the feasibility of performing RT-qPCR, unfortunately, insufficient quantity was extracted from this experiment.

Positive IF staining for all glomerular cell markers was demonstrated in isolated human glomeruli, except for ezrin (Figure 69). Strong positive staining for POD markers, podocin, synaptopodin, nephrin, GLEPP1, and podocalaxyin could be seen, with specific patterns of staining seen with them (Figure 69, A-K). Staining against POD markers WT1 and CD2AP was weaker and more diffuse (Figure 69, L and N). There was also positive staining for MC marker αSMA and GEC markers PDGFR-β and CD31 (Figure 69, O-Q). No staining was seen with either the isotype control or no primary antibody control (Figure 69, R and S). This work demonstrated that the glomerular cell IF antibodies could be successfully used in the analysis of isolated human glomeruli using cytospin to deposit human glomeruli onto slides.

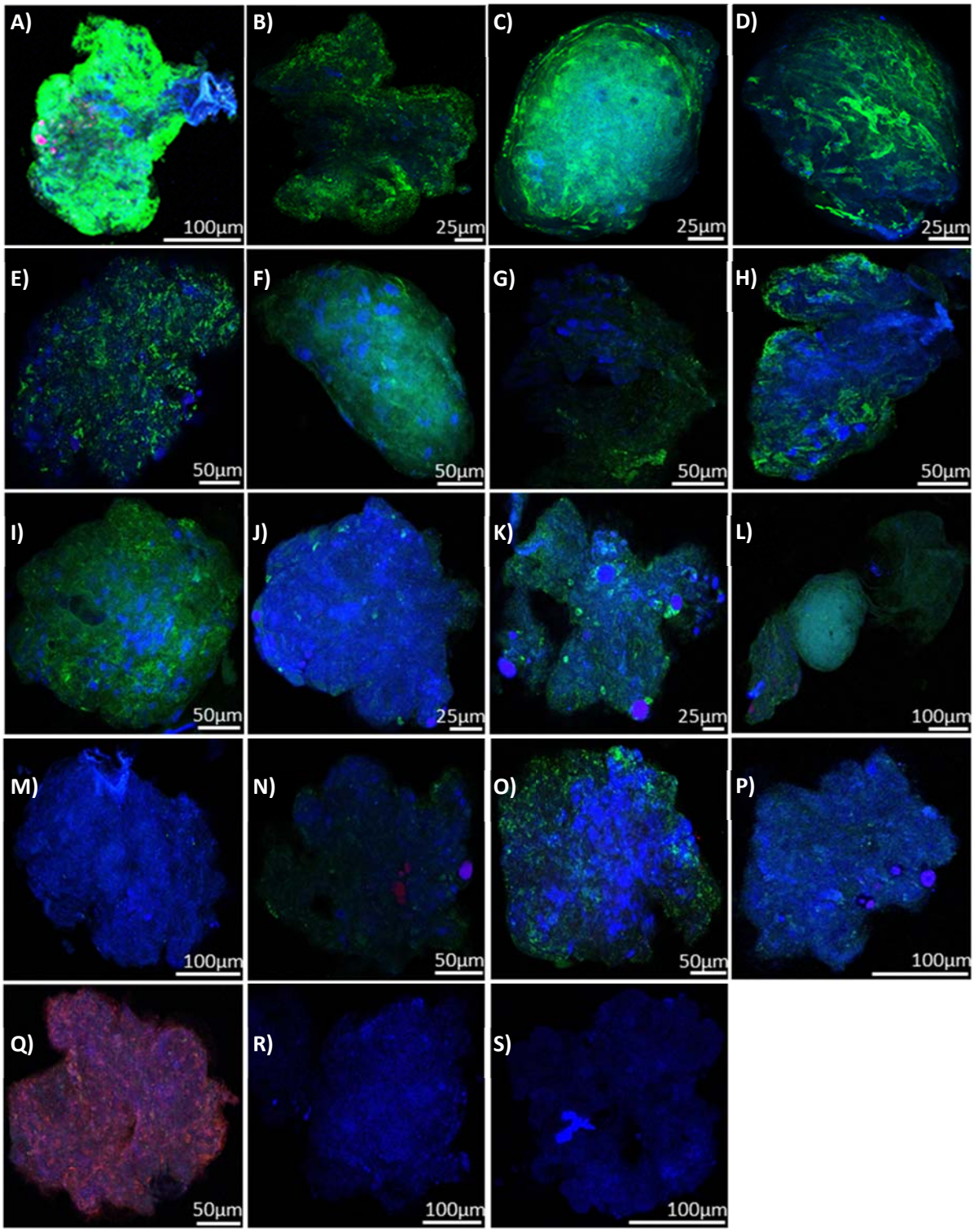

Figure 69. IF of isolated human glomeruli.

IF of isolated human glomeruli following cytospin on day 6 of culture as human glomeruli did not attach to plasticware. Glomerular cell markers were used to examine glomeruli. For PODs, this was podocin (green, A-C), synaptopodin (green, D-E), nephrin (green, F-G), GLEPP1 (green, H-I), podocalaxyin (green, J-K), WT1 (green, L), ezrin (green, M) and CD2AP (green, N). For MCs, αSMA (green, O). For GECs PDGFR-β (green, P) and CD31 (red, Q). Isotype control (green, R). No primary antibody control (green, S). Nuclei were counterstained with DAPI (blue). 20X magnification.

This human glomeruli isolation experiment established that human glomeruli could be successfully isolated from renal cortex tissue in good numbers. The level of glomeruli decapsulation varied, potentially some collagenase treatment could be optimised to remedy this. The significant problem demonstrated was that human glomeruli would not attach to plasticware as reported in the literature, therefore no cellular outgrowth could occur, rendering the aim of using isolated human glomeruli to source human PODs unachievable. Further investigation and optimisation outside the scope of this Thesis would have been required to attempt to resolve this. The valuable resource of human renal tissue was instead used to create HOC to reproduce 3D tri-culture experimental treatments to examine whether responses aligned.

HOC

HOC of human renal tissue is established in the Bradley laboratory.[105] However, RNA extraction from human renal HOC for RT-qPCR analysis was not habitually performed and so some optimisation work was required to ensure both sufficient quantity and quality of RNA from HOC. This optimisation revolved around the methodology of homogenisation and lysis of HOC, where cutting of HOC finely with a scalpel over ice before addition of lysis buffer and use of a tissue disperser was required for sufficient RNA yield. HOC were cultured for 6hrs or 24hrs and stimulated with panels of treatments used in the 3D tri-culture model. Firstly a panel using TGF-β, TNF-α, and ALK5i, then a panel using TGF-β and anti-αvβ8 antibody. The RT-qPCR data shall be separated into these treatment panels for clarity. When setting up a HOC experiment some tissue is set aside in lysis buffer as a control for tissue before culture. This sample is named T0 and RT-qPCR data was analysed and presented using the T0 sample as the reference sample.

TGF-β, TNF-α & ALK5i

HOCs were treated with TGF-β, TNF-α, or ALK5i alone or in combinations for 6hrs or 24hrs, data shall be divided into these timepoints for clarity. The panel of genes examined in these experiments were collagen genes COL1A1, COL3A1, and COL4A1, and ECM genes ACTA2, FN1, and LAMB2. This data is at N=1 and so no statistical analysis was performed, therefore observed data trends were noted.

6hr HOC

HOCs were treated with TGF-β, TNF-α, or ALK5i alone or in combinations for 6hrs, collagen gene expression will be examined first (Figure 70). The CT average for GAPDH was 23.70 and the T0 CT average for GAPDH was 25.70, indicating a good level of GAPDH expression in this data set. No data was acquired for COL1A1 expression with the control sample (Figure 70). TGF-β treatment appeared to evoke COL1A1 expression slightly above the T0 value; while all other treatments caused decreased

expression. ALK5i used in combination with TGF-β resulted in the largest decrease in COL1A1 expression compared to TGF-β used alone, suggesting ALK5i prevented TGF-β mediated COL1A1 expression. The average CT value for COL1A1 was 36.00 and the T0 CT average was 35.10, this suggests COL1A1 expression was low in these HOC samples. Expression of COL3A1 (Figure 70) decreased in culture with the control group compared to T0. TGF-β treatment appeared to evoke an increase in COL3A1 expression compare to both T0 and control values. TNF-α treatment resulted in COL3A1 expression slightly below T0 value, yet greater than that of control value. Co-treatment of TGF-β and TNF-α resulted in a level of COL3A1 expression that remained at T0 value, suggesting TNF-α had an inhibitory effect upon TGF-β evoked COL3A1 expression. ALK5i treatment did not change COL3A1 expression from control value. Co-treatment of TGF-β and ALK5i resulted in a similar level of expression as control, suggesting ALK5i prevented TGF-β evoked COL3A1 expression. The average CT value for COL3A1 was 28.80 and the average T0 CT value for COL3A1 was 30.10, suggesting a low level of expression. COL4A1 expression (Figure 70) decreased slightly in culture with the control group compared to the T0 sample, while TGF-β treatment resulted in an increase in COL4A1 expression compared to both control and T0. TNF-α treatment appeared to cause a decrease in COL4A1 expression when used in isolation and also inhibited TGF-β evoked COL4A1 expression when used in combination. This pattern was followed by ALK5i treatments. The average CT value for COL4A1 was 29.40 and the average T0 CT value for COL4A1 was 30.00, suggestive of a low expression.

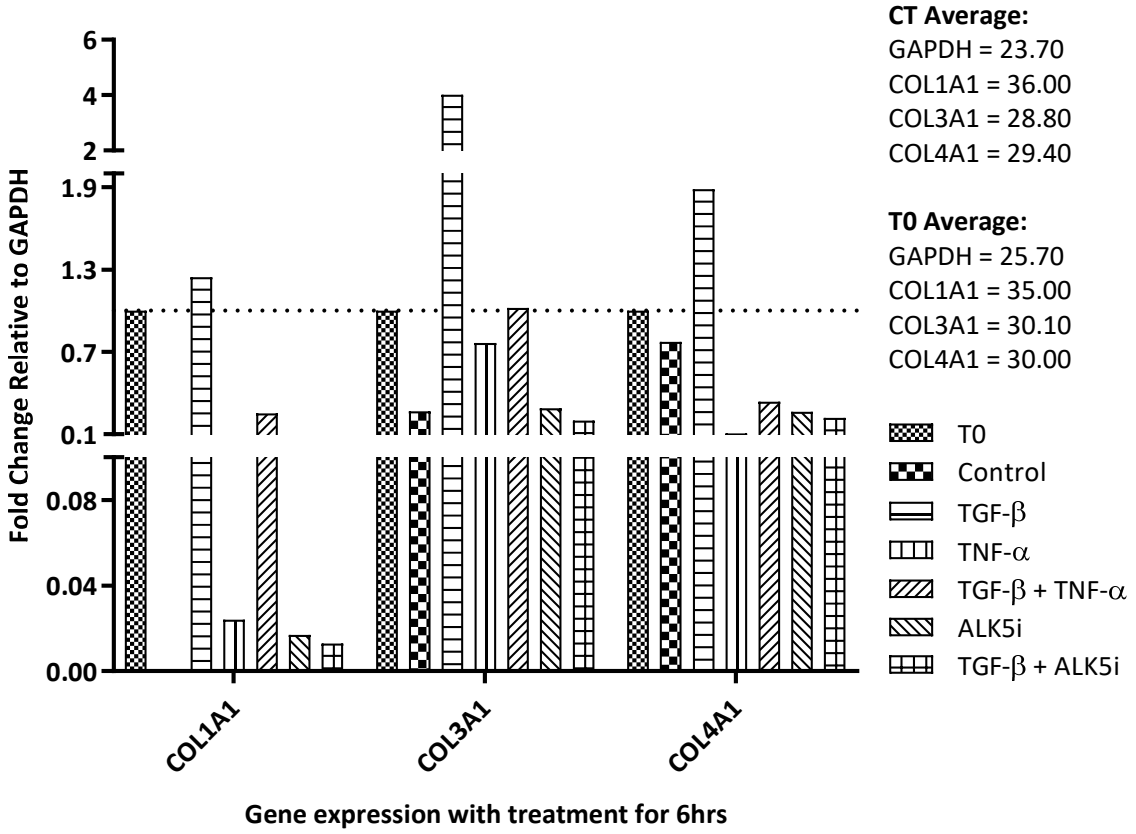

Figure 70. Collagen gene expression in renal HOC treated with TGF-β, TNF-α, and ALK5i for 6hrs. RT-qPCR was performed on renal HOC treated with TGF-β, TNF-α, and ALK5i for 6hrs. ΔΔCT analysis to look at the relative fold-change of the gene of interest against housekeeping gene GAPDH, with T0 set as the reference sample. N=1. Gene CT averages and the T0 average for reference.

ECM genes (Figure 71) examined shall be presented next. The CT average for GAPDH was 20.30 and the T0 CT average for GAPDH was 25.60, indicating there was a good level of GAPDH expression in this data set. No data was acquired for ACTA2 expression with the control sample (Figure 71). TGF-β treatment appeared to result in a slight increase in ACTA2 expression in HOC, compared to T0. TNF-α treatment seemed to elicit a decrease in ACTA2 expression compared to T0. When in co-treatment with TGF-β, TNF-α prevented any increase in ACTA2 expression and instead resulted in a decrease in expression compared with both T0 and TGF-β treatment. ALK5i treatment resulted in a downregulation in ACTA2 expression, and when used in combination with TGF-β inhibited any effect of TGF-β upon ACTA2 expression. The average CT value for ACTA2 was 24.20 and the average T0 CT value for ACTA2 was 23.30, suggesting a good level of ACTA2 expression in these HOC samples. Expression of FN1 (Figure 71) was reduced in culture with the control group compared to the T0 sample. TGF-β treatment resulted in an upregulation in FN1 expression compared to both control and T0. TNFα appeared to evoke some degree of FN1 downregulation, and when used in combination

with TGF-β brought expression down to T0 value. ALK5i treatment did not alter FN1 expression from that of control value and appeared to inhibit TGF-β evoked FN1 expression. The average CT value for FN1 was 26.60 and the average T0 CT value for FN1 was 32.20, demonstrating there was low expression in the T0 sample which increased in cultured HOC samples. LAMB2 expression (Figure 71) was slightly decreased in culture with the control group compared to the T0 sample. Treatment with TGF-β appeared to evoke an increase in LAMB2 expression compared with both control and T0 values. TNF-α treatment resulted in a decrease in LAMB2 expression compared to both control and T0 values, when used in co-treatment TNF-α prevented the TGF-β mediated increase in LAMB2 expression. ALK5i treatment appeared to downregulate LAMB2 expression to a similar degree as TNF-α treatment and following the pattern in preventing the TGF-β evoked increase in LAMB2 expression. The average CT value for LAMB2 was 27.90 and the average T0 CT value for LAMB2 was 30.40, demonstrating expression was lower in T0 samples and increased in HOC samples.

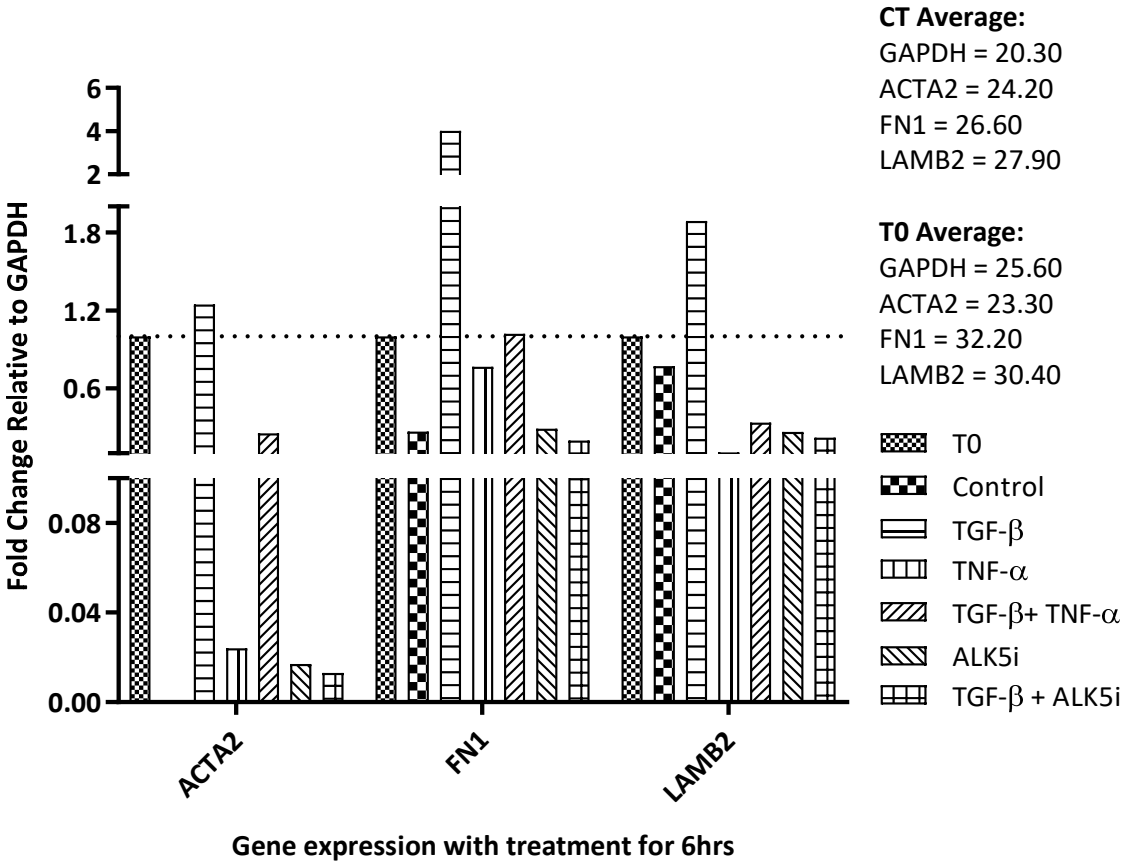

Figure 71. ECM gene expression in renal HOC treated with TGF-β, TNF-α, and ALK5i for 6hrs.
RT-qPCR was performed on renal HOC treated with TGF-β, TNF-α, and ALK5i for 6hrs. ΔΔCT analysis to look at the relative fold-change of the gene of interest against housekeeping gene GAPDH, with T0 set as the reference sample. N=1. Gene CT averages and the T0 average for reference.

24hr HOC

HOCs were treated with TGF-β or TNF-α alone or in combination for 24hrs, collagen gene expression will be examined first (Figure 72). The CT average for GAPDH was 22.40 and the T0 CT average for GAPDH was 25.70, indicating a good level of GAPDH expression in this data set. No data was acquired for COL1A1 expression with the control sample or the TGF-β and TNF-α co-treatment sample (Figure 72). TGF-β treatment appeared to result in downregulated COL1A1 expression while TNF-α treatment seemed to evoke an increase in COL1A1 expression. This was a different expression pattern as seen in 6hr HOCs (Figure 70). The average CT value for COL1A1 was not recorded as no data was acquired for COL1A1 expression with the control sample or the TGF-β and TNF-α co-treatment sample. The average T0 CT value for COL1A1 was 35.00, demonstrating low expression in the T0 sample. COL3A1 expression (Figure 72) was downregulated with every treatment group compared to T0. Control HOC and TGF-β treated HOC resulted in a similar level of COL3A1 downregulation, while TNF-α treatment caused a greater degree of COL3A1 downregulation. Co-treatment of TGF-β and TNF-α resulted in a level of COL3A1 downregulation similar to that of control and TGF-β, suggesting that TGF-β had an inhibitory effect upon TNF-α evoked COL3A1 downregulation. The average CT value for COL3A1 was 31.50 and the average T0 CT value for COL3A1 was 30.01, demonstrating a low-level expression. Expression of COL4A1 (Figure 72) appeared to be downregulated with all treatment groups compared with T0. The average CT value for COL4A1 was 28.50 and the average T0 CT value for COL4A1 was 30.00, demonstrating a low-level expression both before and during HOC.

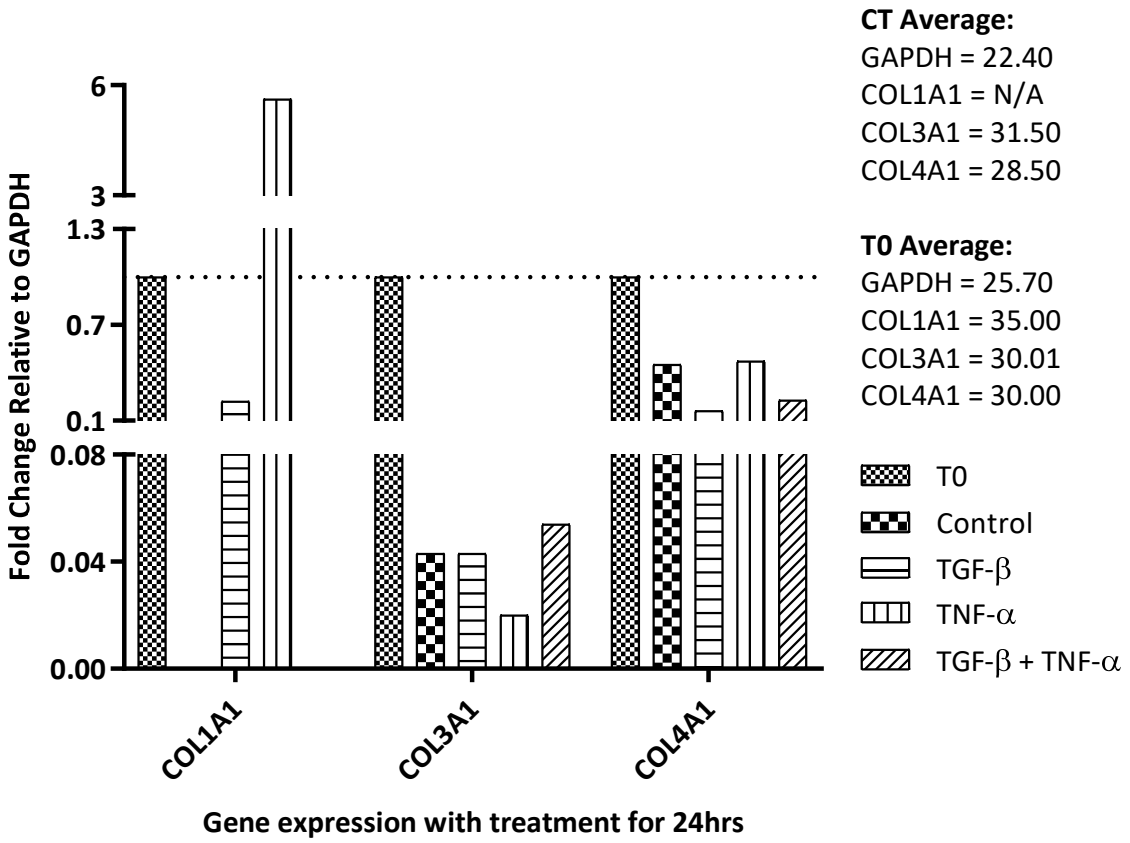

Figure 72. Collagen gene expression in renal HOC treated with TGF-β and TNF-α for 24hrs.
RT-qPCR was performed on renal HOC treated with TGF-β and TNF-α for 24hrs. ΔΔCT analysis to look at the relative fold-change of the gene of interest against housekeeping gene GAPDH, with T0 set as the reference sample. N=1. Gene CT averages and the T0 average for reference.

ECM gene expression (Figure 73) shall be presented next. The CT average for GAPDH was 20.30 and the T0 CT average for GAPDH was 25.60, indicating a good level of GAPDH expression in this data set. ACTA2 expression (Figure 73) was downregulated across all treatments compared with T0. The average CT value for ACTA2 was 24.20 and the average T0 CT value for ACTA2 was 23.30, demonstrating a good expression both before and during HOC. Expression of FN1 (Figure 73) appeared to decrease in control HOC compared to T0. TGF-β evoked increased FN1 expression compared with control and T0, as did TNF-α treatment. Co-treatment of TGF-β and TNF-α caused no change in FN1 expression compared to T0, while there was increased FN1 expression compared to control. The average CT value for FN1 was 26.60 and the average T0 CT value for FN1 was 32.20, demonstrating a low-level expression before HOC which increased during HOC. LAMB2 expression (Figure 73) decreased with all HOC treatments, including the control culture, compared to T0. The average CT value for LAMB2 was 27.90 and the average T0 CT value for LAMB2 was 30.40, demonstrating a low-level expression before HOC which increased during HOC.

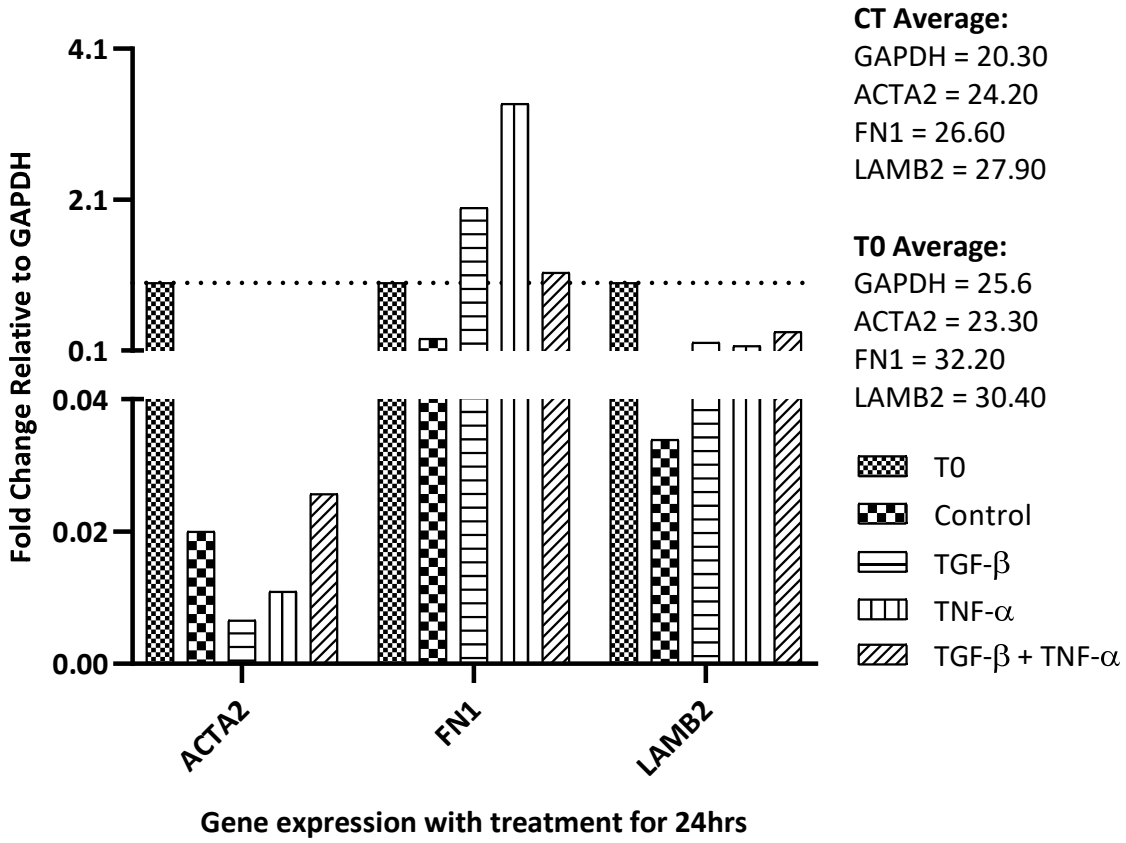

Figure 73. ECM gene expression in renal HOC treated with TGF-β and TNF-α for 24hrs.
RT-qPCR was performed on renal HOC treated with TGF-β and TNF-α for 24hrs. ΔΔCT analysis to look at the relative fold-change of the gene of interest against housekeeping gene GAPDH, with T0 set as the reference sample. N=1. Gene CT averages and the T0 average for reference.

This data set demonstrated a clear difference in HOC gene expression between 6hr and 24hr cultures. Generally, 6hr HOC showed some gene upregulation, while 24hr HOC depicted mainly downregulation, suggesting degradation of HOC by the 24hr time point. When comparing to 3D tri-culture data it was apparent that there were some similarities in gene expression in response to the same treatments, such as FN1 expression upregulation with TGF-β, the comparisons between these models of renal fibrosis shall be examined further in the discussion. As introduced earlier, further work using the HOC model of fibrosis using the anti-αvβ8 antibody was performed.

TGF-β & αvβ8 antibody

HOCs were treated with TGF-β and/or anti-αvβ8 antibody alone or in combination for either 6hrs or 24hrs, data shall be divided into these timepoints for clarity. In this experiment anti-αvβ8 antibody

was used at three different concentrations; 15µg/ml, 30µg/ml, and 60µg/ml, as opposed to the set concentration of 15µg/ml used in all earlier experimental setups using the anti-αvβ8 antibody. Higher concentrations were used in the N=2 set up as N=1 data had shown no substantive action with the 15µg/ml anti-αvβ8 treatment in HOC. The panel of genes examined in these experiments were collagen genes COL1A1, COL3A1, and COL4A1, and ECM genes ACTA2, FN1, and LAMB2.

6hr HOC

HOCs were treated with TGF-β and anti-αvβ8 antibody alone or in combination for 6hrs, collagen gene expression will be examined first (Figure 74). The CT average for GAPDH was 20.29 and the T0 CT average for GAPDH was 24.74, indicating there was a good level of GAPDH expression in this data set. COL1A1 expression (Figure 74) was significantly decreased with all HOC treatments compared with T0. The average CT value for COL1A1 was 31.67 and the average T0 CT value for COL1A1 was 32.02, demonstrating a low-level expression both before and after HOC. Expression of COL3A1 (Figure 74) did not change with any statistical significance with any treatment group. Treatments of anti-αvβ8 antibody at 30µg/ml and 60µg/ml alone or in combination with TGF-β demonstrated a non-significant trend of COL3A1 downregulation. The average CT value for COL3A1 was 26.13 and the average T0 CT value for COL3A1 was 30.44, demonstrating a relatively low-level expression before HOC, while after HOC there was greater COL3A1 expression. COL4A1 expression (Figure 74) remained unchanged with any statistical significance across any treatment group, with all HOC treatments resulting in COL4A1 downregulation compared to T0 at a similar degree. The average CT value for COL4A1 was 24.92 and the average T0 CT value for COL4A1 was 27.82, demonstrating a reasonable level expression both before and after HOC.

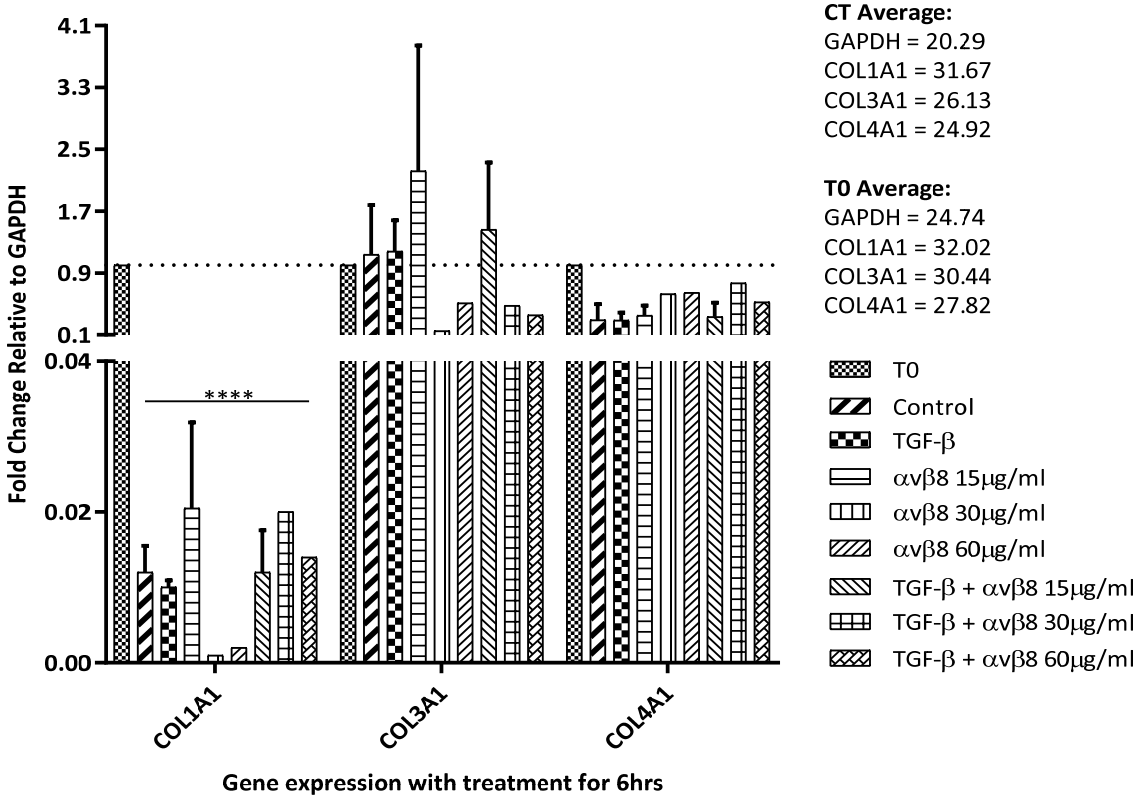

Figure 74. Collagen gene expression in renal HOC treated with TGF-β and anti-αvβ8 antibody for 6hrs. RT-qPCR was performed on renal HOC treated with TGF-β and anti-αvβ8 antibody for 6hrs. ΔΔCT analysis to look at the relative fold-change of the gene of interest against housekeeping gene GAPDH, with T0 set as the reference sample. N=2 (T0, Control, TGF-β, anti-αvβ8 15μg/ml & TGF-β + anti-αvβ8 15μg/ml), N=1 (anti-αvβ8 30μg/ml, anti-αvβ8 60μg/ml, TGF-β + anti-αvβ8 30μg/ml & TGF β + anti-αvβ8 60μg/ml), SEM error bars, One-way ANOVA; COL1A1 p-value <0.0001 (****); COL3A1 p value 0.9582 (ns); COL4A1 p-value 0.0545 (ns); followed by Tukey's multiple comparison post-tests. Gene CT averages and the T0 average for reference.

ECM gene expression (Figure 75) shall be presented next. The CT average for GAPDH was 20.36 and the T0 CT average for GAPDH was 26.48, indicating there was a good level of GAPDH expression in this data set. ACTA2 expression (Figure 75) was significantly decreased with treatments of TGF-β, anti-αvβ8 antibody of all concentrations, and TGF-β, and 15μg/ml anti-αvβ8 antibody co-treatment, compared with T0. All other HOC treatments resulted in a non-statistically significant decrease in ACTA2 expression. Treatment with either 30μg/ml or 60μg/ml of anti-αvβ8 antibody evoked the greatest apparent decrease in ACTA2 expression, attenuated slightly with co-treatment of TGF-β. The average CT value for ACTA2 was 23.26 and the average T0 CT value for ACTA2 was 26.36, demonstrating a reasonable level of expression both before and after HOC, with expression increasing during HOC.

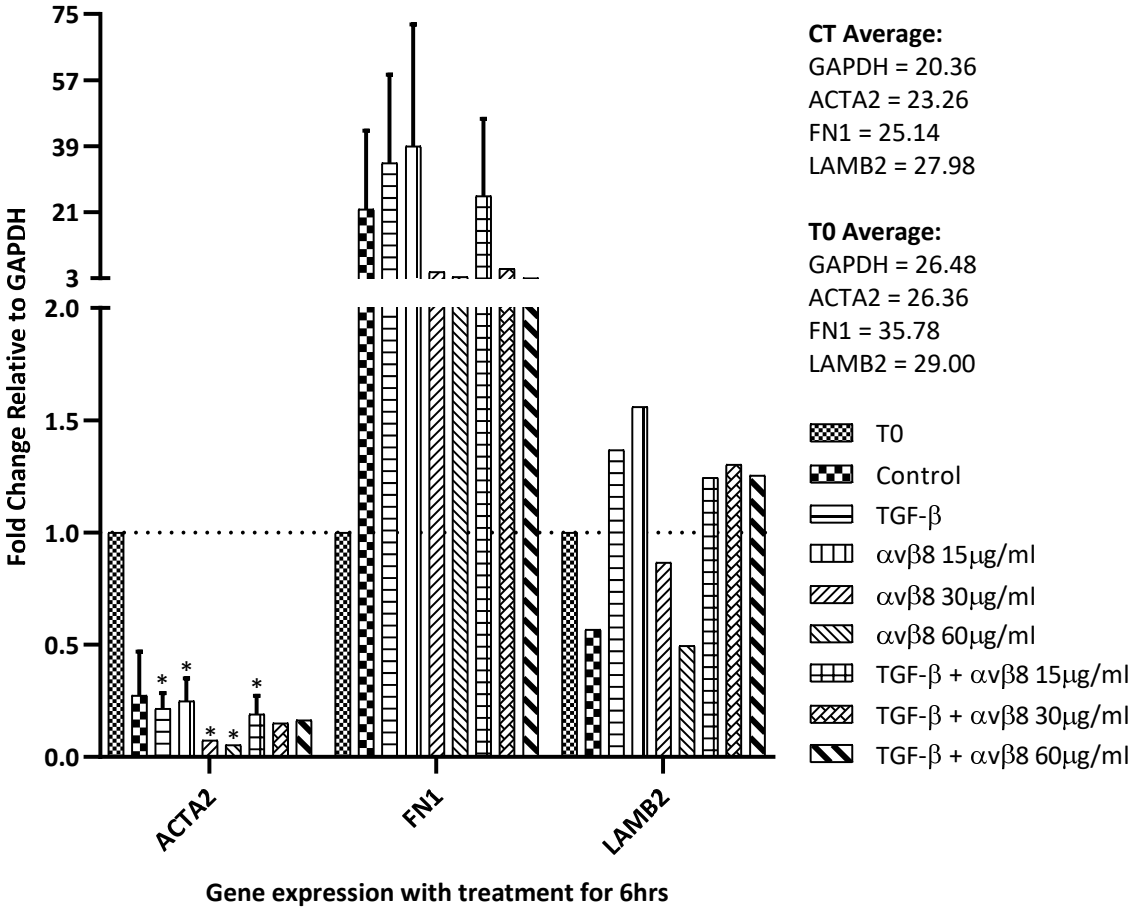

Figure 75. ECM gene expression in renal HOC treated with TGF-β and anti-αvβ8 antibody for 6hrs. RT-qPCR was performed on renal HOC treated with TGF-β and anti-αvβ8 antibody for 6hrs. ΔΔCT analysis to look at the relative fold-change of the gene of interest against housekeeping gene GAPDH, with T0 set as the reference sample. N=2 (T0, Control, TGF-β, anti-αvβ8 15μg/ml & TGF-β + anti-αvβ8 15μg/ml), N=1 (anti-αvβ8 30μg/ml, anti-αvβ8 60μg/ml, TGF-β + anti-αvβ8 30μg/ml, TGF-β + anti-αvβ8 60μg/ml & LAMB2 data), SEM error bars, One-way ANOVA; ACTA2 p-value 0.0307 (*); FN1 p-value 0.9093 (ns); followed by Tukey's multiple comparison post-tests. Gene CT averages and the T0 average for reference.

FN1 expression (Figure 75) did not change with any statistical significance across any treatment, yet all HOC treatments induced a trend of increased FN1 expression, compared to T0, which did to achieve statistical significance. Co-treatment of TGF-β and 15μg/ml anti-αvβ8 antibody resulted in FN1 expression around average control values. Treatments of 30μg/ml or 60μg/ml anti-αvβ8 antibody either alone or in combination with TGF-β evoked a similar degree of FN1 expression, which was lower than that of control HOC. This suggests that anti-αvβ8 antibody at these concentrations inhibits both basal and exogenous TGF-β evoked FN1 expression. The average CT value for FN1 was 25.14 and the average T0 CT value for FN1 was 35.78, demonstrating a low-level expression before

HOC, with expression increasing during HOC. Expression of LAMB2 (Figure 75) was at N1 so no statistical analysis could be made and so data trends were noted. LAMB2 expression decreased in control HOC compared to T0, while TGF-β and 15µg/ml anti-αvβ8 antibody treatments evoked an apparent increase in LAMB2 expression compared with both control HOC and T0. HOC treatment with 30µg/ml anti-αvβ8 antibody resulted in a slight decrease in LAMB2 expression from T0, this was higher than that of control HOC, while 60µg/ml anti-αvβ8 antibody evoked a decrease in LAMB2 expression from T0 to a similar degree as control HOC. All co-treatments evoked a similar increase in LAMB2 expression from both T0 and control HOC. This suggested that the anti-αvβ8 antibody did not affect TGF-β mediated LAMB2 expression at any concertation tested. The average CT value for LAMB2 was 27.98 and the average T0 CT value for LAMB2 was 29.00, demonstrating a lower level expression before HOC, with expression increasing to some extent during HOC.

24hr HOC

These data sets are at N1, therefore no statistical analysis had been performed and so data trends were noted. HOCs were treated with TGF-β and anti-αvβ8 antibody alone or in combination for 24hrs, collagen gene expression will be examined first (Figure 76). The CT average for GAPDH was 20.52 and the T0 CT average for GAPDH was 23.36, indicating a good level of GAPDH expression in this data set. COL1A1 expression (Figure 76) decreased with all HOC treatments compared with T0 and no discernible trend in data could be seen. The average CT value for COL1A1 was 33.40 and the average T0 CT value for COL1A1 was 28.56, demonstrating a lower level expression before HOC, which decreased further with HOC. Expression of COL3A1 (Figure 76) was downregulated with all HOC treatments compared to T0, as with COL1A1, no discernible trend in data could be seen. The average CT value for COL3A1 was 26.68 and the average T0 CT value for COL3A1 was 25.67, demonstrating a good level of expression both before and after HOC. COL4A1 expression (Figure 76) expression was also downregulated with all HOC treatments in comparison to T0. The largest decrease in COL4A1 expression was control HOC. Therefore, when compared to control HOC, all other HOC treatments resulted in an upregulation of COL4A1. The treatments of anti-αvβ8 antibody at 30µg/ml and 60µg/ml demonstrated a similar, slightly lower level of COL4A1 expression than other treatment combinations. Co-treatment of TGF-β and 15µg/ml αvβ8 antibody demonstrated a lower degree of COL4A1 expression than either treatment demonstrated alone, suggesting some interaction between these treatments inhibiting COL4A1 expression. The average CT value for COL4A1 was 24.93 and the average T0 CT value for COL4A1 was 24.63, demonstrating a good level of expression both before and after HOC.

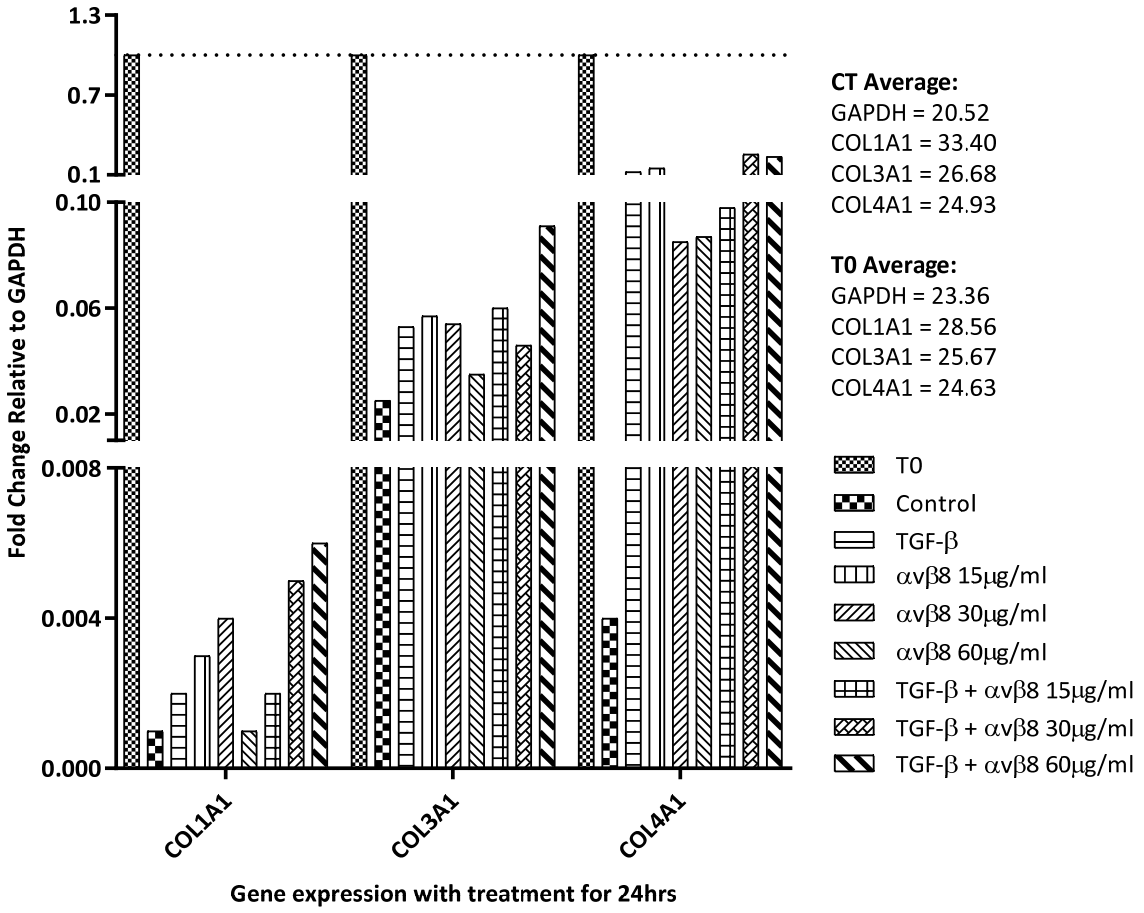

Figure 76. Collagen gene expression in renal HOC treated with TGF-β and anti-αvβ8 antibody for 24hrs.

RT-qPCR was performed on renal HOC treated with TGF-β and anti-αvβ8 antibody for 24hrs. ΔΔCT analysis to look at the relative fold-change of the gene of interest against housekeeping gene GAPDH, with T0 set as the reference sample. N=1. Gene CT averages and the T0 average for reference.

ECM gene expression (Figure 77) shall be presented next. The CT average for GAPDH was 20.37 and the T0 CT average for GAPDH was 23.61, indicating there was a good level of GAPDH expression in this data set. ACTA2 expression (Figure 77) decreased with all HOC treatments compared to T0. TGF-β and 30μg/ml anti-αvβ8 antibody treatments resulted in a higher level of ACTA2 expression than that of control HOC, implying that these treatments evoked some ACTA2 upregulation in HOC. Treatment of 15μg/ml anti-αvβ8 antibody resulted in ACTA2 expression below control HOC level, with 60μg/ml anti-αvβ8 antibody treatment resulting in a degree of ACTA2 expression lower again. Co-treatments of all concentrations of anti-αvβ8 antibody with TGF-β brought ACTA2 expression to below control HOC level. This suggested the anti-αvβ8 antibody could prevent TGF-β mediated ACTA2 upregulation and to some degree basal ACTA2 expression. The average CT value for ACTA2 was 23.81 and the average T0 CT value for ACTA2 was 22.46, demonstrating a good level of expression both before and after HOC.

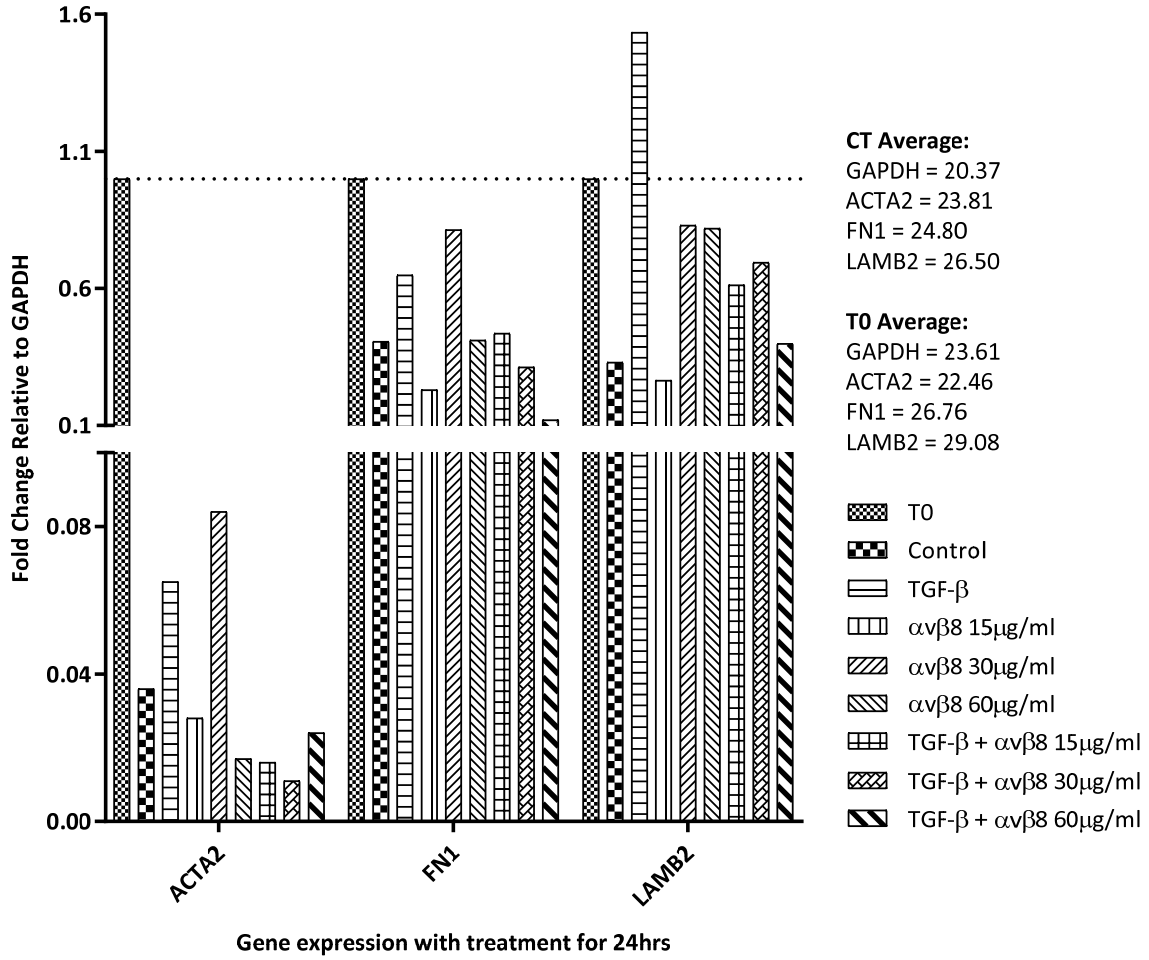

Figure 77. ECM gene expression in renal HOC treated with TGF-β and anti-αvβ8 antibody for 24hrs. RT-qPCR was performed on renal HOC treated with TGF-β and anti-αvβ8 antibody for 24hrs. ΔΔCT analysis to look at the relative fold-change of the gene of interest against housekeeping gene GAPDH, with T0 set as the reference sample. N=1. Gene CT averages and the T0 average for reference.

FN1 expression (Figure 77) was downregulated in all HOC treatments compared to T0. Compared with control HOC, TGF-β treatment, and 30μg/ml anti-αvβ8 antibody treatment resulted in increased FN1 expression in HOC. Treatment with 15μg/ml anti-αvβ8 antibody caused a decrease in FN1 expression compared with both control HOC and T0. Co-treatment of TGF-β with 15μg/ml anti-αvβ8 antibody brought FN1 expression to control HOC value, while 30μg/ml and 60μg/ml anti-αvβ8 antibody treatments brought expression further down to below control HOC value. It appeared the greater the concentration of anti-αvβ8 antibody used in co-treatment with TGF-β, the greater the inhibition of FN1 expression. The average CT value for FN1 was 24.80 and the average T0 CT value for FN1 was 26.76, demonstrating a good level of expression both before and after HOC. Expression of LAMB2 (Figure 77) decreased in control HOC compared to T0, while TGF-β treatment resulted in increased LAMB2 expression in comparison to both control HOC and T0. All anti-αvβ8 antibody treatments resulted in a downregulation of LAMB2 compared with T0. When used in co-treatment with TGF-β, all concentrations of anti-αvβ8 antibody inhibited TGF-β induced LAMB2 expression to some degree, the highest concentration causing the greatest inhibition. The average CT value for LAMB2 was 26.50 and the average T0 CT value for LAMB2 was 29.08, demonstrating a lower level of expression before HOC which increased following HOC.

As with the TGF-β and TNF-α HOC data set, this data demonstrated differences in HOC gene expression with treatments between 6hr and 24hr cultures, with more downregulation compared to T0 with the 24hr timepoint. Further supporting the theory that at this longer time point the HOC is undergoing some degree of degradation. Again, when comparing with 3D tri-culture data some trends can be seen to be replicated in HOC. Comparisons shall be outlined fully, more appropriately, in the discussion section but across all the HOC demonstrated in this chapter it is apparent some parallels can be made. CT averages were generally good, showing variation in response to HOC. This chapter has demonstrated the use of human renal tissue to both study renal fibrosis, and ascertain the clinical relevance of the 3D tri-culture model. This chapter concludes the results of this Thesis and shall be followed by the discussion.

Chapter 9 – Discussion

The discussion is divided into the corresponding results chapters, with reference between sections where appropriate.

Characterisation of Glomerular Cell Types (Chapter 4)

An important aspect of using cell culture for analysis is the characterisation of the cell types. Morphological changes and de-differentiation are often seen when cells are cultured *in vitro*, limiting the validity of results. fGEC and fMC cell types use in this work had previously undergone characterisation in the Bradley laboratory, therefore only the fPOD cells underwent extensive characterisation,[193, 194] involving IF, EM, RT-qPCR, and WB analysis.

Celprogen fPODs

The first primary human fPODs acquired were from Celprogen. They were cultured in 2D and characterised using IF and EM. POD markers used were ezrin, WT-1, synaptopodin, podocin, and nephrin (Figure 1). These are expressed by PODs *in vivo* and commonly used as POD markers *in vitro*.[202, 204] Ezrin expression (Figure 1) was ring-like around 2D Celprogen fPOD nuclei with strong expression at the plasma membrane of interacting cells, mirroring the pattern of expression seen by Hugo *et al.*[205] in rat PODs. Nuclear WT-1 expression (Figure 1) was demonstrated as reported.[200, 202] Synaptopodin expression has been characterised as a marker of the differentiated POD, cytoplasmic synaptopodin expression (Figure 1) was demonstrated in 2D Celprogen fPOD.[200, 202, 204] Expression of podocin (Figure 1) was primarily cytoplasmic, with some strong expression as fPOD cells interacted. This pattern of expression has been reported in differentiated cultured PODs Saleem *et al*.[200] Nephrin expression is described as "diffuse cytoplasmic" in undifferentiated PODs and having "punctuated cell surface and cytoplasmic distribution" in differentiated PODs by Saleem *et al.*[200] Figure 1 demonstrates such punctuated nephrin expression in 2D Celprogen fPODs. Therefore, all five POD phenotypic markers are expressed with similar localisation patterns in 2D Celprogen fPODs as in mature *in vivo* PODs.

Some IF was performed using fMC as a control for POD markers, therefore MC markers were utilised for their phenotype identification. Expression of MC phenotypic markers Thy1 and NG2 was weak (Figure 2); NG2 is a common marker of pericytes, including MCs, but not exclusive to this cell type.[206] While Thy1 is an important marker in fibrosis, especially in the Thy-1 nephritis animal model; and a common marker used for identification of rodent MCs, this is not the case for human MCs, thus may be an inappropriate marker for these cells.[207-209] Thus this poor marker expression is most likely due to poor choice of markers rather than the validity of the cell type. The morphology and tubulin staining (Figure 2) indicate an MC cell type.

SEM (Figure 3) and TEM (Figure 4) of 2D Celprogen fPODs exposed the morphology of these cells, where SEM displayed foot-like processes similar to those reported by Saleem *et al*.[200], while TEM (Figure 4, E) of these foot-like processes revealed similarity to TEM images of POD foot processes *in situ*.[12] TEM (Figure 4, D) revealed a slit diaphragm-like junction approximately 20-40nm wide in between neighbouring 2D cultured fPODs, comparable to such as structure reported by Reiser *et al*.[210], and analogous to TEM imaging of the slit diaphragm seen *in vivo*.

Celprogen fPODs were cultured in 3D to assess any changes in morphology or phenotype expression (Figure 5). Phenotypic markers were ezrin, podocin, synaptopodin, nephrin, and α-SMA; with both 3D fMCs and 3D fGECs also examined. In 3D, Celprogen fPODs demonstrated the same pattern as in 2D, suggesting 3D mono-culture of Celprogen fPODs did not affect expression of these POD markers (Figure 5). Unexpectedly, there was some positive staining for podocin, synaptopodin, and nephrin in 3D fMCs and 3D fGECs (Figure 5), suggesting some non-specific staining.

SEM of 3D Celprogen fPOD cultures (Figure 6) showed foot-like processes, similar to those seen with SEM of 2D fPODs.[200] Interaction of cell processes between multiple fPOD cells could be seen, adding to the 2D TEM data (Figure 4) junction formation between cultured fPODs.

RT-qPCR also characterised these cells, examining the effects of TGF-β and BMP7, cytokines which had been used by the Bradley laboratory to examine their effects upon both fMC cultures and fGEC cultures.[194, 201] In 3D mono-cultures BMP7 prevented fGEC tubule network regression caused by TGF-β treatment, while BMP7 could not prevent TGF-β induced nodule formation in fMC cultures with data demonstrating that BMP7 could modulate TGF-β evoked SMAD responses in fGECs but not fMCs.[194, 201] Therefore SMAD3 gene expression was examined in response to TGF-β and BMP7 treatments, as well as CTGF expression, and CTGF is a downstream mediator of TGF-β. Both 6hr (Figure 7) and 24hr (Figure 8) timepoints were tested in 2D Celprogen fPODs, SMAD3 expression was unchanged, while a significant increase in CTGF expression was demonstrated with TGF-β, that BMP7 did not affect. This pattern of expression was observed in 3D Celprogen fPOD cultures (Figure 9), where SERPINE1 expression was investigated and followed the same pattern as CTGF expression. SERPINE1 encodes Plasminogen activator inhibitor type-1 (PAI-1), the main function of which is inhibition of fibrinolysis, therefore increased PAI-1 is associated with ECM accumulation in many renal diseases.[211, 212]

The literature corroborates this potent induction of CTGF expression by TGF-β.[40, 43] Brennan *et al*.[213] applied next-generation sequencing to identify gene expression profiles associated with TGF-β stimulation in renal epithelial cells and reported these same responses with CTGF and SERPINE1 expression. The RT-qPCR data here suggests that fPODs could be a source of CTGF, Fuchshofer *et al.*[214] used an animal model of FSGS to demonstrate that CTGF and its mRNA were highly upregulated in PODs, correlating with glomerulosclerosis. While Yokoi *et al.*[215] established that

there was exacerbation of glomerular damage in transgenic mice with PODs overexpressing CTGF in diabetes induced by streptozotocin. CTGF upregulation appears to be greater in Celprogen fPODs cultured in 3D than those in 2D, an initial indication of how 3D culture can affect cellular behaviour.

WB analysis was used as a final element of Celprogen fPOD characterisation. BMP7 had been investigated to understand any antagonistic effect upon canonical TGF-β SMAD2/SMAD3 signalling at a protein level in fMCs and fGECs.[194, 201] 2D Celprogen fPOD culture SMAD signalling was interrogated. The expected canonical inductions of pSMAD2 (Figure 10 and Figure 11) and pSMAD3 (Figure 12) with TGF-β; and pSMAD1/5 (Figure 14) with BMP7 were demonstrated. No change in response could be seen with co-treatment. Interestingly, BMP7 treatment significantly increased pSMAD3 expression to the same level as TGF-β treatment (Figure 12). This is unexpected as SMAD3 a downstream effector of TGF-β; however, it has been shown that the distinction between SMADs supposed to be associated with either TGF-β or BMP7 is somewhat blurred; BMP7 induced pSMAD3 in breast cancer cells and TGF-β has been documented to induce pSMAD1.[216]

Total expression of SMAD3 (Figure 13) decreased with TGF-β and co-treatment, suggestive of a negative feedback mechanism on tSMAD3, such downregulation of SMAD3 in response to TGF-β has been reported.[217, 218]

The characterisation data of Celprogen fPOD provide good evidence that Celprogen fPOD were PODs and behaved as thus.

Further Characterisation of Subsequent lots of Celprogen fPODs

Quality control validation at MedImmune detected mycoplasma contamination. Testing of Bradley laboratory Celprogen fPODs was negative (Table 1).

STR profiling by MedImmune of Celprogen fPODs found CHO cell gDNA. At this time problems in attaining RT-qPCR data from Celprogen fPOD cultures for this project had begun. Vials of Celprogen fPODs at the Bradley laboratory tested positive for CHO DNA by RT-qPCR using CHO primers to varying extents (Table 2). 3D tri-cultures had been created using Celprogen fPODs, both in the development and optimisation of 3D tri-cultures, as well as in generating data with different experimental set-ups. To understand the effect of this contamination on data generated, another source of human fPODs was identified, with these cells undergoing characterisation and used in 3D tri-culture to compare results.

The type of fPOD used in each experiment has been documented throughout this thesis. The extent to which CHO contamination may or may not have affected data will be difficult to fully ascertain. During the discussion of 3D tri-culture data, where appropriate, this is noted and commented on. The characterisation of Celprogen fPOD data demonstrates that PODs were present in early work. Some vials may have had low-level CHO contamination, that grew with culture and passage, resulting

in difficulty acquiring RT-qPCR data from Celprogen fPOD cultures. This indicates that, as RT-qPCR is specific to the primers used, the effect upon data will be that less fPOD RNA was available. CHO cells are abundantly studied and are a vital cell line for therapeutic protein production through their adaptability and quick growth.[219] These characteristics suggest CHO cells would overtake a cell culture. Assessment of the effects of this upon 3D tri-cultures will be attempted in the following discussion.

Lonza fPODs

These primary fPODs underwent the same characterisation as Celprogen fPODs. Bright field imaging of 2D Lonza fPODs (Figure 15) where typical cobblestone morphology, with some flattening and arborisation, in line with the literature.[202, 204] IF performed on 2D Lonza fPODs (Figure 16) using the same POD phenotypic markers of ezrin, WT-1, synaptopodin, podocin, and nephrin mirrored the patterns of expression seen with Celprogen fPODs (Figure 1 and Figure 2) and the literature; except for WT-1, where no expression was seen.[200, 202, 204, 205] Three further POD markers were used, podocalyxin, GLEPP1, and CD2AP; no expression of CD2AP was demonstrated. CD2AP is localised to the slit diaphragm of mature PODs, as 2D Lonza fPODs in Figure 16 are spread out and fairly sparse and it may be that explains the lack of CD2AP expression. Expression of podocalyxin and GLEPP1 was localised to the cell membrane, as described in the literature.[202, 204]

TEM of 2D Lonza fPODs (Figure 17) confirmed analogous morphology to Celprogen fPODs (Figure 4) as described by the literature, demonstrating primary and secondary foot-like processes.[12] The effect of TGF-β upon the morphology of 2D Lonza fPODs examined under TEM (Figure 18) depicted ultrastructural damage with membrane rupture and vacuolisation in some cells. Kriz *et al*.[220] used TEM to summarise POD structural changes with injury in animal models of kidney disease, replicating those seen in TGF-β treated Lonza fPODs.

3D Lonza fPOD cultures demonstrated similar IF staining patterns (Figure 19) for the POD phenotypic markers, with the addition of positive CD2AP staining, generally stronger staining was seen in the Lonza fPODs cultured in 3D than those in 2D. Establishing another indication that 3D culture results in changes in cellular behaviour.

Finally, RT-qPCR was used for the characterisation of Lonza fPODs cultured in 2D (Figure 20) and 3D (Figure 21) using TGF-β and BMP7 treatments. Data established the same increases in CTGF expression with TGF-β treatment as seen with Celprogen fPODs (Figure 7, Figure 8, and Figure 9). A degree of SMAD3 downregulation was demonstrated, unlike Celprogen fPODs (Figure 7, Figure 8, and Figure 9), this would however correspond with Celprogen fPOD WB data and reports in the literature.[217, 218] SERPINE1 expression was again upregulated with TGF-β treatment in both 2D and 3D Lonza fPODs cultures, as with Celprogen fPODs (Figure 9). TGFB1 expression was examined, with

expression increased in both 2D and 3D Celprogen fPOD cultures with TGF-β treatment and BMP7 appearing to downregulate expression and causing some degree of inhibition to TGF-β evoked TGFB1 expression. The interplay between TGF-β and BMP7 and their opposing effects are well documented and this dynamic of control over TGFB1 expression fits the narrative.[35, 36, 38, 125, 221] Riser *et al.*[222] demonstrated that TGF-β could autoinduce in rat MCs.

Characterisation provided a credible demonstration that both sources of fPODs were indeed PODs with both phenotypic and morphological observation, as well as with functional responses. As such, both were used in the formation of a 3D tri-culture to model human glomerulosclerosis *in vitro*. Like with the culture of all primary cells, consideration is made of the differentiation state as cells were proliferated through several subcultures.

3D Tri-culture Development & Characterisation (Chapter 5)

3D Tri-culture Development

The development of the 3D tri-culture model of human glomerulosclerosis required some optimisation of three key parameters; the composition of the gel matrix, both the total cell number and the glomerular cell type ratio, and the media composition.

The gel matrix used in this work follows from previous works by the Bradley laboratory, a matrix consisting of rat tail type I collagen and human plasma fibronectin.[193, 194] Gel matrix composition requires consideration to provide the desired 3D environment for cells, gels must be porous for cellular exchange of nutrients and waste, as well as to enable stimulation with treatments; along with the need to possess mechanical properties enabling self-support.[223] Use of natural ECM, such as collagen and fibronectin is advantageous as they can be re-modelled easily by cells and inherently retain biological activity. Conversely, this can result in complication, Matrigel® is a partially defined matrix of collagens and laminin which contains several growth factors that can vary between batch.[224] The simple collagen/fibronectin gel used here avoids these complications and by using rat collagen, enables the assessment of human collagen deposition. A limitation to collagen gels is the modulation of gel stiffness cannot be changed without the simultaneous alteration of density, pore size, and permeability.[223] Gel contraction is a well-documented phenomenon of 3D cultures and is desirable for some studies.[225-227] Elements involved in gel contraction include cell number, cell type, collagen concentration, and collagen type, as well as treatments, with TGF-β reported to stimulate collagen matrix contraction.[226, 228] Such gel contract is not desirable with this work, earlier work in the Bradley laboratory found firstly the slight changes in collagen batches required compensating for to avoid gel contractions and secondly use of a PGA mesh strengthened gels against contraction.[193, 194] PGA mesh has become a routine material for porous scaffolding in 3D gels, the requirement for PGA mesh for 3D tri-cultures was assessed (Table 3), and it was determined not to be required. Earlier

works described had involved the culture of endothelial and mural cells, it seems that upon introduction of an epithelial cell type in fPODs combined with the low fMC number negated the need for PGA mesh to prevent gel contraction.

Cell number and the ratio of each cell type introduced to a gel matrix were optimised to enable first and foremost the formation of a vascular network of interacting fGECs and fPODs with fMCs contained within the gel. There was also the requirement of mimicking the proportionate number of each cell type in vivo, where GEC numbers would be highest, followed by both PODs and MCs; as well as needing high enough RNA yield for RT-qPCR analysis of 3D tri-cultures. As intimated earlier, cell number also impacts upon matrix contraction and so was another parameter for consideration. By optimisation, as required in all 3D culture systems, detailed in Table 3 the appropriate seeding ratio and cell ratio were achieved.

Media composition optimisation allowed for a 3D tri-culture system that sustained each glomerular cell type. Starting with the basal medium required for each cell type, using the literature and modifying the FBS levels while monitoring 3D tri-cultures (Table 3) allowed creation of the tri-culture media V2 used for all 3D tri-culture model work.[184, 185, 202] Such optimisation of culture medium is an essential and standard step when creating a successful culture system of multiple cell types.[229, 230]

3D Tri-culture Characterisation

Appropriate quantifiable and defined read-outs are required of all scientific models to allow for analysis and, ultimately, formation of conclusions.

Confocal microscopy was used qualitatively to image the 3D tri-culture model, revealing the assemblies and interactions of glomerular cells (Figure 23 and Figure 24), as well as the effect of TGF-β (Figure 25). The cell-cell interactions formed by 3D tri-culture mimic the *in vivo* glomerulus, with fGECs forming tubule networks with branching which fPODs interact with and fMCs sit within the matrix. fPODs display long extensions, foot-like processes where the intimately associate with the other glomerular cell types. fPOD labelling could perhaps be improved, as the fine foot-like processes are not imaged as clearly. The well documented damaging effect of TGF-β upon glomerular cell types was demonstrated, providing a depiction of how the glomerulus is injured *in vivo*.[17, 18, 26, 27] Loss of fGEC networks with TGF-β treatment opposes the reported response by Sankar *et al*.[196], whose work was discussed in the literature review, where TGF-β promoted network formation in rat capillary endothelial cells; this could be due to such responses to TGF-β being both context and cell-specific with endothelial cells from rat epididymal fat pads and primary human fGECs. Indeed, such GEC network loss has been observed in previous works by the Bradley laboratory and glomerular capillary network loss due to GEC apoptosis is an *in vivo* characteristic of glomerulosclerosis.[18, 194, 201] Apparent increased fMC number with TGF-β treatment correlates well with the characteristic

enlarged mesangial compartment in glomerulosclerosis where enlargement is partially due to MC proliferation.[10, 17] fPODs in 3D tri-culture response of seeming decreased number and rounding in morphology also mimics the *in vivo* situation with glomerulosclerosis.[19, 20]

The structures and interactions seen in these 3D tri-cultures, along with the visual responses seen with TGF-β provide evidence to this tri-culture system as a model for glomerulosclerosis. No quantitative data was captured here, to do so in further works would be advantageous to underpin these observations

Chief read-outs defined for the 3D tri-culture system were nodule counts and RT-qPCR analysis of gene expression. Nodule formation by 3D tri-cultures is evident by eye with treatment of TGF-β; this is analogous to the fibrotic response of the MC *in vivo*, where there is proliferation, hypertrophy, and excessive matrix deposition. This response has been demonstrated previously in the Bradley laboratory, as well as by others, described in the literature review.[194, 195, 201] Antibody staining for both human collagens type I and III verified positive staining for these proteins located within and around identified nodules, whilst not detected elsewhere within the 3D culture matrix.[201]

Nodule formation in 3D tri-cultures follows the same pattern as in 3D fMC cultures, including BMP7 demonstrating no effect upon TGF-β evoked nodules formation.[201] This is despite the lower number of fMCs compared to the other cell types, suggesting that fGECs and fPODs may contribute to nodule formation. This is possible as both cell types contribute to the healthy GBM *in vivo*; while processes of epithelial to mesenchymal transition (EMT) and endothelial to mesenchymal transition (EndMT) induced by TGF-β, described in the literature, could also result in these cell types becoming sources of excessive ECM deposition.[231-233] It may simply be that the fMCs are highly activated in response to TGF-β, possibly with fGECs and fPODs expressing further pro-fibrotic signals, the cross-talk between glomerular cell types and the contribution of this to glomerulosclerosis is much evidenced.[197, 234-237]

It was presented earlier that TGF-β results in a significant increase in CTGF expression by fPODs, it is possible that this response in the 3D tri-culture potentiates fMC activation and ECM deposition, indeed the literature supports this effect of CTGF upon MCs.[126, 222]

Nodule counts in 3D tri-cultures may also support the observation that fMC numbers increased with TGF-β treatment, with nodule formation also increased.

Preliminary work to achieve a more high-throughput method of counting nodules proved promising, such a methodology would prevent any variability made by individual human assessment and offer potential for more acute analysis, such as quantity of ECM per nodule.

RT-qPCR to quantify gene expression is an important and widely used tool to study the effect of treatment upon a culture system or animal model. Extraction of RNA, the first step in RT-qPCR, is complicated when cells are grown in 3D as opposed to 2D cultures as gel degradation is required,

this is a disadvantage of a gel-based 3D culture system. Protocol optimisation resulted in successful, reproducible RNA extraction from 3D culture gels.

The gene expression response of the 3D tri-culture model to TGF-β was characterised with cultures treated with either TGF-β and/or BMP7 (Figure 29). This enabled comparison of the glomerular cell's response to these stimuli when grown together in 3D tri-culture versus each alone in 3D mono-culture in earlier works.[201] ECM genes, COL1A1 and COL4A1, followed the same expression pattern, upregulation with TGF-β treatment while BMP7 had little effect. This intimates fibrosis initiation in the 3D tri-culture model with TGF-β, which also corresponds with nodule data, as well as with 3D fMC mono-culture data.[201] This is an accepted response much evidenced in the literature of TGF-β increasing COL1A1 and COL4A1 expression.[17, 18, 238, 239] CTGF, SERPINE1, and SMAD3 expression were consistent with the fPOD data and literature discussed earlier.

The data establishes that the culture of the three glomerular cell types in 3D allows these cells to intimately interact both physically and via signalling mechanisms and so mimic the *in vivo* state both morphologically and pathophysiologically. TGF-β treatment evokes a fibrotic response in the 3D tri-culture model which allows for the modelling of human glomerulosclerosis *in vitro*. Examination into the potential antagonism by BMP7 over TGF-β confirmed no such action in the 3D tri-culture model, differing from when glomerular cells are cultured in isolation.[201, 240] This highlights the role glomerular cell interaction and microenvironment plays in behaviour.

3D Tri-culture Model, Cytokines & Growth Factors (Chapter 6)

The 3D tri-culture model tested several cytokines and growth factors to further model and understand glomerulosclerosis.

TGF-β & TNF-α

The pattern of nodule formation with either TGF-β or TNF-α alone, or in co-treatment demonstrated nodule formation was TGF-β dependent and TNF-α had no effect upon this in Celprogen fPOD 3D tri-cultures (Figure 30). Corroborating the fibrotic response to TGF-β in the 3D tri-culture model. The literature defines TGF-β as inducing fibrosis by stimulation of matrix deposition and proliferation whilst TNF-α is more involved in the inflammatory response involved in glomerulosclerosis.[65, 241]

3D tri-cultures with Celprogen fPODs were examined for changes in COL1A1, COL4A1, CTGF, SMAD3, SERPINE1, CCL2, and CXCL8 gene expression (Figure 31). Of particular interest is the expression pattern of COL1A1 expression which significantly increased with TGF-β treatment, while TNF-α alone resulted in a non-statistically significant decrease and co-treatment did not change expression from control values. COL4A1 expression increased without statistical significance with both TGF-β and co-treatments and TNF-α evoked no change in expression. This response indicates differential effects

of these cytokines, with COL1A1 expression TNF-α can inhibit the activity of TGF-β but not COL4A1 expression. TNF-α inhibiting TGF-β induced COL1A1 is characterised in the literature, summarised in a review by Verrecchia and Mauviel[242], while there seems to be no such antagonism with COL4A1. Grande *et al.*[243] studied possible modulation of TGF-β induced COL1A and COL4A expression by several cytokines, including TNF-α, in murine fibroblast-like cells. No effect was concluded with TGF-β and TNF-α co-treatment upon COL4A expression but antagonism was seen with COL1A expression.[243] 3D tri-culture model data therefore supports and confirms these findings. Taking these findings with nodule data (Figure 30), where TNF-α had no apparent effect upon increased formation with TGF-β, the seeming inhibition of TGF-β induced COL1A1 expression by TNF-α in 3D tri-cultures suggests that COL4A1 is the major constituent of nodule formation in the tri-culture. Tamsma *et al.*[244] demonstrated that patient biopsies with diabetic nephropathy that nodular lesions had increased MC staining with COL4A staining. During development there is an isoform switch in COL4A expression from α1 and α2 to α3, α4, and α5 networks, which are believed to be able to better withstand filtration forces and endoproteolysis; due to mutations in α3, α4, and α5 chains in Alport syndrome, there is no such isoform switch in COL4A expression, which results in a GBM that is less robust and thus deteriorates.[245, 246] These findings corroborate that COL4A1 is a major contributor to fibrosis and glomerular dysfunction seen in glomerulosclerosis, further demonstrating the 3D tri-culture as modelling glomerulosclerosis *in vitro*.

CTGF expression upregulation with all treatments was partially expected, as TGF-β is a potent inducer of CTGF, demonstrated with earlier data.[40, 43] The literature provides some evidence that TNF-α can result in CTGF downregulation as well as inhibiting that evoked by TGF-β.[247-250] The literature does suggest incubation times with stimulus alter this effect. While TGF-β induced nodule formation is unaffected by TNF-α treatment despite COL1A1 downregulation, the increase in CTGF expression may be driving nodule formation.

SMAD3 expression mirrored earlier data, the downregulation in SMAD3 expression in response to TGF-β treatment implies downregulation via a negative feedback mechanism, Poncelet *et al*.[218] demonstrated a similar phenomenon in cells with a "myofibroblastic" phenotype from UUO murine models. Increased SERPINE1 expression with all treatments corresponds with literature reports of TGF-β and TNF-α both inducers of SERPINE1 expression, suggesting the contribution of SERPINE1 in renal fibrosis has redundancy, making it an attractive target.[211, 251-254]

Inflammation-associated genes CCL2 and CXCL8, both chemokines, were interrogated being implicated in immune infiltration in kidney fibrosis. CCL2 expression with TGF-β decreased, without statistical significance, the literature suggests that CCL2 expression is downregulated by TGF-β in endothelial but upregulated in epithelial cell types.[255, 256] The 3D tri-culture model has fGECs in the greatest abundance compared with fPODs and fMCs. Wolf *et al.*[257] demonstrated a regulatory loop

existing between CCL2 and TGF-β in *ex vivo* mouse kidney; where CCL2 stimulates collagen expression through upregulation of TGF-β, where TGF-β exerts negative feedback upon CCL2 expression. This may be what is seen in this data. TNF-α treatment alone evokes an expected increase in CCL2 expression, as did co-treatments. CCL2 has been implicated in human renal disease for its role in monocyte recruitment and activation, yet its relationship with TGF-β may also be important to disease pathogenesis.[258-260] CXCL8 expression appeared increased with all treatments; TGF-β mediated CXCL8 downregulation has been reported in endothelial cells by Smith *et al.*[261], while in proximal tubular cells the literature demonstrated TGF-β induces upregulation of CXCL8.[255, 262] As TGF-β induces a trend of increased CXCL8 expression in 3D tri-cultures it suggests that despite the higher numbers of fGECs within the tri-culture model, the other cell types are evoking an overpowering upregulation of CXCL8. TNF-α induction of CXCL8 was expected due to its inflammatory role, confirmed in the literature.[263, 264] In human renal diseases CXCL8 expression has been noted as a potentially useful marker of disease progression.[265, 266]

The same genes assessed by Lonza fPOD 3D tri-cultures, with TGF-β induced COL1A1 expression inhibition by TNF-α replicated in these cultures (Figure 32). Expression of COL4A1, SMAD3, and SERPINE1 was also reproduced, some differences could be seen with CTGF, CCL2, and CXCL8 genes, however, the fundamental and canonical changes in expression discussed above were demonstrated (Figure 32, Figure 33, and Figure 34). Therefore this data set indicates 3D tri-cultures composed of either Celprogen fPODs or Lonza fPODs respond consistently, suggesting the presence of CHO in early cultures had little effect upon gene expression data.

Additional genes were examined in Lonza fPOD 3D tri-cultures, COL3A1 (Figure 32) and CTNNB1 (Figure 34) demonstrated little change in expression across treatments, despite both reported as implicated in renal fibrosis, COL3A1 in ECM accumulation, and CTNNB1 with EMT.[120, 267-269] ACTA2, FN1, and LAMB2 expression were used as further identifiers of fibrosis and ECM deposition (Figure 32). A marker of myofibroblasts and therefore a state of fibrosis, ACTA2 demonstrated the anticipated increase in expression with TGF-β, TNF-α had no effect.[6, 270, 271] Likewise, FN1 and LAMB2 expression followed the expected increase in expression with TGF-β.[272-274] Interestingly, co-treatment resulted in LAMB2 expression to be statistically increased, suggesting synergy between TGF-β and TNF-α, genetic mutations in LAMB2 have been identified as causing glomerular disease.[275] SMAD2 and BMP7 were examined for their signalling association with TGF-β (Figure 33). SMAD2 expression was increased with a seemingly cooperative action of TGF-β and TNF-α co-treatment, there is some evidence of this effect in the literature which results in EMT/EndMT.[276, 277] There is also evidence that SMAD2 acts in a renoprotective manner, therefore TNF-α may be promoting this effect and antagonising the pro-fibrotic action if TGF-β.[278] TNF-α treatment resulting in pSMAD2 but not pSMAD3 has been demonstrated in fGECs (data not shown). BMP7 expression

appeared increased with all treatments, as BMP7 has been described by the literature as both anti-fibrotic and anti-inflammatory, this response may indicate a feedback mechanism to try and prevent further fibrotics and inflammatory response (Figure 34).[279]
Finally, TGM2 expression was examined due to the role of transglutaminase 2 plays in fibrosis by catalysis of ECM cross-linking. TGF-β caused significant TGM2 downregulation, which TNF-α had no impact upon, which differs from the literature where upregulation is reported (Figure 34).[280]

The different roles TGF-β and TNF-α play in the development and progression of glomerulosclerosis is demonstrated by this data, which also suggests there is some interplay between these cytokines. The data presented here again clearly determines the 3D tri-culture model as mimicking the *in vivo* condition, as well as highlighting areas for further analysis and potential therapeutic targets.

TGF-β, CTGF nAb & ALK5i
With data pointing to CTGF has playing a significant role in the fibrotic response both in the 3D tri-culture model and *in vivo*, targeting of CTGF was investigated, along with the classical inhibition of the TGF-β receptor ALK5. The basis of ALK5 inhibition comes from its role in TGF-β signal transduction, and indeed more complex than this, TGF-β receptors form a heteromer that can be either heterodimeric or heterotrimeric.[281] While TGF-β signalling via a TGF-βR-II and ALK5 heterodimer SMAD2/3 phosphorylation occurs, promoting fibrosis.[18] When signalling via a TGF-βR-II, ALK5 and ALK1 heterotrimer SMAD1/5/8 phosphorylation occurs, suppressing fibrosis.[281] Therefore, decreasing the availability of ALK5 may have the dual function of suppressing SMAD2/3 phosphorylation while promoting SMAD1/5/8 phosphorylation. Celprogen fPODs were used in these 3D tri-cultures.
Nodule formation (Figure 35) was diminished when either inhibition was used in co-treatment with TGF-β, but both were required to bring nodule number back to control values, this indicates that both ALK5 and CTGF are necessary for TGF-β driven nodule formation in 3D tri-culture. Comparing this with data where ALK5i was sufficient to prevent TGF-β induced nodule formation in 3D fMC mono-cultures.[201] This firstly demonstrates the effect of culturing multiple cells and permitting the interplay between them, whilst also indicating that increased CTGF expression fPODs respond with the treatment of TGF-β plays a significant role in driving nodule formation in the 3D tri-culture model. As has been described, much evidence has been gathered for the role CTGF plays in fibrosis. While TGF-β is an inducer of CTGF, a more synergistic relationship between the two cytokines has emerged, which this nodule count data supports.[41, 43, 282]
COL1A1 expression in the 3D tri-culture model is ALK5 dependent, with only ALK5i successfully prevented TGF-β evoked expression (Figure 36), suggesting CTGF has little involvement with this

upregulation. A similar pattern of expression was seen with COL4A1 expression. Relating this with nodule data suggests that while is ALK5i required for TGF-β induced COL1A1 and COL4A1 expression, it is not sufficient to bring nodule counts to control values. CTGF nAb is additionally required, suggesting other ECM proteins are contributing to nodule formation in 3D tri-cultures.

Expression of CTGF evoked by TGF-β appeared to be partially inhibited with ALK5i, while inhibition of CTGF itself had no effect. ALK5 is therefore again highlighted as key to TGF-β mediated gene responses, with CTGF itself not required for further gene expression.

As described in the literature review, ALK5i has been used successfully to inhibit early-stage fibrosis in the UUO mouse model.[122] Inhibition of CTGF has been demonstrated as successfully ameliorating fibrosis in animal models, where CTGF inhibition resulted in decreased expression of both collagen and CTGF itself, as well as resulting in a reduction of albuminuria in patients with diabetic kidney disease.[41, 128, 129]

Clearly and as would be expected ALK5i has a significant impact upon fibrosis in the 3D tri-culture system, however inhibition of CTGF was also required to prevent TGF-β mediated nodule formation. Establishing that there is redundancy in the development of fibrotic response in the system which requires targeting of multiple components for attenuation, as has been realised in the human disease.

TGF-β, TNF-α & CTGF nAb

The impact of CTGF inhibition upon TNF-α in addition to TGF-β was investigated with the differential roles involved with inflammation and fibrosis in mind. Celprogen fPODs were used in these 3D tri-cultures. Nodule data (Figure 37) again demonstrated TNF-α and inhibition of CTGF did not prevent TGF-β evoked nodule formation. Expression of COL1A1 and COL4A1 (Figure 38) generally replicated previous expression patterns with these treatments, except for TNF-α resulting in an apparent inhibition of TGF-β evoked COL4A1 expression, yet with no statistical analysis, this is an unsubstantiated trend. Co-treatment of TNF-α and CTGF nAb providing no attenuation in TGF-β evoked collagen expression. This indicates that despite the key role CTGF plays in fibrosis, TGF-β alone is sufficient in eliciting fibrotic response, indeed, the CTGF expression evoked by TGF-β may be greater than the CTGF inhibition level used here. Likewise, CTGF (Figure 39) and CCL2 (Figure 40) expression replicated earlier data. A degree of TGF-β evoked ACTA2 expression (Figure 38) attenuation with TNF-α treatment was demonstrated, this response has been reported in human dermal fibroblasts by Goldberg *et al.*[283] Expression of TGFB1 itself was downregulated with TNF-α treatment and to a lesser extent, with CTGF inhibition (Figure 39). There is some evidence of this effect of CTGF inhibition upon TGFB1 expression in the literature.[284] However the effect of TNF-α is

less clear, there is some evidence of induction of TGFB1 expression in some cell types, however, the complex and often antagonistic relationship between these cytokines is clear, meaning such a response in the 3D tri-culture model is entirely plausible.[285, 286] CDH1 expression, which is the gene that codes for E-cadherin, a marker of EMT, is downregulated by all treatments (Figure 40). Such loss of CDH1 is suggestive of EMT, with TGF-β and TNF-α both described in the literature as capable of stimulating EMT.[231, 232, 287, 288] Surprisingly, the greatest CDH1 downregulation was seen in co-treatment of TGF-β, TNF-α, and CTGF nAb, with CTGF also reported to play a key role in EMT.[289, 290] Anti-CTGF antibodies are reported to have two modes of action in the inhibition of fibrotic response, that is inhibition of TGF-β and the induction of BMP7 signalling.[23] Dudas *et al.*[291] reported that BMP7 was unable to attenuate TGF-β induced EMT, indeed the data presented using the 3D tri-culture model demonstrates BMP7 as failing to prevent any TGF-β evoked fibrotic response. Therefore, it may be that any promotion of BMP7 signalling by CTGF nAb is ineffective. It is additionally prudent to note that the average CT value of CDH1 expression in this data set was 32.89, suggesting a low-level basal expression which makes a reliable analysis more difficult. Finally, CLDN1 expression (Figure 40) was reduced with TGF-β treatment, an anticipated response claudin-1 being another EMT marker.[292]

The data here replicated many previous findings demonstrated in the 3D tri-culture model, further validating the system and indicating reproducibility. Evidence of EMT is established by this data set, signalling further replication of the *in vivo* response in glomerular disease by the 3D tri-culture system. Inhibition of CTGF again did not reveal any significant inhibition of TGF-β induced gene responses. The CTGF nAb used in these experiments is a polyclonal rabbit antibody that reacts with human CTGF, with neutralisation listed as a tested application. Wang *et al.*[41] reported that a CTGF nAb (FG-3019, an anti-CTGF monoclonal antibody) attenuated fibrosis in animal models of kidney fibrosis. As discussed, potentially the mode of CTGF nAb action was ineffective or the dosage was. However, the CTGF nAb was effective in reducing TGF-β induced nodule formation, doing so most effectively with ALK5i to bring nodule counts back to control values.

TGF-β & CTGF

CTGF evoked nodule formation to a similar degree as TGF-β, with no additive effect seen when TGF-β and CTGF were used in combination. The contribution CTGF has to fibrosis has been discussed and therefore this response correlates with the literature.[41, 215, 250] Collagen expression was not upregulated with CTGF treatment (Figure 42); the literature generally reports CTGF has inducing collagen expression, however mainly fibroblasts have been studied and there are reports of no such induction.[293-296] ACTA2 expression (Figure 42) appeared to be largely unaffected by CTGF, ACTA2

expression has been reported to increase with CTGF treatment, again in fibroblasts.[297] However, upregulation of FN1 was demonstrated with both TGF-β and CTGF treatments (Figure 42). It is possible that within the 3D tri-culture model, where the human glomerulus is being modelled, that CTGF is evoking fibronectin expression, and as data has indicated CTGF produced by fPODs can drive nodule formation, fibronectin may be a constituent of those nodules. CTGF evoked FN1 expression is detailed in the literature.[296, 298] Interestingly, LAMB2 expression was downregulated with both cytokines, with TGF-β resulting in the most significant decrease (Figure 42), differing from earlier data. LAMB2 is described as expressed in the normal GBM and not within normal mesangium, with increased expression seen in the mesangium across many renal diseases.[299] Potentially the expression of LAMB2 in the 3D tri-culture is different without a fully established GBM and lower fMCs numbers compared with the other glomerular cells. Additionally, the average CT value for LAMB2 was 27.90 which indicates LAMB2 expression was low overall. CTGF appeared to not affect SMAD3, SERPINE1, or its expression, with TGF-β evoking expression as demonstrated in earlier data sets (Figure 43). Coupled with CTGF inhibition data the implication is that CTGF has no impact upon these genes itself or when TGF-β mediated. Meanwhile, CTGF appeared to induce CCL2 where TGF-β has consistently shown little effect (Figure 43). The literature provides evidence of CTGF promoting infiltration of inflammatory cells, with CCL2 upregulation a demonstrated response in this process.[45, 46] Interestingly, TGF-β prevented this response to CTGF; presumably performing in the anti-inflammatory role it can take.

This data set again underlines and re-affirms earlier findings with the 3D tri-culture model, noting that Celprogen fPODs were used in these experiments. CTGF inhibition had been demonstrated as necessary to prevent TGF-β mediated nodule fibrotic response. Only ECM gene, FN1, was shown as upregulated by CTGF, crucially implicating fibronectin as a key ECM responder in the fibrotic response in the 3D tri-culture model. Further, CTGF has demonstrated its ability to promote an inflammatory response.

TGF-β, bFGF, IL-1α, PDGF-BB & HGF

As anticipated, cytokines bFGF, IL-1α, and PDGF-BB elicited a fibrotic response in the 3D tri-culture model with the induction of nodule formation (Figure 44), with the literature reporting such effects.[130, 131, 150, 165] HGF had no effect, in line with the literature purporting this cytokine as anti-fibrotic.[60, 63] All cytokines appeared to evoked COL1A1 and FN1 expression to some degree, while COL4A1 expression appeared unchanged with IL-1α, spread in the data does make analysis difficult (Figure 45). ACTA2 expression was evoked with TGF-β, emulating earlier results, and discussed literature, with all other treatments indicating some degree of ACTA2 upregulation (Figure 45). LAMB2 appeared to be upregulated with HGF treatment while largely unaffected with other

treatments, HGF has been implicated in the modulation of matrix turnover in glomeruli (Figure 45).[186] As described, mutations in LAMB2 can result in glomerular disease, potentially LAMB2 is a protective element of the ECM in maintaining a healthy GBM and so is upregulated by an anti-fibrotic cytokine such as HGF. Again, it must be noted that the average CT values were reasonably high for LAMB2.

CTGF expression was demonstrated as only elicited with TGF-β; while SERPINE1 was induced with all cytokines, with bFGF and IL-1α doing so second to TGF-β (Figure 46). Such a response with bFGF has been seen in HUVECs, while only IL-1β and not IL-1α has been specified to induce SERPINE1.[300, 301] HGF evoked a level of TGM2 expression that was significantly higher than that treated with TGF-β (Figure 46). The literature plainly illustrates that TGM2 has functional activities beyond enzymatic catalysis of ECM cross-linking, such a cell survival, potentially why renotropic HGF would cause an upregulation.[302]

Cytokines other than TGF-β, CTGF, and TNF-α are widely known to be involved in the melee of glomerulosclerosis. bFGF, IL-1α, PDGF-BB, and HGF all demonstrate responses in the 3D tri-culture model in line with the literature and the *in vivo* situation, noting that Celprogen fPODs were used in these experiments, further strengthening the validity of the model system while highlighting these cytokines further as potential targets in renal fibrosis.

TGF-β, CTGF, IL-1α, IL-1β, PDGF-BB, EGF, bFGF & HGF

All treatments, except HGF, resulted in some increased nodule formation in the 3D tri-culture model, as with previous data. Expression of collagen generally followed earlier data, TGF-β evoking the greatest COL1A1 and COL4A1 responses. COL6A1 was investigated, identified in the normal mesangium, with increased formation observed in more severe CKD patients.[303, 304] Expression of COL1A1, COL4A1 and ACTA2 followed earlier data sets, with TGF-β evoking the greatest response and some lesser responses with other cytokines (Figure 48). Neither TGF-β or EGF appeared to affect COL6A1 expression in the 3D tri-culture model, while the other cytokines seemed to evoke varying degrees of upregulation. With SMAD3 binding sequences identified in the promoter regions of COL6A1, an upregulation may have been anticipated, yet as indicated above, it could be that COL6A1 deposition and turnover are seen in late disease and the 3D tri-culture model had not progressed to that state within the 24hr timepoint.[278] CTGF expression demonstrated the expected upregulation with TGF-β, with this data set also demonstrating some upregulation with CTGF, IL-1α, IL-1β, PDGF-BB, and EGF, differing from earlier data sets (Figure 49). Yet with large error between repeated values at N=2, little credence can be given to this. Expression of BMP7 increased with TGF-β (Figure 49), demonstrating the same response as described earlier (Figure 33). IL-1α, and to a lesser extent,

IL-1β and PDGF-BB appeared to also promote BMP7 expression (Figure 49), once more indicating a feedback mechanism in an attempt to control and prevent further fibrosis and inflammation.[279] Inflammatory genes CCL2 and CXCL8 were predictably upregulated with IL-1α and IL-1β treatments, with PDGF-BB also evoking a similar response (Figure 50). PDGF-BB evoked CCL2 expression has been demonstrated in MCs, while the response with IL-8 has only been described in corneal and orbital fibroblasts.[48, 305] This data presents PDGF-BB as promoting inflammation in the 3D tri-culture model, there is evidence in the literature of upregulation of PDGFRs during inflammation.[306] IL-1α and IL-1β both evoked increased CLDN1 expression, such response has been demonstrated in several cell types where such upregulation correlated with tight junction dysfunction and a disease state.[307-309] Induction of claudin-1 in PODs in a transgenic mouse model resulted in destabilisation of the slit diaphragm and proteinuria and inflammatory glomerular crescents in diabetic patients have demonstrated claudin-1 expression.[310, 311] Therefore, taken together, this data suggests in the 3D tri-culture model IL-1 promotes CLDN1 expression, which may result in aberrations of the slit diaphragm.

This data set further illustrates how a multitude of cytokines are involved in the development and progression of glomerulosclerosis. TGF-β has been demonstrated as the major mediator throughout these 3D tri-culture experiments, mirroring the findings of the literature. However, other cytokines play key roles that are both TGF-β dependant and TGF-β independent, mediating both fibrotic and inflammatory responses as well as regulating one another, as is the case with CTGF. This all helps build a fuller picture of the *in vivo* situation by mimicking these cytokine insults in the 3D tri-culture model, demonstrating that potential therapeutic targets can be identified and tested. Furthermore, importantly, the direct targeting of TGF-β is not practical therapeutically due to the varied and widespread actions of the cytokine throughout the body, without highly specific targeting. Meaning other factors involved must be explored and indeed it may be that multiple targets need to be utilised clinically.

The experimental set up using TGF-β and TNF-α was performed using 3D tri-cultures with Celprogen fPODs and Lonza fPODs. The resultant data established that there was consistency between the 3D tri-cultures regardless of fPOD used, providing some reassurance that data gathered from Celprogen fPOD 3D tri-cultures can be used and interrogated.

It should be noted, a large panel of genes was explored here, indeed this was the case for the majority of experimental setups. The reason for this was simply the amount of RNA that was available from each experiment versus the time between running 3D tri-cultures, as to achieve sufficient glomerular cell numbers for 3D tri-cultures cell culture periods were often prolonged. Therefore, a large panel

of genes with involvement in renal fibrosis was explored. Additionally, the intention was to run samples in MedImmune laboratories where such a large panel of genes could be run quickly.

3D Tri-culture Model & αvβ8 (Chapter 7)

Background Data for αvβ8

The integrin αvβ8 has been identified as a potential target in renal fibrosis due to its role in the activation of TGF-β, with the hypothesis that it can enable indirect modulation of TGF-β signalling that is specific to the kidney. The specific localisation of αvβ8 is therefore of great importance, as discussed, expression has been demonstrated primarily in the kidney, brain, and female reproductive organs; with expression of αvβ8 in mouse kidney identified in MCs.[171, 172] IF analysis of αvβ8 expression in the glomerular cell types of the 3D tri-culture model indicated that αvβ8 is primarily expressed in fPODs, with some weak staining in fMCs (Figure 51). Vogetseder *et al.*[312] also report moderate to strong expression of αvβ8 in PODs in normal human tissue, along with moderate expression in distal tubules and no expression in proximal tubules. Taken with the IF data here, there is strong indication that renal αvβ8 expression in humans is predominately localised to PODs, with expression in MCs noted in mice tissue.[172, 313] Indeed, IHC of human renal tissue presented in this work also demonstrated glomerular staining with acute staining localised to PODs (Figure 52).

This data supports the hypothesis of utilising αvβ8 to modify TGF-β for specific targeting in the treatment of fibrotic glomerular disease.

Anti-αvβ8 in 3D Tri-culture

MedImmune developed an anti-αvβ8 antibody which was used in the 3D tri-culture model, as a key part of the development and conception of modelling glomerulosclerosis *in vitro* was to enable both identification and testing of potential therapeutic targets.

Celprogen and Lonza fPODs were used in these experiments, additionally, LTGF-β and 1D11 were utilised. As αvβ8 is involved in the activation of TGF-β, a true assessment of its inhibition requires LTGF-β as opposed to active TGF-β. 1D11 acts as a control for total TGF-β inhibition. As CTGF had demonstrated the ability to induce nodule formation and CTGF inhibition indicated a degree of TGFB1 downregulation, CTGF was also employed in this experimental setup.

Nodule data demonstrated that αvβ8 was able to partially inhibit TGF-β, LTGF-β, and CTGF induced nodule formation (Figure 53 and Figure 54). Indicating that the anti-αvβ8 antibody was successfully preventing αvβ8 mediated TGF-β activation and therefore reducing TGF-β pro-fibrotic signalling. Earlier CTGF inhibition was described to cause TGFB1 downregulation (Figure 39), suggesting CTGF is involved in TGFB1 expression and so the effect upon CTGF induced nodule formation by αvβ8 may reflect inhibition of the activation of TGF-β generated by this mechanism.[284] TGF-β upregulation of

CTGF is a driver of This adheres with previously described evidence of RGD integrin antagonists reducing fibrosis in models of renal disease, with the difference of knowing the specific integrin targeted.[175, 176]

No change in ECM gene expression was detected with the anti-αvβ8 antibody compared with TGF-β evoked responses in Celprogen fPOD 3D tri-cultures (Figure 55). There did appear to be some inhibition of TGF-β evoked CTGF expression with the anti-αvβ8 antibody, which would seem sensible considering αvβ8 inhibition would prevent activation of endogenous TGF-β (Figure 56). The literature reports RGD integrin inhibition results in suppression of CTGF expression in kidney fibroblasts both with and without exogenous TGF-β.[314]

Lonza fPOD 3D tri-cultures similarly demonstrated no change in TGF-β evoked COL1A1 and ACTA2 expression with αvβ8 inhibition; however, response with LTGF-β did appear to be attenuated to some degree (Figure 57 and Figure 59). While unlike earlier data, both TGF-β and LTGF-β evoked COL4A1 expression appeared inhibited by the anti-αvβ8 antibody in this data set at N=1 (Figure 58). An interesting result as data has suggested that COL4A1 is the major constituent of nodule formation in the 3D tri-culture model, therefore partly explaining decreased nodule formation with αvβ8 inhibition. LTGF-β did not appear to substantially evoke FN1, therefore again no change in FN1 with αvβ8 was demonstrated (Figure 60). Earlier data had demonstrated that CTGF could evoke increased FN1 expression (Figure 42), no such response is seen here (Figure 60). This variability suggests there could be degradation in recombinant CTGF aliquots used in these experiments.

TGF-β evoked CTGF expression did not appear to change with αvβ8 inhibition in this data set, while expression evoked with LTGF-β was attenuated to some degree (Figure 61). This may partly explain the effect of αvβ8 inhibition upon nodule counts, with exogenous TGF-β treatment free to induce CTGF expression while LTGF-β is inhibited from doing so by the anti-αvβ8 antibody. SERPINE1 upregulation by TGF-β was again unaffected by αvβ8 inhibition (Figure 62). While LTGF-β evoked SERPINE1 expression to a lesser extent, some attenuation in this response could be seen with the anti-αvβ8 antibody.

Despite the low N numbers, this data set truly validates the anti-αvβ8 antibody as preventing TGF-β activation and consequently, TGF-β mediated fibrosis in the 3D tri-culture model, the effects seen clearly when LTGF-β was used in the system. In many instances, the inhibition of αvβ8 was as effective, if not more so, in preventing LTGF-β mediated pro-fibrotic gene expression. The 3D tri-culture model is also demonstrated further as an important tool in the assessment of such therapeutics upon glomerular fibrosis, allowing valuable insight before further clinical investigations. Once again there was little difference between data acquired from 3D tri-cultures using Celprogen fPODs or Lonza fPODs, especially considering the low N numbers.

Glomeruli Isolation & HOC (Chapter 8)

Glomeruli Isolation

Exploration of glomeruli isolation was made as a potential avenue to isolate PODs for the 3D tri-culture model. Both mouse and human glomeruli isolations were performed, where collagenase was identified as not essential in the isolation procedure. Cellular outgrowth from mouse glomeruli displayed both POD and MC markers, suggesting heterogeneity in the cells that were in the outgrowth and so indicating a requirement for a further isolation step to harvest only PODs (Figure 64, Figure 65, and Figure 66). Literature does reference strategies for obtaining a homogenous cell culture.[185] Human glomeruli were found not to adhere to plasticware as described in the literature, this was similarly experienced by collaborators. Further investigation and optimisation outside the scope of this project were required to remedy this.

This work demonstrated successful isolation of glomeruli from both mouse and human tissue, where there was certainly POD outgrowth from mouse glomeruli.

HOC

HOC was created to reproduce 3D tri-culture experimental treatments to examine whether responses aligned which would add further credence to the clinical relevance of the 3D tri-culture model. It is important to note here that renal tissue used for HOC is obtained from two sources; one provides normal renal tissue from biopsies and one is from donor kidneys, where solely cortex tissue can therefore be supplied. The consequence of this is that renal tissue from biopsies may have only a few or no glomeruli, the sources of tissue shall be noted in the data discussions below. Two timepoints were used in this work, the 24hr timepoint used in all 3D tri-culture model experimentation and a 6hr timepoint. Literature reports a limitation with HOC of incubation length, therefore a shorter timepoint of 6hr was examined which has successfully been used with renal HOC.[104, 105, 315]

TGF-β, TNF-α & ALK5i

The renal tissue used in these HOC was from biopsies; additionally, this is an early data set of N=1, therefore only limited observations can be taken from it. At the 6hr timepoint, TGF-β treatment resulted in upregulation of COL1A1, COL3A1, and COL4A1 (Figure 70). COL3A1 upregulation with TGF-β was not commonly seen in the 3D tri-culture model. Increased collagen III is reported in glomerulosclerosis; however, there is evidence of cell-specific regulation where fibroblasts respond with collagen III expression when stimulated with TGF-β.[267, 316] Fibroblasts are not present in the 3D

tri-culture model, while likely within the HOC, which may explain the disparity here. ALK5 inhibition attenuated all TGF-β evoked collagen upregulation, as would be anticipated, while TNF-α had a similar effect. Inhibition of TGF-β evoked COL1A1 expression has been demonstrated in the 3D tri-culture model (Figure 31 and Figure 32), but not for COL4A1 or COL3A1. TNF-α mediated inhibition of COL3A1 has been reported in dermal fibroblasts, however, it is prudent to consider when looking at this data that N=1 and the signal from the tubulointerstitium may be stronger than of the glomerular tissue in HOC.

ECM genes ACTA2, FN1, and LAMB2 genes were all upregulated with TGF-β at the 6hr timepoint (Figure 71). A response demonstrated in the 3D tri-culture model; except LAMB2, where TGF-β generally had little effect. Once again while ALK5 inhibition appeared to attenuate all TGF-β evoked ECM genes, TNF-α had a similar effect. This effect had been observed with ACTA2 expression in the 3D tri-culture model (Figure 38). Such a response with ACTA2 and FN1 expression has been demonstrated in human dermal fibroblasts.[283, 317]

Data at the 24hr timepoint generally illustrates a downregulation in all gene expression, regardless of treatment, compared to the T0 control tissue (Figure 72 and Figure 73). This indicates deterioration of the HOC as a whole due to the length of culture, in-line with the literature as discussed earlier. Due to this evident effect upon HOC condition at the 24hr timepoint, no further discussion of these data shall be made as it is flawed with many assumptions and cautions required for analysis.

The gene expression profiles seen in HOC in this data are very similar to those seen with the 3D tri-culture model. TNF-α does appear to behave in a more antagonistic manner in HOC compared with 3D tri-culture. The antagonistic relationship of TNF-α can have upon TGF-β is well documented, pro-inflammatory TNF-α suppression of anti-inflammatory TGF-β is a system for maintenance of homeostasis.[247, 283, 317-319]

It is important to remember however that firstly this data is very early/preliminary data with no repeated measures and crucially, the amount of glomerulus in this renal tissue at this point is unknown, and much of the signal measured could be coming from other cell types and structures, like tubules, which are most abundant in the renal cortex.

TGF-β & anti-αvβ8 antibody

Renal tissue used in these data sets was from biopsies. Unlike the previous data set, collagen gene expression was generally lower in HOC samples than T0 control, despite the 6hr timepoint (Figure 74). This suggests some degree of degradation in the HOC, indeed, this data demonstrates no discernible changes or patterns in collagen expression with treatments.

ECM genes demonstrated a downregulation in ACAT2 expression across all HOC compare with T0, again indicating some HOC degradation (Figure 75). Conversely, FN1 expression was increased with HOC, where there was an indication of αvβ8 inhibition attenuating the TGF-β mediated FN1 response. Additionally, the higher concentrations of anti-αvβ8 antibody in HOC alone appeared to reduce basal FN1 expression, suggesting that the antibody was behaving as designed in preventing activation of endogenous LTGF-β. A similar pattern is demonstrated with LAMB2 expression. However, as noted, this is very preliminary data with no statistical power to it.

This data set appears to reveal HOC experiencing some degradation, where collagens and ACAT2 were primarily affected. Yet, does provide some early indication that αvβ8 inhibition is having the anti-fibrotic effect it was designed to provide. This data also indicates that the higher concentrations of the anti-αvβ8 antibody are more effective and these higher concentrations may be worth investigating in the 3D tri-culture model. This validates HOC as a potential tool in the prediction of required drug dosage, use of HOC in drug development is reported in the literature.[102, 183]

As with the earlier data set, the precise renal origin of tissue from renal biopsies is unknown without any further analytical investigation, making assessment or comparison of this HOC data against the 3D tri-culture model difficult. Further work is required to fully utilise HOC and enable such comparison to the 3D tri-culture model, this preliminary work demonstrates promising responses in modelling renal fibrosis.

Chapter 10 – Conclusions & Future Work

The data presented in this Thesis validates the 3D tri-culture as an *in vitro* model of glomerulosclerosis. TGF-β induced physical nodule formation, replicating ECM deposition, with increased fibrotic and inflammatory gene expression demonstrated by the 3D tri-culture model are all some of the clinical markers of glomerulosclerosis.[4-6, 127, 212]

There is a large body of literature supporting the role of TGF-β in ECM accumulation in kidney disease[26, 320] both *in vitro*[110-112], in animal models[108, 109], and *in vivo*[28, 107]. This data adds to and supports this. TNF-α is also a key cytokine of kidney disease, and its complex relationship with TGF-β is also highlighted by this data.[67, 69, 70, 243, 247, 249] TGF-β is seen as the main pro-fibrotic cytokine involved in fibrotic kidney disease whilst TNF-α is the key mediator of inflammation and they can target one another, as demonstrated in the 3D tri-culture model with TNF-α treatment inhibiting TGF-β induced COL1A1 expression. Certainly, a complex relationship is at play between these cytokines, which is compounded by their individual dualities, in the 3D tri-culture model TGF-β and TNF-α in combination promote fibrosis and inflammation above that seen when used separately.

The importance of CTGF in the fibrotic response is also supported by this data, implicated in COL4A1 and TGFB1 expression.[40, 41, 43, 284] Inhibition of CTGF was required, alongside ALK5i, to prevent TGF-β evoked nodule formation. Coupling this observation with that of CTGF promoting TGFB1 results in the premise that; TGF-β upregulates CTGF, both contribute to nodule formation and CTGF induces TGFB1 expression. Therefore, either inhibition of CTGF or TGF-β signalling will only attenuate part of the fibrotic response and so both require targeting. A simple schematic of this relationship between TGF-β and CTGF, with the points of inhibition used in this body of work, is detailed in Figure 78.

PODs are identified as a source of CTGF in this Thesis, an observation supported by the literature.[213-215] This is a further demonstration of the importance of culturing the three glomerular cell types together, in allowing a greater recapitulation of the glomerular microenvironment where glomerular crosstalk is essential to both homeostasis and the development of disease.

Antagonism of TGF-β mediated with proposed natural antagonists BMP7 and HGF proved ineffective in the 3D tri-culture model. Other cytokines involved in the fibrotic and inflammatory melee of glomerulosclerosis explored, PDGF-BB, EGF, bFGF, IL-1α, and IL-1β certainly elicited some fibrotic/inflammatory effect in the 3D tri-culture model. With some interesting responses indicated, such as IL-1 induction of CLDN1 expression, which may result in slit diaphragm abnormalities. However, the data marks TGF-β as the master cytokine of fibrosis in this system, correlating with the extensive literature determining this. TGF-β is an attractive target to have a substantive impact on the development and progression of renal fibrosis. Integrin αvβ8 has been evidenced as a viable target to indirectly modify TGF-β activity. As depicted in the schematic of Figure 78, αvβ8 inhibition

is unlikely to solely fully attenuate renal fibrosis, with CTGF activity playing a key role, re-introducing the concept of multiple targets for treatment.

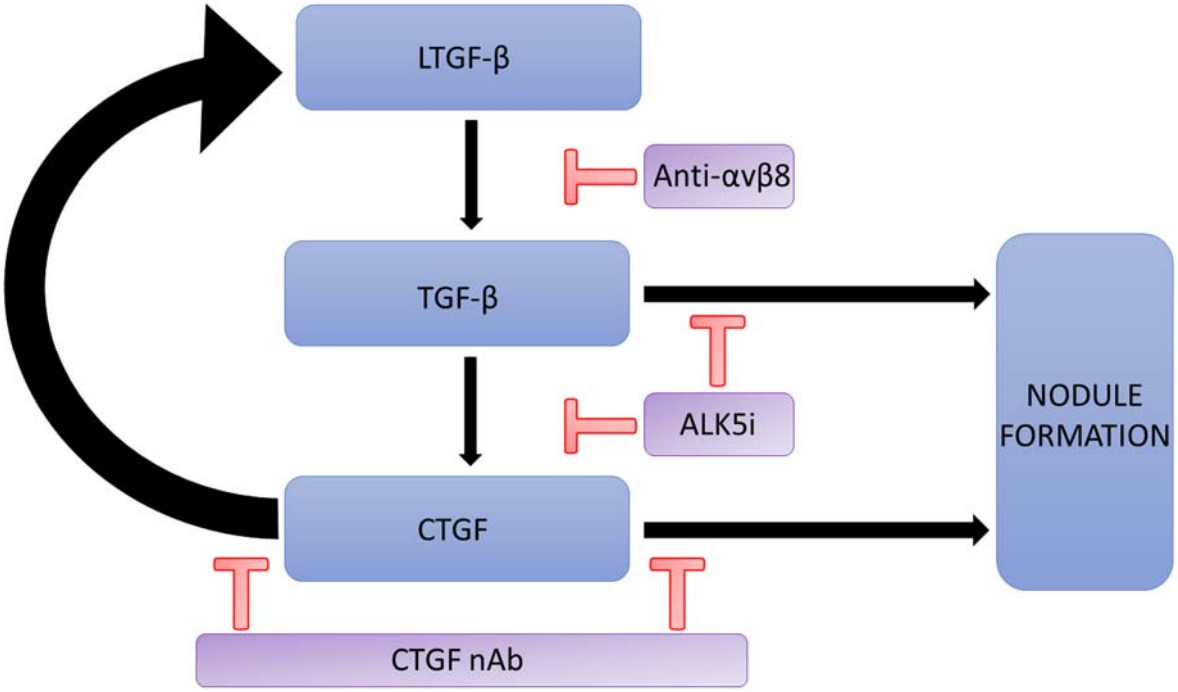

Figure 78. TGF-β and CTGF co-operative interaction induce nodule formation in 3D tri-culture.

The culture of the three glomerular cell types in 3D allows these cell types to intimately interact both physically and via signalling mechanisms and mimic the *in vivo* state both morphologically and pathophysiologically. This has made apparent the many factors at play in glomerulosclerosis, revealing it is highly likely that for a successful treatment and attenuation that avoids adverse effects, multiple elements require targeting. TGF-β and CTGF are key in fibrosis and good potential targets in preventing disease progression considering the synergy that exists between these cytokines in driving disease progression. The targeting of integrin αvβ8 allows for cell and tissue-specific modification of TGF-β activity avoiding a total universal inhibitory blockade of activity which would result in undesirable systemic outcomes. Of the foremost importance is data that is of clinical relevance and this research demonstrates the 3D tri-culture model can translate to pertinent information about glomerulosclerosis and kidney disease. The 3D tri-culture model provides further detail and complexity than a simple 2D mono-culture while simplifying the view seen with animal models where disease aetiology is not reflected, also allowing the desired move away from the use of animals.

On balance, the 3D tri-culture model allows for the best compromise for studying and assessing treatments for glomerulosclerosis, a tool that can aid evaluation in drug development. A system that models human glomerulosclerosis *in vitro*.

Future Work

A multitude of possible avenues and directions are conceivable with the 3D tri-culture model. Firstly work could be done to increase N numbers of existing data to add greater power and confirm preliminary findings, with the panel of genes studied could be narrowed and refined

Work could be done for further optimisation of 3D tri-culture read-outs. The system could be made more high-throughput using 384-well plates where, using high content microscopy and the HALO software introduced earlier, defined fibrotic end-points could be assessed. This could include nodule formation with staining for collagens, as well as other ECM proteins such as fibronectin, as well as assessing fGEC network lengths with branching. Certainly, a quantitative measure of the response of each cell type in the model to TGF-β would be advantageous in comparing with the *in vivo* condition, which would be fGEC network loss, fPOD loss, fMC proliferation. Indeed, cell death has not been analysed in the 3D culture system, it would be informative to know the extent of basal cell death and then with treatments, especially TNF-α with its role in cell death. Cell viability assays may also be useful to assess any change in fPOD cell numbers with TGF-β to provide a functional response that represents *in vivo*.

Additional elements added to the 3D tri-culture model could be explored. As has been discussed, the immune element of renal fibrosis has become to be shown as an important one. The addition of a further immune element, either the secretome of an immune cell type or the addition of an immune cell itself to the 3D tri-culture model would be an interesting avenue to explore. Flow and related mechanical stress play a central role in the pathogenesis of glomerulosclerosis.[321] Recapitulating this in the 3D tri-culture model would further add to the clinical relevance of the system. There is an immediate avenue where this could be explored, ibidi® plasticware was used successfully to create 3D tri-cultures, ibidi® have a cell culture under flow system that could be employed to study flow in the 3D tri-culture.[322]

Further analysis of the underlying molecular mechanisms of cytokine signalling could be made. For example, how TNF-α antagonises TGF-β, where the literature implicates NF-κB and JNK signalling, and how CTGF induces TGFB1, where it is only known not to involve SMAD2 or SMAD7.[284, 318]

Another key research area in the complicated mix of renal fibrosis mechanisms is EMT/EndMT, this has mainly been described in tubular epithelial cells therefore, it may be interesting to study the 3D tri-culture further for EMT/EndMT.

A source of CTGF in the 3D tri-culture model was identified as fPODs, this finding is based on RT-qPCR data, therefore further investigation of this would be of interest. Such as seeing if this response is demonstrated at a protein level and potentially fPOD specific CTGF knockdown to see how considerable an effect fPOD produced CTGF has upon fibrosis in the 3D tri-culture.

Experiments with αvβ8 inhibition resulted in some interesting preliminary data, where the αvβ8 integrin proved an effective potential target in glomerulosclerosis. Further experimentation with the higher concentrations of anti-αvβ8 antibody would be prudent, along with exploration of the effect of inhibition when using other inducers of TGF-β in the 3D tri-culture, such as exposure to high glucose.

Further work with HOC would be advantageous as discussed, it can enable an analysis of patient tissues for similarities in active pathways or targets seen within the model. Either HOC would be focussed on using tissue where the precise renal origin is known, or assessment would be made for glomerular markers, to facilitate making the desired comparisons with HOC and 3D tri-culture. IHC of HOC to examine protein expression of identified markers of fibrosis, such as fibronectin and CTGF would be valuable. Work to obtain PODs from isolated glomeruli could be furthered, while perhaps an exploration of culturing isolated human glomeruli to model glomerulosclerosis could be of interest. Utilising isolated glomeruli in this manner was introduced in the literature review and enable interrogation with clear clinical relevance.[186, 323]

References

1. *Are you Kidney Aware?* 2019; Available from: http://www.worldkidneyday.co.uk/are-you-kidney-aware/.
2. Gale, E.A.M., *The Rise of Childhood Type 1 Diabetes in the 20th Century.* Diabetes, 2002. **51**(12): p.3353-3361.
3. Wild, S., et al., *Global Prevalence of Diabetes.* Estimates for the year 2000 and projections for 2030, 2004. **27**(5): p.1047-1053.
4. Eddy, A.A. and E.G. Neilson, *Chronic Kidney Disease Progression.* Journal of the American Society of Nephrology, 2006. **17**(11): p.2964-2966.
5. Liu, Y., *Cellular and molecular mechanisms of renal fibrosis.* Nat Rev Nephrol, 2011. **7**(12): p.684-696.
6. Duffield, J.S., *Cellular and molecular mechanisms in kidney fibrosis.* J Clin Invest, 2014. **124**(6): p.2299-306.
7. Makino, H., et al., *Ultrastructural changes of extracellular matrices in diabetic nephropathy revealed by high resolution scanning and immunoelectron microscopy.* Laboratory investigation; a journal of technical methods and pathology, 1993. **68**(1): p.45-55.
8. Alsaad, K.O. and A.M. Herzenberg, *Distinguishing diabetic nephropathy from other causes of glomerulosclerosis: an update.* Journal of Clinical Pathology, 2007. **60**(1): p.18-26.
9. Rydel, J.J., et al., *Focal segmental glomerular sclerosis in adults: Presentation, course, and response to treatment.* American Journal of Kidney Diseases, 1995. **25**(4): p.534-542.
10. Schlondorff, D. and B. Banas, *The mesangial cell revisited: no cell is an island.* J Am Soc Nephrol, 2009. **20**(6): p.1179-87.
11. Sison, K., et al., *Glomerular Structure and Function Require Paracrine, Not Autocrine, VEGF–VEGFR-2 Signaling.* Journal of the American Society of Nephrology, 2010. **21**(10): p.1691-1701.
12. Pavenstädt, H., W. Kriz, and M. Kretzler, *Cell Biology of the Glomerular Podocyte.* Physiological Reviews, 2003. **83**(1): p.253-307.
13. Grahammer, F., C. Schell, and T.B. Huber, *The podocyte slit diaphragm - from a thin grey line to a complex signalling hub.* Nat Rev Nephrol, 2013. **9**(10): p.587-598.
14. Peterson, J.C., et al., *Blood pressure control, proteinuria, and the progression of renal disease: the Modification of Diet in Renal Disease Study.* Annals of internal medicine, 1995. **123**(10): p.754-762.
15. Garg, P. and T. Rabelink, *Glomerular Proteinuria: A Complex Interplay Between Unique Players.* Advances in Chronic Kidney Disease, 2011. **18**(4): p.233-242.
16. Consortium, C.K.D.P., *Association of estimated glomerular filtration rate and albuminuria with all-cause and cardiovascular mortality in general population cohorts: a collaborative meta-analysis.* The Lancet, 2010. **375**(9731): p.2073-2081.
17. Loeffler, I. and G. Wolf, *Transforming growth factor-β and the progression of renal disease.* Nephrology Dialysis Transplantation, 2013.
18. Böttinger, E.P. and M. Bitzer, *TGF-ß Signaling in Renal Disease.* Journal of the American Society of Nephrology, 2002. **13**(10): p.2600-2610.
19. Kriz, W. and M. Lehir, *Pathways to nephron loss starting from glomerular diseases-insights from animal models.* Kidney International, 2005. **67**(2): p.404-419.
20. Wiggins, R.C., *The spectrum of podocytopathies: A unifying view of glomerular diseases.* Kidney International, 2007. **71**(12): p.1205-1214.
21. Fioretto , P., et al., *Reversal of Lesions of Diabetic Nephropathy after Pancreas Transplantation.* New England Journal of Medicine, 1998. **339**(2): p.69-75.
22. Zeisberg, M., et al., *BMP-7 counteracts TGF-beta1-induced epithelial-to-mesenchymal transition and reverses chronic renal injury.* Nat Med, 2003. **9**(7): p.964-8.
23. Tampe, D. and M. Zeisberg, *Potential approaches to reverse or repair renal fibrosis.* Nat Rev Nephrol, 2014. **10**(4): p. 226-37.

24. Grande, M.T., et al., *Snail1-induced partial epithelial-to-mesenchymal transition drives renal fibrosis in mice and can be targeted to reverse established disease.* Nat Med, 2015. **21**(9): p. 989-97.
25. Jun, J.-I. and L.F. Lau, *Resolution of organ fibrosis.* The Journal of Clinical Investigation, 2018. **128**(1): p.97-107.
26. Schnaper, H.W., et al., *TGF-β signal transduction and mesangial cell fibrogenesis.* American Journal of Physiology - Renal Physiology, 2003. **284**(2): p.F243-F252.
27. LEASK, A. and D.J. ABRAHAM, *TGF-β signaling and the fibrotic response.* The FASEB Journal, 2004. **18**(7): p.816-827.
28. Yamamoto, T., et al., *Expression of transforming growth factor-beta isoforms in human glomerular diseases.* Kidney Int, 1996. **49**(2): p.461-9.
29. Lee, S., et al., *Expression of transforming growth factor-beta1 and hypoxia-inducible factor-1alpha in renal transplantation.* Transplant Proc, 2008. **40**(7): p.2147-8.
30. Pohlers, D., et al., *TGF-β and fibrosis in different organs — molecular pathway imprints.* Biochimica et Biophysica Acta (BBA) - Molecular Basis of Disease, 2009. **1792**(8): p.746-756.
31. Massagué, J., *Receptors for the TGF-β family.* Cell, 1992. **69**(7): p.1067-1070.
32. Derynck, R., Y. Zhang, and X.-H. Feng, *Transcriptional Activators of TGF-b Responses: Smads.* Cell, 1998. **95**(6): p.737-740.
33. Massague, J., *How cells read TGF-b signals.* Nat Rev Mol Cell Biol, 2000. **1**(3): p.169-178.
34. Zeisberg, M., *Bone morphogenic protein-7 and the kidney: current concepts and open questions.* Nephrology Dialysis Transplantation, 2006. **21**(3): p.568-573.
35. Mitu, G.M., S. Wang, and R. Hirschberg, *BMP7 is a podocyte survival factor and rescues podocytes from diabetic injury.* Am J Physiol Renal Physiol, 2007. **293**(5): p.F1641-8.
36. Yanagita, M., *Inhibitors/antagonists of TGF-β system in kidney fibrosis.* Nephrology Dialysis Transplantation, 2012. **27**(10): p.3686-3691.
37. Simon, M., et al., *Expression of bone morphogenetic protein-7 mRNA in normal and ischemic adult rat kidney.* American Journal of Physiology - Renal Physiology, 1999. **276**(3): p.F382-F389.
38. WANG, S.-N., J. LAPAGE, and R. HIRSCHBERG, *Loss of Tubular Bone Morphogenetic Protein—7 in Diabetic Nephropathy.* Journal of the American Society of Nephrology, 2001. **12**(11): p.2392-2399.
39. Wetzel, P., et al., *Bone morphogenetic protein-7 expression and activity in the human adult normal kidney is predominantly localized to the distal nephron.* Kidney Int, 2006. **70**(4): p. 717-23.
40. Goldschmeding, R., et al., *Connective tissue growth factor: just another factor in renal fibrosis?* Nephrology Dialysis Transplantation, 2000. **15**(3): p.296-299.
41. Wang, Q., et al., *Cooperative interaction of CTGF and TGF-beta in animal models of fibrotic disease.* Fibrogenesis Tissue Repair, 2011. **4**(1): p.4.
42. Kok, H.M., et al., *Targeting CTGF, EGF and PDGF pathways to prevent progression of kidney disease.* Nat Rev Nephrol, 2014. **10**(12): p.700-711.
43. Yokoi, H., et al., *Role of connective tissue growth factor in profibrotic action of transforming growth factor-b: A potential target for preventing renal fibrosis.* American Journal of Kidney Diseases, 2001. **38**(4): p.S134-S138.
44. Nguyen, T.Q., et al., *CTGF Inhibits BMP-7 Signaling in Diabetic Nephropathy.* Journal of the American Society of Nephrology, 2008. **19**(11): p.2098-2107.
45. Liu, S.C., Hsu, C. J., Fong, Y. C., Chuang, S. M. & Tang, C. H., *CTGF induces monocyte chemoattractant protein-1 expression to enhance monocyte migration in human synovial fibroblasts.* Biochim. Biophys. Acta, 2013. **1833**(5): p.1114–1124.
46. Sánchez-López, E., et al., *CTGF Promotes Inflammatory Cell Infiltration of the Renal Interstitium by Activating NF-κB.* Journal of the American Society of Nephrology, 2009. **20**(7): p.1513-1526.

47. Andrae, J., R. Gallini, and C. Betsholtz, *Role of platelet-derived growth factors in physiology and medicine.* Genes & Development, 2008. **22**(10): p.1276-1312.
48. Floege, J., F. Eitner, and C.E. Alpers, *A New Look at Platelet-Derived Growth Factor in Renal Disease.* Journal of the American Society of Nephrology, 2008. **19**(1): p.12-23.
49. Boor, P., T. Ostendorf, and J. Floege, *PDGF and the progression of renal disease.* Nephrology Dialysis Transplantation, 2014. **29**(suppl_1): p.i45-i54.
50. Chen, J., et al., *EGFR Signaling Promotes TGFβ-Dependent Renal Fibrosis.* Journal of the American Society of Nephrology, 2012. **23**(2): p.215-224.
51. Citri, A. and Y. Yarden, *EGF–ERBB signalling: towards the systems level.* Nature Reviews Molecular Cell Biology, 2006. **7**(7): p.505-516.
52. Tsau, Y.K. and C.H. Chen, *Urinary Epidermal Growth Factor Excretion in Children with Chronic Renal Failure.* American Journal of Nephrology, 1999. **19**(3): p.400-404.
53. Strutz, F., et al., *Basic fibroblast growth factor expression is increased in human renal fibrogenesis and may mediate autocrine fibroblast proliferation.* Kidney International, 2000. **57**(4): p.1521-1538.
54. Floege, J., et al., *Basic fibroblast growth factor augments podocyte injury and induces glomerulosclerosis in rats with experimental membranous nephropathy.* The Journal of Clinical Investigation, 1995. **96**(6): p.2809-2819.
55. Messmer, U.K., V.A. Briner, and J. Pfeilschifter, *Basic Fibroblast Growth Factor Selectively Enhances TNF-α—Induced Apoptotic Cell Death in Glomerular Endothelial Cells: Effects on Apoptotic Signaling Pathways.* Journal of the American Society of Nephrology, 2000. **11**(12): p.2199-2211.
56. Slavin, J., *Fibroblast growth factors: at the heart of angiogenesis.* Cell Biol Int, 1995. **19**(5): p.431-44.
57. Itoh, N., *The Fgf families in humans, mice, and zebrafish: their evolutional processes and roles in development, metabolism, and disease.* Biol Pharm Bull, 2007. **30**(10): p.1819-25.
58. Strutz, F., *The role of FGF-2 in renal fibrogenesis.* Front Biosci (Schol Ed), 2009. **1**: p.125-31.
59. Yang, J., C. Dai, and Y. Liu, *Hepatocyte Growth Factor Suppresses Renal Interstitial Myofibroblast Activation and Intercepts Smad Signal Transduction.* The American Journal of Pathology, 2003. **163**(2): p.621-632.
60. Dai, C. and Y. Liu, *Hepatocyte growth factor antagonizes the profibrotic action of TGF-beta1 in mesangial cells by stabilizing Smad transcriptional corepressor TGIF.* J Am Soc Nephrol, 2004. **15**(6): p.1402-12.
61. Mizuno, S. and T. Nakamura, *Suppressions of chronic glomerular injuries and TGF-beta 1 production by HGF in attenuation of murine diabetic nephropathy.* Am J Physiol Renal Physiol, 2004. **286**(1): p.F134-43.
62. Lekushi, K., et al., *Hepatocyte growth factor attenuates renal fibrosis through TGF-β1 suppression by apoptosis of myofibroblasts.* Journal of Hypertension, 2010. **28**(12): p.2454-2461.
63. Liu, Y., *Hepatocyte growth factor in kidney fibrosis: therapeutic potential and mechanisms of action.* American Journal of Physiology-Renal Physiology, 2004. **287**(1): p.F7-F16.
64. Organ, S.L. and M.-S. Tsao, *An overview of the c-MET signaling pathway.* Therapeutic advances in medical oncology, 2011. **3**(1 Suppl): p.S7-S19.
65. Wynn, T.A., *Cellular and molecular mechanisms of fibrosis.* J Pathol, 2008. **214**(2): p.199-210.
66. Navarro-Gonzalez, J.F., et al., *Inflammatory molecules and pathways in the pathogenesis of diabetic nephropathy.* Nat Rev Nephrol, 2011. **7**(6): p.327-40.
67. Wada, J. and H. Makino, *Inflammation and the pathogenesis of diabetic nephropathy.* Clin Sci (Lond), 2013. **124**(3): p.139-52.
68. Betjes, M.G., *Immune cell dysfunction and inflammation in end-stage renal disease.* Nat Rev Nephrol, 2013. **9**(5): p.255-65.

69. Kurts, C., et al., *The immune system and kidney disease: basic concepts and clinical implications.* Nat Rev Immunol, 2013. **13**(10): p. 738-753.
70. Awad, A.S., et al., *Macrophage-derived tumor necrosis factor-alpha mediates diabetic renal injury.* Kidney Int, 2015. **88**(4): p. 722-33.
71. Wu, J., et al., *Immune activation caused by vascular oxidation promotes fibrosis and hypertension.* J Clin Invest, 2016. **126**(1): p. 50-67.
72. Baud, L., et al., *Production of tumor necrosis factor by rat mesangial cells in response to bacterial lipopolysaccharide.* Kidney Int, 1989. **35**(5): p. 1111-8.
73. Hruby, Z.W. and R.P. Lowry, *Spontaneous release of tumor necrosis factor alpha by isolated renal glomeruli and cultured glomerular mesangial cells.* Clin Immunol Immunopathol, 1991. **59**(1): p. 156-64.
74. Navarro, J.F., et al., *Renal pro-inflammatory cytokine gene expression in diabetic nephropathy: effect of angiotensin-converting enzyme inhibition and pentoxifylline administration.* Am J Nephrol, 2006. **26**(6): p. 562-70.
75. Wajant, H., K. Pfizenmaier, and P. Scheurich, *Tumor necrosis factor signaling.* Cell Death Differ, 2003. **10**(1): p. 45-65.
76. Dinarello, C.A. and S.M. Wolff, *The Role of Interleukin-1 in Disease.* New England Journal of Medicine, 1993. **328**(2): p. 106-113.
77. Sims, J.E. and D.E. Smith, *The IL-1 family: regulators of immunity.* Nature Reviews Immunology, 2010. **10**: p. 89.
78. Kovacs, E., *Fibrogenic cytokines: The role of immune mediators in the development of scar tissue*. Vol. 12. 1991. 17-23.
79. Anders, H.-J., *Of Inflammasomes and Alarmins: IL-1β and IL-1α in Kidney Disease.* Journal of the American Society of Nephrology, 2016. **27**(9): p. 2564-2575.
80. Ruoslahti, E., *Integrins.* The Journal of clinical investigation, 1991. **87**(1): p. 1-5.
81. Hynes, R.O., *Integrins: Bidirectional, Allosteric Signaling Machines.* Cell, 2002. **110**(6): p. 673-687.
82. Pozzi, A. and R. Zent, *Integrins in kidney disease.* J Am Soc Nephrol, 2013. **24**(7): p. 1034-9.
83. Conroy, K.P., L.J. Kitto, and N.C. Henderson, *alphav integrins: key regulators of tissue fibrosis.* Cell Tissue Res, 2016.
84. Lee, V.W. and D.C. Harris, *Adriamycin nephropathy: A model of focal segmental glomerulosclerosis.* Nephrology, 2011. **16**(1): p. 30-38.
85. Like, A. and A. Rossini, *Streptozotocin-induced pancreatic insulitis: new model of diabetes mellitus.* Science, 1976. **193**(4251): p. 415-417.
86. Tesch, G.H. and T.J. Allen, *Rodent models of streptozotocin-induced diabetic nephropathy (Methods in Renal Research).* Nephrology, 2007. **12**(3): p. 261-266.
87. Sharma, K., P. McCue, and S.R. Dunn, *Diabetic kidney disease in the db/dbmouse.* American Journal of Physiology - Renal Physiology, 2003. **284**(6): p. F1138-F1144.
88. Cefalu, W.T., *Animal Models of Type 2 Diabetes: Clinical Presentation and Pathophysiological Relevance to the Human Condition.* ILAR Journal, 2006. **47**(3): p. 186-198.
89. Yang, H.-C., Y. Zuo, and A.B. Fogo, *Models of chronic kidney disease.* Drug Discovery Today: Disease Models, 2010. **7**(1–2): p. 13-19.
90. Miner, J.H. and J.R. Sanes, *Molecular and functional defects in kidneys of mice lacking collagen alpha 3(IV): implications for Alport syndrome.* The Journal of Cell Biology, 1996. **135**(5): p. 1403-1413.
91. Cosgrove, D., et al., *Collagen COL4A3 knockout: a mouse model for autosomal Alport syndrome.* Genes & Development, 1996. **10**(23): p. 2981-2992.
92. Griffin, K.A., M. Picken, and A.K. Bidani, *Method of renal mass reduction is a critical modulator of subsequent hypertension and glomerular injury.* Journal of the American Society of Nephrology, 1994. **4**(12): p. 2023-31.

93. Gava, A.L., et al., *Effects of 5/6 nephrectomy on renal function and blood pressure in mice.* International Journal of Physiology, Pathophysiology and Pharmacology, 2012. **4**(3): p. 167-173.
94. Chevalier, R.L., M.S. Forbes, and B.A. Thornhill, *Ureteral obstruction as a model of renal interstitial fibrosis and obstructive nephropathy.* Kidney Int, 2009. **75**(11): p. 1145-52.
95. Abbott, A., *Cell culture: Biology's new dimension.* Nature, 2003. **424**(6951): p. 870-872.
96. Pampaloni, F., E.G. Reynaud, and E.H.K. Stelzer, *The third dimension bridges the gap between cell culture and live tissue.* Nat Rev Mol Cell Biol, 2007. **8**(10): p. 839-845.
97. Antoni, D., et al., *Three-dimensional cell culture: a breakthrough in vivo.* Int J Mol Sci, 2015. **16**(3): p. 5517-27.
98. Edmondson, R., et al., *Three-Dimensional Cell Culture Systems and Their Applications in Drug Discovery and Cell-Based Biosensors.* Assay and Drug Development Technologies, 2014. **12**(4): p. 207-218.
99. Weaver, V.M., et al., *Reversion of the malignant phenotype of human breast cells in three-dimensional culture and in vivo by integrin blocking antibodies.* J Cell Biol, 1997. **137**(1): p. 231-45.
100. Warburg, O., *Versuche und uberledbeudem carcinomgewebe (methoden).* Biochem Z, 1923. **142**: p. 317-333.
101. Ruegg, C.E., et al., *Preparation of positional renal slices for study of cell-specific toxicity.* Journal of Pharmacological Methods, 1987. **17**(2): p. 111-123.
102. De Kanter, R., et al., *Organ Slices as an In Vitro Test System for Drug Metabolism in Human Liver, Lung and Kidney.* Toxicology in Vitro, 1999. **13**(4): p. 737-744.
103. Stribos, E.G.D., et al., *Precision-cut human kidney slices as a model to elucidate the process of renal fibrosis.* Translational Research, 2016. **170**: p. 8-16.e1.
104. Stribos, E.G.D., et al., *Renal fibrosis in precision-cut kidney slices.* European Journal of Pharmacology, 2016. **790**: p. 57-61.
105. Al-Lamki, R.S., J.R. Bradley, and J.S. Pober, *Human Organ Culture: Updating the Approach to Bridge the Gap from In Vitro to In Vivo in Inflammation, Cancer, and Stem Cell Biology.* Frontiers in Medicine, 2017. **4**(148).
106. Sharma, K., et al., *Increased renal production of transforming growth factor-beta1 in patients with type II diabetes.* Diabetes, 1997. **46**(5): p. 854-9.
107. Iwano, M., et al., *Quantification of glomerular TGF-β1 mRNA in patients with diabetes mellitus.* Kidney International, 1996. **49**(4): p. 1120-1126.
108. MOZES, M.M., et al., *Renal Expression of Fibrotic Matrix Proteins and of Transforming Growth Factor-β (TGF-β) Isoforms in TGF-β Transgenic Mice.* Journal of the American Society of Nephrology, 1999. **10**(2): p. 271-280.
109. Kim, H.W., et al., *Heterozygous mice for TGF-betaIIR gene are resistant to the progression of streptozotocin-induced diabetic nephropathy.* Kidney Int, 2004. **66**(5): p. 1859-65.
110. Wang, S. and R. Hirschberg, *BMP7 antagonizes TGF-β-dependent fibrogenesis in mesangial cells.* American Journal of Physiology - Renal Physiology, 2003. **284**(5): p. F1006-F1013.
111. MacKay, K., et al., *Transforming growth factor-beta. Murine glomerular receptors and responses of isolated glomerular cells.* Journal of Clinical Investigation, 1989. **83**(4): p. 1160-1167.
112. Poncelet, A.-C. and H.W. Schnaper, *Regulation of human mesangial cell collagen expression by transforming growth factor-β1.* American Journal of Physiology - Renal Physiology, 1998. **275**(3): p. F458-F466.
113. Border, W.A., et al., *Suppression of experimental glomerulonephritis by antiserum against transforming growth factor [beta]1.* Nature, 1990. **346**(6282): p. 371-374.
114. Kulkarni, A.B. and S. Karlsson, *Transforming growth factor-beta 1 knockout mice. A mutation in one cytokine gene causes a dramatic inflammatory disease.* The American Journal of Pathology, 1993. **143**(1): p. 3-9.

115. Wang, W., et al., *Signaling mechanism of TGF-beta1 in prevention of renal inflammation: role of Smad7.* J Am Soc Nephrol, 2005. **16**(5): p. 1371-83.
116. Monteleone, G., et al., *TGF-b1 and Smad7 in the regulation of IBD.* Mucosal Immunol, 2008. **1**(1s): p. S50-S53.
117. Nakao, A., K. Okumura, and H. Ogawa, *Smad7: a new key player in TGF-β-associated disease.* Trends in molecular medicine, 2002. **8**(8): p. 361-363.
118. Yan, X., Z. Liu, and Y. Chen, *Regulation of TGF-β signaling by Smad7.* Acta Biochimica et Biophysica Sinica, 2009. **41**(4): p. 263-272.
119. Li, J.H., et al., *Smad7 Inhibits Fibrotic Effect of TGF-β on Renal Tubular Epithelial Cells by Blocking Smad2 Activation.* Journal of the American Society of Nephrology, 2002. **13**(6): p. 1464-1472.
120. Lan, H.Y., et al., *Inhibition of renal fibrosis by gene transfer of inducible Smad7 using ultrasound-microbubble system in rat UUO model.* J Am Soc Nephrol, 2003. **14**(6): p. 1535-48.
121. Yang, J., et al., *Downregulation of Smad Transcriptional Corepressors SnoN and Ski in the Fibrotic Kidney: An Amplification Mechanism for TGF-β1 Signaling.* Journal of the American Society of Nephrology, 2003. **14**(12): p. 3167-3177.
122. Moon, J.A., et al., *IN-1130, a novel transforming growth factor-beta type I receptor kinase (ALK5) inhibitor, suppresses renal fibrosis in obstructive nephropathy.* Kidney Int, 2006. **70**(7): p. 1234-43.
123. Meng, X.-m., D.J. Nikolic-Paterson, and H.Y. Lan, *TGF-b: the master regulator of fibrosis.* Nat Rev Nephrol, 2016. **12**(6): p. 325-338.
124. Lu, A., et al., *Blockade of TSP1-Dependent TGF-b; Activity Reduces Renal Injury and Proteinuria in a Murine Model of Diabetic Nephropathy.* The American Journal of Pathology, 2011. **178**(6): p. 2573-2586.
125. Vukicevic, S., et al., *Osteogenic protein-1 (bone morphogenetic protein-7) reduces severity of injury after ischemic acute renal failure in rat.* J Clin Invest, 1998. **102**(1): p. 202-14.
126. Murphy, M., et al., *Suppression Subtractive Hybridization Identifies High Glucose Levels as a Stimulus for Expression of Connective Tissue Growth Factor and Other Genes in Human Mesangial Cells.* Journal of Biological Chemistry, 1999. **274**(9): p. 5830-5834.
127. Ito, Y., et al., *Expression of connective tissue growth factor in human renal fibrosis.* Kidney Int, 1998. **53**(4): p. 853-61.
128. Yokoi, H., et al., *Reduction in connective tissue growth factor by antisense treatment ameliorates renal tubulointerstitial fibrosis.* J Am Soc Nephrol, 2004. **15**(6): p. 1430-40.
129. Adler, S.G., et al., *Phase 1 study of anti-CTGF monoclonal antibody in patients with diabetes and microalbuminuria.* Clin J Am Soc Nephrol, 2010. **5**(8): p. 1420-8.
130. FLOEGE, J., et al., *Mitogenic effect of platelet-derived growth factor in human glomerular mesangial cells: modulation and/or suppression by inflammatory cytokines.* Clinical & Experimental Immunology, 1991. **86**(2): p. 334-341.
131. Hudkins, K.L., et al., *Exogenous PDGF-D Is a Potent Mesangial Cell Mitogen and Causes a Severe Mesangial Proliferative Glomerulopathy.* Journal of the American Society of Nephrology, 2004. **15**(2): p. 286-298.
132. OSTENDORF, T., et al., *Specific Antagonism of PDGF Prevents Renal Scarring in Experimental Glomerulonephritis.* Journal of the American Society of Nephrology, 2001. **12**(5): p. 909-918.
133. Nakagawa, T., et al., *Role of PDGF B-Chain and PDGF Receptors in Rat Tubular Regeneration after Acute Injury.* The American Journal of Pathology, 1999. **155**(5): p. 1689-1699.
134. Holbro, T. and N.E. Hynes, *ErbB Receptors: Directing Key Signaling Networks Throughout Life.* Annual Review of Pharmacology and Toxicology, 2004. **44**(1): p. 195-217.
135. Jørgensen, P.E., et al., *Renal uptake and excretion of epidermal growth factor from plasma in the rat.* Regulatory Peptides, 1990. **28**(3): p. 273-280.

136. Taira, T., et al., *Urinary epidermal growth factor levels in patients with acute renal failure.* Am J Kidney Dis, 1993. **22**(5): p. 656-61.
137. Terzi, F., et al., *Targeted expression of a dominant-negative EGF-R in the kidney reduces tubulo-interstitial lesions after renal injury.* J Clin Invest, 2000. **106**(2): p. 225-34.
138. Chen, J., J.-K. Chen, and R.C. Harris, *EGF Receptor Deletion in Podocytes Attenuates Diabetic Nephropathy.* Journal of the American Society of Nephrology, 2015. **26**(5): p. 1115-1125.
139. Liu, N., et al., *Genetic or Pharmacologic Blockade of EGFR Inhibits Renal Fibrosis.* Journal of the American Society of Nephrology, 2012. **23**(5): p. 854-867.
140. FRANÇOIS, H., et al., *Prevention of renal vascular and glomerular fibrosis by epidermal growth factor receptor inhibition.* The FASEB Journal, 2004. **18**(7): p. 926-928.
141. Bou Matar, R.N., J.D. Klein, and J.M. Sands, *Erlotinib preserves renal function and prevents salt retention in doxorubicin treated nephrotic rats.* PLoS One, 2013. **8**(1): p. e54738.
142. Zhang, M.-Z., et al., *The Role of the EGF Receptor in Sex Differences in Kidney Injury.* Journal of the American Society of Nephrology, 2019. **30**(9): p. 1659-1673.
143. Kim, B.W., et al., *Association between epidermal growth factor (EGF) and EGF receptor gene polymorphisms and end-stage renal disease and acute renal allograft rejection in a Korean population.* Renal Failure, 2020. **42**(1): p. 98-106.
144. Humes, H.D., et al., *Epidermal growth factor enhances renal tubule cell regeneration and repair and accelerates the recovery of renal function in postischemic acute renal failure.* The Journal of Clinical Investigation, 1989. **84**(6): p. 1757-1761.
145. Wang, Z., et al., *Importance of Functional EGF Receptors in Recovery from Acute Nephrotoxic Injury.* Journal of the American Society of Nephrology, 2003. **14**(12): p. 3147-3154.
146. Silver, B.J., F.E. Jaffer, and H.E. Abboud, *Platelet-derived growth factor synthesis in mesangial cells: induction by multiple peptide mitogens.* Proceedings of the National Academy of Sciences, 1989. **86**(3): p. 1056-1060.
147. Ballermann, B.J., *Regulation of bovine glomerular endothelial cell growth in vitro.* American Journal of Physiology-Cell Physiology, 1989. **256**(1): p. C182-C189.
148. Takeuchi, A., et al., *Basic fibroblast growth factor promotes proliferation of rat glomerular visceral epithelial cells in vitro.* The American journal of pathology, 1992. **141**(1): p. 107.
149. Strutz, F., et al., *TGF-ß1 induces proliferation in human renal fibroblasts via induction of basic fibroblast growth factor (FGF-2).* Kidney International, 2001. **59**(2): p. 579-592.
150. Floege, J., et al., *Infusion of platelet-derived growth factor or basic fibroblast growth factor induces selective glomerular mesangial cell proliferation and matrix accumulation in rats.* The Journal of Clinical Investigation, 1993. **92**(6): p. 2952-2962.
151. Dolivo, D.M., S.A. Larson, and T. Dominko, *Fibroblast Growth Factor 2 as an Antifibrotic: Antagonism of Myofibroblast Differentiation and Suppression of Pro-Fibrotic Gene Expression.* Cytokine & Growth Factor Reviews, 2017. **38**: p. 49-58.
152. Taman, M., et al., *Increase urinary hepatocyte growth factor excretion in human acute renal failure.* Clinical nephrology, 1997. **48**(4): p. 241-245.
153. Oka, M., et al., *Hepatocyte Growth Factor–Secreting Mesothelial Cell Sheets Suppress Progressive Fibrosis in a Rat Model of CKD.* Journal of the American Society of Nephrology, 2019. **30**(2): p. 261-276.
154. Hasegawa, G., et al., *Possible role of tumor necrosis factor and interleukin-1 in the development of diabetic nephropathy.* Kidney Int, 1991. **40**(6): p. 1007-12.
155. Nakamura, T., et al., *mRNA expression of growth factors in glomeruli from diabetic rats.* Diabetes, 1993. **42**(3): p. 450-6.
156. Moriwaki, Y., et al., *Elevated levels of interleukin-18 and tumor necrosis factor-alpha in serum of patients with type 2 diabetes mellitus: relationship with diabetic nephropathy.* Metabolism, 2003. **52**(5): p. 605-8.

157. Niewczas, M.A., et al., *Serum concentrations of markers of TNFalpha and Fas-mediated pathways and renal function in nonproteinuric patients with type 1 diabetes.* Clin J Am Soc Nephrol, 2009. **4**(1): p. 62-70.
158. Lin, J., et al., *Lipid and inflammatory biomarkers and kidney function decline in type 2 diabetes.* Diabetologia, 2010. **53**(2): p. 263-7.
159. DiPetrillo, K., B. Coutermarsh, and F.A. Gesek, *Urinary tumor necrosis factor contributes to sodium retention and renal hypertrophy during diabetes.* Am J Physiol Renal Physiol, 2003. **284**(1): p. F113-21.
160. Hong, S., et al., *Smad7 binds to the adaptors TAB2 and TAB3 to block recruitment of the kinase TAK1 to the adaptor TRAF2.* Nat Immunol, 2007. **8**(5): p. 504-13.
161. Garlanda, C., C.A. Dinarello, and A. Mantovani, *The interleukin-1 family: back to the future.* Immunity, 2013. **39**(6): p. 1003-1018.
162. Lonnemann, G., et al., *Cytokines in human renal interstitial fibrosis. II. Intrinsic interleukin (IL)-1 synthesis and IL-1-dependent production of IL-6 and IL-8 by cultured kidney fibroblasts.* Kidney International, 1995. **47**(3): p. 845-854.
163. Niemir, Z.I., et al., *Podocytes are the major source of IL-1 alpha and IL-1 beta in human glomerulonephritides.* Kidney International, 1997. **52**(2): p. 393-403.
164. Lorenz, G., M.N. Darisipudi, and H.-J. Anders, *Canonical and non-canonical effects of the NLRP3 inflammasome in kidney inflammation and fibrosis.* Nephrology Dialysis Transplantation, 2013. **29**(1): p. 41-48.
165. Shahzad, K., et al., *Nlrp3-inflammasome activation in non-myeloid-derived cells aggravates diabetic nephropathy.* Kidney International, 2015. **87**(1): p. 74-84.
166. Lemos, D.R., et al., *Interleukin-1β Activates a MYC-Dependent Metabolic Switch in Kidney Stromal Cells Necessary for Progressive Tubulointerstitial Fibrosis.* Journal of the American Society of Nephrology, 2018. **29**(6): p. 1690-1705.
167. Lei, Y., et al., *Interleukin-1β Inhibition for Chronic Kidney Disease in Obese Mice With Type 2 Diabetes.* Frontiers in Immunology, 2019. **10**(1223).
168. Ozawa, A., et al., *Molecular Basis of the Ligand Binding Specificity of αvβ8 Integrin.* Journal of Biological Chemistry, 2016. **291**(22): p. 11551-11565.
169. Mu , D., et al., *The integrin αvβ8 mediates epithelial homeostasis through MT1-MMP–dependent activation of TGF-β1.* Journal of Cell Biology, 2002. **157**(3): p. 493-507.
170. Campbell, M.G., et al., *Cryo-EM Reveals Integrin-Mediated TGF-β Activation without Release from Latent TGF-β.* Cell, 2020. **180**(3): p. 490-501.e16.
171. Moyle, M., M.A. Napier, and J.W. McLean, *Cloning and expression of a divergent integrin subunit beta 8.* Journal of Biological Chemistry, 1991. **266**(29): p. 19650-8.
172. Lakhe-Reddy, S., et al., *β8 integrin binds Rho GDP dissociation inhibitor-1 and activates Rac1 to inhibit mesangial cell myofibroblast differentiation.* Journal of Biological Chemistry, 2006. **281**(28): p. 19688-19699.
173. Aluwihare, P., et al., *Mice that lack activity of αvβ6- and αvβ8-integrins reproduce the abnormalities of Tgfb1- and Tgfb3-null mice.* Journal of Cell Science, 2009. **122**(2): p. 227-232.
174. Hatley, R.J.D., et al., *An αv-RGD Integrin Inhibitor Toolbox: Drug Discovery Insight, Challenges and Opportunities.* Angewandte Chemie International Edition, 2018. **57**(13): p. 3298-3321.
175. Bon, H., et al., *Spontaneous Extracellular Matrix Accumulation in a Human in vitro Model of Renal Fibrosis Is Mediated by αV Integrins.* Nephron, 2019. **142**(4): p. 328-350.
176. Basta, J., et al., *Pharmacologic inhibition of RGD-binding integrins ameliorates fibrosis and improves function following kidney injury.* Physiological Reports, 2020. **8**(7): p. e14329.
177. Reichart, F., et al., *Selective targeting of integrin αvβ8 by a highly active cyclic peptide.* Journal of medicinal chemistry, 2019. **62**(4): p. 2024-2037.
178. Chen, A., et al., *Experimental focal segmental glomerulosclerosis in mice.* Nephron, 1998. **78**(4): p. 440-52.

179. Sakemi, T., et al., *Sex difference in progression of adriamycin-induced nephropathy in rats.* Am J Nephrol, 1996. **16**(6): p. 540-7.
180. Becker, G.J. and T.D. Hewitson, *Animal models of chronic kidney disease: useful but not perfect.* Nephrology Dialysis Transplantation, 2013.
181. Mosley, K., J. Collar, and V. Cattell, *Mesangial cell necrosis in Thy 1 glomerulonephritis – an ultrastructural study.* Virchows Archiv, 2000. **436**(6): p. 567-573.
182. Jensen, M.S., et al., *Activation of the prostaglandin E2 EP2 receptor attenuates renal fibrosis in unilateral ureteral obstructed mice and human kidney slices.* Acta Physiologica, 2019. **227**(1): p. e13291.
183. Bigaeva, E., et al., *Predictive Value of Precision-Cut Kidney Slices as an Ex Vivo Screening Platform for Therapeutics in Human Renal Fibrosis.* Pharmaceutics, 2020. **12**(5): p. 459.
184. Wilson, H.M. and K.N. Stewart, *Glomerular Epithelial and Mesangial Cell Culture and Characterization*, in *Human Cell Culture Protocols*, R.R. Mitry and R.D. Hughes, Editors. 2012, Humana Press: Totowa, NJ. p. 187-201.
185. Ni, L., M. Saleem, and P.W. Mathieson, *Podocyte culture: tricks of the trade.* Nephrology (Carlton), 2012. **17**(6): p. 525-31.
186. Esposito, C., et al., *Hepatocyte growth factor (HGF) modulates matrix turnover in human glomeruli.* Kidney International, 2005. **67**(6): p. 2143-2150.
187. Poosti, F., et al., *Precision-cut kidney slices (PCKS) to study development of renal fibrosis and efficacy of drug targeting ex vivo.* Disease Models & Mechanisms, 2015. **8**(10): p. 1227-1236.
188. Genovese, F., et al., *Precision-cut kidney slices as a tool to understand the dynamics of extracellular matrix remodeling in renal fibrosis.* Biomarker insights, 2016. **11**: p. BMI. S38439.
189. Stribos, E.G., et al., *Murine precision-cut kidney slices as an ex vivo model to evaluate the role of transforming growth factor-β1 signaling in the onset of renal fibrosis.* Frontiers in physiology, 2017. **8**: p. 1026.
190. Ruigrok, M.J.R., et al., *siRNA-Mediated RNA Interference in Precision-Cut Tissue Slices Prepared from Mouse Lung and Kidney.* The AAPS Journal, 2017. **19**(6): p. 1855-1863.
191. Tan, R.J., et al., *Tubular injury triggers podocyte dysfunction by β-catenin–driven release of MMP-7.* JCI Insight, 2019. **4**(24).
192. Paish, H.L., et al., *A Bioreactor Technology for Modeling Fibrosis in Human and Rodent Precision-Cut Liver Slices.* Hepatology, 2019. **70**(4): p. 1377-1391.
193. Waters, J.P., et al., *In vitro self-assembly of human pericyte-supported endothelial microvessels in three-dimensional coculture: a simple model for interrogating endothelial-pericyte interactions.* J Vasc Res, 2013. **50**(4): p. 324-31.
194. Waters, J., *3-dimensional culture of endothelial and mural cells allowing interrogation of the role of TGF-β/BMP7 signaling in human glomerular endothelial and mesangial cells in glomerulosclerosis* in *Department of Medicine*. 2015, University of Cambridge.
195. Marx, M., et al., *Spatial organization of the extracellular matrix modulates the expression of PDGF-receptor subunits in mesangial cells.* Kidney International, 1993. **43**(5): p. 1027-1041.
196. Sankar, S., et al., *Modulation of transforming growth factor beta receptor levels on microvascular endothelial cells during in vitro angiogenesis.* J Clin Invest, 1996. **97**(6): p. 1436-46.
197. Byron, A., et al., *Glomerular cell cross-talk influences composition and assembly of extracellular matrix.* J Am Soc Nephrol, 2014. **25**(5): p. 953-66.
198. Li, M., et al., *Three-dimensional podocyte-endothelial cell co-cultures: Assembly, validation, and application to drug testing and intercellular signaling studies.* Eur J Pharm Sci, 2016. **86**: p. 1-12.
199. Takasato, M., et al., *Kidney organoids from human iPS cells contain multiple lineages and model human nephrogenesis.* Nature, 2015. **526**(7574): p. 564-568.

200. Saleem, M.A., et al., *A Conditionally Immortalized Human Podocyte Cell Line Demonstrating Nephrin and Podocin Expression.* Journal of the American Society of Nephrology, 2002. **13**(3): p. 630-638.
201. Waters, J.P., et al., *A 3D tri-culture system reveals that activin receptor-like kinase 5 and connective tissue growth factor drive human glomerulosclerosis.* The Journal of Pathology, 2017. **243**(3): p. 390-400.
202. Krtil, J., et al., *Culture methods of glomerular podocytes.* Kidney Blood Press Res, 2007. **30**(3): p. 162-74.
203. Nyengaard, J.R. and T.F. Bendtsen, *Glomerular number and size in relation to age, kidney weight, and body surface in normal man.* Anat Rec, 1992. **232**(2): p. 194-201.
204. Shankland, S.J., et al., *Podocytes in culture: past, present, and future.* Kidney Int, 2007. **72**(1): p. 26-36.
205. Hugo, C., et al., *The plasma membrane-actin linking protein, ezrin, is a glomerular epithelial cell marker in glomerulogenesis, in the adult kidney and in glomerular injury.* Kidney Int, 1998. **54**(6): p. 1934-44.
206. Smith, S.W., S. Chand, and C.O.S. Savage, *Biology of the renal pericyte.* Nephrology Dialysis Transplantation, 2012.
207. Haeryfar, S.M.M. and D.W. Hoskin, *Thy-1: More than a Mouse Pan-T Cell Marker.* The Journal of Immunology, 2004. **173**(6): p. 3581-3588.
208. Bradley, J.E., G. Ramirez, and J.S. Hagood, *Roles and regulation of Thy-1, a context-dependent modulator of cell phenotype.* BioFactors, 2009. **35**(3): p. 258-265.
209. Scindia, Y.M., U.S. Deshmukh, and H. Bagavant, *Mesangial pathology in glomerular disease: targets for therapeutic intervention.* Advanced drug delivery reviews, 2010. **62**(14): p. 1337-1343.
210. REISER, J., et al., *The Glomerular Slit Diaphragm Is a Modified Adherens Junction.* Journal of the American Society of Nephrology, 2000. **11**(1): p. 1-8.
211. Eddy, A.A. and A.B. Fogo, *Plasminogen Activator Inhibitor-1 in Chronic Kidney Disease: Evidence and Mechanisms of Action.* Journal of the American Society of Nephrology, 2006. **17**(11): p. 2999-3012.
212. Małgorzewicz, S., E. Skrzypczak-Jankun, and J. Jankun, *Plasminogen activator inhibitor-1 in kidney pathology (Review).* Int J Mol Med, 2013. **31**(3): p. 503-10.
213. Brennan, E.P., et al., *Next-generation sequencing identifies TGF-β1-associated gene expression profiles in renal epithelial cells reiterated in human diabetic nephropathy.* Biochimica et Biophysica Acta (BBA) - Molecular Basis of Disease, 2012. **1822**(4): p. 589-599.
214. Fuchshofer, R., et al., *Connective tissue growth factor modulates podocyte actin cytoskeleton and extracellular matrix synthesis and is induced in podocytes upon injury.* Histochemistry and Cell Biology, 2011. **136**(3): p. 301.
215. Yokoi, H., et al., *Overexpression of connective tissue growth factor in podocytes worsens diabetic nephropathy in mice.* Kidney Int, 2008. **73**(4): p. 446-55.
216. Sieber, C., et al., *Recent advances in BMP receptor signaling.* Cytokine Growth Factor Rev, 2009. **20**(5-6): p. 343-55.
217. Yanagisawa, K., et al., *Induction of apoptosis by Smad3 and down-regulation of Smad3 expression in response to TGF-β in human normal lung epithelial cells.* Oncogene, 1998. **17**(13): p. 1743-1747.
218. Poncelet, A.-C., et al., *Cell phenotype-specific down-regulation of Smad3 involves decreased gene activation as well as protein degradation.* Journal of Biological Chemistry, 2007. **282**(21): p. 15534-15540.
219. Dahodwala, H. and K.H. Lee, *The fickle CHO: a review of the causes, implications, and potential alleviation of the CHO cell line instability problem.* Current Opinion in Biotechnology, 2019. **60**: p. 128-137.

220. Kriz, W., et al., *The podocyte's response to stress: the enigma of foot process effacement.* American Journal of Physiology-Renal Physiology, 2013. **304**(4): p. F333-F347.
221. Weiskirchen, R. and S.K. Meurer, *BMP-7 counteracting TGF-beta1 activities in organ fibrosis.* Front Biosci (Landmark Ed), 2013. **18**: p. 1407-1434.
222. RISER, B.L., et al., *Regulation of Connective Tissue Growth Factor Activity in Cultured Rat Mesangial Cells and Its Expression in Experimental Diabetic Glomerulosclerosis.* Journal of the American Society of Nephrology, 2000. **11**(1): p. 25-38.
223. Baker, B.M. and C.S. Chen, *Deconstructing the third dimension – how 3D culture microenvironments alter cellular cues.* Journal of Cell Science, 2012. **125**(13): p. 3015-3024.
224. Hughes, C.S., L.M. Postovit, and G.A. Lajoie, *Matrigel: A complex protein mixture required for optimal growth of cell culture.* PROTEOMICS, 2010. **10**(9): p. 1886-1890.
225. Allen, T.D. and S.L. Schor, *The contraction of collagen matrices by dermal fibroblasts.* J Ultrastruct Res, 1983. **83**(2): p. 205-19.
226. Chevallay, B. and D. Herbage, *Collagen-based biomaterials as 3D scaffold for cell cultures: applications for tissue engineering and gene therapy.* Medical and Biological Engineering and Computing, 2000. **38**(2): p. 211-218.
227. Klumpers, D.D., et al., *Cell mediated contraction in 3D cell-matrix constructs leads to spatially regulated osteogenic differentiation.* Integr Biol (Camb), 2013. **5**(9): p. 1174-83.
228. Montesano, R. and L. Orci, *Transforming growth factor beta stimulates collagen-matrix contraction by fibroblasts: implications for wound healing.* Proc Natl Acad Sci U S A, 1988. **85**(13): p. 4894-7.
229. Ma, J., et al., *Coculture of osteoblasts and endothelial cells: optimization of culture medium and cell ratio.* Tissue Eng Part C Methods, 2011. **17**(3): p. 349-57.
230. Goers, L., P. Freemont, and K.M. Polizzi, *Co-culture systems and technologies: taking synthetic biology to the next level.* J R Soc Interface, 2014. **11**(96).
231. Sam, R., et al., *Glomerular epithelial cells transform to myofibroblasts: early but not late removal of TGF-β1 reverses transformation.* Translational Research, 2006. **148**(3): p. 142-148.
232. Li, Y., et al., *Epithelial-to-Mesenchymal Transition Is a Potential Pathway Leading to Podocyte Dysfunction and Proteinuria.* The American Journal of Pathology, 2008. **172**(2): p. 299-308.
233. Cho, J.G., et al., *Endothelial to Mesenchymal Transition Represents a Key Link in the Interaction between Inflammation and Endothelial Dysfunction.* Front Immunol, 2018. **9**: p. 294.
234. Siddiqi, F.S. and A. Advani, *Endothelial-Podocyte Crosstalk: The Missing Link Between Endothelial Dysfunction and Albuminuria in Diabetes.* Diabetes, 2013. **62**(11): p. 3647-3655.
235. Dimke, H., Y. Maezawa, and S.E. Quaggin, *Crosstalk in glomerular injury and repair.* Current opinion in nephrology and hypertension, 2015. **24**(3): p. 231.
236. Lennon, R. and S. Hosawi, *Glomerular cell crosstalk.* Current Opinion in Nephrology and Hypertension, 2016. **25**(3): p. 187-193.
237. Daehn, I.S., *Glomerular endothelial cell stress and cross-talk with podocytes in early diabetic kidney disease.* Frontiers in Medicine, 2018. **5**: p. 76.
238. Suzuki, S., et al., *Transcriptional activation of matrix genes by transforming growth factor beta 1 in mesangial cells.* Experimental nephrology, 1993. **1**(4): p. 229-237.
239. Park, I.S., et al., *Expression of transforming growth factor-beta and type IV collagen in early streptozotocin-induced diabetes.* Diabetes, 1997. **46**(3): p. 473-80.
240. Wang, S. and R. Hirschberg, *BMP7 antagonizes TGF-beta -dependent fibrogenesis in mesangial cells.* Am J Physiol Renal Physiol, 2003. **284**(5): p. F1006-13.
241. Klahr, S. and J.J. Morrissey, *The role of vasoactive compounds, growth factors and cytokines in the progression of renal disease.* Kidney International, 2000. **57**: p. S7-S14.
242. Verrecchia, F. and A. Mauviel, *TGF-beta and TNF-alpha: antagonistic cytokines controlling type I collagen gene expression.* Cell Signal, 2004. **16**(8): p. 873-80.

243. Grande, J.P., D.C. Melder, and A.R. Zinsmeister, *Modulation of collagen gene expression by cytokines: Stimulatory effect of transforming growth factor-β1, with divergent effects of epidermal growth factor and tumor necrosis factor-α on collagen type I and collagen type IV.* Journal of Laboratory and Clinical Medicine, 1997. **130**(5): p. 476-486.
244. Tamsma, J.T., et al., *Expression of glomerular extracellular matrix components in human diabetic nephropathy: decrease of heparan sulphate in the glomerular basement membrane.* Diabetologia, 1994. **37**(3): p. 313-20.
245. Miner, J.H., *Renal basement membrane components.* Kidney international, 1999. **56**(6): p. 2016-2024.
246. Harvey, S.J., et al., *Role of distinct type IV collagen networks in glomerular development and function.* Kidney Int, 1998. **54**(6): p. 1857-66.
247. Abraham, D.J., et al., *Tumor Necrosis Factor α Suppresses the Induction of Connective Tissue Growth Factor by Transforming Growth Factor-β in Normal and Scleroderma Fibroblasts.* Journal of Biological Chemistry, 2000. **275**(20): p. 15220-15225.
248. Xie, S., et al., *Regulation of TGF-β1-induced connective tissue growth factor expression in airway smooth muscle cells.* American Journal of Physiology - Lung Cellular and Molecular Physiology, 2005. **288**(1): p. L68-L76.
249. Cooker, L.A., et al., *TNF-α, but not IFN-γ, regulates CCN2 (CTGF), collagen type I, and proliferation in mesangial cells: possible roles in the progression of renal fibrosis.* American Journal of Physiology - Renal Physiology, 2007. **293**(1): p. F157-F165.
250. Sánchez-López, E., et al., *Connective tissue growth factor (CTGF): a key factor in the onset and progression of kidney damage.* Nefrologia, 2009. **29**(5): p. 382-391.
251. Chen, Y.Q., et al., *Differential mechanisms of plasminogen activator inhibitor-1 gene activation by transforming growth factor-beta and tumor necrosis factor-alpha in endothelial cells.* Thromb Haemost, 2001. **86**(6): p. 1563-72.
252. Kishida, M., et al., *PGE1 inhibits the expression of PAI-1 mRNA induced by TNF-alpha in human mesangial cells.* Exp Clin Endocrinol Diabetes, 2005. **113**(7): p. 365-71.
253. Swiatkowska, M., J. Szemraj, and C.S. Cierniewski, *Induction of PAI-1 expression by tumor necrosis factor alpha in endothelial cells is mediated by its responsive element located in the 4G/5G site.* Febs j, 2005. **272**(22): p. 5821-31.
254. Fogo, A.B., *Renal fibrosis: not just PAI-1 in the sky.* Journal of Clinical Investigation, 2003. **112**(3): p. 326-328.
255. Qi , W., et al., *TGF-1 induces IL-8 and MCP-1 through a connective tissue growth factor-independent pathway.* American Journal of Physiology - Renal Physiology, 2006. **290**(3): p. F703-F709.
256. Weiss, J.M., C.A. Cuff, and J.W. Berman, *TGF-beta downmodulates cytokine-induced monocyte chemoattractant protein (MCP)-1 expression in human endothelial cells. A putative role for TGF-beta in the modulation of TNF receptor expression.* Endothelium, 1999. **6**(4): p. 291-302.
257. Wolf, G., et al., *Existence of a regulatory loop between MCP-1 and TGF-β in glomerular immune injury.* American Journal of Physiology - Renal Physiology, 2002. **283**(5): p. F1075-F1084.
258. Viedt, C. and S.R. Orth, *Monocyte chemoattractant protein-1 (MCP-1) in the kidney: does it more than simply attract monocytes?* Nephrology Dialysis Transplantation, 2002. **17**(12): p. 2043-2047.
259. Wada, T., et al., *Monocyte chemoattractant protein-1: does it play a role in diabetic nephropathy?* Nephrology Dialysis Transplantation, 2003. **18**(3): p. 457-459.
260. Yadav, A., V. Saini, and S. Arora, *MCP-1: chemoattractant with a role beyond immunity: a review.* Clinica chimica acta, 2010. **411**(21): p. 1570-1579.
261. Smith, W.B., et al., *Transforming growth factor-beta 1 inhibits the production of IL-8 and the transmigration of neutrophils through activated endothelium.* The Journal of Immunology, 1996. **157**(1): p. 360-8.

262. Gerritsma, J.S., et al., *Transforming growth factor-β1 regulates chemokine and complement production by human proximal tubular epithelial cells.* Kidney international, 1998. **53**(3): p. 609-616.
263. Schmouder, R.L., et al., *In vitro and in vivo interleukin-8 production in human renal cortical epithelia.* Kidney international, 1992. **41**(1): p. 191-198.
264. Navarro, J.F. and C. Mora-Fernández, *The role of TNF-α in diabetic nephropathy: pathogenic and therapeutic implications.* Cytokine & growth factor reviews, 2006. **17**(6): p. 441-450.
265. Wada, T., et al., *Detection of urinary interleukin-8 in glomerular diseases.* Kidney international, 1994. **46**(2): p. 455-460.
266. SEGERER, S., P.J. NELSON, and D. SCHLÖNDORFF, *Chemokines, Chemokine Receptors, and Renal Disease: From Basic Science To Pathophysiologic and Therapeutic Studies.* Journal of the American Society of Nephrology, 2000. **11**(1): p. 152-176.
267. Yoshioka, K., et al., *Glomerular localization of type III collagen in human kidney disease.* Kidney International, 1989. **35**(5): p. 1203-1211.
268. Wang, D., et al., *Canonical Wnt/beta-catenin signaling mediates transforming growth factor-beta1-driven podocyte injury and proteinuria.* Kidney Int, 2011. **80**(11): p. 1159-69.
269. Liu, Y., *New insights into epithelial-mesenchymal transition in kidney fibrosis.* J Am Soc Nephrol, 2010. **21**(2): p. 212-22.
270. Boor, P. and J. Floege, *The renal (myo-)fibroblast: a heterogeneous group of cells.* Nephrology Dialysis Transplantation, 2012. **27**(8): p. 3027-3036.
271. Novakovic, Z.S., et al., *The interstitial expression of alpha-smooth muscle actin in glomerulonephritis is associated with renal function.* Medical Science Monitor: International Medical Journal of Experimental and Clinical Research, 2012. **18**(4): p. CR235.
272. McKay, N.G., et al., *The effect of transforming growth factor beta 1 on mesangial cell fibronectin synthesis: increased incorporation into the extracellular matrix and reduced pI but no effect on alternative splicing.* Exp Mol Pathol, 1993. **59**(3): p. 211-24.
273. Ikeya, M., M. Nagase, and N. Honda, *Intraglomerular distribution of fibronectin in primary glomerular diseases.* Clin Nephrol, 1985. **24**(2): p. 53-9.
274. Sugiyama, D., K. Kulkeaw, and C. Mizuochi, *TGF-beta-1 up-regulates extra-cellular matrix production in mouse hepatoblasts.* Mechanisms of Development, 2013. **130**(2): p. 195-206.
275. Chen, Y.M. and H. Liapis, *Focal segmental glomerulosclerosis: molecular genetics and targeted therapies.* BMC nephrology, 2015. **16**(1): p. 101.
276. Liao, S.-J., et al., *TGF-β1 and TNF-α synergistically induce epithelial to mesenchymal transition of breast cancer cells by enhancing TAK1 activation.* Journal of cell communication and signaling, 2019. **13**(3): p. 369-380.
277. Yoshimatsu, Y., et al., *TGF-beta and TNF-alpha cooperatively induce mesenchymal transition of lymphatic endothelial cells via activation of Activin signals.* PLOS ONE, 2020. **15**(5): p. e0232356.
278. Lan, H.Y., *Diverse Roles of TGF-β/Smads in Renal Fibrosis and Inflammation.* International Journal of Biological Sciences, 2011. **7**(7): p. 1056-1067.
279. Li, R.X., W.H. Yiu, and S.C. Tang, *Role of bone morphogenetic protein-7 in renal fibrosis.* Frontiers in physiology, 2015. **6**: p. 114.
280. Quan, G., et al., *TGF-beta1 up-regulates transglutaminase two and fibronectin in dermal fibroblasts: a possible mechanism for the stabilization of tissue inflammation.* Arch Dermatol Res, 2005. **297**(2): p. 84-90.
281. Upton, P.D. and N.W. Morrell, *TGF-beta and BMPR-II pharmacology--implications for pulmonary vascular diseases.* Curr Opin Pharmacol, 2009. **9**(3): p. 274-80.
282. Abreu, J.G., et al., *Connective-tissue growth factor (CTGF) modulates cell signalling by BMP and TGF-b.* Nat Cell Biol, 2002. **4**(8): p. 599-604.
283. Goldberg, M.T., et al., *TNF-α Suppresses α-Smooth Muscle Actin Expression in Human Dermal Fibroblasts: An Implication for Abnormal Wound Healing.* The Journal of investigative dermatology, 2007. **127**(11): p. 2645-2655.

284. Li, G., et al., *Inhibition of connective tissue growth factor by siRNA prevents liver fibrosis in rats.* J Gene Med, 2006. **8**(7): p. 889-900.
285. Sullivan, D.E., et al., *TNF-α induces TGF-β1 expression in lung fibroblasts at the transcriptional level via AP-1 activation.* Journal of cellular and molecular medicine, 2009. **13**(8b): p. 1866-1876.
286. Yamane, K., et al., *Antagonistic effects of TNF-alpha on TGF-beta signaling through down-regulation of TGF-beta receptor type II in human dermal fibroblasts.* J Immunol, 2003. **171**(7): p. 3855-62.
287. Strutz, F., et al., *Role of basic fibroblast growth factor-2 in epithelial-mesenchymal transformation.* Kidney International, 2002. **61**(5): p. 1714-1728.
288. Zhao, C., et al., *Role of tumor necrosis factor-α in epithelial-to-mesenchymal transition in transplanted kidney cells in recipients with chronic allograft dysfunction.* Gene, 2018. **642**: p. 483-490.
289. Burns, W.C., et al., *Connective Tissue Growth Factor Plays an Important Role in Advanced Glycation End Product–Induced Tubular Epithelial-to-Mesenchymal Transition: Implications for Diabetic Renal Disease.* Journal of the American Society of Nephrology, 2006. **17**(9): p. 2484-2494.
290. Sonnylal, S., et al., *Connective tissue growth factor causes EMT-like cell fate changes in vivo and in vitro.* Journal of cell science, 2013. **126**(10): p. 2164-2175.
291. Dudas, P.L., R.L. Argentieri, and F.X. Farrell, *BMP-7 fails to attenuate TGF-beta1-induced epithelial-to-mesenchymal transition in human proximal tubule epithelial cells.* Nephrol Dial Transplant, 2009. **24**(5): p. 1406-16.
292. Ikenouchi, J., et al., *Regulation of tight junctions during the epithelium-mesenchyme transition: direct repression of the gene expression of claudins/occludin by Snail.* Journal of cell science, 2003. **116**(Pt 10): p. 1959-1967.
293. Gupta, S., et al., *Connective tissue growth factor: Potential role in glomerulosclerosis and tubulointerstitial fibrosis.* Kidney International, 2000. **58**(4): p. 1389-1399.
294. Gore-Hyer, E., et al., *Selective stimulation of collagen synthesis in the presence of costimulatory insulin signaling by connective tissue growth factor in scleroderma fibroblasts.* Arthritis & Rheumatism, 2003. **48**(3): p. 798-806.
295. Wang, S., et al., *Connective tissue growth factor in tubulointerstitial injury of diabetic nephropathy.* Kidney International, 2001. **60**(1): p. 96-105.
296. Mason, R.M., *Connective tissue growth factor(CCN2), a pathogenic factor in diabetic nephropathy. What does it do? How does it do it?* Journal of Cell Communication and Signaling, 2009. **3**(2): p. 95-104.
297. Zhang, C., et al., *Connective tissue growth factor regulates the key events in tubular epithelial to myofibroblast transition in vitro.* Cell Biol Int, 2004. **28**(12): p. 863-73.
298. Blom, I.E., et al., *In vitro evidence for differential involvement of CTGF, TGFβ, and PDGF-BB in mesangial response to injury.* Nephrology Dialysis Transplantation, 2001. **16**(6): p. 1139-1148.
299. Setty, S., et al., *Differential expression of laminin isoforms in diabetic nephropathy and other renal diseases.* Modern Pathology, 2012. **25**(6): p. 859-868.
300. Kaneko, T., et al., *Induction of Plasminogen Activator Inhibitor-1 in Endothelial Cells by Basic Fibroblast Growth Factor and Its Modulation by Fibric Acid.* Arteriosclerosis, Thrombosis, and Vascular Biology, 2002. **22**(5): p. 855-860.
301. Rerolle, J.-P., et al., *Plasminogen activator inhibitor type 1 is a potential target in renal fibrogenesis.* Kidney International, 2000. **58**(5): p. 1841-1850.
302. Nurminskaya, M.V. and A.M. Belkin, *Cellular functions of tissue transglutaminase*, in *International review of cell and molecular biology*. 2012, Elsevier. p. 1-97.
303. Mason, R.M. and N.A. Wahab, *Extracellular Matrix Metabolism in Diabetic Nephropathy.* Journal of the American Society of Nephrology, 2003. **14**(5): p. 1358-1373.

304. Rasmussen, D.G.K., et al., *Collagen turnover profiles in chronic kidney disease.* Scientific Reports, 2019. **9**(1): p. 16062.
305. van Steensel, L., et al., *Platelet-Derived Growth Factor-BB: A Stimulus for Cytokine Production by Orbital Fibroblasts in Graves' Ophthalmopathy.* Investigative Ophthalmology & Visual Science, 2010. **51**(2): p. 1002-1007.
306. Fellström, B., et al., *Platelet-derived growth factor receptors in the kidney—Upregulated expression in inflammation.* Kidney International, 1989. **36**(6): p. 1099-1102.
307. Duffy, H.S., et al., *Reciprocal regulation of the junctional proteins claudin-1 and connexin43 by interleukin-1beta in primary human fetal astrocytes.* The Journal of neuroscience : the official journal of the Society for Neuroscience, 2000. **20**(23): p. RC114.
308. Abe, T., et al., *Interleukin-1β and Barrier Function of Retinal Pigment Epithelial Cells (ARPE-19): Aberrant Expression of Junctional Complex Molecules.* Investigative Ophthalmology & Visual Science, 2003. **44**(9): p. 4097-4104.
309. Fujita, H., et al., *Claudin-1 expression in airway smooth muscle exacerbates airway remodeling in asthmatic subjects.* Journal of Allergy and Clinical Immunology, 2011. **127**(6): p. 1612-1621.e8.
310. Gong, Y., et al., *Inducible expression of claudin-1 in glomerular podocytes generates aberrant tight junctions and proteinuria through slit diaphragm destabilization.* Journal of the American Society of Nephrology, 2017. **28**(1): p. 106-117.
311. Gaut, J.P., et al., *Claudin 1 and nephrin label cellular crescents in diabetic glomerulosclerosis.* Human pathology, 2014. **45**(3): p. 628-635.
312. Vogetseder, A., et al., *αv-Integrin isoform expression in primary human tumors and brain metastases.* International Journal of Cancer, 2013. **133**(10): p. 2362-2371.
313. Khan, S., et al., *Mesangial cell integrin αvβ8 provides glomerular endothelial cell cytoprotection by sequestering TGF-β and regulating PECAM-1.* Am J Pathol, 2011. **178**(2): p. 609-20.
314. Zhou, X., et al., *An integrin antagonist (MK-0429) decreases proteinuria and renal fibrosis in the ZSF1 rat diabetic nephropathy model.* Pharmacol Res Perspect, 2017. **5**(5).
315. Al-Lamki, R.S., et al., *Tumor necrosis factor receptor 2-signaling in CD133-expressing cells in renal clear cell carcinoma.* Oncotarget, 2016. **7**(17).
316. Bertelli, R., et al., *Cell-specific regulation of alpha1 (III) and alpha2 (V) collagen by TGF-beta1 in tubulointerstitial cell models.* Nephrology, dialysis, transplantation: official publication of the European Dialysis and Transplant Association-European Renal Association, 1998. **13**(3): p. 573-579.
317. Mauviel, A., et al., *Tumor necrosis factor inhibits collagen and fibronectin synthesis in human dermal fibroblasts.* FEBS Letters, 1988. **236**(1): p. 47-52.
318. Verrecchia, F. and A. Mauviel, *TGF-β and TNF-α: antagonistic cytokines controlling type I collagen gene expression.* Cellular Signalling, 2004. **16**(8): p. 873-880.
319. Verrecchia, F., et al., *Tumor necrosis factor-alpha inhibits transforming growth factor-beta /Smad signaling in human dermal fibroblasts via AP-1 activation.* J Biol Chem, 2000. **275**(39): p. 30226-31.
320. Ziyadeh, F.N., *Mediators of Diabetic Renal Disease: The Case for TGF-β as the Major Mediator.* Journal of the American Society of Nephrology, 2004. **15**(1 suppl): p. S55-S57.
321. Chagnac, A., et al., *Consequences of Glomerular Hyperfiltration: The Role of Physical Forces in the Pathogenesis of Chronic Kidney Disease in Diabetes and Obesity.* Nephron, 2019. **143**(1): p. 38-42.
322. Reiser, A., et al. *Changes in cell-cell contacts of endothelial cells (HUVEC) under long term shear stress conditions*. in *ANGIOGENESIS*. 2014. SPRINGER VAN GODEWIJCKSTRAAT 30, 3311 GZ DORDRECHT, NETHERLANDS.
323. Hale, L.J., et al., *3D organoid-derived human glomeruli for personalised podocyte disease modelling and drug screening.* Nature Communications, 2018. **9**(1): p. 5167.